THE REMOVAL OF LEAD POLLUTANTS FROM EFFLUENTS USING ZEOLITES

by

JAMES FRANCIS O'CONNOR

A Thesis Submitted for the Degree of
Doctor of Philosophy

The City University
Department of Chemistry
August 1989

To my wife Anne,

Without your love, patience and understanding I could never have done it.

CONTENTS

LIST OF TABLES

LIST OF FIGURES

ACKNOWLEDGEMENTS

Firstly, my thanks go to my supervisor Dr. R. P. Townsend for his advice and encouragement throughout this project.

My thanks also go to [redacted], who were the collaborating industrial body, for their financial and technical support.

I would also like to thank all my friends and colleagues at City University for their help and advice - I got there in the end.

Finally, my thanks go to [redacted] for the friendly persuasion and provision of resources, and to [redacted] for sorting out the mess and turning out such a professionally typed thesis.

I hereby grant powers of discretion to the University Librarian to allow this thesis to be copied without further reference to the author.

ABSTRACT

To provide an effective method for the removal of trimethyllead ions from effluents, a detailed examination of both the kinetics and equilibrium thermodynamics of ion exchange of trimethyllead into a variety of zeolites of varying ion exchange capacities was required.

As a base upon which the research programme could be built, a study of the kinetics and equilibrium properties of the exchange of lead ions in a range of zeolites, having varying framework silica to alumina ratios, were examined at 25°C and at total solution normalities of 0.05 and 0.1g equiv. dm^{-3}. Ion exchange isotherms were constructed for all systems, but non-stoichiometric behaviour was observed in all cases. Selectivity sequences for the lead exchanges could nevertheless be deduced, and as a general rule it was found that the more siliceous the zeolite, the lower the preference for lead. Ion exchange behaviour can be rationalized in terms of ion hydration and electrostatic ion binding energies. The selectivity sequences are discussed in terms of simple dielectric theory, which is shown to have serious limitations in predicting affinity trends in zeolites of different framework charge.

The kinetics and equilibrium selectivity characteristics of the trimethyllead/sodium binary system in NaX and NaY were initially examined to clarify both the influences of silica to alumina ratio, and the ion size and shape, on the exchange properties of these zeolites. The effects of changes in sodium chloride content on the selectivity of the zeolites for the trimethyllead ion was of particular interest because of the nature of effluents currently

obtained. Exchange limits suggested a possible dissociation within the zeolite. The high degree of selectivity exhibited by these zeolites for the inorganic lead ion did not extend to this organolead ion, and subsequently a study of the selectivity for the trimethyllead ion by acid treated clinoptilolite samples was carried out to note the effect, if any, that higher silica contents may have on the preferential sorption of organics from water.

An initial examination of hydronium ion exchange as a function of pH is also reported. The importance of hydronium exhange has frequently been underestimated in past studies and it is felt that it should be taken into account not only during preparation, but also in ion exchange of zeolites.

LIST OF PRINCIPLE SYMBOLS

a_o	Unit cell diameter
a_U	Activity of ion U in solution
$\bar{a}_U$	Activity of ion U in the crystal
d_f	Framework density (number of tetrahedra per 1000Å^3)
E_d	Polarographic deposition potential
E_U	Solution phase equivalent fraction of ion U
$\bar{E}_U$	Crystal phase equivalent fraction ion U
e	Charge on one electron (C)
F	Helmoltz free energy of charge formation
f_N	Normalisation factor
G	Gibb's free energy of charge formation
ΔG^θ	Standard free energy of exchange
g_U	Crystal phase activity coefficient of ion U
H	Enthalpy
I	Ionic strength of solution (mol dm^{-3})
K_a	Thermodynamic equilibrium constant
K_c	Corrected selectivity coefficient (Kielland quotient)
K_m	Mass action quotient
L	Avagadro's constant (mol^{-1})
m_U	Concentration of ion U in the solution phase (mol dm^{-3})
$\bar{m}_U$	Concentration of ion U in the crystal phase (mol kg^{-1})

N	Solution concentration (g equiv. dm^{-3})
(N)	Used as a superscript indicates normalised value
n	Number of moles
P, p	Pressure
$\bar{Q}$	Exchange capacity of a zeolite
R	Gas constant (8.314 kJ mol^{-1})
r_U	Radius of ion U
S	Entropy
T	Absolute temperature (273 K)
V	Volume
V_f	Void fraction
w	work
X_i	Equivalent fraction of cations in the ith set of cation sites
z_U	Valency of ion U
α	Molar separation factor
α'	Separation factor (in terms of equivalent fractions)
Δ	Crystal phase water activity term
Γ	Ratio of the solution phase activity coefficients
$\gamma_{\pm}^{(VX)}$ UX	Mean molal stoichiometric activity coefficient of salt UX in a solution of VX
ε	Permittivity of medium ($CV^{-1}m^{-1}$)
μ	Chemical potential

v	Molar volume
$^-$	As superscript indicates crystal phase

CHAPTER 1 - INTRODUCTION

1.1 ANTIKNOCK COMPOUNDS

The principal commercial application of organolead compounds is in their use as antiknock agents. These are additives for aviation and motor gasolines which are incorporated in order to suppress the reactions that produce the undesirable phenomenon of "knock" in the internal combustion engine. "Knock" frequently limits the power output of an engine and if it is sufficiently severe, it may damage it. It may also preclude the use of higher compression ratios, which are more efficient thermodynamically, allowing greater power output or greater economy as desired.

The phenomenon of engine "knock" is described in detail in a standard reference work (Lewis and von Elbe 1961).

When a petrol/air mixture enters the engine cylinder, it is compressed by the piston and ignited by the sparking plug. During normal combustion the charge is consumed smoothly and progressively by the advancing flame front. Under certain conditions, those parts of the charge which are remote from the source of ignition (often referred to as "end gas") become overheated by radiation from the advancing flame front and through compression by the expanding gas behind it. The result is that the end gas becomes unstable, and detonates before the flame front can reach it to produce normal combustion. The shock waves from these detonations produce an audible metallic sound commonly referred to as "knocking". Detonation produces mechanical and heat stresses on the engine which reduce efficiency, and may in extreme cases result in early engine failure. Combustion of the

fuel without detonation is therefore necessary in order to achieve maximum efficiency. This is achieved by ensuring that the fuel is of an adequate quality, and the most effective means of accomplishing this is by the addition of a small amount of "antiknock" compound.

The phenomenon of "knock" was observed and studied almost from the inception of the spark ignition engine. The principal pioneers in this work were Hodgkinson and Ricardo in England and Kettering and Midgley in the U.S.A. These research workers discovered a relationship between "knock" and the molecular structure of the fuel components: aromatics or branched-chain structures were more resistant to "knock" than straight chain paraffins. However, it was impractical at that time to increase substantially the aromatic and branched-chain content in petrol by refining, and so a search was started for chemical compounds which, when added to petrol in small amounts, could increase its resistance to "knock". This search led eventually to the discovery (Midgley and Boyd 1922) of tetraethyllead (TEL). The cost-effectiveness of TEL so far exceeded that of all other "antiknock" agents investigated that it has been used commercially in petrol since 1923. Shortly afterwards, the closely related, but more volatile, tetramethyllead (TML) was found to be equally effective.

During combustion, lead oxides are formed which, if allowed to build up in the engine, reduce performance. Thus the need to add "scavengers" to convert this lead into volatile compounds was soon appreciated, and dichloroethane and dibromoethane were found to be most effective.

1.1.1 Manufacture of Teraalkyllead Compounds

The manufacturing processes for "antiknock" compounds (either in batch or continuous reactors) are virtually the same. TEL and TML are commonly manufactured by reaction, with lead-sodium alloy, of ethyl chloride (equation 1.1) and methyl chloride (equation 1.2) respectively:-

$$4NaPb + 4C_2H_5Cl \rightarrow (C_2H_5)_4Pb + 3Pb + 4NaCl \qquad 1.1$$

$$4NaPb + 4CH_3Cl \rightarrow (CH_3)_4Pb + 3Pb + 4NaCl \qquad 1.2$$

The TEL or TML is next separated by steam distillation and the metallic lead residue is refined in a furnace for re-use in the manufacturing process.

All operations involving the use of sodium are carried out under a blanket of nitrogen. Lead sodium alloy is prepared by mixing weighed quantities of molten lead and sodium (produced by electrolysis of molten salt in Down's multiple electrode cells) in a reaction pot. At the completion of the reaction the alloy is transferred through resistance-heated feed lines to a distribution pot. It is fed to a flaking machine which consists of a drum, cooled internally, rotating in a bath of molten alloy. The drum becomes covered with a film of solid alloy which is removed in the form of flakes by a stripping blade. The alloy is weighed into hoppers for transportation to the alkylation building.

The batch process for the production of TEL or TML is carried out in specially designed autoclaves which are housed in multi-storey buildings. In order to make use of a gravity flow for the product and residues, the reaction materials are transported to the top

floor, and from there the correct amount of alloy for either TEL or TML is discharged into the autoclave.

Ethyl chloride (to produce TEL) or methyl chloride plus a catalyst (to produce TML) is then added under carefully controlled conditions. Both reactions are strongly exothermic, the temperature of the autoclave being controlled both by water cooling of the jacket, and by the evaporation and reflux of ethyl chloride or methyl chloride. After the reaction, the excess alkyl chloride is vented off for recovery, and the autoclave contents are discharged into a steam-still for recovery of TEL or TML (toluene is always added during the manufacture of TML, and the product is always a TML/toluene mixture). Various "still aids" may be added to prevent conglomeration of solids and to aid removal of tetraalkyllead. These additives include sodium thiosulphate, surfactants and ferrous sulphate. All the excess alkyl chloride vented from the autoclave and distillation kettle is passed through a refrigeration unit and then condensed.

The TEL or TML is blended with the "scavengers" (either a mixture of dichloroethane and dibromoethane, or dibromoethane alone) to produce the range of "antiknock" compounds, which contain different proportions of lead alkyls. All types of "antiknock" compund are formulated to have the same lead content, namely 39.39% w/w Pb.

1.1.2 Effluent Treatment

The sludge remaining in the distillation kettle consists mainly of lead and sodium chloride. There will also be present some unreacted lead-sodium alloy, tetraalkylead and its decomposition

products, alkyl chlorides and the "still aids", all in intimate contact with the water. This sludge is discharged to holding pits, from where the lead is recovered for re-use in the manufacturing process. The remaining supernatant aqueous liquors form the major part of the liquid effluent problem.

The aqueous effluents in the sludge pit contain large amounts of inorganic lead. This lead can be in the form of elemental lead in suspension (3 moles of elemental lead produced per mole of tetraalkylead), or as divalent lead salts, both in solution and as insoluble lead hydroxide. These salts are formed either by the reaction of previously unreacted lead-sodium alloy with water, or by the action of extremely alkaline aqueous liquors on elemental lead to give the soluble plumbite ion:

$$Pb \rightarrow Pb^{2+} + 2e^- \qquad 1.3$$

$$Pb^{2+} + 2OH^- \rightarrow Pb(OH)_2 \qquad 1.4$$

$$\text{Excess alkali} \quad Pb(OH)_2 + OH^- \rightarrow HPbO_2^- + H_2O \qquad 1.5$$

Tetraalkyllead which was not removed during steam distillation forms the major insoluble organolead constituent of the effluent. Soluble organolead compounds are mainly the trialkyllead ion, although a small quantity of dialkyllead ion is also present. These ionic species can be formed as decomposition and disproportionation products in the steam distillation process, or by oxidation of tetraalkyllead compounds in the sludge pit itself:

$$R_4Pb + Cl_2 \rightarrow R_3PbCl + RCl \qquad 1.6$$

$$R_3PbCl + Cl_2 \rightarrow R_2PbCl_2 + RCl \qquad 1.7$$

In a recent study Graves and McArthey (A.O.C. internal report) suggest that sludge pit oxidation mechanisms are mainly responsible for the formation of these soluble organolead compounds.

The alkyllead salts are thermally unstable and will decompose at high temperatures through disproportionation reactions:

$$2R_3PbX \rightarrow R_4Pb + R_2PbX_2 \qquad 1.8$$

$$2R_2PbX_2 \rightarrow R_3PbX + (RPbX_3) \qquad 1.9$$

$$(RPbX_3) \rightarrow RX + PbX_2 \qquad 1.10$$

where X is an ionic species (frequently the chloride ion).

A second type of decomposition which results in the formation of hydrocarbons was also observed:

$$2R_3PbX \rightarrow R_4Pb + PbX_2 + R\text{-}R \qquad 1.11$$

$$R_2PbX_2 \rightarrow PbX_2 + R\text{-}R \qquad 1.12$$

It has been shown (Calingaert, Dykistra and Shapiro 1948) that under steam distillation conditions, both disproportionation and decomposition reactions occur in tri- and dialkyllead salts and these reactions have been proposed as a source of alkyllead salts in sludge pit effluent (Lill, A.O.C. internal report).

A typical composition of sludge pit effluent has been given (Lill, A.O.C. internal report) as follows:

Soluble inorganic lead	50 ppm
Insoluble inorganic lead	2000 ppm

Soluble organic lead	10 ppm
Insoluble organic lead	100 ppm
Sodium chloride	5-8% w/w
Sodium thiosulphate	0.5-1% w/w
Ferrous sulphate	200 ppm
pH	12

In the past, the sludge pit effluents have been treated by pH adjustment followed by settlement and/or filtration.

A typical flow scheme consists of primary settlement to remove elemental lead and insoluble lead salts followed by pH control to between 8.5 and 9.0 (at which lead salts have a minimum solubility). The precipitation occurs in a final settlement tank which removes the resultant solids from solution.

A well designed effluent treatment plant will be able to remove inorganic lead and insoluble organic lead compounds down to concentration levels of the order of several parts per million. However, these plants have little effect upon the levels of the soluble organolead compounds (tri and dialkyllead ions).

The treated effluent from such a plant would typically be:

Inorganic lead	2 ppm
Trialkyllead chloride	10 ppm
Dialkyllead chloride	0-1 ppm
Sodium chloride	50,000 ppm

Sodium thiosulphate	500 ppm

Plus minor components of effluent stream.

pH	8.5-9.0

The soluble organolead salts become the major source of lead in the treated effluent. The quantity of PbR_2^{2+} ions (< 1 ppm) is such that this species is not a serious problem, but the PbR_3^{+} ion is the most difficult to remove from the effluent.

1.1.3 Removal of Organolead Salts from Aqueous Solution

1.1.3.1 Cleavage of the lead to carbon bonds

Probably the simplest way of removing organolead salts from aqueous solution would be to oxidise them to some inorganic lead species which may then be easily removed from solution by precipitation. Several oxidising agents have been suggested to achieve this, such as chlorine, bromine, potassium permanganate, hydrogen peroxide or persulphuric acid (Levenspiel 1966; Lill, A.O.C. internal report; Shapiro and Frey 1968). At ambient temperatures most oxidising agents are ineffective unless used in large excess. Even in large excess, although reagents can oxidise trialkyllead ions to dialkyllead ions, few will further oxidise the dialkyllead species to inorganic lead, and even when this is possible, this step occurs so slowly as to be of no practical use.

Some studies have been conducted using chlorine at an aqueous phase temperature of 80°C (Lill, A.O.C. internal report). The alkyllead chloride concentrations can be reduced from 10 ppm to < 1 ppm in twenty minutes. However, the cost of heating large volumes of industrial effluent to 80°C from ambient, and then

having to cool it again before final discharge of the effluent stream, makes any high temperature process economically unacceptable. High temperature chlorine also poses severe corrosion problems.

Alternatively, one may make use of the reaction between organolead salts and ultraviolet light to produce the inorganic species. It was found (Lill, A.O.C. internal report) that to convert sufficient lead to the inorganic form, on an industrial scale, required long residence times (30 minutes). On an industrial scale this would require a large optical surface, and the power consumption to generate the ultraviolet light would be very high. There is also a high probability of the deposition of opaque films on the optical surfaces. Other industrially available ultraviolet processes generally work on very short residence times (up to one minute), and are not effective in conditions where fouling can occur. This process is therefore not applicable for organolead effluents.

In summary, the energy requirement for complete oxidation of trialkyllead chlorides to inorganic lead is much too great. Add to this the fact that they are present in very dilute solution, and it becomes apparent that the above disruptive processes are not economically viable.

1.1.3.2 Reduction methods

Several reactions have been discovered in which trialkyllead chloride in aqueous solution can be reduced to the corresponding water insoluble tetralkyllead or hexaalkyldilead compounds.

Metal borohydrides (in particular sodium borohydride) in proportionate quantities of 10-50% weight borohydride to the weight of dissolved lead, have been shown to reduce lead levels in solution to < 2 ppm at pH 8.0-9.5 (Lores and Moore 1973).

The following stoichiometry has been proposed:

$$8R_3Pb^+ + BH_4^- + 8OH^- \rightarrow 4H_2O + B(OH)_4^- + 4R_6Pb_2 \qquad 1.13$$

One mole of borohydride reduces 8 moles of trialkyllead ion in this mechanism. However, there is some evidence that further reduction to inorganic lead may take place:

$$R_3Pb^+ + BH_4^- \rightarrow R_3PbBH_4 \qquad 1.14$$

$$R_3PbBH_4 \rightarrow R_3PbH + BH_3 \qquad 1.15$$

$$R_3PbH + 2H_2O \rightarrow Pb + 3RH + 2OH^- \qquad 1.16$$

In this reaction 1 mole of borohydride reduces 1 mole of trialkyllead ion.

The reduced lead compounds can be seen as a fine white precipitate, which may be extracted from the effluent by filtration, sedimentation or solvent extraction.

A modification to this procedure involves the removal of the water insoluble lead compounds from the aqueous effluent by adsorption on activated carbon (Edmondson 1977). This activated carbon has a high capacity for adsorbing the water insoluble organolead compounds formed in these reactions, and provides a solid lead-containing product which can be handled readily and disposed of as such, by burning. Alternatively, the lead-containing

compounds can be removed from the carbon by extraction with a suitable solvent and the carbon then re-used.

Unfortunately, to ensure sufficient precipitation of the lead compounds, excess borohydride needs to be added, which, as well as being wasteful, is itself a pollution hazard since it is an extremely strong reducing agent. This excess could be destroyed by addition of a suitable oxidising agent, but the precipitate must be kept separate from such an agent to prevent the organolead compounds redissolving.

1.1.3.3 Chemical combination methods

The reaction of alkyllead chlorides in aqueous solution illustrates the ionic nature of the Pb-Cl bond. Alkyllead chlorides are highly ionised in solution:

$$R_3PbCl \rightleftharpoons R_3Pb^+ + Cl^- \qquad 1.17$$

$$R_2PbCl_2 \rightleftharpoons R_2PbCl^+ + Cl^- \rightleftharpoons R_2Pb^{2+} + Cl^- \qquad 1.18$$

The ionic nature of these compounds enables them to be used to prepare other organolead salts by metathesis reactions:

$$R_3PbCl + MY \rightarrow R_3PbY + MCl \qquad 1.19$$

$$R_2PbCl_2 + 2MY \rightarrow R_2PbY_2 + 2MCl \qquad 1.20$$

Thus if a trialkyllead salt could be found with a very low solubility in the aqueous phase, such a reaction could be used to precipitate the said trialkyllead salt from solution.

A precipitant comprising an alkali metal sulphide having at least one N-C-S group in the molecule (e.g. dialkyldithiocarbamates and related sulphur containing compounds) has been found to produce

insoluble trialkyllead salts. However, the resultant precipitates are so fine that conventional filtration and settlement techniques will not remove them from solution. This problem was overcome by using a precipitation/solvent extraction technique with the precipitate remaining dissolved in a hydrocarbon solvent phase (Edmondson 1975). The aqueous and organic phases are separated and the organic phase is treated to obtain the extracted lead compounds in a readily disposable form, either by evaporation of the solvent, or further reaction of the lead compounds therein with bromine to precipitate out the lead from the organic solvent. A modification to this procedure involves the removal of the water-insoluble compound from the precipitant treated aqueous effluent by their adsorption onto activated carbon, as described previously (Edmondson 1977).

Further complications are encountered however. In high concentrations of chloride ions, anionic chloride complexes are formed:

$$R_3Pb^+ + nCl^- \rightleftharpoons R_3PbCl_n^{1-n} \quad (n = 0,1,2) \qquad 1.21$$

$$R_2Pb^{2+} + nCl^- \rightleftharpoons R_2PbCl_n^{2-n} \quad (n = 0,1,2,3) \qquad 1.22$$

In the sludge pit effluent trialkyllead chlorides exist mainly in the form of the anionic chloro complex $R_3PbCl_2^-$ (equation 1.23), which being negatively charged, is not open to combination with other negative species. To overcome this, large excesses of reagent must be used in the aqueous phase to displace the equilibrium and encourage formation of the trialkyllead dithiocarbamate (equation 1.24):

$$R_3Pb^+ + 2Cl^- \rightleftharpoons [R_3PbCl_2]^- \qquad 1.23$$

$$R_3Pb^+ + Et_2NCSS^- \rightleftharpoons R_3PbEt_2NCSS \qquad 1.24$$

Diethyldithio carbamate — Trialkyllead diethyldithiocarbamate

As a result, problems arise from the possible toxic effects of adding large excesses of these sulphur containing compounds to the aqueous phase.

1.1.3.4 Foam separation

Surface active solutes may be removed by passing a stream of air bubbles through the solution. The solute will adsorb onto the air/liquid interface and be carried to the surface where it will form a foam, rich in solute. which may be removed (Sebba 1959; Levenspiel 1966).

Trialkyllead chlorides and dialkyllead dichlorides do not possess a high degree of surface activity. To be floated out of solution they must be chemically combined with a surface active agent, which has a high degree of selectivity for alkyllead ions (known as the collector), to form a surface active organolead product. In a similar way to precipitation reactions, collectors with negative charges will not be effective in removing the alkyllead ions if they exist primarily in the form of the anionic chloro complex. Tests on triethyllead chloride solution in the presence and absence of sodium chloride, with a wide range of surface active agents did not produce very promising results (Lill, A.O.C. internal report). This is probably due to the low selectivity of collectors in samples of synthetic effluent containing high

concentrations of chloride ions.

1.1.3.5 Adsorption methods

Tetraalkyllead compounds may be removed from petrol by adsorption onto several materials, including activated clays (Neef 1945) and silica gel (Jezl and Mills 1956). Organolead compounds adsorb onto glassware from both aqueous and organic solvent systems. This is a well-known laboratory phenomenon, requiring the deleading of glassware by washing with concentrated nitric acid. This information in itself suggests that organolead compounds have some affinity for silica containing compounds. The mechanism of attraction may be electrostatic, as all the siliceous material used have polar surfaces, and would therefore attract charged organolead ions or induce dipoles within the lead-carbon bonds. This adsorption mechanism would be expected to work well in non-polar solvents, but would not be nearly so successful in aqueous solutions where other polar species may interfere at the adsorption sites. Alternatively the lead-silica attraction may involve a more specific type of bonding. These materials have been combined together in other circumstances (e.g. manufacture of glassware). Furthermore, both elements are members of group IVb of the periodic table and silicon, like lead, can combine with carbon to form organosilicon compounds. These results are largely for covalent solvent systems, at relatively high lead concentrations for tetraalkyllead species, but under aqueous conditions with much lower concentrations of trialkyllead chloride, different mechanisms may be operating and the systems may not be as successful. Differences in the structures of tetraalkyllead and trialkyllead cations, tetrahedral and trigonal

planar respectively (Figure 1.1), mean that a material which can adsorb one compound may not remove the other due to steric effects.

Several studies have been conducted using ion exchange resins (Nozaki 1967; Lill, A.O.C. internal report; A.O.C. internal report 1970). Cationic resins will remove triethyllead cations from aqueous solution in the absence of sodium chloride (equation 1.25), but in the presence of high chloride ion concentrations triethyllead exists in solution mainly as the anionic complex $Et_3PbCl_2^-$ (equation 1.26):

$$\underset{\text{resin}}{-\,COO^-Na^+} + \underset{\text{solution}}{Et_3Pb^+} \rightleftharpoons \underset{\text{resin}}{-\,COO^-Et_3Pb^+} + \underset{\text{solution}}{Na^+} \qquad 1.25$$

$$Et_3Pb^+ + 2Cl^- \rightleftharpoons [Et_3PbCl_2]^- \qquad 1.26$$

Anionic resins, on the other hand, will remove triethyllead from solution in the presence of high concentrations of chloride ions (equation 1.27), but not otherwise.

$$\underset{\text{resin}}{-\,N^+Cl^-} + \underset{\text{solution}}{Et_3PbCl_2^-} \rightleftharpoons \underset{\text{resin}}{-\,N^+Et_3PbCl_2^-} + \underset{\text{solution}}{Cl^-} \qquad 1.27$$

The available literature shows, therefore, that alkyllead compounds may be adsorbed onto several materials in a variety of physical situations. It must then be decided whether any of these adsorbents are effective enough to be used on an industrial scale under the limited conditions of the effluent stream. Adsorption reactions generally have several inherent advantages in this particular situation if a suitable adsorbent can be found. Very low effluent concentrations may be achieved by adsorbents, and

Figure 1.1

(a) Tetraalkyllead

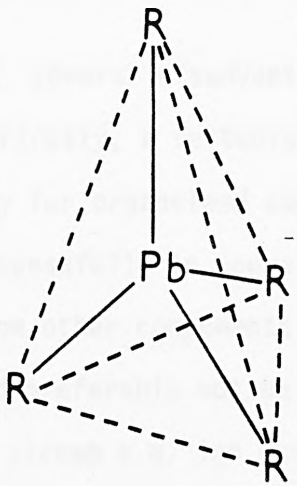

(b) Trialkyllead cation

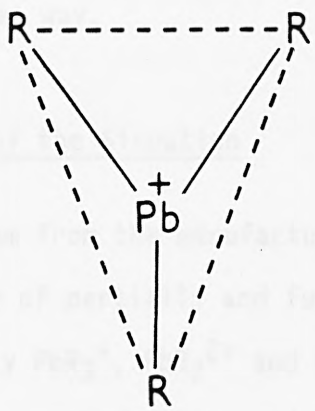

levels well below 1 ppm Pb in the final effluent are not impossible. Adsorption is a very common unit operation, which is fairly well understood. It is a "clean" process in the sense that nothing is added to the effluent which may cause a further pollution problem.

In this context, several disadvantages to an adsorption process are apparent. Firstly, a suitable adsorbent with a sufficiently high selectivity for organolead compounds must be found, which must operate successfully in industrial conditions without interference from other components in the effluent stream. An adsorbent should preferably not be dependent on external factors in the effluent stream e.g. ion exchange resins, and of course zeolites, are completely dependent on chloride ion concentration to operate successfully which is not a readily controlled effluent parameter. Adsorbents are generally expensive, and to be economically viable must either achieve a very high loading or be capable of regeneration. Furthermore, adsorption is not an absolute method of disposal, in that the organolead compound is not destroyed but exists on the adsorbent and must still be disposed of in some way.

1.1.4 Summary of the Situation

The effluent stream from the manufacture of lead tetraalkyls contains a variety of partially and fully oxidised lead ion species, especially PbR_3^+, PbR_2^{2+} and Pb^{2+}. The Pb^{2+} ions are readily removed by precipitation, and the quantity of PbR_2^{2+} ions (< 1 ppm) is such that this species is not a serious problem. The most difficult ion to remove from the effluent is PbR_3^+. Methods

have been developed to effect this removal, but problems of pollution from reagents used to remove lead, and the ever-rising costs of organic solvents, reagents and energy itself all render current methods less than ideal. A possible different approach, which is the subject of this research, is to use a suitable ion exchanger having also pronounced sorptive properties, which could further decrease the (already low) R_4Pb level within the effluent. Requirements for an ion exchanger to be useful in this context are that

(i) it should have a high exchange capacity;

(ii) exchange and sorption of lead should occur rapidly, so that effluent treatment times are minimised;

(iii) its selectivity for lead should be moderate (if recovery is required) or high (if no lead reclamation is contemplated);

(iv) the exchanger should be cheap (especially if recovery of lead is not contemplated);

(v) the exchanger itself should not be a harmful pollutant.

It should be possible to meet all requirements by the choice of a suitable zeolite. This thesis describes some initial studies on the exchange and adsorption of lead and organolead species on zeolites.

CHAPTER 2 - ZEOLITES

The first practical use of zeolites probably occurred about 2000 years ago when natural zeolite rock was quarried for use as building stone (Mumpton 1977), although it was not until the discovery of stilbite in 1756 that zeolites were first recognised as a new group of minerals consisting of hydrated aluminosilicates of the alkali and alkaline earth metals (Cronstedt 1756). The first physico-chemical property of zeolites which had an application (reversible cation exchange) was investigated over 100 years ago (Eichhorn 1858). This led to the development of synthetic, amorphous aluminosilicates as commercial cation exchange materials (permutites) in the early 20th century (Shreve 1930). These materials were used primarily in water softening.

The advent of the polymeric organic resin exchangers rendered all previously used inorganic exchangers obsolete for many commercial ion exchange processes, for two main reasons. Firstly, the organic resins were much more resistant to attack in acid or alkaline solution than were either zeolites or permutites, and secondly, their more open structure meant that very rapid exchange of ions could be effected. Thus using the organic resins, a rapid exchange could be coupled with a rapid "through-put" of solution in an ion exchange column.

Syntheses of so-called "zeolites" have been reported since the middle of the 19th century (Morey and Ingerson 1937), but few of these reports can be substantiated due to lack of essential data for identification. During the 1950's and 1960's, zeolites of high chemical purity and completely regular crystal structures

were synthesized (Manson and Sheppard 1974). Of these, zeolite A (which has no known natural analogue), zeolites X, Y (which are analogues of faujasite) and Zeolon (which is an analogue of natural mordenite) are readily available commercially (Sand 1967; Flanigen 1980). More recently, with the development of very high silica porous tectosilicates, in which the content of framework aluminium can be so low as to be no more than a trace impurity, molecular sieves have become available which have lost much of their polar character (Mobil Co. 1971; Argauer and Landolt 1972; Kokotailo and Meier 1979). These materials, the ZSM series, represent a significant departure from earlier zeolites in their properties, and it has been proposed that they be named "2nd generation zeolites" (Flanigen 1980). A pure silica analogue, silicalite, has been claimed (Flanigen and Bennett 1978) and because this series of structures is so closely related (characterised by a very high number of 5-rings) a single generic name, Pentasil, has been proposed to encompass all the series members (Kokatailo and Meier 1979).

As early as 1840 it was observed that crystals of zeolites could be reversibily dehydrated without any apparent change in morphology (Damour 1840). Dehydrated chabazite crystals were observed to adsorb rapidly the vapours of water, methyl alcohol, ethyl alcohol and formic acid; however, when exposed to acetone, ether or benzene, essentially no adsorption occurred (Wiegel and Steinhoff 1925). McBain (1932) deduced from these observations that the pore openings in chabazite crystals must be less than 5 $\mathring{A}$ in diameter (see note at bottom of page), and he originated the term "molecular sieve" to define porous solid materials which

NB $1\mathring{A} = 10^{-1}$ nm throughout this thesis

exhibit the property of acting as sieves on a molecular scale. The use of zeolites as molecular sieves has grown enormously, the shapes and sizes of various molecules being the criteria of exclusion. Alteration of the molecular sieving character of a zeolite by means of exchanging the cations originally in the zeolite for cations of different ionic radii is a well-known technique for "tailoring" basic types to perform different separations. For example, zeolite 4A (the sodium form with 8-oxygen window aperture dimensions of 4Å) will not adsorb propane, but if the Na^+ ions are replaced by Ca^{2+} ions to give zeolite 5A then propane is adsorbed (Breck 1956). Similarly, exchanging Na^+ ions by K^+ ions, in zeolite 4A, gives zeolite 3A with a significantly reduced size of the 8-oxygen window aperture. This form precludes essentially any oxygen adsorption (Breck 1956). More recently, separations have been shown to be possible by using combinations of different ions (Takaishi, Yatsurgi, Yusa and Kuratomi 1975). For example, it is in principle possible to use zeolite A with a Zn^{2+} fraction of 0.6 and K^+ of 0.4 to separate trans-but-2-ene and cis-but-2-ene, the kinetic diameters of which are 4.5 and 4.8 Å respectively. The material is referred to as "4.5" A, implying a zeolite molecular sieve with an apparent pore size between 4A and 5A. It would appear that further "fine tuning" of this type may be practical to achieve other separations.

Another area of great significance began to attract attention in the 1960's and has resulted in a major burst of activity, particularly in the petroleum industry. Zeolite-based catalysts became important when it was discovered that rare earth and hydrogen forms of certain zeolites possessed a cracking activity

which was several orders of magnitude greater than that formed with conventional silica-alumina catalysts. The performance of cracking catalysts based on zeolite Y (first introduced by the Mobil Company in 1962) won them rapid recognition. They gave less coking, increased production capacity, and improved gasoline yields by as much as 25%.

Ion exchange often forms the first stage in catalyst preparations, but the nature of the zeolite itself plays an essential part in catalytic activity by providing reactions sites and a shape-selective substrate. In hydrogen-zeolites it is believed that Brønsted acid centres are formed (Venuto and Landis 1968):

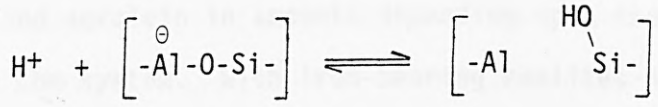

By proton transfer from these acid centres the formation of carbonium ions can result, and these reactive intermediates can be involved in polymerization, isomerization and cracking. Since these acid centres occur throughout the body of the zeolite, its molecular sieving and catalytic functions can be harnessed simultaneously. Thus, in catalysts based upon erionite or zeolite A, n-paraffins can enter the crystals and reach intracrystalline acid sites, but not branched chain hydrocarbons, cycloparaffins (naphthenates) or aromatics. The n-paraffins can therefore be selectively cracked while the other hydrocarbons are relatively unchanged (Weisz and Frilette 1960). Zeolite-based isomerization catalysis and molecular sieving can also be combined, using zeolite Y in the isomerization reactors and zeolite CaA in the subsequent units, which filter out unchanged n-paraffins (Barrer 1978(a)). The n-paraffins may then be desorbed and returned to

the reactant stream. In this way virtually complete isomerization of raffinates to branched chain paraffins, cycloparaffins and aromatics can be envisaged, with improved antiknock properties even without the addition of tetraalkyl lead.

Catalytic selectivity for molecules of particular shapes has been demonstrated for mixtures other than those referred to above (Weisz, Frilette, Maatman and Mower 1962; Chen and Weisz 1967).

Synthetic zeolites containing transition metal ions are active for oxidation of H_2, CO, C_2H_4 and NH_3 (Minachev and Isakov 1973). With oxygen and Cr- or Ag- bearing zeolites, ammonia yielded N_2O and N_2; with Cu(II)Y propylene gave 2-propanol, acetaldehyde, acetone and acrolein in amounts depending upon the quantity of water in the system. With iron-bearing zeolites A, X or Y, mixtures of propylene, ammonia and oxygen yielded CH_2=CH-CN and water. In Ni- and Pd- faujasites benzene underwent hydrodimerization to phenylcyclohexane. The addition of lead to nickel containing zeolite Y (Davidova, Valcheva and Shapov 1981) and high silica zeolites (Cha and Kaeding 1983) as petrochemical catalysts has been shown to improve their performance. These examples are a small selection of the many reactions effected with zeolite-based catalysts (Venuto and Landis 1968; Turkevich and Ono 1969; Venuto 1971; Penchev, Davidova, Kanazirev, Minchev and Neinska 1973). The examples do however serve to indicate their versatility.

For large scale removal of pollutants from river effluents the high cost of organic resins renders them at a disadvantage to many natural or synthetic zeolites. Thus, much work has been published on the use of zeolites (particularly clinoptilolite) to remove

from effluents ammonia and ammonium ions, which are not only toxic to fish and other forms of aquatic life, but also contribute to the rapid growth of algae, leading in turn to eutrophic conditions in lakes and rivers (Mercer and Ames 1970; Stamberg, Bishop and Kumke 1972; Johnson and Sieburth 1974; Joergensen, Libor, Graber and Barkacs 1976). Due to this severe problem, local and national environmental protection agencies have limited the amount of nitrogen that is permissible in municipal and industrial waste effluents to only 1 ppm (Mumpton 1976). Zeolites, and especially clinoptilolite, are now being used as anti-pollutants, employing several designs (Mumpton 1976; Sato, Mikio and Fukagawa 1976; Liberti, Boari, and Passino 1979; Liberti and Boari 1981). For example, Semmens carried out studies in which NH_4^+-saturated clinoptilolite is regenerated with sodium nitrate brine (Semmens 1980). As NH_4^+ ions are released they are oxidised by nitrifying bacteria, the overall process yielding sodium clinoptilolite, sodium nitrate, water and carbon dioxide.

Another cause of eutrophic conditions in freshwater lakes is phosphate ions, arising from fertilizer washed off the land, or from polyphosphate salts which are mixed with detergents in order to soften water during the washing process. Statutory pressures have caused detergent manufacturers to seek replacements for polyphosphate salts, and zeolites have been indicated as being a particularly suitable substitute (Schwuger and Smolka 1976; Schwuger and Smolka 1977; Kurzendorfer, Schwuger and Smolka 1979). For ideal detergent performance this "builder" must lower (in the presence of very large excess concentrations of Na^+ ions) the amount of free Ca^{2+} and Mg^{2+} ions by sequestering (e.g. sodium tripolyphosphate) or by ion exchange (e.g. NaX). Final Ca^{2+} and

Mg^{2+} ion concentrations of less than 10^{-5} mol dm^{-3} and 10^{-4} mol dm^{-3} respectively are required. Although NaA is known to be very effective for removal of Ca^{2+} ions, it is not effective for the removal of Mg^{2+} ions, particularly at ambient temperature, due to the slow rate of exchange. In contrast, magnesium exchanges rapidly into NaX. A combination of the two zeolites is claimed to produce a synergistic effect: zeolite A is more effective in removing Ca^{2+} ions and zeolite X more effective in the removal of Mg^{2+} ions (Breck 1980; Kuhl and Sherry 1980).

Zeolites, being resistant to severe levels of ionizing radiation and relatively high temperatures, offer significant advantages over organic resins in some radiochemical applications. One of the earliest applications of zeolites in ion exchange was the removal by clinoptilolite of caesium-137 (^{137}Cs) and strontium-90 (^{90}Sr) out of low level waste streams from nuclear installations (Ames 1959; Ames 1960). The ions can be extracted with high efficiency from the effluent and either stored indefinitely in the zeolite, or removed by elution for subsequent purification and recovery. The zeolites investigated and used in this respect include chabazite, clinoptilolite, synethetic mordenite and Linde AW-500 (Mercer and Schmidt 1965; Breck 1980). ^{85}Kr encapsulation ($t_{\frac{1}{2}}$ = 10.7 years) in zeolite materials such as sodalite has also been studied (Foster, Pence and Staples 1974; Bendixen and Knecht 1976), and leakage has been demonstrated to be very low. Selective adsorption of $^{14}CO_2$ ($t_{\frac{1}{2}}$ = 5760 years) by zeolite 5A has been shown to be possible, with susequent desorption and recovery as $CaCO_3$ after scrubbing with a lime slurry (Brown 1976). The solid $CaCO_3$ is packaged for storage in metal containers. One method for the separation and retention of gaseous ^{129}I

($t_{\frac{1}{2}}$ = 1.6 x 10^6 years) is based upon the use of silver-loaded adsorbents such as AgX. Regeneration of the ^{129}I loaded AgX by passing H_2 over the material produces HI, which can be chemisorbed onto PbX. The spent PbX is sent for solid waste disposal and the expensive AgX is re-used (Maeck, Pence and Keller 1968; Donner and Tamberg 1972).

Zeolites exchanged with the nutrient ions NH_4^+ and K^+ can be added to soils as ionic type fertilizers, where the nutrient ions are released gradually over a long period of time. In addition to carrying the primary nutrients (K and N), micronutrients such as iron, copper, manganese and zinc can be supplied by the zeolite. For soil application, relatively impure natural zeolites may have an application, since costs must be kept low. Additionally, the zeolite may function as soil conditioners, improving its physical properties. In Japan, clinoptilolite added to soils greatly improved the growth and yield of farm crops (Torii 1978). The assumption was made that the enhancement effect is due to adsorption and retention of ammonia-nitrogen and potassium, or better maintenance of water content, and the prevention of root decay.

Zeolite minerals in Japan, in particular clinoptilolite and mordenite, have been added to the diets of pigs, chickens and ruminants (Mumpton and Fishman 1977). Significant increases in gain of body weight per unit of feed were achieved, particularly in chickens, and there was claimed to be a general improvement in the well-being of the animals. There is no quantitative evidence to show how these improvements are brought about beyond such observations as reduced ammonia levels in portal blood (Pond, Yen and Hill 1981) and increased calcium uptake (Cool and Willard

1982). In the feeding of ruminants, zeolites may be introduced into the rumen prior to the feeding of non-protein nitrogen - N.P.N. (e.g. urea), so that NH_4^+ levels are partially reduced by cation exchange, and then subsequently released by Na^+ and K^+ ions which enter the rumen in the saliva.

The high ion exchange and adsorption capacities of zeolites give them many other actual or potential applications, such as in malodour control, carriers of herbicides and pesticides, artifical kidney dialysate regeneration, beverage carbonation, flame extinguishers, isotopic enrichment and even weather modification (Breck 1980).

With zeolites finding many new applications in the field of ion exchange, detailed knowledge of the kinetics and thermodynamics of exchange for a variety of metal ions in various zeolites is obviously desirable, and for many systems such studies have already been carried out. This is partly because their regular crystalline structure and framework rigidity make them useful, relatively simple, model systems from which the principles governing exchange processes can be elucidated, and partly because ion exchange is frequently involved in the preparation of zeolites for use as molecular sieves and catalysts. Initially, the studies largely concentrated on exchange processes involving the alkali and alkaline earth cations (Sherry 1975), though there is much interest in noble (Fletcher and Townsend 1983) and transition metal ion exchanged zeolites as potential catalysts (Gal, Jankovic, Malcic, Radovanov and Todorovic 1971; Gal and Radovanov 1975; Maes and Cremers 1975; Barrer and Townsend 1976(a) and (b); Fletcher and Townsend 1980(a); Fletcher and Townsend 1981). The potential uses of zeolites as ion exchangers to selectively

separate and recover metals from industrial effluents and in the recovery of precious and semi-precious metals is obviously of great significance.

In recent years the need to control the heavy metal content of wastewaters has caused increasing concern. Where polluting metals are present in high concentrations, oxidation, reduction and precipitation processes may be used effectively. However, recovery is more difficult when the offending metals are found in low concentrations and yet in the presence of high concentrations of other salts. In these cases, procedures such as solvent extraction and ion exchange may be preferred (Edmondson 1975; Edmondson 1977). Studies on zeolites for this purpose have been very limited so far. The affinity of clinoptilolite for certain heavy metals (lead, silver, cadmium, zinc and copper) was identified by Chelishchev and co-workers (1974), in which they observed a selectivity sequence of $Pb^{2+} > Ag^{+} > Cd^{2+}$, Zn^{2+}, $Cu^{2+} > Na^{+}$. This work was extended to include mercury and thallium (Filizova 1974), and it was reported that thallium, mercury and silver (as well as caesium) all caused recrystallisation and breakdown of the original clinoptilolite structure. Their examination of silver exchange was contrary to the conclusions of Chelishchev and co-workers (Chelishchev, Martynova, Fakina and Berenshtein 1974; Chelishchev, Berenshtein and Martynova 1975). Studies by Semmens and co-workers on clinoptilolite have indicated very high selectivities for Ba^{2+} and Pb^{2+}, and somewhat lower selectivities for Cu^{2+}, Zn^{2+} and Cd^{2+} (Semmens and Seyfarth 1978), whilst a selectivity sequence of $Pb^{2+} > Ag^{2+} > Cd^{2+}$ was noted in which competing cations (Ca^{2+}, Mg^{2+} and Na^{+}) influenced removal of these metals, particularly Cd^{2+} (Semmens and Martin 1979).

Semmens has commented upon the possibility of hydroxide precipitation within the channels and at the surface of the zeolite due to the high internal pH of these zeolites combined with the high internal metal concentrations (Semmens 1981).

Examinations of analcite (Barrer and Hinds 1953) and chabazite (Barrer, Davies and Rees 1969(a)) have demonstrated that these ion exchangers show a high preference for Pb^{2+} over Na^{+} ions. Barrer and Hinds (1953) proposed a mechanism to account for over-exchange of lead in analcite in which it was suggested that lead entered the crystal as the univalent complex $PbOH^{+}$.

Zeolite A, which for some time has been recognised as a useful replacement "builder" for STPP in detergents, could subsequently influence metal removal during the primary sedimentation stage of sewage treatment, thus the behaviour of this material has been studied by many workers. In their investigation of the exchange of Cd^{2+}, Zn^{2+}, Co^{2+} and Ni^{2+} ions in NaA, Gal and co-workers showed that the standard free energy of exchange ($\Delta G^{\ominus}$) increased with decrease in size of the hydrated divalent cations (Gal, Jankovic, Malcic, Radovanov and Todorovic 1971). Hertzenberg and Sherry (1980) used these data and extended the work to demonstrate that the selectivity of NaA for Cd^{2+} as a function of co-anion was $NO^{-} > CH_3COO^{-} > Cl^{-}$. However, on repeating the studies of Gal and co-workers (1971), Hertzenberg and Sherry (1980) showed that NaA exhibited a higher selectivity for Cd^{2+} in the Cl^{-} system (-6.86 kJ/equiv. compared with -4.56 kJ/equiv.), which modified the selectivity sequence to $NO^{-} > CH_3COO^{-} \sim Cl^{-}$. The difference in selectivities was suggested by Hertzenberg and Sherry (1980) to be related to the difference in batches of zeolites and has been commented upon elsewhere for Ca^{2+} exchange with NaA (Wiers, Grosse

and Cilley 1982). The ion exchange of heavy metal ions with a mixed Ca^{2+}/Na^{+} zeolite A (which is the form of the material one might expect to encounter in the environment) as a function of various parameters produced the following selectivity sequence (Schwuger, Smolka and Kurzendorfer 1976):

$$Pb^{2+} > Ag^{+} > Cu^{2+} >> Cd^{2+} > Zn^{2+} >> Co^{2+}, Ni^{2+}, Mn^{2+}$$

To estimate the impact of Ca^{2+}-charged zeolite A on the removal of heavy metals from sewage, laboratory simulations of the activated sludge process have been carried out. These indicated that whilst the order of selectivity was similar to that of Schwuger and co-workers (1976) the zeolite did not significantly affect the concentrations of the metals (Stoveland, Lester and Perry 1980). Removal of some of the metals by this zeolite was in fact less than in the presence of STPP, and under conditions of "shock loading" (to simulate the effect of a "wash day") the improvement in metal removal which had been observed with STPP was not observed when zeolite A was added under similar conditions.

The ion exchange behaviour and hydrolysis rate of CaA were studied in a variety of artificial and natural water samples (Allen, Cho and Neubecker 1983). The selectivity series $Pb^{2+} >> Cd^{2+} > Zn^{2+} > Cu^{2+} >> Ni^{2+}$ was said to be in general agreement with that of Schwuger and co-workers (1976). Generally, exchange in natural waters was similar to or less than that in artificial water, though selectivity for Cd^{2+} was markedly lower in the natural waters used (i.e. in natural water the sequence was $Pb^{2+} > Zn^{2+} > Cu^{2+} > Cd^{2+} > Ni^{2+}$). This is probably because of the relatively high affinity of these metals for soluble organic and inorganic complexing materials in natural waters. Such discrepancies have

been noted elsewhere (Obeng, Carrondo, Perry and Lester 1981; Rossin, Perry and Lester 1982). Zeolite A hydrolysed extensively in natural waters, with a typical half-life of 1-2 months. The rate was accelerated at low pH and retarded by high concentration of hydrolysis products.

A specific method for the removal of heavy metal ion impurities has been described (Gradl, Schimmel and Krause 1983) in which a wet process phosphoric acid containing 16 ppm Cd^{2+}, 33 ppm Cu^{2+}, 0.1 ppm Pb^{2+} and 0.005 ppm Hg^{+} was brought into contact with a sample of zeolite A onto which a thioester had previously been adsorbed. The subsequent filtrate contained < 1 ppm Cd^{2+}, < 1 ppm Cu^{2+}, < 0.005 ppm Pb^{2+} and < 0.001 ppm Hg^{+}. Equilibrium isotherm data for CaA exchange with Pb^{2+}, Cd^{2+} and Cu^{2+} gave a selectivity sequence of $Pb^{2+} > Cd^{2+} > Cu^{2+}$ (Wiers, Grosse and Cilley 1982). Near-stoichiometric exchange was observed in the case of Pb^{2+} and Cd^{2+}, whereas over-exchange has been observed elsewhere for the same exchanges in NaA (Hertzenberg and Sherry 1980; McCusker and Seff 1982; Ronay and Seff 1984). Hertzenberg and Sherry (1980) accounted for this in terms of the presence of small amounts of excess aluminium occluded in the sodalite cages, whilst McCusker and Seff (1982) thought the partial preference of the zeolite framework for the monopositive ion $CdOH^{+}$, present in the somewhat acidic $CdCl_2$ exchange solution could explain the observed over-exchange; the monopositive $CdOH^{+}$ ion was considered to more evenly balance the local anionic charge of the zeolite framework. These workers also observed over-exchange of NaA in a relatively neutral cadmium acetate/cadmium hydroxide solution. Wiers et al (1982) surmised that by virtue of the alkaline pH developed in NaA slurries, exchange of hydrolysed lead and cadmium cations occurs

(field-induced precipitation), whereas Pb^{2+} and Cd^{2+} ions exist predominantly under the conditions of their work. However, by the use of a flow through technique (Ronay and Seff 1982), it was shown that over-exchange with NaA still occurred when only Pb^{2+} cations were present. Although a somewhat greater uptake of Pb^{2+} from aqueous nitrate than from aqueous acetate was reported by Hertzenberg and Sherry (1980), using batch-method equilibrium experiments, Ronay and Seff (1984) found the capacity of NaA for Pb^{2+} to be much greater from aqueous acetate solution. They observed 9 lead ions per unit cell (a 50% over-exchange) which they suggested was due to increased cation hydrolysis at the higher pH of acetate solutions, compared to nitrate (pH6 and pH4.3 respectively).

In their study of Ca^{2+} exchange in NaA, Wiers, Grosse and Cilley (1982) revealed shortages in the total concentration of exchangeable ions as compared with Al^{3+} recoveries. This was attributed to the proton-exchange effect and is of importance not only in the understanding of possible environmental water effects on zeolite A, but also in the thermodynamic treatment of isotherm data.

Extreme conditions of ion exchange (such as for instance highly concentrated solutions, high temperatures or long exchange periods) which are necessary for the production of highly exchanged alkaline earth forms of zeolite A have been shown to cause destruction of crystals (Lutz, Fahlke, Lohse, Bulow and Richter-Mendau 1983). Reduced stability of zeolite A crystals in the presence of alkaline earth ions was reported to be due to hydrolysis of crystal lattice by the influence of protons whose concentration is increased beyond the dissociation equilibrium of

water owing to the formation of weakly dissociated alkaline earth ion hydroxides. Zeolite NaMgA was structurally degraded much more than NaCaA because of the smaller solubility of magnesium hydroxide.

The studies of Cook, Cilley, Savitsky and Wiers (1982) on NaA hydrolysis and degradation indicated that on addition of cations with higher binding affinities, such as Ca^{2+} or Pb^{2+} the rate of extent of proton exchange was reduced. Their results were explained on the basis of an incongruent dissolution mechanism that is initiated by proton exchange and is then followed by silicic acid release yielding possibly a mixture of gibbsite, $Al_2O_3.3H_2O$, and halloysite, $Al_2Si_2O_5(OH)_4$. Under the alkaline conditions developed by NaA slurries a tentative mechanism has been proposed in which the hydrolysis process is auto-catalytic with further release of H^+ continuing the reaction (Drummond, De Jonge and Rees 1983). The rate of hydrolysis eventually decreased due to the apparent stability of H-A.

The use of ion exchange processes involving zeolites X and Y have, in the main, been with their use as catalysts in view, as mentioned previously. Investigations into their use as agents for the removal of metals from wastewater has received very little attention but their potential use is obvious (Gal and Radovanov 1975; Maes and Cremers 1975; Fletcher and Townsend 1980(a); Fletcher and Townsend 1981).

In studies of the ion exchange of Cu^{2+} ions with NaX and NaY evidence has been given for the presence of surface hydroxylated species (Schoonheydt and Velghe 1976; Dyer and Barri 1977), a conclusion in accord with the comments of Semmens (1981).

Deterioration of the ability of a zeolite to function satisfactorily as an ion exchanger is most often indicated by a decrease in the exchange capacity. The problems of acid attack and accompanying aluminium extraction are probably the most common hazard encountered in exchange studies, and these phenomena must be considered whenever appreciable hydronium ion exchange may take place. Hydronium ion exchange can occur quite unintentionally, especially in solutions of acidic salts. In fact, a high degree of exchange (about 20%) for sodium ions can occur by prolonged washing of NaX with distilled water (Bolton 1971). Ion exchange of NaX and NaY with Co^{2+}, Zn^{2+} and Ni^{2+} was shown, long ago, to be non-stoichiometric at low bivalent ion occupancy, the hydrolytic sodium loss being about twice as large for NaX ($\sim$5Na^{+} ions lost per unit cell) as for NaY, the effect being more pronounced at high temperature (Maes and Cremers 1973). Proof that awareness on the part of authors is increasing is evidenced by the fact that they are more frequently indicating the importance of hydrogen-ion exchange in the preparation and use of many of the so-called metal-cation forms of zeolites (Bolton 1971).

Many ion exchange complexes of layer silicates of the clay minerals group have been prepared, in which organic ions have replaced the exchangeable metallic cations, and there have been detailed studies of their properties (Marshall 1964; Barrer 1964). On the other hand there have been relatively few investigations of exchange involving organic cations in the crystalline zeolites. Barrer, Buser and Grutter (1956) measured extents of exchange in Linde Sieve X from 2N or 1N solution of various methyl- and ethylammonium halides and ammonium chloride. They established an ion sieve exclusion of $(C_2H_5)_4N^{+}$, while the methylammonium cations

showed extents of exchange which decreased as the number of methyl groups increased. Barrer and Meier (1958; 1959) extended this work to Linde Sieve A, for the ions $CH_3(CH_2)_xNH_3^+$ where x = 0,1,2,3 and 5, and also to $CH_3(CH_2)_4CH(CH_3)NH_3^+$, $(CH_3)_3NH$, $(CH_3)_4N^+$ and $(C_2H_5)_4N^+$. Ion-sieve exclusion was demonstrated for the last two cations, and a steric effect which was not of an ion sieve character was also established. Thus, the larger organic cations fill the intracrystalline volume before 100% exchange, so that complete exchange is then impossible. Kinetic and equilibrium studies have also been made of exchanges of alkylammonium ions with Na-clinoptilolite (Barrer, Papadopoulos and Rees 1967). $(CH_3)_4N^+$ and $(C_4H_9)_4N^+$ ions were excluded from the channel system in clinoptilolite by an ion-sieve action, but NH_4^+, $CH_3NH_3^+$, $(CH_3)_2NH_2^+$, $(C_2H_5)NH_3^+$ and $nC_3H_7NH_3^+$ replaced all the Na^+, while the $(CH_3)_3NH^+$, iso-$C_3H_7NH_3^+$ and $nC_4H_9NH_3^+$ only partial exchange occurred due to steric effects. The work of Barrer, Buser and Grutter (1956) was repeated and extended, at a lower solution total normality (0.05g equiv. dm^{-3}), for the exchange and adsorption of NH_4^+, $CH_3NH_3^+$, $C_2H_5NH_3^+$, $nC_3H_7NH_3^+$, iso-$C_3H_7NH_3^+$, $nC_4H_9NH_3^+$, $(CH_3)_2NH_2^+$, $(C_2H_5)_2NH_2^+$, $(CH_3)_3NH^+$ and $(C_2H_5)_3NH^+$ on Linde Sieves X and Y (Theng, Vansant and Uytterhoeven 1968). For steric reasons, none of these ions could effect a complete replacement of the Na^+ ions initially present in the zeolite, so the exchange reaction was confined to the large cavities in the crystal. The maximum extent of exchange decreased with an increase in molecular weight and polarizability of the cations, but was always below the limit imposed by the space requirement of the respective ions. This decrease was also greater for the di- and trialkyl derivatives than for monoalkylammonium ions of comparable weight, and was more pronounced in X than in Y. These observations have been

interpreted in terms of the increased difficulty of packing the larger and more branched species in the spherical large cavities of the crystal, and in terms of the affinities of the organic ions for the zeolite.

A patent has been published which describes a procedure for the removal of tetraalkyllead impurities (tetramethyl-, tetraethyl-, trimethylethyl-, dimethyldiethyl-, etc.) from liquid hydrocarbons, in order to prevent poisoning of cracking catalysts (Audeh 1978). The method involves contacting liquid hydrocarbons with a suitable sorbent (i.e. an amorphous or crystalline material such as zeolites X, Y, mordenite, ZK4 or ZSM5) which act as carriers for anhydrous hydrogen chloride. A displacement reaction with the tetraalkyllead compounds occurs (equation 2.1) to form a gaseous product, RH, and the resulting insoluble alkyllead salt, R_3PbCl, remains on the sorption material:

$$R_4Pb + HCl \rightarrow RH + R_3PbCl \qquad 2.1$$

Studies have demonstrated that a naphtha starting material, doped with 75 ppm alkyllead, after contact with the sorbent HCl/NaX, contains less than 5 ppb alkyllead impurities. Regeneration of the sorption materials was also possible.

2.1 STRUCTURE OF ZEOLITES

Zeolites are porous, crystalline aluminosilicates made up of SiO_4 and AlO_4 tetrahedra arranged in a three dimensional framework structure through shared oxygen atoms. Within the structure are cavities which are occupied by cations and water molecules, both of which have considerable freedom of movement.

The isomorphous substitution of Al^{3+} for Si^{4+} within the framework leads to a charge deficiency of -1, which results in an overall delocalised negative charge throughout the framework. To maintain electroneutrality the presence of an appropriate cation (normally alkali metal or alkaline earth metal) is required. It is these exchangeable cations which result in the ion exchange properties of zeolites. The number of charged sites is limited in accordance with Loewenstein's rule (Loewenstein 1954) which states that AlO_4-tetrahedra are not linked directly to other AlO_4-tetrahedra, so that when SiO_2/AlO_4 = 1 Si and Al alternate upon the tetrahedral sites, giving ordered frameworks.

Zeolites may be represented by the empirical formula (Breck 1973(a)):

$$M_{2/n}O.Al_2O_3.xSiO_2.\ yH_2O$$

where n is the valence of cation M, and x is equal to or greater than two.

The crystalline struture of zeolites enables one to express their composition using a unit cell formula (Breck 1973(a)):

$$M_{x/n}\ [(AlO_2)_x\ .\ (SiO_2)_y]\ .\ wH_2O$$

where M is an exchangeable cation (valance n), w is the number of water molecules and the ratio y/x usually has values of 1-5 depending upon the structure. The sum (x+y) is the total number of tetrahedra in the unit cell. The portion in square brackets represents the framework composition.

Zeolites are so diverse that secondary structural units, based on small groupings of linked tetrahedra, are needed to describe and

systematise their structures. Meier proposed the secondary building units (SBU's) shown in Figure 2.1 as the smallest number of such units from which then known zeolite structures could be built (Meier 1967). In the SBU's shown the Al or Si atoms are present at each corner or termination. The oxygens are not shown; they are located near the mid-points of the lines joining each pair of T atoms (Si or Al). In some cases, the zeolite framework can be considered conveniently in terms of the polyhedral units which are shown in Figure 2.2. These are cage-like units designated by Greek letters : α, ß, γ, etc. The α cage refers to the largest unit - the truncated cuboctrahedron.

In the classification used by Breck zeolites are categorised in terms of the SBU's that comprise the framework (Breck 1973(b)). However, ways of formulating zeolite framework structures have been developed, involving structural units of greater complexity than the SBU's (Barrer 1982).

2.2 CATION SITINGS IN ZEOLITES

Zeolite frameworks usually provide more than one kind of site for the exchangeable cations. The number of electrochemical equivalents of cations needed to balance the anionic framework charge may also be considerably less than the total number of available cation sites. Thus when the cations distribute themselves among the sites so as to minimise the overall free energy of the system there may be partial occupancy of some or all of the types of sites available. Factors which decide the cation distribution pattern within the framework are complex, and involve properties of the cationic species such as valency, ionic radius, hydration energy, electronic stucture, as well as properties of

Figure 2.1 Secondary Building Units (SBU's)

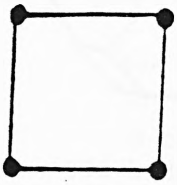

S4R

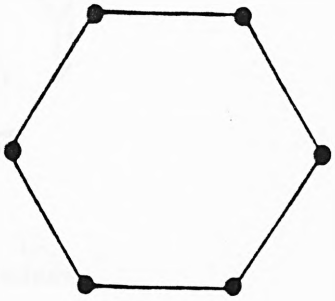

S6R

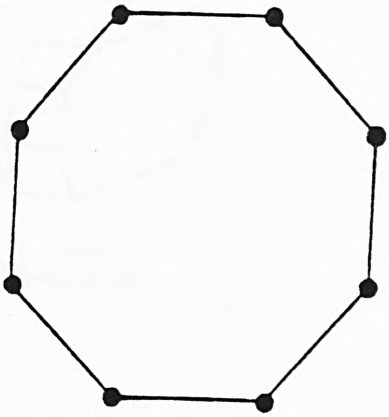

S8R

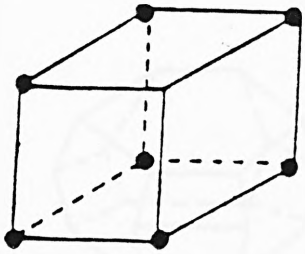

D4R

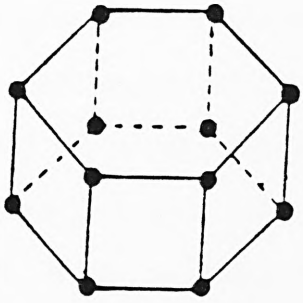

D6R

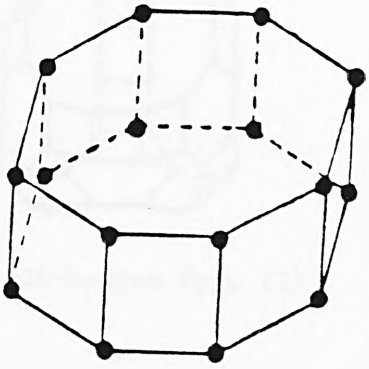

D8R

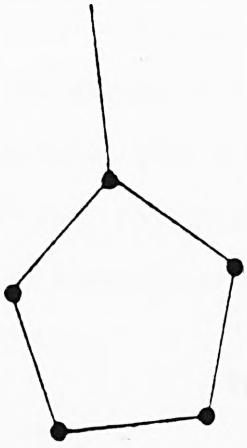

5-1

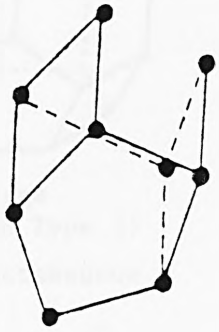

4-4-1

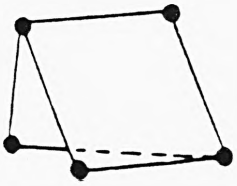

4-1

Figure 2.2 Polyhedral voids

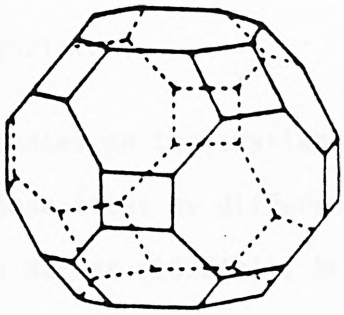

α cage
(26-hedron Type I)
Truncated cuboctahedron

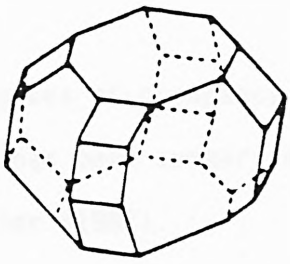

γ cage
(18-hedron)

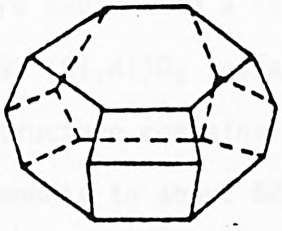

ε cage
(11-hedron)

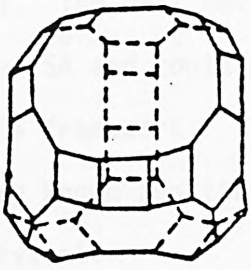

(26-hedron Type II)

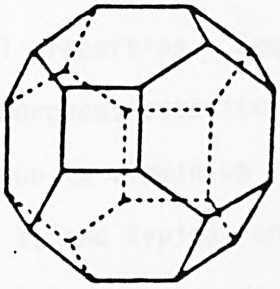

β cage
(14-hedron Type I)
Truncated octahedron

the zeolite such as its water content, temperature and framework charge. Due to these complexities, ion site distribution data from different samples and investigators are not always consistent.

Studies on the available ion sites and the degrees of occupancy of these sites by differently exchanged zeolites has been summarised by Barrer (1978(b)), Breck (1973(c)) and Mortier (1982).

2.3 ZEOLITES X AND Y

Zeolites X, Y and faujasite have topologically similar aluminosilicate framework structures, although they are distinct zeolite species with characteristic differences. The unit cells are cubic with a large cell dimension of nearly 25Å and contains 192 $(Si,Al)O_4$ tetrahedra. The remarkably stable framework structure contains the largest void space of any known zeolite and amounts to about 50 vol. % of the dehydrated crystal.

The chemical compositions of zeolites X and Y are related to the synthesis method (Breck 1973(d)). The zeolites are distinguished on the basis of chemical composition, structure, and their related physical and chemical properties. Zeolite X differs from Y only by the degree of isomorphous substitution of Al for Si within the framework. The silicon to aluminium ratio can vary with both zeolites, especially Y, and typical unit cell formulae are given below together with their corresponding Si/Al ratios (Breck 1973(e)):

Zeolite X:-

$$Na_{86}[(AlO_2)_{86}(SiO_2)_{106}].\ 264\ H_2O \quad Si/Al = 1\text{-}1.5$$

Zeolite Y:-

$$Na_{56}[(AlO_2)_{56}(SiO_2)_{136}].\ 250\ H_2O \quad Si/Al = 1.5\text{-}3$$

The framework of these faujasites consists of a tetrahedral arrangement of the truncated octahedra (sodalite units i.e. ß-cages - see Figure 2.2) i.e. the octahedra are linked at some of the octahedral faces by hexagonal prisms, each containing 12 SiO_4 or AlO_4 tetrahedra which are formed by linking (but not sharing) of two 6-oxygen windows, one from each sodalite unit (see Figure 2.3). This produces the characteristic double-6-ring, D6R, as the secondary building unit in their structural framework and creates the 26-hedra type II void or 'supercage' (see Figure 2.2). Thus these zeolites can be considered to comprise two independent but inter-connecting three-dimensional networks of cavities because of the way the linked sodalite units are arranged topologically. One such network consists of the supercages joined to each other by the sharing of 12-oxygen windows of free diameter 7.4 Å, and the other is the linking of the sodalite units via hexagonal prisms, with 6-oxygen windows which have free diameters of 2.5Å.

Barrers' classification (1978) of cation sites in faujasites, shown below, is based on work done by Smith (1971):

Site I - In the centre of hexagonal prisms (16 sites per unit cell)

Site I' - In sodalite cages, i.e. 14-hedra, adjacent to 6-oxygen windows leading to hexagonal prisms (32 sites per unit cell)

Site U - In the centre of sodalite cages (8 sites per unit cell)

Figure 2.3 Structure of faujasite

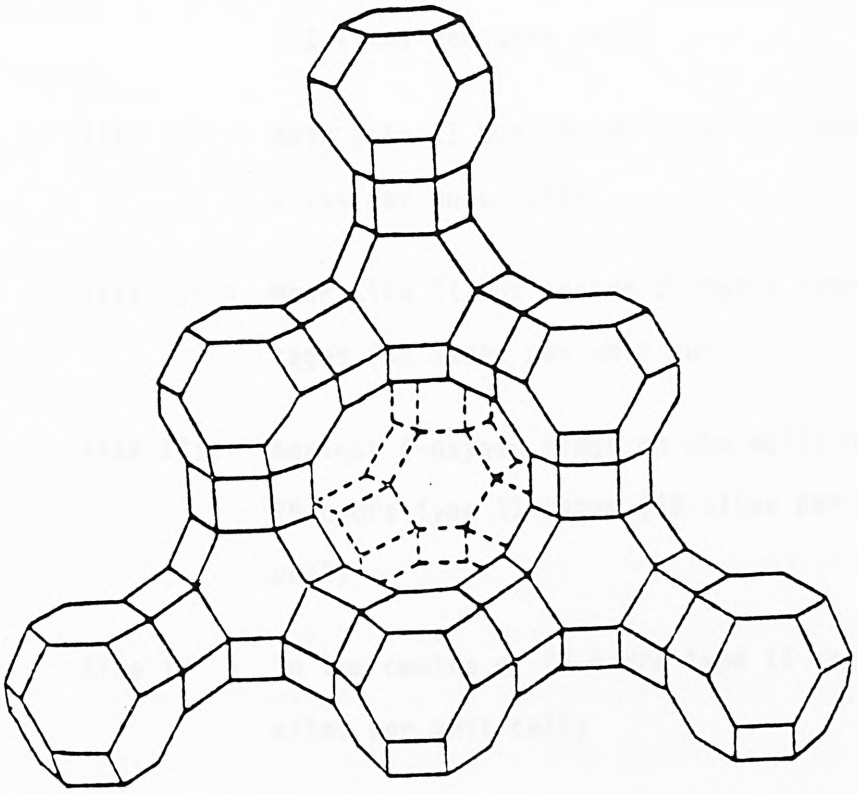

Figure 2.4 Structure of zeolite A

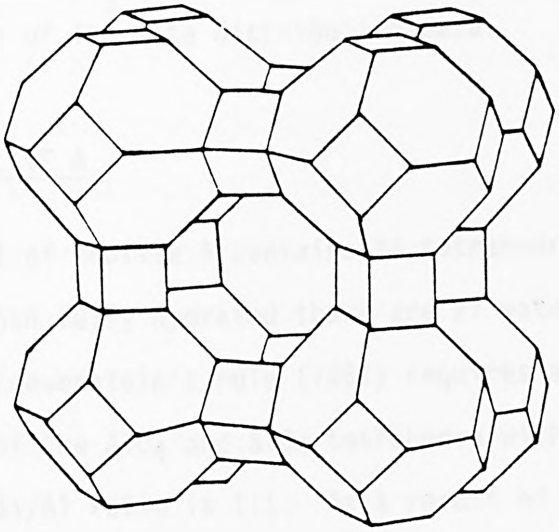

Site II - In the plane of the 6-oxygen windows linking the sodalite cages and 26-hedra type II cages (32 sites per unit cell)

Site II′ - Near site II but inside sodalite cages (32 sites per unit cell)

Site II* - Near Site II but inside 26-hedra type II cages (32 sites per unit cell)

Site III - Against 4-oxygen rings on the walls of 26-hedra type II cages (48 sites per unit cell)

Site IV - In the centre of 26-hedra type II cages (8 sites per unit cell)

Site V - In the 12-oxygen rings of the 26-hedra type II cages (16 sites per unit cell).

The different approaches and findings of Breck (1973(f)) and Mortier (1982) illustrate the complexities involved in the determination of ion site distribution data.

2.4 ZEOLITE A

The unit cell of zeolite A contains 24 tetrahedra (12 AlO_4 and 12 SiO_4). When fully hydrated there are 27 water molecules per unit cell. Loewenstein's rule (1954) requires a rigorous alternation of the AlO_4 and SiO_4 tetrahedra within the framework, because the Si/Al ratio is 1:1. As a result of this the lattice constant of the true unit cell of zeolite A must be 24.6Å and must contain 192 tetrahedra. However it is often more convenient to

consider the pseudo-cell of 12.3Å. In these terms, the unit cell composition is as follows:

Zeolite A:-

$$Na_{12}[(AlO_2)_{12}(SiO_2)_{12}].\quad 27H_2O \qquad Si/Al = 1$$

In many preparations, chemical analyses of zeolite A have indicated a Si/Al ratio of slightly less than 1. This would appear to imply that deviations from a 4:0 ordering scheme occur in the lattice (in 4:0 ordering, each Si^{4+} is linked, via oxygen bridges, to four Al^{3+} ions, and each Al^{3+} likewise to four Si^{4+}). Indeed a 3:1 ordering scheme (where each Si^{4+} is surrounded, via oxygen bridges, to three Al^{3+} and one Si^{4+}, and vice versa) was recently proposed based on results obtained with ^{29}Si "magic angle spinning" nuclear magnetic resonance data (Bursill, Lodge and Thomas 1981). This conclusion was rejected however when it was demonstrated that these workers had failed to appreciate the degree to which the chemical shift of the 4:0, 3:1 peaks depended on the topology, and that the chemical shift of the 4:0 peak in zeolite A is quite different compared to other materials. Thus what appeared to be a 3:1 ordering was in fact 4:0 (Melchior, Vaughan, Jarmen and Jacobson 1982). Bursill, Lodge and Thomas (1981) had used zeolite X as a standard, but zeolites X and A are markedly different structurally. It is now appreciated that one needs to use iso-structural materials (e.g. zeolites A and ZK4) to calibrate. The occlusion of $NaAlO_2$ within the sodalite cages has been postulated as the reason for a Si/Al ratio of less than 1 (Barrer and Meier 1958), but there has been no evidence to support this.

The aluminosilicate framework of zeolite A can be described in terms of two types of polyhedra. One is a simple cubic arrangement of eight tetrahedra, the double 4-ring (D4R); the other is the truncated octahedron, or sodalite cage (see Figures 2.1 and 2.2). The aluminosilicate framework of zeolite A is generated by placing the D4R units ($Si_4Al_4O_{16}$) along the centres of all the edges of a cube of edge 12.3Å. This arrangement produces truncated octahedral units centred at the corners of the cube (Figure 2.4). Each corner of the cube is thus occupied by a sodalite unit, comprising a cavity with a free diameter of 6.6Å. This cubic arrangement of eight sodalite units creates a large cavity of free diameter 11.4Å, which is a truncated cuboctahedron. There are therefore two interconnecting, three dimensional channel systems: one consists of connected supercages, 11.4Å in diameter, separated by 8-oxygen windows of free diameter 4.2Å, and the other system consists of sodalite cages, alternating with the supercages and separated by 6-oxygen windows of free diameter 2.2Å (Reed and Breck 1956). Barrer's (1978(b)) classification of cation sites in zeolite A is as follows:

S1 - In the 8-ring (3 sites per pseudo unit cell)

S2 - In the 6-ring (8 sites per pseudo unit cell)

S2′ - In the sodalite cage but adjacent to the 6-ring (8 sites per pseudo unit cell)

S2* - In the 26-hedra type I cage adjacent to the 6-ring (8 sites per pseudo unit cell)

S3 - Against the 4-rings on the walls of the 26-hedra type I cage (12 sites per pseudo unit cell)

SU - In the centre of the sodalite cages (1 site per pseudo unit cell)

S4 - In the centre of the 26-hedra type I cage (1 site per pseudo unit cell).

2.5 CLINOPTILOLITE

The structure of clinoptilolite remained uncertain and controversial until fairly recently. Alberti (1975) confirmed that clinoptilolite is isostructural with heulandite, the structure of which had been determined previously (Merkle and Slaughter 1968). Typical unit cell compositions are as follows:

Heulandite:-

$Ca_4[(AlO_2)_8(SiO_2)_{28}].\ 24H_2O$ Si/Al = 2.47-3.73

Clinoptilolite:-

$Na_6[(AlO_2)_6(SiO_2)_{30}].\ 24H_2O$ Si/Al = 4.25-5.25

In the natural material, calcium, sodium and potassium are the major cationic constituents with high calcium generally prevailing for the lower Si/Al ratio heulandite and high potassium in the higher Si/Al ratio clinoptilolite. The effect of dehydration upon the low silica calcium heulandites is that their structure changes at 215°C to Heulandite "B" (structure unknown) and between 500-550°C the material tends to degrade (Breck 1973(g); Alletti 1972), whilst potassium-exchanged heulandites and various

potassium and hydrogen clinoptilolites are stable up to 800°C (Barrer and Makki 1964; Araya and Dyer 1981). Alberti (1975) showed that the markedly greater stability of clinoptilolite could be explained in terms of a lowering of the charge density in clinoptilolite compared to heulandite. The Si/Al ratio is higher in clinoptilolite than in heulandite; there are therefore fewer exchangeable cations per unit cell within the channels of clinoptilolite, and an extra cation site exists at the origin of the unit cell, which contributes significantly towards the thermal stability of the zeolite.

The SBU in clinoptilolite is the 4-4-1 unit proposed by Meier (1968). Each tetrahedron belongs to both 4- and 5-rings of silicon and aluminium, and the ($Si_{10}Al_{10}O_{20}$) units are arranged in layers, which accounts for the lamellar morphologies and the cleavage properties of these zeolites (Breck 1973(g)). Each layer is cross-linked to other layers by Si-O-Si and Si-O-Al bonds, which create, between each pair of layers, two dimensional networks of channels of three kinds. Movement into and along one set of channels is governed by elliptical 10-ring windows having approximate free dimensions of 7.9Å x 3.5Å (Figure 2.5). The other channels have one set of windows with free dimensions of about 4.4Å x 3.0Å (Barrer, Papadopoulos and Rees 1967).

Four cation sites have been identified (Mortier 1982) - three in the channels of the structure, co-ordinated mainly to water molecules, while the other occupies a position close to the centre of the 8-ring.

Figure 2.5 The ab crystallographic plane of heulandite (Merkle and Slaughter 1965).

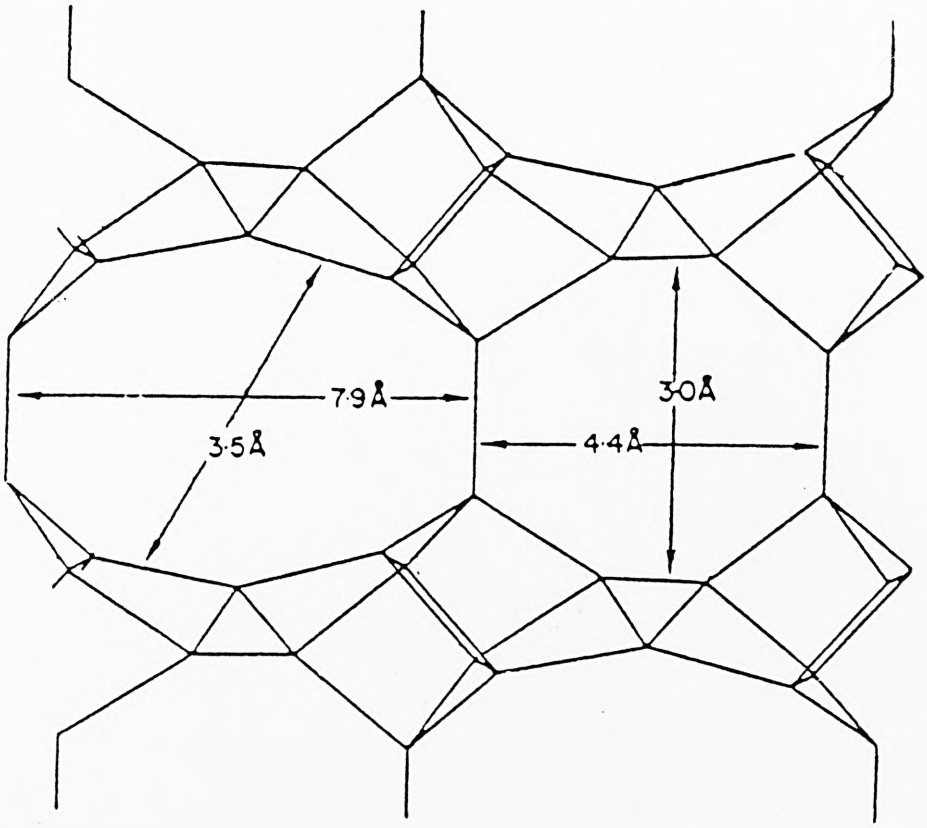

CHAPTER 3 - ION EXCHANGE

3.1 BINARY ION EXCHANGE

Ion exchange can be defined as the reversibile interchange of ions between two phases, occurring in such a way that there is no gross change in the solid. For a binary exchange, the reaction may be written as

$$z_A\bar{M}_B^{z_B^+} + z_BM_A^{z_A^+} \rightleftharpoons z_AM_B^{z_B^+} + z_B\bar{M}_A^{z_A^+} \qquad 3.1$$

where z_A, z_B are the valencies of the exchange cations $M_A^{z_A^+}$ and $M_B^{z_B^+}$ and $\bar{M}$ and M refer to the exchanger and solution phases respectively. The ion B, initially in the zeolite, is frequently referred to as the counter ion.

The equilibrium properties of an ion exchange system are depicted by an isotherm. This is an equilibrium plot of the concentration of an exchanging ion in solution against the concentration of that same ion in the exchanger at constant solution concentration (g equiv. dm^{-3}) and temperature. The isotherm is plotted in terms of the equivalent fraction E_A of the ingoing ion in solution against that for the same ion in the zeolite, $\bar{E}_A$. For a binary exchange (Dyer, Enamy and Townsend 1981) the equivalent fractions are defined by

$$E_A = \frac{z_Am_A}{z_Am_A + z_Bm_B} \qquad 3.2$$

and

$$\bar{E}_A = \frac{z_A \bar{m}_A}{z_A \bar{m}_A + z_B \bar{m}_B} \qquad 3.3$$

where m_A, m_B are the concentrations (mol dm^{-3}) of ions $M_A^{z_A+}$, $M_B^{z_B+}$ in solution and $\bar{m}_A$, $\bar{m}_B$ are the concentrations (mol kg^{-1}) of the ions in the exchanger phase (normally by convention not the dry exchanger, but that which has taken up a known quantity of water by equilibration at constant temperature under a known and constant water vapour pressure).

An isotherm is obtained experimentally by equilibrating solutions of constant total normality T_N (g equiv. dm^{-3}) but containing different proportions of cations $M_A^{z_A+}$ and $M_B^{z_B+}$, with known weights of either the homoionic M_A or homoionic M_B zeolite. The experiments are carried out over a period of time which is sufficient for equilibrium to be attained. Following this, the equilibrium compositions of the zeolite and solution phases are found by chemical analysis.

T_N must be kept constant because the selectivity of the zeolite for the ion A can be not only a function of $\bar{E}_A$ but also of the total normality. Different total normalities will then correspond to different isotherms; for a given value of $\bar{E}_A$, the magnitude of E_A can range from 0 to 1 according to the magnitude of T_N.

For a binary exchange, the concentrations (mol dm^{-3}) of the ions $M_A^{z_A+}$ and $M_B^{z_B+}$ can be determined from the expressions

$$m_A = \frac{E_A T_N}{z_A} \qquad 3.4$$

$$T_N = z_A m_A + z_B m_B \qquad 3.5$$

$$m_B = \frac{(1 - E_A)\, T_N}{z_B} = \frac{E_B T_N}{z_B} \qquad 3.6$$

since $E_B = 1 - E_A$ and $\bar{E}_B = 1 - \bar{E}_A$.

The preference of an exchanger for one cation over another is expressed as a separation factor, α' :

$$\alpha' = \frac{(\bar{E}_A/E_A)}{(\bar{E}_B/E_B)} = \frac{\bar{E}_A E_B}{\bar{E}_B E_A} \qquad 3.7$$

Since isotherms are usually plotted with E_A as the ordinate and $\bar{E}_A$ as the abscissa, the value of α' can be graphically obtained as shown in Figure 3.1, as the ratio

$$\alpha' = \frac{\text{Area I}}{\text{Area II}} \qquad 3.8$$

In an ion exchange system where the zeolite shows equal preference for both ions, $\bar{E}_A$ equals $\bar{E}_B$, and the isotherm plot is linear, following the diagonal in the diagram (Figure 3.1).

Ion exchange preferences can be summarised in terms of the separation factor as follows:

$\alpha' > 1$: zeolite exhibits preference for ingoing ion (M_A)

$\alpha' = 1$: zeolite exhibits no preference

$\alpha' < 1$: zeolite exhibits preference for outgoing ion (M_B)

Figure 3.1 Graphical determination of α and α'

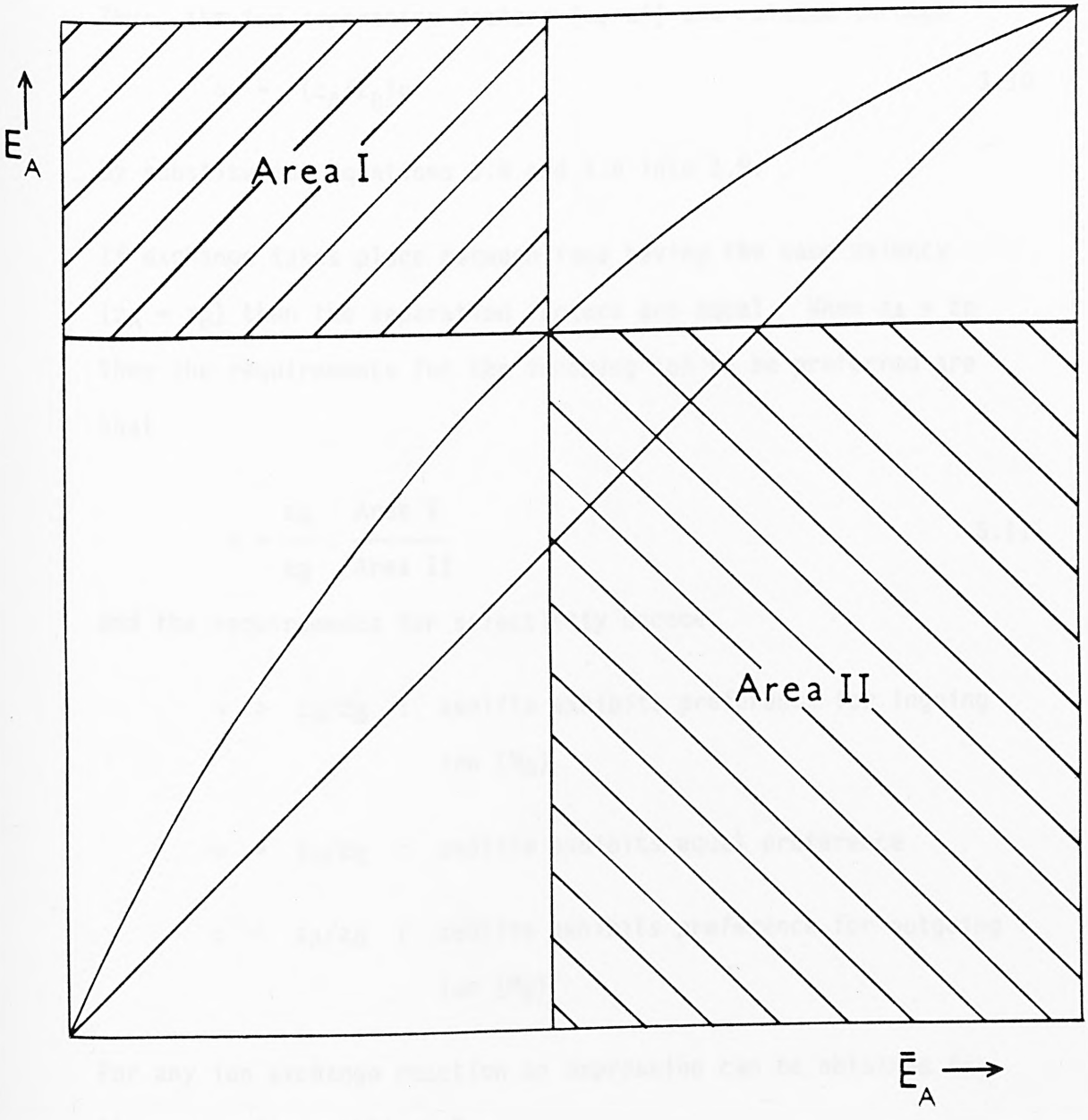

Since thermodynamic quantities describing ion exchange in zeolites are usually expressed in terms of molar concentrations (mol dm^{-3}) in solutions, the separation factors can also be expressed in the same way. This molar separation factor is given by

$$\alpha = \frac{(\bar{E}_A/m_A)}{(\bar{E}_B/m_B)} = \frac{\bar{E}_A m_B}{\bar{E}_B m_A} \qquad 3.9$$

Thus, the two separation factors (α, α') are related through

$$\alpha = (z_A/z_B)\alpha' \qquad 3.10$$

by substituting equations 3.4 and 3.6 into 3.9.

If exchange takes place between ions having the same valency ($z_A = z_B$) then the separation factors are equal. When $z_A \neq z_B$ then the requirements for the incoming ion to be preferred are that

$$\alpha = \frac{z_A}{z_B} \cdot \frac{\text{Area I}}{\text{Area II}} \qquad 3.11$$

and the requirements for selectivity become

$\alpha > z_A/z_B$: zeolite exhibits preference for ingoing ion (M_A)

$\alpha = z_A/z_B$: zeolite exhibits equal preference

$\alpha < z_A/z_B$: zeolite exhibits preference for outgoing ion (M_B)

For any ion exchange reaction an expression can be obtained for the mass action quotient K_m.

Considering equation 3.1,

$$K_m = \frac{\bar{E}_A^{\,z_B}\, m_B^{\,z_A}}{\bar{E}_B^{\,z_A}\, m_A^{\,z_B}} \qquad 3.12$$

The separation factor can be related (Barrer and Klinowski 1974) to the mass action quotient K_m.

Rearranging equation 3.12

$$K_m^{\,1/z_A} = \frac{m_B}{\bar{E}_B} \cdot \left[\frac{\bar{E}_A}{m_A}\right]^{z_B/z_A}$$

$$K_m^{\,1/z_A} = \frac{\bar{E}_A m_B}{\bar{E}_B m_A} \cdot \left[\frac{E_A}{m_A}\right]^{\frac{z_B - z_A}{z_A}} \qquad 3.13$$

Since

$$\alpha = \bar{E}_A m_B / \bar{E}_B m_A$$

Then

$$K_m^{\,1/z_A} = \alpha \left[\frac{\bar{E}_A}{m_A}\right]^{\frac{z_B - z_A}{z_A}}$$

$$\alpha = K_m^{\,1/z_A} \cdot \left[\frac{\bar{E}_A}{m_A}\right]^{\frac{z_A - z_B}{z_A}} \qquad 3.14$$

Equation 3.14 can be used to find the relation between α and K_m for any ion exchange system.

In cases where the two ions have the same valencies ($z_A = z_B$) then $\alpha = K_m^{1/z_A}$ and thus for the simplest case (when $z_A = z_B = 1$, uni-univalent exchange) $\alpha = K_m$.

3.1.1 Classification of Isotherms

Ion exchange isotherms for zeolite studies can be arranged in three groups and are shown in Figures 3.2 - 3.4.

Isotherms of the first kind are shown in Figure 3.2. When the valencies of the cations are equal, the figures represent the following preferences.

a - zeolite shows preference for outing ion eg. Li/NaX, Li/NaY (Sherry 1966)

b - zeolite shows equal preference eg. Sr/Na phillipsite (Barrer and Munday 1971)

c - zeolite shows preference for ingoing ion eg. Pb/NaA (Hertzenberg and Sherry 1980), Pb/Na clinoptilolite (Semmens and Seyfarth 1981), Ag/NaX, Ag/NaY (Sherry 1966).

If the exchanging ions have different valencies, the selectivity is not visually obvious since

$$\alpha = \frac{z_A}{z_B} \cdot \frac{\text{Area I}}{\text{Area II}} \qquad 3.11$$

Isotherms of the second kind (Figure 3.3) are characterised by a sigmoid curve and are often observed when the selectivity is dependent upon cation composition, and the selectivity is reversed

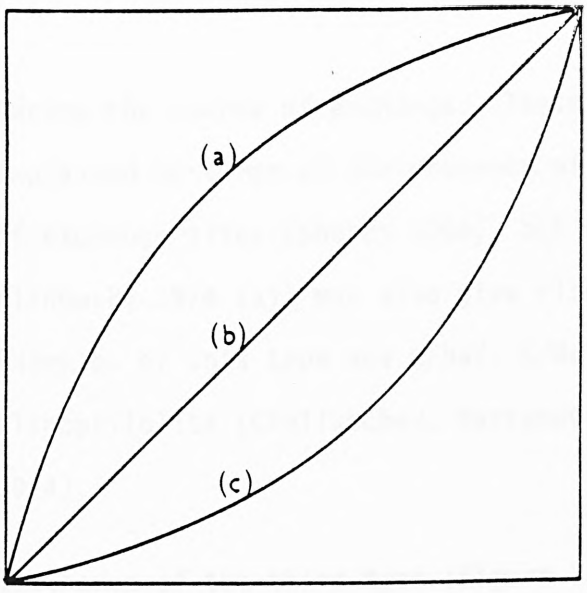

Figure 3,2

Isotherms of the 1st kind

(a) outgoing ion preferred

(b) equal preference

(c) ingoing ion preferred

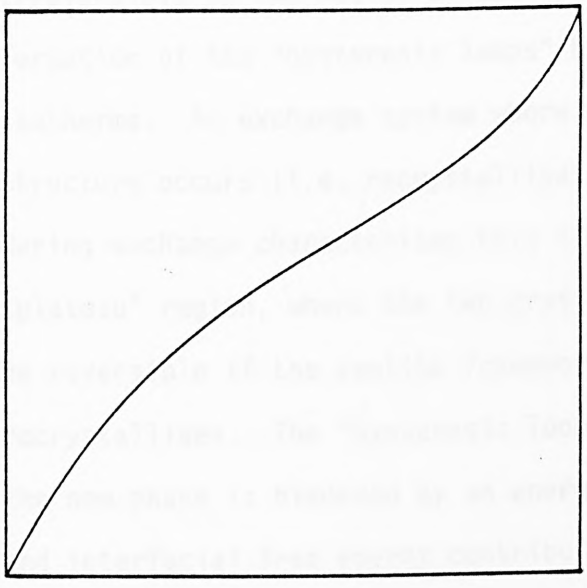

Figure 3.3

Isotherm of the 2nd kind

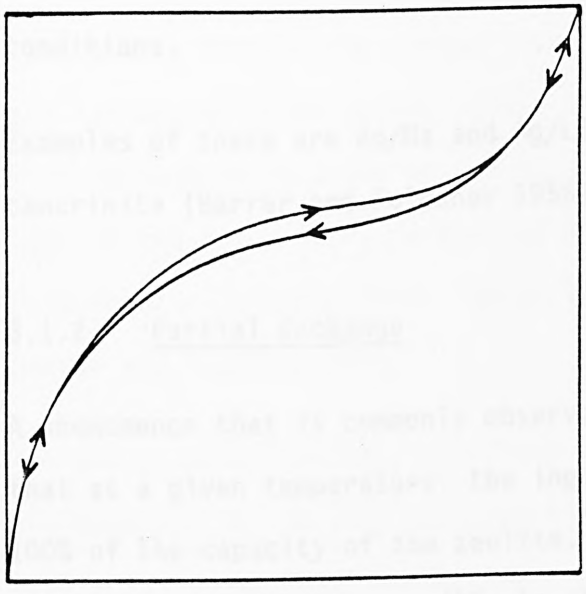

Figure 3.4

Isotherms of the 3rd kind

during the course of exchange. These sigmoidal curves have been explained in terms of the presence of two or more different types of exchange sites (Sherry 1966), but other factors (Barrer and Klinowski 1974 (a)) may also give rise to curves of this form. Examples of this type are K/NaX, K/NaY (Sherry 1966), Pb/Na clinoptilolite (Chelishchev, Martynova, Fakina and Berenshtein 1974).

Isotherms of the third type (Figure 3.4) are found to be partially irreversible in the region of the "plateau", leading to the formation of the "hysteresis loops" between forward and reverse isotherms. An exchange system where a change in the framework structure occurs (i.e. recrystallisation of the zeolite phase) during exchange characterises this type of isotherm. The "plateau" region, where the two crystal phases co-exist, can also be reversible if the zeolite framework is flexible and readily recrystallises. The "hysteresis loops" arise when the growth of the new phase is hindered by an energy barrier caused by strain and interfacial free energy contributions (Townsend 1977), and these isotherms are said to be characteristic of metastable conditions.

Examples of these are Ag/Na and Ag/Li exchanges in basic cancrinite (Barrer and Falconer 1956).

3.1.2 Partial Exchange

A phenomenon that is commonly observed in zeolite ion exchange is that at a given temperature, the ingoing ion fails to exchange to 100% of the capacity of the zeolite. In effect, some sites within the crystal remain inaccessible to the entering ion.

Figures 3.5 - 3.7 depict the isotherms which apply to partial ion exchange processes, and these correspond to their respective total ion exchange isotherms as shown in Figures 3.2 - 3.4.

The cause of this phenomenon may be the rigid, regular crystalline structure of the zeolite. Entering ions larger than the channel size within the crystal are excluded, and the zeolite acts as a sieve. This "ion sieving" is often observed when the ions themselves have ionic radii which should not cause their exclusion from zeolite channels. These ions are usually strongly hydrated in aqueous solution, and their exclusion is considered to be associated with this factor. The ion-sieve effect may be total as in the case of the $(CH_3)_4N^+$ and $(C_2H_5)_4N^+$ ions and zeolite A, from which they are completely excluded (Barrer and Meier 1958; Barrer and Meier 1959), or partial, leading to incomplete exchange (Barrer, Rees and Shamsuzzoha 1966; Sherry 1966; Sherry 1968; Barrer and Klinowski 1974; Maes and Cremers 1975; Fletcher and Townsend 1981). The zeolite channels may also cause ion exclusion in another manner, connected with the total void volume of the channels, when ions are partially excluded, not because they cannot pass through the channel windows, but because they fill all the intracrystalline volume before 100% exchange is achieved. This phenomenon is known as the volume-steric exclusion mechanism (Barrer and Meier 1958; Barrer and Meier 1959; Barrer, Papadopoulos and Rees 1967; Theng, Vansant and Uytterhoeven 1968; Barrer and Townsend 1978).

Ion sieve and volume-steric effects are not the only explanations for partial exchange however, and a more comprehensive explanation has been put forward (Barrer and

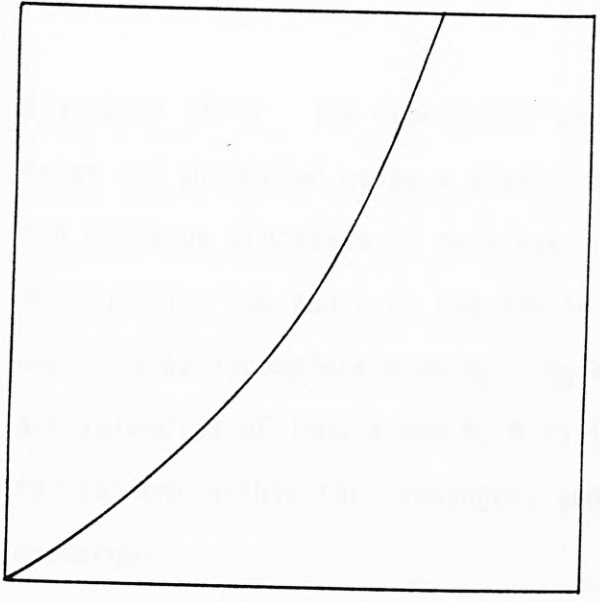

Figure 3.5

Isotherm of the 4th kind

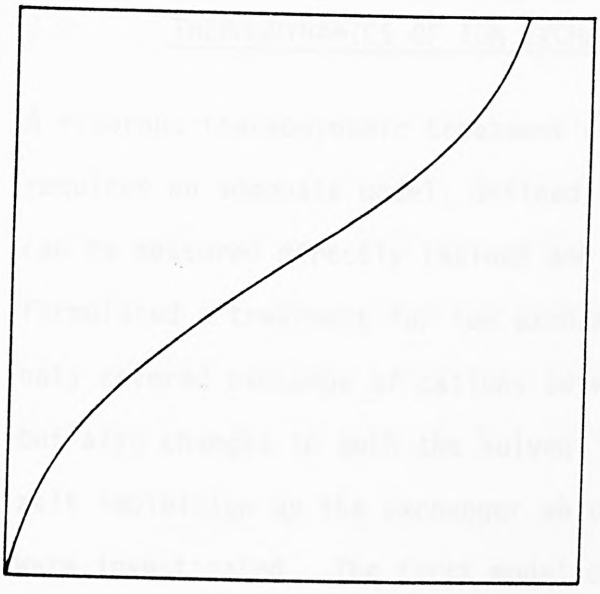

Figure 3.6

Isotherm of the 5th kind

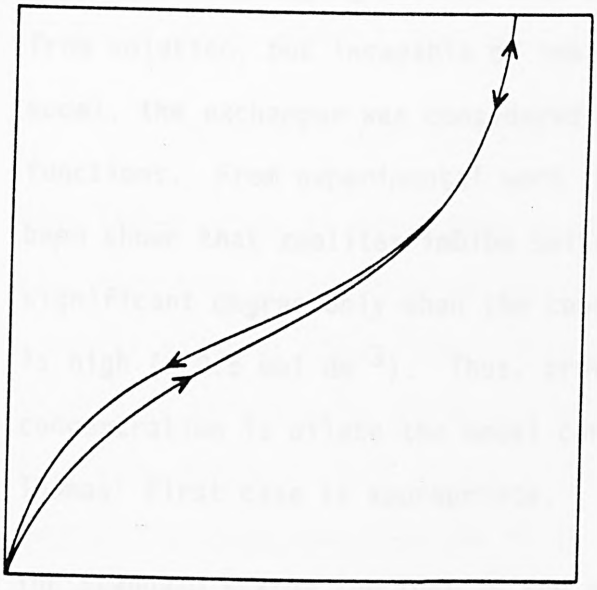

Figure 3.7

Isotherms of the 6th kind

Klinowski 1977). The conditions under which partial exchange may arise was predicted using a statistical thermodynamic model of the ion exchange processes in zeolites. It was shown that if A is the entering ion and B is the ion in the crystal, then exchange can only be incomplete when $z_A < z_B$ and $N/N_o < 1/z_A$. Here z_A, z_B are valencies of ions A and B, N is the number of available sites for cations within the exchanger, and N_o the total charge on the exchanger.

3.2 THERMODYNAMICS OF ION EXCHANGE

A rigorous thermodynamic treatment of the ion exchange reaction requires an adequate model, defined in terms of quantities that can be measured directly (Gaines and Thomas 1953). These workers formulated a treatment for ion exchange in clay minerals which not only covered exchange of cations between solution and exchanger but also changes in both the solvent content and the degree of salt imbibition by the exchanger which may take place. Two cases were investigated. The first model consisted of an exchanger capable of exchanging cations with solution and adsorbing solvent from solution, but incapable of imbibing anions. In the second model, the exchanger was considered capable of all three functions. From experimental work (Barrer and Walker 1964) it has been shown that zeolites imbibe salts from solution to a significant degree only when the concentration of salt in solution is high (> 0.5 mol dm^{-3}). Thus, provided the solution concentration is dilute the model corresponding to Gaines and Thomas' first case is appropriate.

The standard states for ions in the solution phase are defined in terms of the hypothetical ideal molal solutions of salts, obeying

Henry's law. Thus for ion $M_A^{z_A+}$, $m_A = a_A = \gamma_A = 1$ in the standard state, where m_A is the concentration (mol kg^{-1}), a_A is the activity of ion $M_A^{z_A+}$ in the solution and γ_A is the "individual ion activity coefficient" in solution (which of course cannot be evaluated - see Section 3.2.1). For the exchanger phase the standard states are chosen in terms of Raoult's law, and this requires the exchanger being in the respective homoionic forms. The exchanger imbibes water and the extent of imbibition varies for different ion exchange forms of the same exchanger. In the Gaines and Thomas treatment the exchanger phase is taken as the wet solid so that the definition incorporates the free energy of hydration of each homoionic form, thus avoiding complicated calculations arising from the model. The treatment involves considering all three phases (vapour, solution and exchanger) and since at equilibrium it must be true that the chemical potentials of water (μ_w) be the same in all phases, then

$$\mu_w(v) = \mu_w(s) = \mu_w(c)$$

where (v) refers to the vapour phase. This implies that in the standard state, when it must be true that

$$\mu_w(v) = \mu_w^{\theta}(v),\ \mu_w(s) = \mu_w^{\theta}(s) \text{ and } \mu_w(c) = \mu_w^{\theta}(c)$$

then the activity of water must be unity in all phases. For the exchanger this occurs when the zeolite has imbibed its equilibrium quantity of water after immersing the homoionic exchanger in an infinitely dilute solution of the same ion (i.e. pure water). Thus, the standard state of the exchanger phase is the homoionic form of the exchanger immersed in an infinitely dilute solution of the same ion. Then for ion $M_A^{z_A+}$ in the exchanger in the standard

state, $\bar{E}_A = \bar{a}_A = g_A = 1$, where $\bar{a}_A$ is the activity of the ion in the exchanger phase, and g_A is the activity coefficient of ion $M_A^{z_A+}$ in association with its equivalent of exchanger framework (Gaines and Thomas 1953).

For the binary ion exchange reaction

$$z_A\bar{M}_B^{z_B+} + z_BM_A^{z_A+} \rightleftharpoons z_AM_B^{z_B+} + z_B\bar{M}_A^{z_A+} \qquad 3.1$$

the thermodynamic equilibrium constant is defined as

$$K_a = \frac{\bar{a}_A^{z_B} \cdot a_B^{z_A}}{a_A^{z_B} \cdot \bar{a}_B^{z_A}} \qquad 3.15$$

where $\bar{a}_A$ and a_A are the activities of $M_A^{z_A+}$ in the crystal and solution phases respectively.

In terms of concentrations and activity coefficients this becomes

$$K_a = \frac{\bar{E}_A^{z_B} \cdot g_A^{z_B} \cdot m_B^{z_A} \cdot \gamma_B^{z_A}}{m_A^{z_B} \cdot \gamma_A^{z_B} \cdot \bar{E}_B^{z_A} \cdot g_B^{z_A}} \qquad 3.16$$

where g_A, g_B are the crystal phase activity coefficients (Gaines and Thomas convention) and γ_A, γ_B the solution phase activity coefficients of the ions $M_A^{z_A+}$, $M_B^{z_B+}$ respectively.

From equations 3.12 and 3.16 it is apparent that K_a and K_m are related by

$$K_a = K_m \cdot \frac{g_A^{z_B} \cdot \gamma_B^{z_A}}{g_B^{z_A} \cdot \gamma_A^{z_B}} \qquad 3.17$$

A third quotient is also used to characterise the equilibrium. Because it includes the solution phase activity correction, it is sometimes known as the corrected selectivity coefficient. To avoid confusion with α, and for historical reasons, it has usually been known as the Kielland quotient (Kielland 1935) but this latter term is disappearing in favour of the former.

$$K_c = K_m \Gamma \qquad 3.18$$

where

$$\Gamma = \frac{\gamma_B^{z_A}}{\gamma_A^{z_B}} \qquad 3.19$$

Thus from equations 3.16 and 3.18,

$$K_a = K_c \cdot (g_A^{z_B} / g_B^{z_A}) \qquad 3.20$$

The determination of K_a from isotherm data involves two steps. The first of these is the solution phase activity correction, which gives K_c. The second involves an evaluation of the activity coefficients of the ions in the zeolite, to finally obtain K_a.

The standard free energy of exchange is given by

$$\Delta G^{\theta} = -(RT/z_A z_B) \cdot \ln K_a \qquad 3.21$$

3.2.1 Determination of Solution Phase Activity Coefficients

An expression for the "individual ion activity coefficients" may be derived theoretically using the Debye-Hückel approach (Robinson and Stokes 1970), but values cannot be separately determined by experiment since ions in solution must be accompanied by an equivalent number of oppositely charged ions. A ratio of single ion activity coefficients, Γ (equation 3.19), can however be determined from experimentally measured mean molal stoichiometric activity coefficients $\gamma_{\pm AX}$ and $\gamma_{\pm BX}$, where the subscripts AX, BX refer to salts with a common anion X.

The relations between $\gamma_{\pm AX}$ and $\gamma_{\pm BX}$ and the activity coefficients of the individual ions γ_A, γ_B are obtained from the definitions of the mean molal activity coefficients:

$$\gamma_{\pm AX} = (\gamma_A^{z_X} \cdot \gamma_X^{z_A})^{\frac{1}{z_A+z_X}} \qquad 3.22$$

$$\gamma_{+BX} = (\gamma_B^{z_X} \cdot \gamma_X^{z_B})^{\frac{1}{z_B+z_X}} \qquad 3.23$$

Thus

$$\ln\gamma_{\pm AX} = \frac{1}{z_A+z_X}\left[z_X \ln\gamma_A + z_A \ln\gamma_X\right] \qquad 3.24$$

$$\ln\gamma_{\pm BX} = \frac{1}{z_B+z_X}\left[z_X \ln\gamma_B + z_B \ln\gamma_X\right] \qquad 3.25$$

Multiplying 3.24 by $z_B(z_A+z_X)/z_X$ and 3.25 by $z_A(z_B+z_X)/z_X$ gives

$$\frac{z_B(z_A+z_X)}{z_X} \ln\gamma_{\pm AX} = z_B \ln\gamma_A + \left[\frac{z_A z_B}{z_X}\right] \ln\gamma_X \qquad 3.26$$

and

$$\frac{z_A(z_B+z_X)}{z_X} \ln\gamma_{\pm BX} = z_A \ln\gamma_B + \left[\frac{z_A z_B}{z_X}\right] \ln\gamma_X \qquad 3.27$$

Subtracting 3.26 from 3.27 gives

$$\ln\Gamma = \ln\left[\frac{\gamma_B^{z_A}}{\gamma_A^{z_B}}\right] = \frac{1}{z_X}\left[z_A(z_B+z_X)\ln\gamma_{\pm BX} - z_B(z_A+z_X)\ln\gamma_{\pm AX}\right] \qquad 3.28$$

This expression yields Γ in terms of the mean molal stiochiometric activity coefficients of pure solutions. What is required is an expression for Γ which corresponds to the experiemental situation (i.e. in terms of the mean molal activity coefficients of AX and BX in mixed solution, respectively denoted by the symbols $\gamma_{\pm AX}$ (BX) and $\gamma_{\pm BX}$ (AX)). By extending Guggenheim's (1935) original theory, Glueckauf (1949) derived expressions for these quantities in terms of the pure salt mean molal activity coefficients, and these are shown below:

$$\log \gamma_{\pm AX}(BX) = \log \gamma_{\pm AX} - \frac{m_B}{4I}\left[k_1 \log \gamma_{\pm AX} - k_2 \log \gamma_{\pm BX} - \frac{k_3}{I+I^{-\frac{1}{2}}}\right] \qquad 3.29$$

and

$$\log \gamma_{\pm BX}(AX) = \log \gamma_{\pm BX} - \frac{m_A}{4I}\left[k_4 \log \gamma_{\pm BX} - k_5 \log \gamma_{\pm AX} - \frac{k_6}{I+I^{-\frac{1}{2}}}\right] \quad 3.30$$

where

$$k_1 = z_B(2z_B - z_A + z_X)$$

$$k_2 = z_A(z_B+z_X)^2(z_A+z_X)^{-1}$$

$$k_3 = \tfrac{1}{2}z_A z_B z_X(z_A-z_B)^2(z_A+z_X)^{-1}$$

$$k_4 = z_A(2z_A - z_B + z_X)$$

$$k_5 = z_B(z_A+z_X)^2(z_B+z_X)^{-1}$$

$$k_6 = \tfrac{1}{2}z_A z_B z_X(z_B-z_A)^2(z_B+z_X)^{-1}$$

and I is ionic strength of the solution ($=\frac{1}{2}\Sigma_i m_i z_i^2$).

The procedure is therefore to determine $\gamma_{\pm AX}(BX)$ and $\gamma_{\pm BX}(AX)$ in terms of $\gamma_{\pm AX}$ and $\gamma_{\pm BX}$ over the range of I values covered by the isotherm solutions and then by analogy with equation 3.28, Γ as a function of composition can be obtained from

$$\ln\Gamma = \frac{1}{z_X}\left[z_A(z_B+z_X)\ln\gamma_{\pm BX}(AX) - z_B(z_A+z_X)\ln\gamma_{\pm AX}(BX)\right] \quad 3.31$$

3.2.2 Determination of Zeolite Phase Activity Coefficients

The means of determining the solid phase activity coefficients was first rigorously formulated by Gaines and Thomas (1953). For the three phase system to be at equilibrium it must be true that the chemical potential of the water be the same for all phases, at a given temperature and pressure, viz:

$$\mu_W(v) = \mu_W(s) = \mu_W(c) = \mu_W^{\theta}(c) + RT\ln a_W \qquad 3.32$$

where $\bar{a}_W$ is the activity of water in the exchanger.

Similarly, for equilibrium

$$\mu_A(s) = \mu_A(c) = \mu_A^{\theta}(c) + RT\ln a_A = \mu_A^{\theta}(c) + RT\ln(\bar{E}_A g_A) \qquad 3.33$$

and

$$\mu_B(s) = \mu_B(c) = \mu_B^{\theta}(c) + RT\ln \bar{a}_B = \mu_B^{\theta}(c) + RT\ln(\bar{E}_B g_B) \qquad 3.34$$

From the general thermodynamic extensive d (intensive) relationship

$$SdT - VdP + \Sigma_i n_i d\mu_i = 0 \qquad 3.35$$

the Gibbs-Duhem equation is obtained at constant temperature and pressure: -

$$\Sigma_i n_i d\mu_i = 0 \qquad 3.36$$

where n_i is the number of moles of the ith component of a particular phase. This becomes applicable to the exchanger phase if

(i) all the independently variable components in the exchanger which affect the equilibrium are included in the summation

(ii) salt imbibition is ignored

(iii) the total number of exchange sites per mole of exchanger is constant (a variable exchange capacity, which could arise in the case of salt imbibition requires the inclusion of this factor as an independently variable component).

Combining equations 3.32, 3.33, 3.34 and 3.36

$$n_w RT d\ln\bar{a}_w + n_A RT d\ln\bar{E}_A g_A + n_B RT d\ln\bar{E}_B g_B = 0 \qquad 3.37$$

The terms in RT cancel, and multiplying throughout by $z_A z_B/(z_A n_A + z_B n_B)$ puts the equation in terms of equivalent fractions of ions in the zeolite

$$\left[\frac{n_w z_A z_B}{z_A n_A + z_B n_B}\right] d\ln\bar{a}_w + \left[\frac{n_A z_A z_B}{z_A n_A + z_B n_B}\right] d\ln\bar{E}_A g_A + \left[\frac{n_B z_A z_B}{z_A n_A + z_B n_B}\right] d\ln\bar{E}_B g_B = 0 \qquad 3.38$$

Examination of the terms in brackets shows that the denominator is $\bar{E}_A + \bar{E}_B = 1$ and the second and third terms are just equivalent fractions of ions in the zeolite. Then

$$\nu_w z_A z_B d\ln\bar{a}_w + z_B\bar{E}_A d\ln\bar{E}_A g_A + z_A\bar{E}_B d\ln\bar{E}_B g_B = 0 \qquad 3.39$$

Separating the logarithmic terms and simplifying

$$\nu_w z_A z_B d\ln\bar{a}_w + z_B d\bar{E}_A + z_A d\bar{E}_B + \bar{E}_A d\ln g_A^{z_B} + \bar{E}_B d\ln g_B^{z_A} = 0 \qquad 3.40$$

where $\nu_w = n_w/(z_A n_A + z_B n_B)$ and is the number of moles of water per unit exchanger capacity

$g_A^{z_B}$ or $g_B^{z_A}$ may be eliminated by introducing equation 3.20

$$K_a = K_c \cdot g_A^{z_B}/g_B^{z_A} \qquad 3.20$$

Taking the logarithms of equation 3.20

$$\ln K_a = \ln K_c + \ln g_A^{z_B} - \ln g_B^{z_A} \qquad 3.41$$

and

$$0 = d\ln K_c + d\ln g_A^{z_B} - d\ln g_B^{z_A} \qquad 3.42$$

Combining equations 3.40 and 3.42, explicit expressions for g_A and g_B can be derived by elimination of either g_A or g_B to give

$$d\ln g_A^{z_B} = (z_B - z_A)d\bar{E}_B - \bar{E}_B d\ln K_c - \nu_w z_A z_B d\ln \bar{a}_w \qquad 3.43$$

$$d\ln g_B^{z_A} = -(z_B - z_A)d\bar{E}_A - \bar{E}_A d\ln K_c - \nu_w z_A z_B d\ln \bar{a}_w \qquad 3.44$$

Gaines and Thomas (1953) evaluated these expressions by integrating between standard states and the experimental value of $\bar{E}_A$. Thus for the case of g_A, the integration is between $g_A^{z_B} = \bar{E}_A = 1$ and $g_A^{z_B}$ at $\bar{E}_A$. In the case of a zeolite it can generally be assumed that the water activity term is negligible (Barrer and Klinowski 1974 (a)) and this will be discussed later (see section 3.2.2.1). If the water activity term is ignored then $g_A^{z_B} = 1$ at $\bar{E}_A = 1$ even when the concentration of ions in the

solution phase is not zero (Fletcher and Townsend 1981). This simplifies the integration path (Gaines and Thomas 1953) and equation 3.43 becomes

$$\int_{g_A=\bar{E}_A=1}^{g_A(\bar{E}_A)} d\ln g_A^{z_B} = (z_B-z_A)\int_{1,0}^{\bar{E}_A,\bar{E}_B} d\bar{E}_B - \int_{K_c(\bar{E}_A=1)}^{K_c(\bar{E}_A)} (1-\bar{E}_A)d\ln K_c \qquad 3.45$$

giving

$$\ln g_A^{z_B} = (z_B-z_A)\bar{E}_B - \int_{K_c(\bar{E}_A=1)}^{K_c(\bar{E}_A)} (1-\bar{E}_A)d\ln K_c \qquad 3.46$$

This integral can be transformed since

$$\int(1-\bar{E}_A)d\ln K_c = (1-\bar{E}_A)\ln K_c + \int \ln K_c d\bar{E}_A \qquad 3.47$$

If $\ln K_c^{(\bar{E}_A)}$ is the value of $\ln K_c$ at $\bar{E}_A$, then

$$\ln g_A^{z_B} = (z_B-z_A)\bar{E}_B - (1-\bar{E}_A)\ln K_c^{(\bar{E}_A)} + \int_{\bar{E}_A}^{1} \ln K_c d\bar{E}_A \qquad 3.48$$

Similarly, integrating equation 3.44

$$\int_{g_B=\bar{E}_B=1}^{g_B(\bar{E}_B)} d\ln g_B^{z_A} = -(z_B-z_A)\int_{1,0}^{\bar{E}_B,\bar{E}_A} d\bar{E}_A + \int_{K_c(\bar{E}_B=1)}^{K_c(\bar{E}_B)} \bar{E}_A d\ln K_c \qquad 3.49$$

between limits gives

$$\ln g_B^{z_A} = -(z_B - z_A)\bar{E}_A + \int_{K_c(\bar{E}_B=1)}^{K_c(\bar{E}_B)} \bar{E}_A d\ln K_c \qquad 3.50$$

This integral can be transformed since

$$\int \bar{E}_A d\ln K_c = \bar{E}_A \ln K_c - \int \ln K_c d\bar{E}_A \qquad 3.51$$

Thus if $\ln K_c^{(\bar{E}_A)}$ is the value of $\ln K_c$ at $\bar{E}_A$ then

$$\ln g_B^{z_A} = -(z_B - z_A)\bar{E}_A + \bar{E}_A \ln K_c - \int_0^{\bar{E}_A} \ln K_c d\bar{E}_A \qquad 3.52$$

substituting equations 3.48 and 3.52 into equation 3.41 yields finally

$$\ln K_a = (z_B - z_A) + \int_0^1 \ln K_c d\bar{E}_A \qquad 3.53$$

This equation allows the thermodynamic equilibrium constant to be evaluated from isotherm data by integration of the plot of $\ln K_c$ against $\bar{E}_A$ over the complete range of $\bar{E}_A$ values from 0 to 1.

3.2.2.1 Exchanger Phase Water Activity Term

It has generally been assumed that for zeolites, the water activity terms in the Gaines and Thomas (1953) treatment may be ignored when calculating zeolite phase activity coefficients and standard free energy values. If this assumption is not valid,

the integration of $\ln K_c$ between the limits $\bar{E}_A = 0$ and $\bar{E}_A = 1$ to give K_a (equation 3.53) may give a value for ΔG^{θ} that is substantially in error. The cause of this lies in the fact that the standard states for the zeolite phase are each homoionic solid in equilibrium with an infinitely dilute solution of the relevant ion (Gaines and Thomas 1953). Since the actual exchange experiments are carried out at a total solution normality, T_N, and the exchanger undergoes a substantial amount of osmotic swelling in transition from the infinitely dilute solution to a solution strength, T_N, then the activity of water in each of the homoionic M_A and M_B zeolites when contacted respectively with solutions of $M_A^{z_A+}$ and $M_B^{z_B+}$ of normality T_N will not necessarily be unity. Consequently, from the Gibbs-Duhem equation, it follows that the activity coefficients, g_A in the M_A zeolite and g_B in the M_B zeolite, will deviate from unity, even though the zeolite is still in the relevant homoionic form (Fletcher and Townsend 1981(b)). A rigorous thermodynamic treatment therefore requires an integration path involving three steps, as shown in Figure 3.8, which is a modification of the original diagram of Gaines and Thomas (1953).

The expression for K_a in the binary case is

$$\ln K_a = (z_B - z_A) + \int_0^1 \ln K_c \, d\bar{E}_A + \Delta \qquad 3.54$$

where (Barrer and Munday 1971)

Figure 3.8 Diagrammatic representation of the three step integration path for thermodynamic treatment

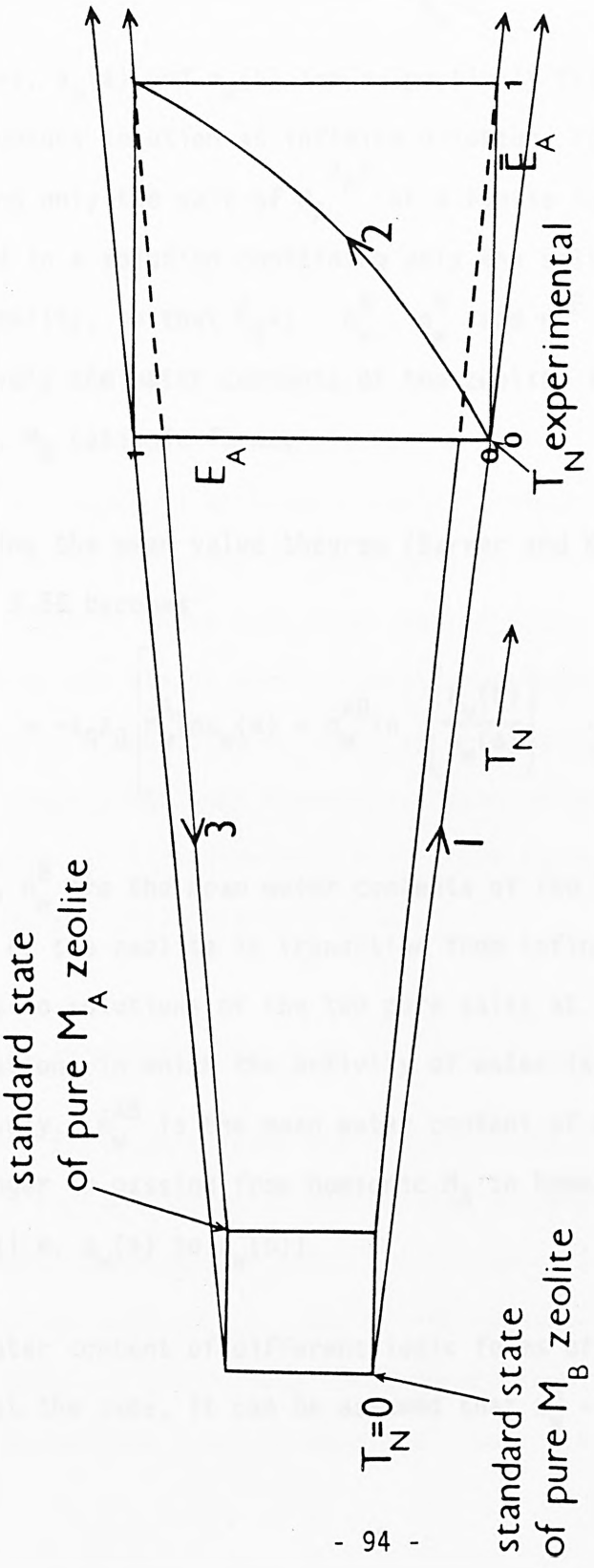

$$\Delta = -z_A z_B \left[\int_{a_w=1}^{a_w(a)} n_w^A \, d\ln a_w + \int_{a_w(a)}^{a_w(b)} n_w^{AB} \, d\ln a_w - \int_{a_w=1}^{a_w(b)} n_w^B \, d\ln a_w \right] \qquad 3.55$$

where $a_w=1$, $a_w(a)$ and $a_w(b)$ are respectively the activity of water in the aqueous solution at infinite dilution; in a solution containing only the salt of $M_A^{z_A+}$ at a finite normality, so that $\bar{E}_A=1$; and in a solution containing only the salt of $M_B^{z_B+}$ at the same normality, so that $\bar{E}_B=1$. n_w^A, n_w^B and n_w^{AB} represent respectively the water contents of the zeolite in its M_A, M_B and mixed M_A, M_B cationic forms.

By applying the mean value theorem (Barrer and Klinowski 1974(a)) equation 3.55 becomes

$$\Delta = -z_A z_B \left[\bar{n}_w^A \ln a_w(a) + \bar{n}_w^{AB} \ln \left(\frac{a_w(b)}{a_w(a)} \right) - \bar{n}_w^B \ln a_w(b) \right] \qquad 3.56$$

where $\bar{n}_w^A$, $\bar{n}_w^B$ are the mean water contents of the homoionic M_A and M_B forms of the zeolite in transition from infinitely dilute solutions to solutions of the two pure salts at the finite concentrations in which the activity of water is $a_w(a)$ and $a_w(b)$ respectively. $\bar{n}_w^{AB}$ is the mean water content of the mixed M_A, M_B exchanger in passing from homionic M_A to homoionic M_B zeolite (i.e. $a_w(a)$ to $a_w(b)$).

If the water content of different ionic forms of the exchanger are almost the same, it can be assumed that $n_w^A = n_w^B = \bar{n}_w^{AB}$ and Δ

becomes zero. However, if the water content of the different ionic forms differ and the amount of swelling is not negligible, but the exchange is carried out in dilute solutions, then the activities of the water in solutions of pure electrolytes at the same normality are approximately the same and almost independent of the mole fractions of the individual cations in solution (since Raoult's law applies). Then equation 3.56 can be written as

$$\Delta = -z_A z_B \left[\bar{n}_w^A - \bar{n}_w^B \right] \ln a_w \qquad 3.57$$

Using equations 3.55 and 3.57 Barrer and Klinowski (1974(a)) calculated values of Δ for exchanges in zeolite A as well as for Cu^{2+}/Na^{+} exchanges in an organic resin. Though the values of the first and third integrals in equation 3.55 could be large the opposite signs of these integrals ensured that their overall contribution was always small. The second term involving n_w^{AB} was generally found to be at least an order of magnitude lower than the other terms and, therefore, insignificant. For determination of K_a, therefore, the Δ term is ignored up to solution normalities of around unity.

3.3 THERMODYNAMIC PROCEDURE FOR PARTIAL EXCHANGE

In many ion exchange systems the maximum level of exchange is less than one. For such cases of partial ion exchange, before thermodynamic treatment of data, the isotherms are "normalised" by expressing the exchange in terms of the exchangeable cations only (Barrer, Rees and Shamsuzzoha 1966; Sherry 1966; Sherry 1968). Thus if the maximum level of exchange observed with the ingoing

ion $M_A^{z_A+}$ is $\bar{E}_{A(max)}$ (Figure 3.5), then the normalised equivalent fraction of ion $M_A^{z_A+}$ in the zeolite, $\bar{E}_A^N$, is related to $\bar{E}_A$ by

$$\bar{E}_A^N = f_N \bar{E}_A \qquad 3.58$$

where the normalising factor $f_N = 1/\bar{E}_{A(max)}$. Then

$$\bar{E}_B^N = 1 - \bar{E}_A^N \qquad 3.59$$

This operation implies that those ions with which the ingoing ion $M_A^{z_A+}$ does not exchange are regarded as part of the zeolite lattice, and are not involved in ion exchange. The standard states remain the homoionic M_A and M_B forms in contact with infinitely dilute solutions of the relevant ion, but the total exchange capacity now corresponds to the maximal level of exchange attainable by $M_A^{z_A+}$ (i.e. $\bar{E}_{A(max)}$) rather than that attainable by $M_B^{z_B+}$. The expression for K_a then becomes (Gaines and Thomas 1953)

$$\ln K_a = (z_B - z_A) + \int_0^1 \ln K_c^N \, d\bar{E}_A^N \qquad 3.60$$

where K_c^N is the normalised Kielland quotient.

Vansant and Uytterhoeven (1971) criticised this approach on two grounds. Firstly, they considered that the normalisation procedure was based on the assumption that the unexchanged fraction of the ions has no influence on the exchange equilibria. Secondly, that the normalisation procedure made no allowance for

$\bar{E}_{A(max)}$ being a function of temperature. They therefore formulated a new procedure which involves four integration steps for the determination of K_a. The first three steps are identical to those used previously (Barrer, Rees and Shamsuzzoha 1966; Sherry 1966; Sherry 1968), but the fourth is an integration from the maximally exchanged M_A form to the fully exchanged M_A form (i.e from $\bar{E}_A^N = 1$ to $\bar{E}_A = 1$). Their "standard states" are therefore the homoionic zeolites in terms of the exchange capacity with respect to the original ion $M_B^{z_B+}$. Since not all sites into which $M_B^{z_B+}$ can exchange are accesible to $M_A^{z_A+}$, it follows that the standard state for the M_A zeolite is physically unattainable. Such a reference state is hypothetical in a different sense to that of other well-known hypothetical standard states, in that its properties cannot be inferred by extrapolation from a situation in which the system is behaving ideally (e.g. in the hypothetical ideal molal salt solution, the properties are inferred by extrapolating from the measured properties of that solution as the molality of the salt $\rightarrow 0$). Therefore, the means of accomplishing, and the physical significance of this fourth integration step, is problematic.

In their reply, Barrer, Klinowski and Sherry (1973) raise this question, and show that the procedure of Vansant and Uytterhoeven (1971) contains other conceptual and mathematical inaccuracies. A rigorous justification of the original normalisation procedure is presented dealing with three possible cases of partial exchange. These are, respectively, a pseudo-equilibrium, partial exchange where $\bar{E}_{A(max)}$ is independent of temperature, and partial exchange where $\bar{E}_{A(max)}$ is a function of temperature. For the latter two cases, thermodynamic treatment of the data is possible.

Barrer, Klinowski and Sherry (1973) argue that if a zeolite has n different sets of sites, the overall standard free energy change ΔG^{θ} may be related to the contributions made by each site group through

$$\Delta G^{\theta} = \sum_{1}^{n} X_i \Delta G_i^{\theta} \qquad 3.61$$

where ΔG_i^{θ} is the standard free energy of exchange per equivalent for the ith set of sites, and the equivalent fraction, X_i, of all cations in the ith set is

$$X_i = \frac{z_A m_A(i) + z_B m_B(i)}{\sum_{1}^{n} (z_A m_A(i) + z_B m_B(i))} \qquad 3.62$$

where $m_A(i)$ and $m_B(i)$ are the molalities of the ion $M_A^{z_A+}$ and $M_B^{z_B+}$ in the ith site set. Similarly, from equation 3.21 it follows that

$$\ln K_a = \frac{-z_A z_B}{RT} \sum_{1}^{n} X_i \Delta G_i^{\theta} \qquad 3.63$$

and

$$\Delta G_i^{\theta} = -(RT/z_A z_B) \ln K_i \qquad 3.64$$

where K_i is the thermodynamic equilibrium constant for the ith set of sites, i.e.

$$K_i = \frac{(\bar{a}_A^i)^{z_B} (a_B)^{z_A}}{(a_A)^{z_B} (\bar{a}_B^i)^{z_A}} \qquad 3.65$$

where $(\bar{a}_A^i)$ is the activity of $M_A^{z_A+}$ in the ith set of sites in the zeolite phase, and (a_A) is the activity of $M_A^{z_A+}$ in the solution phase.

Combining equations 3.63 and 3.64 gives

$$\ln K_a = \sum_1^n X_i \ln k_i \qquad 3.66$$

or

$$K_a = \prod_1^n K_i^{X_i} \qquad 3.67$$

If partial exchange occurs, so that $M_B^{z_B+}$ can exchange into sets 1 to n, but $M_A^{z_A+}$ can only exchange into sets 1 to j, since the total standard free energy change must be the sum of the parts, and these parts only involve sets 1 to j, from 3.61

$$\Delta G^\theta_{(1-j)} = \sum_1^j X_i \Delta G_i^\theta / \sum_1^j X_i \qquad 3.68$$

and similarly from 3.66

$$\ln K_{a(1-j)} = \sum_1^j X_i \ln k_i / \sum_1^j X_i \qquad 3.69$$

But

$$1/\sum_1^j X_i = \frac{\sum_1^n (z_A m_A(i) + z_B m_B(i))}{\sum_1^j (z_A m_A(i) + z_B m_B(i))} \qquad 3.70$$

$$= 1/\bar{E}_{A(max)} = f_N \qquad 3.71$$

Therefore, implicit in a rigorous treatment of partial exchange is the introduction of the normalisation factor f_N. Because the ions in sets k to n are not involved in the exchange, they are not an independently variable component of the crystal phase (Gaines and Thomas 1953) and thus need not be considered directly; their influence is taken into account in the activity coefficients g_A and g_B. Barrer, Klinowski and Sherry (1973) emphasise that each X_i term may or may not be a function of temperature. Thus the alternatives of $\bar{E}_{A(max)}$ being independent, or a function of, temperature are covered, contrary to the inference of Vansant and Uytterhoeven (1971).

The criticism that the earlier normalisation procedure (Barrer, Rees and Shamsuzzoha 1966; Sherry 1966; Sherry 1968) fails to allow for the influence of unexchanged ions on the exchange equilibrium is repeated by Breck (1973(h)), and has appeared in a different form in a review by Cremers (1977). Concerning equations 3.61 and 3.67 Cremers (1977) concludes that implicit for each group of sites are relations such as

$$\mu_A(i) = \mu_A^{\theta}(i) + RT\ln E_A(i).g_A(i) \qquad 3.72$$

where $\mu_A(i)$ is the chemical potential of ion $M_A^{z_A+}$ in the ith site, $\bar{E}_A(i)$ is the equivalent fraction of $M_A^{z_A+}$ in the ith site and $g_A(i)$ the corresponding activity coefficient. The use of equation 3.72 implies that each site set is a separate phase, and such a model is contrary to that of Barrer, Klinowski and Sherry (1973) which is based on that of Gaines and Thomas (1953).

3.4 PREDICTION OF THERMODYNAMIC PARAMETERS USING THE TRIANGLE RULE

The triangle rule has been used (Barrer and Klinowski 1974(b)) to predict thermodynamic reaction parameters for reactions which may be inter-related through appropriate summations and subtractions of the reaction equations. Thus, considering the binary exchange systems M_1/Na-ZEO and M_2/Na-ZEO for which the equilibrium constants K_a and standard free energies $\Delta G^{\ominus}$ have been obtained experimentally using the triangle rule, the thermodynamic parameters for the systems M_1/M_2-ZEO or M_2/M_1-ZEO should be predictable.

For the reactions

$$M_1^{2+} + 2\bar{Na}^{+} \rightleftharpoons \bar{M}_1^{2+} + 2Na^{+} \qquad 3.73$$

$$M_2^{2+} + 2\bar{Na}^{+} \rightleftharpoons \bar{M}_2^{2+} + 2Na^{+} \qquad 3.74$$

$$M_2^{2+} + \bar{M}_1^{2+} \rightleftharpoons \bar{M}_2^{2+} + M_1^{2+} \qquad 3.75$$

where Na^{+}, M_1^{2+}, M_2^{2+} and $\bar{Na}^{+}$, $\bar{M}_1^{2+}$, $\bar{M}_2^{2+}$ are sodium and two different metal ions in solution and crystal phases respectively. Let K_{a1}, K_{a2}, K_{a3} be the equilibrium constants for the reactions 3.73, 3.74 and 3.75 respectively and ΔG_1^{θ}, ΔG_2^{θ}, ΔG_3^{θ} the corresponding standard free energies.

Since

$$K_{a1} = (\bar{a}_{M1} \cdot a_{Na}^2)/(a_{M1} \cdot \bar{a}_{Na}^2) \qquad 3.76$$

$$K_{a2} = (\bar{a}_{M2} \cdot a_{Na}^2)/(a_{M2} \cdot \bar{a}_{Na}^2) \qquad 3.77$$

$$K_{a3} = (\bar{a}_{M2} \cdot a_{M1})/(a_{M2} \cdot \bar{a}_{M1}) \qquad 3.78$$

Then K_{a3} can be expressed in terms of K_{a1}, K_{a2} and

$$K_{a3} = K_{a2}/K_{a1} \qquad 3.79$$

Now consider the reactions

$$M_1^{2+} + 2\overline{Na}^{+} \rightleftharpoons \bar{M}_1^{2+} + 2Na^{+} \qquad 3.80$$

$$M_1^{2+} + 2\overline{NH_4}^{+} \rightleftharpoons \bar{M}_1^{2+} + 2NH_4^{+} \qquad 3.81$$

$$NH_4^{+} + \bar{Na}^{+} \rightleftharpoons \overline{NH_4^{+}} + Na^{+} \qquad 3.82$$

where K_{a4}, K_{a5}, K_{a6} are the equilibrium constants for the reactions 3.80, 3.81 and 3.82 respectively. When K_{a4} and K_{a5} are known, K_{a6} can be predicted since

$$K_{a6} = \left[\frac{K_{a4}}{K_{a5}}\right]^{\frac{1}{2}} \qquad 3.83$$

3.5 IMPORTANCE OF THE THERMODYNAMIC APPROACH

In the discussion so far, the aim has been to calculate the thermodynamic equilibrium constant K_a, which refers to a particular free energy ΔG^{θ} for a given reference state (e.g. 1 atm, 298K). K_a is constant irrespective of the solution strength at which it is determined. In principle, using a thermodynamic approach, the value of K_a so obtained can be used to predict the behaviour of a particular system for a range of conditions without having to carry out further experiments. The

changes in conditions can be in the temperature or pressure of the system, or in the external solution total normality T_N.

3.5.1 Temperature and Pressure Changes

In this section it is indicated how the thermodynamic parameters K_a, ΔG^θ obtained at a particular temperature and pressure can be used to predict the behaviour of the system when the temperature or pressure changes.

From the definition of the Gibb's free energy

$$G = H - TS \qquad 3.84$$

the so-called master equation may be derived

$$dG = VdP - SdT \qquad 3.85$$

combining the first and second laws of thermodynamics. Also, at constant temperature, for a reaction

$$\Delta G^\theta = \Delta H^\theta - T\Delta S^\theta \qquad 3.86$$

where ΔH^θ and ΔS^θ are the standard enthalpy and entropy changes of the system respectively. Under standard conditions the master equation 3.85 becomes

$$d\Delta G^\theta = \Delta V^\theta dP - \Delta S^\theta dT \qquad 3.87$$

where ΔV^θ is the standard volume change of the system (ion exchanger plus solution and vapour).

At constant temperature 3.87 becomes

$$\left[\frac{\partial \Delta G^\theta}{\partial P}\right]_T = \Delta V^\theta \qquad 3.88$$

but

$$\Delta G^{\theta} = -RT\ln k_a \qquad 3.89$$

Substituting 3.89 into 3.88 gives

$$\left[\frac{\partial \ln k_a}{\partial P}\right]_T = -\frac{\Delta V^{\theta}}{RT} \qquad 3.90$$

which describes the relationship between the equilibrium constant and pressure, and is one quantitative description of Le Chatelier's principle.

At constant pressure, equation 3.87 becomes

$$\left[\frac{\partial \Delta G^{\theta}}{\partial T}\right]_P = -\Delta S^{\theta} \qquad 3.91$$

Combining equations 3.91 and 3.86 gives the Gibb's Helmholtz equation, viz:

$$\Delta G^{\theta} = \Delta H^{\theta} + T\left[\frac{\partial \Delta G^{\theta}}{\partial T}\right]_P \qquad 3.92$$

and substituting 3.89 into 3.92 gives

$$-RT\ln k_a = \Delta H^{\theta} + T\left[\frac{\partial}{\partial T}(-RT\ln k_a)\right]_P$$

so that

$$\left[\frac{\partial \ln k_a}{\partial T}\right]_P = \frac{\Delta H^{\theta}}{RT^2} \qquad 3.93$$

This equation is another quantitative description of Le Chatelier's principle, and describes the variation of equilibrium with temperature.

Integration of equations 3.90 or 3.93 enables in principle the evaluation of K_a at any temperature or pressure. In practice ΔV^θ is very small for ion exchange involving zeolites, so that it is not expected that the ion exchange will be markedly affected by pressure changes (equation 3.90). The use of equation 3.93 may be a problem, since the ion site set populations may change with temperature, meaning that the standard states are not comparable. This is a problem which merits further investigation.

3.5.2 Solution Concentration Changes

Helfferich (1962) states that although the Gaines and Thomas (1953) treatment is "thermodynamically exact" and "universally applicable", yet "the dependence of the selectivity on the ionic composition and the concentration of the solution cannot be predicted". Barrer and Klinowski (1974(a)) have shown that this statement should be modified, especially for zeolites, since while the crystal phase activity coefficients g_A and g_B may change markedly with external solution concentration, their ratio remains nearly constant. Thus changes in isotherm shape with the total solution normality T_N may be deduced from changes in Γ, provided an experimental isotherm has been obtained at one value of T_N.

Considering the Gaines and Thomas (1953) treatment once more, and including the water activity terms, then

$$\ln g_A^{z_B} = (z_B - z_A)\bar{E}_B - \ln K_c^{(\bar{E}_A)} + \bar{E}_A \ln K_c^{\bar{E}_A} + \int_{\bar{E}_A}^{1} \ln K_c \, d\bar{E}_A$$

$$- z_A z_B \left[\int_{1}^{a_w(a)} n_w^A \, d\ln a_w + \int_{a_w(a)}^{a_w(\bar{E}_A)} n_w^{AB} d\ln a_w \right] \qquad 3.94$$

$$\ln g_B^{z_A} = -(z_B - z_A)\bar{E}_A + \bar{E}_A \ln K_c^{(\bar{E}_A)} - \int_{0}^{\bar{E}_A} \ln K_c \, d\bar{E}_A$$

$$+ z_A z_B \left[\int_{a_w(E_A)}^{a_w(b)} n_w^{AB} d\ln a_w - \int_{1}^{a_w(b)} n_w^{B} d\ln a_w \right] \qquad 3.95$$

Barrer and Klinowski (1974(a)) evaluated the expressions in the brackets in equations 3.94 and 3.95 and showed that their contributions to $g_A^{z_B}$ and $g_B^{z_A}$ respectively were usually significant, even in zeolites. Therefore as the external solution concentration is changed and the activity of water in each phase correspondingly alters, the $g_A^{z_B}$, $g_B^{z_A}$ values change concomitantly. Thus a given value of $\bar{E}_A$ can correspond to different values of g_A, g_B depending on the external solution concentration.

Combining equations 3.94 and 3.95 gives

$$\ln\left[\frac{g_A^{z_B}}{g_B^{z_A}}\right] = (z_B - z_A) - \ln K_c^{(\bar{E}_A)} + \int_0^1 \ln K_c \, d\bar{E}_A + \Delta \qquad 3.96$$

or (using equation 3.54)

$$\ln\left[\frac{g_A^{z_B}}{g_B^{z_A}}\right] = \ln K_a - \ln K_c^{(\bar{E}_A)} + \Delta \qquad 3.97$$

Since $K_c^{(\bar{E}_A)}$ is the value of the Kielland quotient at a given $\bar{E}_A$, the only physical factors that can affect the ratio of the activity coefficients are the water activity term Δ and the level of salt imbibition. Δ is very small (Barrer and Klinowski (1974(a)) and at low concentrations salt imbibition is neglibible (Barrer and Walker 1964), therefore $g_A^{z_B}/g_B^{z_A}$ must be near-independent of external solution concentration if the total solution normalities are low. Transformation of equations 3.12 and 3.17, for a given value of $\bar{E}_A$, results in the expression

$$\left[\frac{m_B^{z_A}}{m_A^{z_B}}\right]\Gamma = \frac{E_B^{z_A}\,\Gamma}{E_A^{z_B}\,Q} = \frac{K_c \bar{E}_B^{z_A}}{\bar{E}_A^{z_B}} = \frac{K_a g_B^{z_A}\,\bar{E}_B^{z_A}}{g_A^{z_B}\,\bar{E}_A^{z_B}} = \text{constant} \qquad 3.98$$

where $Q = z_B^{z_A} / \left[z_A^{z_B} \cdot T_N^{(z_A - z_B)}\right]$. The significance of equation 3.98 is that since Q is a function of T_N, if the value of E_A is known for a given $\bar{E}_A$ at one value of T_N, provided that activity coefficient data for the two salts (Γ) are known over a range of solution normalities, E_A may be predicted for any T_N. Thus for a chosen $\bar{E}_A$ value at two solution normalities T_{N1}, T_{N2} from

equation 3.98

$$\frac{E_{A1}Q_1}{(1-E_{A1})^{z_A}\Gamma_1} = \frac{E_{A2}Q_2}{(1-E_{A2})^{z_A}\Gamma_2} \qquad 3.99$$

where E_{A1}, Q_1 refer to T_{N1} and E_{A2}, Q_2 refer to T_{N2}. Barrer and Klinowski (1974(a)) solved equation 3.99 iteratively (since $\Gamma = f(E_A)$) from $\bar{E}_A = 0$ to 1, for a range of T_N values. This gave families of isotherms for each different choice of z_A and z_B values. When $z_A \neq z_B$ they noted two important results. Firstly, with increasing dilution, the exchanger displays increasing selectivity for the ion of higher valency, so that at infinite dilution and for $z_A > z_B$ all isotherms become rectangular and the selectivity quotient α (as defined in equation 3.9) becomes infinite (i.e. the exchanger is infinitely selective for the ion of higher valency). Thus, at infinite dilution the properties of the exchanger are of little importance. Secondly, they found that the shape of the isotherm could change completely with T_N, so that an isotherm with no inflexion point could become sigmoid on dilution, and vice-versa. Consequently, the difference between selectivity and thermodynamic affinity is made clear, in that it is obvious that thermodynamic affinity cannot be predicted from the appearance of the isotherm. Also, obtaining a sigmoid isotherm does not in itself indicate that there is more than one type of ion site participating in the exchanger in the zeolite.

3.6 APPLICATION OF DIELECTRIC THEORY TO ION EXCHANGE

Dielectric theory has been used frequently in the past to rationlise various trends in measured ΔG^{θ} values for different ion exchange reactions in zeolites (Barrer, Rees and Shamsuzzoha, 1966;

Barrer and Davies 1969; Barrer, Davies and Rees 1969(b); Barrer and Klinowski 1972; Barrer and Townsend 1976(b); Fletcher and Townsend 1980; Fletcher and Townsend 1981(a)). The reversible work w necessary for the creation of a charge z_e on a sphere of radius r embedded in a medium of permittivity ε is (Bottcher 1952)

$$w = \frac{z^2e^2}{8\Pi r\varepsilon} \qquad 3.100$$

where e is the charge of one electron (1.602×10^{-19} As), and ε is obtained from the relationship $\varepsilon = \varepsilon_r.\varepsilon_o$, where ε_r is the relative permittivity (previously known as the "dielectric constant"). The permittivity of a vacuum, $\varepsilon_o = 8.854 \times 10^{-12}A^2s^4kg^{-1}m^{-3} = 8.854 \times 10^{-12}CV^{-1}m^{-1}$. The reversible work w may be equated to the Helmholtz free energy of charge formation F, since for a condensed phase reaction the work of expansion tends to zero (i.e. $pV \to 0$)

$$w = F \sim G \qquad 3.101$$

and

$$G = H - TS \qquad 3.102(a)$$

$$F = U - TS \qquad 3.102(b)$$

$$H = U + pV \qquad 3.102(c)$$

where G is the Gibb's free energy of charge formation.
Considering the ion exchange reaction

$$z_B E_A^{z_A+} + z_A \bar{E}_B^{z_B+} \rightleftharpoons z_B \bar{E}_A^{z_A+} + z_A E_B^{z_B+} \qquad 3.103$$

It follows that

$$\Delta G = \left[z_B \bar{G}_A + z_A G_B\right] - \left[z_B G_A + z_A \bar{G}_B\right] \quad 3.104$$

If G, $\bar{G}$ refer to the work of charge formation of the ions $M_A^{z_A+}$, $M_B^{z_B+}$ in their respective standard states in the solution and crystal phases, then ΔG becomes a standard free energy change. Then per mole of exchange

$$G^\theta = \frac{Lz^2e^2}{8\pi r\varepsilon} \quad 3.105$$

where L is the Avagadro number (6.023×10^{23} mol^{-1}). Thus, for the above binary exchange

$$\Delta G^\theta = \left[z_B \bar{G}_A^\theta + z_A G_B^\theta\right] - \left[z_B G_A^\theta + z_A \bar{G}_B^\theta\right] \quad 3.106$$

$$\frac{Le^2}{8\pi} \left[\frac{z_B z_A^2}{r_A \bar{\varepsilon}_A} + \frac{z_A z_B^2}{r_B \varepsilon_B} - \frac{z_B z_A^2}{r_A \varepsilon_A} - \frac{z_A z_B^2}{r_B \bar{\varepsilon}_B}\right] \quad 3.107$$

where ε_A, ε_B and $\bar{\varepsilon}_A$, $\bar{\varepsilon}_B$ refer to the permittivities of the ions $M_A^{z_A+}$, $M_B^{z_B+}$ in the solution and crystal phases respectively.

Therefore, dividing by $z_A z_B$ gives the standard free energy change per equivalent

$$\Delta G^\theta = \frac{Le^2}{8\pi} \left[\frac{z_A}{r_A \bar{\varepsilon}_A} + \frac{z_B}{r_B \varepsilon_B} - \frac{z_A}{r_A \varepsilon_A} - \frac{z_B}{r_B \bar{\varepsilon}_B}\right] \quad 3.108$$

3.6.1 Influence of Ionic Radius and Charge

If it is initially assumed (Barrer, Rees and Shamsuzzoha 1966) that the permittivities for pure M_A and M_B zeolites are the same, then

$$\bar{\varepsilon}_A \approx \bar{\varepsilon}_B = \bar{\varepsilon} \qquad 3.109$$

and that the permittivities of the two standard solutions are the same, then

$$\varepsilon_A \approx \varepsilon_B = \varepsilon \qquad 3.110$$

where ε and $\bar{\varepsilon}$ represent the permittivities of the solution and crystal phases respectively. Then relationship 3.108 simplifies to

$$\Delta G^{\theta} = \frac{Le^2}{8\Pi} \left[\left(\frac{z_A}{r_A} - \frac{z_B}{r_B} \right) \left(\frac{1}{\bar{\varepsilon}} - \frac{1}{\varepsilon} \right) \right] \qquad 3.111$$

Experiments and theory have shown (Barrer, Rees and Shamsuzzoha 1966) that for systems involving zeolites and aqueous solutions, $\bar{\varepsilon} < \varepsilon$. Whence

$$\left(\frac{1}{\bar{\varepsilon}} - \frac{1}{\varepsilon} \right) > 0 \qquad 3.112$$

Then the conditions for ΔG^{θ} to be negative (i.e. for the zeolite to show an affinity for ion $M_A^{z_A+}$ over ion $M_B^{z_B+}$) or the converse, are

$$r_A > \left(\frac{z_A}{z_B} \right) r_B \rightarrow \Delta G^{\theta} < 0 \qquad 3.113$$

and

$$r_A < \left[\frac{z_A}{z_B}\right] r_B \rightarrow \Delta G^{\theta} > 0 \qquad 3.114$$

In the case of the uni-univalent exchange, for ΔG^{θ} to be negative the condition is simply that the radius of the ingoing ion should be greater than that of the counter ion. Barrer, Rees and Shamsuzzoha (1966) successfully used conditions 3.112 and 3.113 to provide a semiquantitative explanation for their thermodynamic data. The observed cation affinity sequence for zeolite X, based on their ΔG^{θ} values, is

$$Rb^+ > Ba^{2+} > Cs^+ = Sr^{2+} > K^+ = Ca^{2+} > Na^+ > Li^+$$

Based on the ionic radii of these ions the ion size sequence is

$$Cs^+ > Rb^+ > Ba^{2+} > K^+ > Sr^{2+} > Ca^{2+} > Na^+ > Li^+$$

It is apparent that the affinity sequence is in reasonable agreement with the ion size sequence. The selectivity sequence based on standard free energy changes should only be used as a guide towards understanding the ion exchange behaviour because in a real system selectivities may well be reversed with respect to standard ΔG values. Barrer and Townsend (1976(b)) used this treatment to rationalise the thermodynamic affinity sequence for the exchange of Mn^{2+}, Co^{2+}, Ni^{2+}, Cu^{2+} and Zn^{2+} in synthetic ammonium mordenite. Their affinity sequence (based on measured ΔG^{θ} values) is

$$Mn^{2+} > Cu^{2+} > Co^{2+} > Zn^{2+} > Ni^{2+}$$

which is in good agreement with the theoretical affinity sequence with the single exception of Cu^{2+}

$$Mn^{2+} > Co^{2+} = Zn^{2+} > Ni^{2+} > Cu^{2+}$$

3.6.2 Influence of Zeolite Framework Charge Density

Considering two zeolites of different framework charge densities, equation 3.111 becomes

$$\Delta G^{\theta}_{(lc)} = \frac{Le^2}{8\Pi} \left[\left(\frac{z_A}{r_A} - \frac{z_B}{r_B} \right) \left(\frac{1}{\bar{\varepsilon}_{(lc)}} - \frac{1}{\varepsilon} \right) \right] \qquad 3.115$$

and

$$\Delta G^{\theta}_{(hc)} = \frac{Le^2}{8\Pi} \left[\left(\frac{z_A}{r_A} - \frac{z_B}{r_B} \right) \left(\frac{1}{\bar{\varepsilon}_{(hc)}} - \frac{1}{\varepsilon} \right) \right] \qquad 3.116$$

where the subscripts (lc) and (hc) refers to zeolites having low and high charge densities, respectively. The permittivity of the higher charged zeolite is greater than that found in the lower charged zeolite (Barrer and Klinowski 1972), and since $\bar{\varepsilon}_{(lc)} < \bar{\varepsilon}_{(hc)} < \varepsilon$ (from equation 3.112), then

$$0 < \left(\frac{1}{\bar{\varepsilon}_{(hc)}} - \frac{1}{\varepsilon} \right) < \left(\frac{1}{\bar{\varepsilon}_{(lc)}} - \frac{1}{\varepsilon} \right) \qquad 3.117$$

and it, therefore, must be true that for a given ion exchange reaction

$$\left| \Delta G^{\theta}_{(hc)} \right| < \left| \Delta G^{\theta}_{(lc)} \right| \qquad 3.118$$

Consequently if the sign of ΔG^{θ} (which is determined by one or other of the inequalities 3.113 or 3.114) is positive

$$\Delta G^{\theta}_{(hc)} < \Delta G^{\theta}_{(lc)} \qquad 3.119$$

whereas if the sign is negative

$$\Delta G^{\theta}_{(hc)} > \Delta G^{\theta}_{(lc)} \qquad 3.120$$

Barrer and Klinowski (1972) discussed uni-univalent and uni-divalent exchange in two isostructural chabazites in terms of their framework charge densities, and found that "the ion of larger crystallographic radius is preferred by the zeolite of lower charge density over the entire range of exchanger composition". Earlier work on zeolites X and Y came to a similar conclusion (Barrer, Davies and Rees 1969(b)) and was also confirmed in the case of exchange of amminated silver into NaX, NaY and NaMOR (Fletcher and Townsend 1981(a)).

3.6.3 Modification of Dieletric Theory

The calculated free energy sequence for exchanges has, in certain cases, been shown not to correspond to that predicted by simple dielectric theory (Fletcher and Townsend 1980; Fletcher and Townsend 1981(a)). This may be due to failure of one or both of the two assumptions made in the derivation of equation 3.111 regarding the constancy of the permittivities of the two phases in their two ionic forms. In particular, to assume that $\bar{\varepsilon}_A \approx \bar{\varepsilon}_B = \bar{\varepsilon}$ is an oversimplification if one of the exchanging ions is highly polarisable or if the ion site distributions differ in the two homoionic exchanged forms of the zeolite.

The capacitance of a parallel plate condenser is directly proportional to the permittivity of the medium between the plates (Anderson 1964). Introduction into this medium of species of high polarisability will further increase the capacitance of the condenser, thus reflecting the further increase in the

permittivity of the medium which has occurred. If the ingoing ion $M_A^{z_A+}$ has a substantially higher polarisability than the counter ion $M_B^{z_B+}$, the assumptions that $\varepsilon_B \approx \varepsilon_A$ and that $\bar{\varepsilon}_B \approx \bar{\varepsilon}_A$ must be unjustified. Thus from equation 3.108, the corrected value for the free energy of exchange ΔG^{θ}_{co} becomes

$$\Delta G^{\theta}_{corr} = \frac{Le^2}{8\Pi} \left[\frac{z_A}{r_A} \left(\frac{1}{\bar{\varepsilon}_A} - \frac{1}{\varepsilon_A} \right) - \frac{z_B}{r_B} \left(\frac{1}{\bar{\varepsilon}_B} - \frac{1}{\varepsilon_B} \right) \right] \quad 3.121$$

or, if $z_A = z_B = 1$

$$\Delta G^{\theta}_{corr} = \frac{Le^2}{8\Pi r_a r_B} \left[\left(\frac{r_B}{\bar{\varepsilon}_A} - \frac{r_A}{\bar{\varepsilon}_B} \right) - \left(\frac{r_B}{\varepsilon_A} - \frac{r_A}{\varepsilon_B} \right) \right] \quad 3.122$$

Considering first the solution phase it is obvious that, irrespective of the zeolite involved, providing each zeolite has a common counter ion $M_B^{z_B+}$, the second bracketed term in equation 3.122 will have the same value for all zeolites, even if $\varepsilon_A > \varepsilon_B$. Thus, equation 3.122 becomes

$$\Delta G^{\theta}_{corr} = \frac{Le^2}{8\Pi r_A r_B} \left[\left(\frac{r_B}{\bar{\varepsilon}_A} - \frac{r_A}{\bar{\varepsilon}_B} \right) - k \right] \quad 3.123$$

where k is a constant (Fletcher and Townsend 1981(a)).

Considering now the zeolite phase, if $\bar{\varepsilon}_A > \bar{\varepsilon}_B$ the degree by which the permittivity of $M_A^{z_A+}$ exceeds that of $M_B^{z_B+}$ will be a function of the charge density of the zeolite itself. The higher the charge density of the zeolite, the greater will be the difference in permittivity between the two exchanged forms, since a higher charge density will induce a greater degree of polarisation in

the $M_A^{z_A+}$ ions.

If $r_B < r_A$ it follows that the term in brackets in equation 3.123 is negative, thus

$$\left(\frac{r_B}{\bar{\varepsilon}_{A(hc)}} - \frac{r_A}{\bar{\varepsilon}_{B(hc)}}\right) < \left(\frac{r_B}{\bar{\varepsilon}_{A(lc)}} - \frac{r_A}{\bar{\varepsilon}_{B(lc)}}\right) < 0 \qquad 3.124$$

where $\bar{\varepsilon}_{A(hc)}$, $\bar{\varepsilon}_{A(lc)}$ are the permittivities of ion $M_A^{z_A+}$ in the higher and lower charged zeolites, respectively.

Comparing equations 3.123 and 3.124, it is apparent that allowance for the fact that $\bar{\varepsilon}_A > \bar{\varepsilon}_B$ causes the corrected values of the free energy of exchange ΔG^θ_{corr} to be more negative than the values calculated by the simple theory (equations 3.115 and 3.116), and that correction is greatest for the zeolite of highest charge density. Then

$$(\Delta G^\theta_{corr} - \Delta G^\theta_{uncorr})_{hc} < (\Delta G^\theta_{corr} - \Delta G^\theta_{uncorr})_{lc} < 0 \qquad 3.125$$

Equation 3.123 shows that if $\bar{\varepsilon}_A \neq \bar{\varepsilon}_B$, the direction in which the value of ΔG^θ (as predicted by simple dieletric theory) must be corrected is independent of charges or the ionic radii of the exchanging cations. If $\bar{\varepsilon}_A > \bar{\varepsilon}_B$ the adjustment is in the negative direction, whereas if $\bar{\varepsilon}_A < \bar{\varepsilon}_B$ the converse is true. Thus, for example, the situation may arise where simple dieletric theory predicts a positive value for ΔG^θ but if in fact $\bar{\varepsilon}_A > \bar{\varepsilon}_B$, then not only the calculated value of ΔG^θ but also the sign itself may be predicted erroneously (Fletcher and Townsend 1981(a)).

CHAPTER 4 - EXPERIMENTAL

4.1 RATIONALE OF EXPERIMENTAL WORK

The proposed programme of research involved an examination of the kinetics and equilibrium thermodynamics of ion exchange of trimethyllead cations ($(CH_3)_3\ Pb^+$ or Me_3Pb^+) into a variety of zeolites of different ion exchange capacities (i.e. varying silica : alumina ratios within the aluminosilicate framework). However it was also desirable to study the selectivities of these zeolites for lead only, using conditions which excluded complications arising from the presence of interfering ions. These studies were carried out first. In the moderately acidic Pb^{2+}/Na^+ exchange solutions one might expect the faujasites, X and Y, to be less susceptible to decomposition than zeolite A (Cook, Cilley, Savitsky and Wiers 1982; Wiers, Grosse and Cilley 1982; Allen, Cho and Neubecker 1983; Lutz, Fahlke, Lohse, Bulow and Richter-Mendau 1983) in which the very high selectivity for Pb^{2+} has been demonstrated (Schwuger and Smolka 1976; Hertzenberg and Sherry 1980). Zeolites X and Y are relatively cheap materials that are readily available, and which are known for their high selectivity for some polluting ions. Thus, as a base upon which the research programme could be built, a study of the rate of uptake and selectivity for Pb^{2+} in the presence of Na^+ in a series of five faujasites (zeolite X and four Y-type zeolites having varying silica : alumina ratios) was initiated.

For a given zeolite, comparisons of selectivities for lead over sodium at two different solutions normalities (T_N) should show that the selectivity increases for the divalent ion as the total

concentration of ions in the external solution is decreased (Barrer and Klinowski 1974; Rees 1980). This "valence concentration effect" was tested by examining the above system at two different total normalities of 0.05 and 0.1 equiv. dm^{-3} (throughout this thesis the term "equivalent" means 1 mole of unit positive or negative charges).

The framework charge density of zeolite A is greater than that for zeolite X, hence an examination of the Pb/NaA system was also necessary in order to confirm trends noted for the faujasites, which contradict some literature reports regarding lead exchange in zeolite A (Hertzenberg and Sherry 1980; Cook, Cilley, Savitsky and Wiers 1982; Wiers, Grosse and Cilley 1982), and to test simple dielectric theory predictions (Barrer and Davies 1969; Barrer and Townsend 1976; Fletcher and Townsend 1981(a)).

Application of the "triangle rule" (Barrer and Klinowski 1974(b)) to the systems - Pb/NaX, Pb/CaX and Ca/NaX in order to predict a value of ΔG^{θ} for the Pb/NaX system was also required to confirm dielectric theory predictions (Barrer and Davies 1969; Barrer and Townsend 1976; Fletcher and Townsend 1981(a)). Hence an investigation of the Pb/CaX ion exchange system was undertaken; this would then enable one to compare predicted values of ΔG^{θ} with experiment since the Ca/NaX reaction had already been studied on a similar sample of NaX (Fletcher, Townsend and Loizidou 1983).

An examination of the Pb/CaA ion exchange reaction was also considered necessary in order to check literature data regarding this system (Cook, Cilley, Savitsky and Wiers 1982; Wiers, Grosse and Cilley 1982), and to complete an overall study of Pb^{2+} exchange equilibria as a function of silica : alumina ratio.

Whilst awaiting the arrival of equipment for the study of organic lead exchange in zeolites, Pb/Na ion exchange in two forms of a clinoptilolite sample (raw unexchanged material referred to as natural clinoptilolite-NAT.CLI, and a sodium exchanged sample referred to as fully exchanged clinoptilolite-F.EX.CLI) was investigated since the problem of precipitation had been suspected to occur in some natural zeolites (Barrer and Hinds 1953; Semmens and Seyfarth 1978; Semmens and Martin 1979; Semmens 1981), and clinoptilolite is a cheap, readily available material, known for its high selectivity for some polluting metal ions.

Studies on the equilibrium selectivity characteristics of the ternary exchange system : $Me_3Pb^+/Pb^{2+}/Na^+$, was initiated by concentrating on the Me_3Pb^+/Na^+ binary system in both NaX and NaY. The main aim was to clarify the influences of both the silica : alumina ratio, and the ion size and shape, on the exchange properties of these materials.

In the presence of a high concentration of sodium chloride it was thought that association of the trimethyllead salt to form the anionic complex - $[Me_3PbCl_2]^-$ (which in itself is obviously not exchangeable with a zeolite) could occur. Thus, by comparing the Me_3Pb^+/Na^+ ion exchange characteristics for solutions having a similar Me_3Pb^+ : Na^+ ratio but using anions of sodium of differing complexing ability i.e. chloride, nitrate, perchlorate, it should be possible to note differences, if any, between the three exchanges. Should the association to form the dichloro anionic complex occur in the high chloride background and this conversion be reversible, then as zeolite removed Me_3Pb^+ from solution a shift in the association (equation 4.1) back towards the cation would continue until an equilibrium existed between the three

states:

$$E_{Me_3Pb} \rightleftharpoons E_{[Me_3PbCl_2]^-} \qquad 4.1$$

$$E_{Me_3Pb} \rightleftharpoons \bar{E}_{Me_3Pb}$$

The possible effects of this association reaction to form the anionic complex and subsequently to reach equilibrium with the zeolite also were studied by carrying out exchanges using chloride and nitrate as co-anions for periods up to 2 weeks.

Based upon the above results, examinations of Me_3Pb^+ exchange, in the presence of sodium chloride, were carried out at a total solution concentration of 0.01 equiv. dm^{-3}. These studies required the unambiguous determination of exactly which species of ions were present in which phase. Since in the real effluent system one would be dealing with low levels of Me_3Pb^+ in the presence of high concentrations of sodium chloride, a study of the isotherm at $E_A \rightarrow 0$ was expedited by investigating the removal of up to 100 ppm Me_3Pb^+ in a background of 0.01N NaCl. Subsequently, the concentration of background salt was increased to determine the removal of the same levels of Me_3Pb^+ in a background of 0.01N NaCl.

By the production of acid-treated clinoptilolite one may study the effect, if any, that changes in the framework charge may have on the selectivity for the organolead species Me_3Pb^+, in this natural material. However, since one is dealing with high concentrations of salt in the effluent, it was necessary for the clinoptilolite to be re-exchanged several times with a sodium solution after the acid treatment in order to produce a mixed Na/H clinoptilolite.

By comparing the removal of Me_3Pb^+ by acid-treated clinoptilolite samples with its removal by the original natural zeolite one may determine any changes in selectivity for the organolead species that may occur.

In high-silica zeolites it has been shown that, by careful control of the pH of solution, substantial hydronium exchange may occur without significant structural damage to the zeolite (Chu and Dwyer 1983). However, it has also been shown that zeolite A may undergo hydronium exchange over a range of pH's, and that this may be accompanied by crystal damage (Cook, Cilley, Savitsky and Wiers 1982; Wiers, Grosse and Cilley 1982; Allen, Cho and Neubecker 1983; Drummond, De Jonge and Rees 1983; Lutz, Fahlke Lohse, Bulow and Richter-Mendau 1983). Studies suggest that during any ion exchange study, hydronium exchange also occurs (Bolton 1971; Maes and Cremers 1973). Despite its obvious importance, the mechanism for hydronium exchange in zeolites has been little studied. Thus, as part of this study, aspects of hydronium exchange were also investigated.

4.2 CHEMICAL REAGENTS

All zeolites used in this study were kindly donated by Laporte Industries (Widnes, Cheshire). The synthetic zeolites were obtained as powders (initially in the sodium form) while the clinoptilolite was particulate in nature. Details of the codes which are used in this thesis to distinguish the different batches are given in Table 4.1. All other chemicals used, both for ion exchange experiments and for the analyses were of "AnalaR" grade and were supplied by BDH or Fisons.

Table 4.1

Zeolite type	Si/Al ratio	Batch No.	Code
A	1.00	RD60/81	A
X	1.22	RD61/81	Z1 (or X)
Y	1.48	RD126/81	Z2
Y	1.80	RD127/82	Z3
Y	2.07	RD128/82	Z4
Y	2.39	RD62/81	Z5 (or Y)
Clinoptilolite	5.18	RD173/82	CLI

4.3 PREPARATION OF HOMOIONIC ZEOLITES

4.3.1 Preparation of Sodium Zeolites

Although A, X and the four Y type zeolites were supplied in the sodium form, it was necessary to exchange them with solutions of sodium chloride or sodium nitrate to ensure that they were in the homoionic sodium forms. Approximately 50g of zeolite was exchanged three times for 24 hours at room temperature, with 300 ml of 1N* sodium nitrate (see Section 4.8) in 600 ml polypropylene bottles. Following the final exchange, the zeolite was separated in a centrifuge and then washed carefully with distilled water to minimise hydronium ion (H_3O^+) exchange.

Following washing, the zeolite was dried overnight in an oven at 80°C. The zeolite was then equilibrated with respect to water vapour by placing it in a desiccator over a saturated solution of

*1N refers to 1g equiv. dm^{-3}, hereafter designated by the symbol N

sodium chloride for up to 3 weeks. Subsequently, the zeolite was stored in the dessicator to ensure it maintained its equilibrium quantity of water.

Preparation of the "fully" exchanged sodium form of clinoptilolite (F.EX.CLI) involved exchanging the natural unaltered clinoptilolite (NAT.CLI), (obtained from Laportes), with 1N sodium nitrate up to thirty times.

4.3.2 Preparation of Other Cationic Forms

From the sodium forms of the zeolites a number of other cationic forms were prepared. Samples of CaA and CaX were prepared by exhaustively exchanging, at room temperature, 15g samples of the sodium zeolites with 500 ml aliquots of 0.4N solutions of calcium nitrate (a lower concentration of the divalent salt was used because of the so-called "concentration-valency effect" (Barrer, Klinowski 1974)). After the exchange had been completed the zeolite was separated, washed, dried and equilibrated with water vapour as described in Section 4.3.1.

Trimethyllead exchanged forms of X and Y, used for structural analysis and determination of the lead species in the crystal phase, were prepared in small batches. 3g samples of sodium zeolite were exchanged with 0.01N solutions of trimethyllead chloride at room temperature. The same method of preparation as described previously was followed except that the exchanged forms were dried at 30°C to prevent possible decomposition of the lead species.

Inorganic lead forms of all the zeolites, used for structural analysis, were prepared by exchanging 2g samples of the zeolite with 0.1N solutions of lead nitrate at room temperature, The washing, drying and equilibration procedure was the same as described in Section 4.3.1.

4.4 PREPARATION OF "H-CLINOPTILOLITE"

The preparation of a clinoptilolite sample with a high Si:Al ratio, and possible consequent hydrophobic properties, was also attempted. Two 10g samples of NAT.CLI were taken and one sample treated four times, for 24 hours at room temperature, with 250 ml of 2N hydrochloric acid in a 600 ml polypropylene bottle and the other sample similarly treated with 4N hydrochloric acid. The samples were separated and washed with distilled water then re-exchanged three times with 1N sodium nitrate solution as in Section 4.3.1. The washing, drying and equilibration procedures were the same as in Section 4.3.1.

Hereafter, the samples treated with 2N and 4N hydrochloric acid are designated as 2N CLI and 4N CLI respectively.

The zeolite extracts from successive acid treatments were analysed for aluminium and iron (see Sections 4.6.3 and 4.6.4 respectively), to determine the aluminium content of the remaining zeolite.

4.5 MEASUREMENT OF EQUILIBRIUM ISOTHERMS

4.5.1 Standard Procedure

All ion exchange isotherms were measured at 25°C (298K). The total solution phase concentrations, or total normalities at which the ion exchange systems were studied, are shown in Table 4.2, where the common anion for each system is also included in brackets.

Equilibrium measurements were made by contacting in sealed polypropylene bottles, weighed amounts (0.3 ± 0.005g) of zeolite with 50 ml of solutions of constant total normality T_N, but containing known and varying proportions of the two cations.

During the equilibration the solutions were continually mixed and thermostatted. This consisted of clamping the bottles around the edges of two vertically mounted aluminium wheels, which were driven around by an electric motor, via a central axle. The lower third of each wheel was immersed in water in two thermostatted water bottles so that the bottles passed in and out of the water as the wheels rotate. This allowed continuous mixing of the zeolite and solution phases, and although the bottles were only immersed in water for a third of a revolution thermostatting to within 0.5°C of the temperature of the water bath was obtained.

Isotherm data points in the regions $E_A \longrightarrow 0$ and $E_A \longrightarrow 1$ were obtained by varying the solution to zeolite ratio. In the case of $E_A \longrightarrow 1$, it was necessary in order to obtain some crystal phase compositions to carry out multiple exchanges.

Table 4.2

Total Normalities of Ion Exchange Systems Studied

	Total Normality (T_N)		
	0.1	0.05	0.01
$Pb^{2+}/Na^{+}(NO_3^-)A$	✓	-	-
$Pb^{2+}/Na^{+}(NO_3^-)Z1$	✓	✓	-
$Pb^{2+}/Na^{+}(NO_3^-)Z2$	✓	✓	-
$Pb^{2+}/Na^{+}(NO_3^-)Z3$	✓	✓	-
$Pb^{2+}/Na^{+}(NO_3^-)Z4$	✓	✓	-
$Pb^{2+}/Na^{+}(NO_3^-)Z5$	✓	✓	-
$Pb^{2+}/Na^{+}(NO_3^-)$NAT.CLI	✓	-	-
$Pb^{2+}/Na^{+}(NO_3^-)$F.EX.CLI	✓	-	-
$Pb^{2+}/Ca^{2+}(NO_3^-)A$	✓	-	-
$Pb^{2+}/Ca^{2+}(NO_3^-)Z1$	✓	-	-
$Me_3Pb^{+}/Na^{+}(Cl^-)Z1$	✓a	-	✓
$Me_3Pb^{+}/Na^{+}(Cl^-)Z5$	✓a	-	✓
$Me_3Pb^{+}/Na^{+}(Cl^-)$NAT.CLI	-	-	✓
$Me_3Pb^{+}/Na^{+}(Cl^-)$2N CLI	-	-	✓
$Me_3Pb^{+}/Na^{+}(Cl^-)$4N CLI	-	-	✓

a refers to study of the exchange of 1-100 ppm Me_3Pb^{+} in a background of 0.1 equiv dm^{-3} Na^{+}.

From kinetic studies a period of 7 days was found adequate for the systems to attain equilibrium. When multiple exchanges were used initial exchanges were carried out for 24 hours, followed by a final exchange of 7 days.

After 7 days equilibration, the zeolite and solution phases were separated by centrifuging at 3000 rpm for 5 minutes. The zeolite phase was washed twice with 40 ml portions of distilled water each time. Both phases were then analysed for all exchanging ions. In the case of exchanges with clinoptilolite however, difficulty in the dissolution of the zeolite forced one to determine the crystal phase composition from a knowledge of the original composition and differences in analysis between the solution phase before and after exchange.

4.5.2 Reversibility Tests

Thermodynamics can only be applied to systems which have proved to be reversible over the whole isotherm composition range. Thus, thermodynamic reversibility was checked for all exchanges using the "wet" method (Barrer and Townsend 1976(a)). A normal forward reaction was carried out by exchanging 0.3g of zeolite with 50 cm^3 of exchange solution containing only the ingoing ion. After equilibration the suspension was centrifuged and 25 ml of solution removed and replaced by 25 ml of solution of the same total normality, but with a lower concentration of the ingoing ion. The system was re-equilibrated for 7 days, then separated, and the zeolite washed. Finally, both phases were analysed for all ions as in Section 4.5.1.

An alternative method which has been used in the past is one in which a zeolite which had been exhaustively exchanged with the ingoing ion, is used as the starting material. However, re-distribution of ions may occur during the drying stage and this may result in irreversible exchange (Barrer and Townsend 1976(a)), and therefore this method was not used.

4.6 ZEOLITE ANALYSIS

The bulk zeolite samples were analysed for water, silicon, aluminium and cation content. The crystal phase composition of all isotherm points were also determined by direct analyses of the zeolite for exchangeable cation content (except, as explained above, in the case of clinoptilolite where it had to be inferred).

Analyses of the bulk clinoptilolite samples were kindly carried out, using X-ray fluorescence, by Laporte Industries (Widnes, Cheshire) because of the difficulties involved in dissolution of this zeolite and the number of impurities one normally encounters in such a natural material.

4.6.1 Water

The water content of the zeolite was determined by heating a 0.2g aliquot of zeolite in a platinum crucible at a temperature of 100°C for 1 hour. After cooling in a desiccator the sample was reweighed, and then transferred back to the Meker burners for further heating, until a constant weight was attained. The water content was thus found thermogravimetrically by difference.

4.6.2 Silica

A 0.2g aliquot of zeolite was weighed into a platinum crucible and mixed with about 2g of an equimolar mixture of the anhydrous carbonates of sodium and potassium ("fusion mixture"). The crucible was covered and heated, slowly at first, and then to 1000°C for 1 hour. The crucible was allowed to cool until the salt melt had just solidified and was then immersed in 30 ml of distilled water in a porcelain dish. 30 ml of concentrated hydrochloric acid was added and the dish covered with a watch glass. The dish was warmed on a steam bath for 1 hour, then the platinum crucible was removed after washing carefully to ensure no solid was removed with it. 1 ml of concentrated sulphuric acid was added and the solution evaporated to complete dryness. 30 ml of 1:1 hydrochloric acid solution and a few drops of concentrated sulphuric acid were added, and after the residue had re-dissolved the solution was evaporated to complete dryness again. This process rendered the silica insoluble in dilute acid, while the aluminium remained soluble. Finally, 30 ml of 5% hydrochloric acid were added to the residue and the resulting suspension digested on a steam bath for about 15 minutes. The hot suspension was filtered through a Whatman No. 42 ashless filter paper, and the precipitate washed with hot, very dilute hydrochloric acid, and then with distilled water. The filtrate was made up to 250 ml and put aside for aluminium and iron analysis.

The ashless filter paper was carefully folded and placed in a pre-weighed platinum crucible (weight = W1). The crucible was gently heated over small bunsen burners to dry and char the filter paper, and then the temperature slowly raised, over a period of

hours, until eventually using Meker burners a temperature of 1000°C was attained. This enabled one to completely burn off all the carbon (care must be taken to avoid formation of silicon carbide; hence the slow heating). After heating for 1 hour at 1000°C the crucible was cooled in a dessicator and weighed (weight = W2).

1 ml of water, followed by 7 ml of 48% hydrofluoric acid were then added to the residue. The resulting solution was heated on a hot plate to allow volatile SiF_4 to escape, then when "dry" a similar volume of acid was added and allowed to evaporate to dryness again. The crucible was then transferred to Meker burners and heated at 1000°C for 20 minutes, after which it was cooled in a dessicator and weighed (weight = W3). Consistency of weights before and after this procedure (W3 = W1) indicated that the previous weight difference (W2-W1) was due to the presence of silica only i.e.

$$\%SiO_2 = (W2-W1).100/(\text{wt. of zeolite})$$

In practice, however, W3 tended to be slightly larger than W1, due to traces of sodium and potassium chloride carried over in the filter paper, therefore:

$$\%SiO_2 = (W2-W3).100/(\text{wt. of zeolite})$$

4.6.3 Aluminium

Aluminium was also determined by standard gravimetric analysis Vogel (1978(a)). A 100 ml aliquot of filtrate from the silica analysis was pipetted into a 600 ml beaker and neutralised with 1:1 ammonia solution, 4 ml of 1:1 hydrochloric acid solution were added and the solution was made up to 200 ml with distilled water.

The solution was warmed on a steam bath and 15 ml of 5% oxine reagent (8-hydroxyquinoline) were added. The solution was further warmed to 50°C and 40 ml of 40% ammonium acetate solution slowly added, while stirring. The resulting suspension was heated to 70°C and kept at this temperature (no higher) for 10 minutes.

The solution was cooled to about 40°C, vacuum filtered through a pre-weighed No. 4 sintered glass crucible, and washed thoroughly with hot distilled water. The precipitate was dried at 140°C for 2 hours, then cooled in a desiccator and weighed.

Separate analyses for iron had to be made (Section 4.6.4) since both aluminium and iron are obtained together as the oxinates ($Al(C_9H_6ON)_3$, $Fe(C_9H_6ON)_3$) using this method.

If f grammes of iron were present in the aliquot of filtrate used, the iron present (as the oxine compound) was allowed for as follows:

$$Fe(C_9H_6ON)_3 = \frac{488.31}{55.85} \times f \quad \text{(in grammes)}$$

$$Al = \left[W - \left(\frac{488.31}{55.85} \times f \right) \right] \times \frac{26.9815}{459.44} \quad \text{(in grammes)}$$

where W is the weight of the precipitate in grammes.

4.6.4 Iron

10 ml aliquots of the fusion filtrate were transferred to 50 ml volumetric flasks. To each flask was added 5 ml of 10% hydroxylammonium chloride solution, 5 ml of 1N sodium acetate solution and 4 ml of a 0.25% w/v 1:10 phenanthroline solution. The solutions were made up to 50 ml with distilled water, and then analysed colorimetrically against a reagent blank using an EEL

absorptiometer (604 filter). In the presence of iron, phenanthroline gives a brown-red colour. Beer's law is obeyed up to 6 ppm of iron.

4.6.5 Cation Analysis

4.6.5.1 Extraction of the cations

Before the cation content of the zeolite could be determined, the cations had to be brought into solution. The method used depended on the properties (SiO_2 : Al_2O_3 ratio) of the zeolite under study.

Zeolites A and X (low SiO_2 : Al_2O_3 ratio) were heated at 90°C overnight in a solution 1:1 nitric acid. The solution was then filtered to remove the colloidal silica and then diluted to 250 ml with distilled water.

Zeolite Y did not dissolve completely in nitric acid. The cations were extracted by heating the zeolite at 90°C for three days in a solution 1:1 nitric acid. The solution was then filtered to remove the remaining solid insoluble silica, and then diluted to 250 ml with distilled water.

4.6.5.2 Sodium

Sodium was determined, after suitable dilution, using a Corning 400 flame photometer. The working range was 0-25 ppm and no serious interferences were encountered.

4.6.5.3 Calcium

Calcium was determined, after suitable dilution, using a Perkin-Elmer 370 atomic absorption spectrophotometer at a wavelength of 422.7 nm, and using a nitrous oxide/acetylene flame.

The working range was 0-10 ppm. Aluminium was found to cause interference, and therefore an equal amount of aluminium (in the form of dissolved zeolite) was added to all the standard solutions to allow for this interference. In addition, potassium nitrate (1000 ppm) was added to all solutions as an ionisation buffer (Vogel 1978(b)).

4.6.5.4 Lead

Lead was determined, after suitable dilution, using the absorption spectrophotometer (Section 4.6.5.3), at a wavelength of 283.3 nm and using an air/acetylene flame. The working range was 0-20 ppm. For exchanges involving Me_3Pb^+ the dissolution of the zeolite in 1:1 HNO_3 converts any organolead into the inorganic species. Thus, the number of moles of lead in the crystal phase could be determined using inorganic lead standards.

4.7 ANALYSIS OF CATIONS IN THE SOLUTION PHASE

4.7.1 Sodium and Potassium

Sodium and potassium were determined as described in Section 4.6.5.2. The working range for potassium was, similarly, 0-25 ppm and no interferences were encountered.

4.7.2 Inorganic Lead and Calcium

Lead and calcium were determined by complexometric titrations.

When lead alone was present in solution, the concentration was determined by direct titration with EDTA after the solution had been buffered at pH6 with powdered hexamine, and using xylenol

orange indicator (Vogel 1978(c)). The end-point colour change was red to yellow.

In solutions containing both lead and calcium, methylthymol blue (MTB) allowed lead to be titrated with EDTA at pH6 without interference by calcium, which was subsequently titrated at pH12 (Vogel 1987(d)). An aliquot of solution was pipetted into a 250 ml conical flask and diluted with about 25 ml of distilled water. About 50 mg of 1 MTB:100 KNO_3 mixture was added followed by nitric acid until the solution was yellow, followed by powdered hexamine until the solution had an intense blue colour (pH6). This was titrated with standard EDTA solution to give the lead concentration in solution. 1N sodium hydroxide solution was added until the pH of the solution had risen to 12 (pH meter). Titration of this bright blue solution with EDTA was continued until the colour changed to grey and this gave the concentration of calcium.

Determination of lead and calcium at concentrations too low to titrate was carried out by atomic absorption spectrophotometry. For lead the same procedure as for the zeolite phase (Section 4.6.5.4) was used, while for calcium the same procedure as the zeolite phase (Section 4.6.5.3) was also used except that no aluminium was added to the standards.

The accurate determination of lead at concentrations less than 2 ppm and down to 10 ppb (parts per billion) was carried out voltametrically using a EG & G model 264 polarograph, operating in the differential pulse anodic stripping mode (i.e. DPASV) and employing a hanging mercury drop electrode. The background

solution used was 0.1 mol dm^{-3} $NaNO_3$. Deposition of lead onto the mercury drop was carried out at -0.75V (against a standard Ag/AgCl reference electrode). The stripping scan was performed over the range -0.75V to -0.45V, with the lead peak occurring at a half wave potential of -0.62V. The concentration of lead was determined by standard addition.

4.7.3 Trimethyllead

Trimethyllead was determined, after suitable dilution, using the same procedure as for inorganic lead in Section 4.6.5.4 except that the standards were made up of 0-20 ppm trimethyllead. For samples containing greater than 10^{-2} mol dm^{-3} Na^+ standards had to contain an equal amount of sodium (see Section 6.4.2.1).

For the determination of trimethyllead concentrations less than 1 ppm a modification of the polarographic system described in Section 4.7.2, using a different cell system (Figure 4.1) allowed the detection of organolead species down to 0.02 ppb (Hodges and Noden 1979). The standard DPASV procedure for analysis is as follows (this is the procedure laid down by Associated Octel (Hodges 1984), however the actual procedure used was varied slightly (Section 6.4.2.2.2)):

Special Apparatus

Anodic stripping voltammetry cell.

"Glassy carbon electrode" (diameter of disc 3 mm).

Platinum spiral counter electrode in a salt bridge.

Saturated Calomel reference electrode in a salt bridge.

Figure 4.1 Anodic stripping voltammetry cell

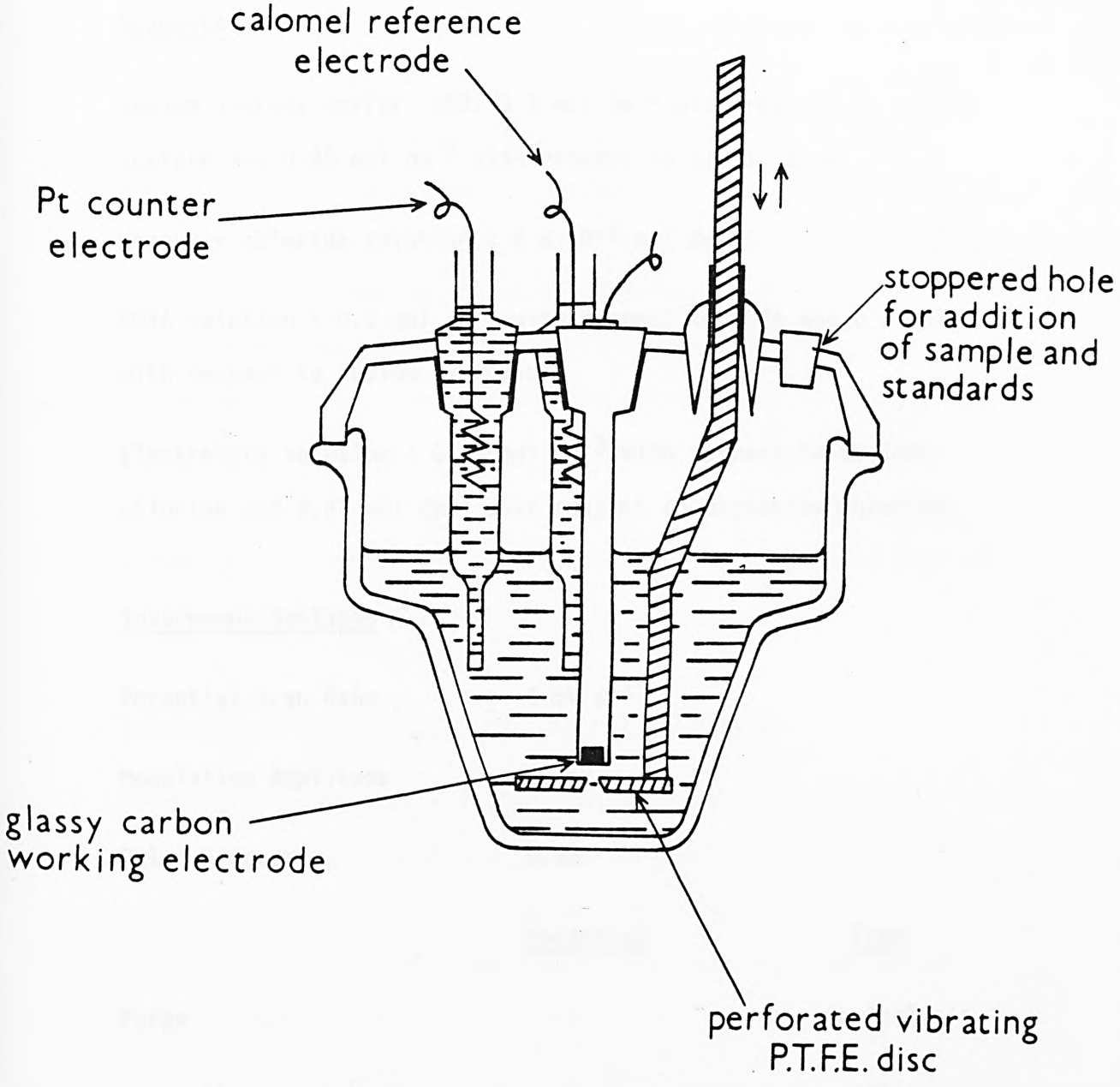

Vibrator/stirrer - a conically perforated PTFE disc fixed to the armature of a Rena 301 aquarium pump.

Deoxygenated nitrogen was passed through distilled water to reduce evaporation in the cell at a controlled flow of 200 ml min^{-1}.

Reagents

Sodium acetate buffer, pH5: 3.2 mol dm^{-3} with respect to sodium acetate and 0.88 mol dm^{-3} with respect to acetic acid.

Mercuric chloride solution : 5 x 10^{-3} mol dm^{-3}.

CDTA solution : 0.2 mol dm^{-3} with respect to CDTA and 0.5 mol dm^{-3} with respect to sodium hydroxide.

Electrolyte solution : 0.51 mol dm^{-3} with respect to sodium chloride and 0.07 mol dm^{-3} with respect to magnesium chloride.

Instrument Settings

Potential Scan Rate	5 mV s^{-1}
Modulation Amplitude	50 mV
Pulse Frequency	0.5s

	Potential	Time
Purge	-	see Analysis
Deposition	see Analysis	120s
Final	-0.20V	-

Analysis

Blank determination

Depending on the size of the aliquot of sample, the volume of electrolyte was varied so that the total volume of the blank plus sample was 50 ml. Therefore up to 48.5 ml of electrolyte solution (see Section 6.4.2.2.2) was measured into the cell, and to this were added 0.5 ml each of acetate buffer, mercuric chloride solution and CDTA solution. The deposition potential was set to -0.70V and the purge time to 4 minutes. The analysis cycle was allowed to run after which there should have been a very small lead peak (<2 mm) at -0.52V. The same blank sample was run again, as previously, but with a deposition potential of -1.00V (in the blank there should not be any lead species present so one may carry out this blank determination just once with a deposition potential of -1.00V). Allowance had to be made for this peak at -0.52V in the determination of the organolead species.

Determination of Alkyllead in the Sample Solution

To the cell containing the electrolyte, a suitable aliquot of the sample was added through the stoppered hole without disturbing the position of the electrodes (Figure 4.1). The deposition potential was set to -0.70V, the purge time to 1 minute, and the analysis cycle allowed to run.

A peak at -0.52V indicated the presence of $(CH_3)_2Pb^{2+}$ (or Me_2Pb^{2+}) in the sample.

The above procedure was repeated but this time with the deposition potential set at -1.00V. An increased peak height over that obtained when depositing at -0.70V indicated the presence of Me_3Pb^+ in the sample.

Calibration by Standard Addition

Trimethyllead (Me_3Pb^+)

Following the above determination, a suitable aliquot of Me_3Pb^+ standard was added to the contents of the cell by means of a microlitre pipette (e.g. 10 µl of 100 ppm standard in 50 ml is an addition of 20 ppb). The deposition and scanning cycle was repeated as before with the deposition potential set on -1.00V.

Dimethyllead (Me_2Pb^{2+})

Following the Me_3Pb^+ calibration, to the contents of the cell a suitable aliquot of Me_2Pb^{2+} standard (100 ppm) was added. The deposition and scanning cycle was repeated as before with the deposition potential set on -0.70V.

Calculation

At E_d = -0.70V, Me_2Pb^{2+} is measured whilst at E_d = 1.00V both Me_2Pb^{2+} and Me_3Pb^+ are measured.

From the peak heights obtained for the different deposition conditions and subsequent standard additions, the concentrations of Me_2Pb^{2+} and Me_3Pb^+ in the orginal sample were calculated.

4.7.4 Magnesium

Magnesium was determined using the atomic absorption spectrophotometer (Section 4.6.5.3) at a wavelength of 285.2 nm using a nitrous oxide/acetylene flame. The working range was 0-2 ppm, and no interferences in the solution phase were encountered.

4.7.5 Aluminium

As part of the study on hydronium exchange a check for aluminium in some exchange solutions was made. Following separation of the two phases (Section 4.5.1) the solutions were filtered under vacuum using a micropore filter (0.45 μm) to remove zeolite fines.

Amongst the reagents that have been used for the colorimetric determination of aluminium is Eriochrome Cyanine R (Vogel 1978(e)). At a pH of 5.9-6.1 zinc, nickel, manganese and cadmium interfere negligibly, but iron and copper must be absent.

An aliquot of the solution was transferred to a 100 ml beaker, 5 ml of 5-volume hydrogen peroxide were added and mixed well. The pH of the solution was adjusted to 6.0 (using either 0.2 mol dm^{-3} sodium hydroxide or 0.2 mol dm^{-3} hydrochloric acid), then 5 ml of 0.1% w/v Eriochrome Cyanine R solution added and mixed well. 50 ml of pH6 buffer solution were added and without delay diluted to 100 ml in a graduated flask. After 30 minutes the absorbance of the solutions were measured using an EEL absorptiometer with a 605 filter.

Standards, up to 3.5 ppm in the final solution, were treated similarly. This method is sensitive down to 0.1 ppm.

For those solutions containing lead it was not possible to use this method as the procedure involved the use of hydrogen peroxide, and a lead oxide precipitate was formed. Also the method was carried out at pH6 and it was shown that lead hydroxide precipitates out of solution at pH5.9 (Section 6.3.1.1). Thus, for the lead containing solutions atomic absorption spectrophotometry (see Section 4.6.5.3) was used at a wavelength of 309.3 nm using a nitrous oxide/acetylene flame. The working range was 0-50 ppm, with a sensitivity of 1 ppm which was lower than the colorimetric method. Potassium nitrate (1000 ppm) was added to all solutions as an ionisation buffer (Vogel 1978(b)).

4.8 PRECIPITATION STUDIES

The homoionic sodium form of zeolite 1 (NaZ1) was initially prepared by exchanging with 1N NaCl solution. When overexchange was noted in the first system studied (Pb^{2+}/Na^{+}Z1 exchange at 0.05N and 0.1N) precipitation of lead chloride due to residual chloride anion remaining adsorbed on the zeolite was considered to be a possible explanation. Thus, a further sample of NaZ1 was prepared (as in Section 4.3.1) by exchange with 1N sodium nitrate solution and samples exchanged with several Pb^{2+}/Na^{+} exchange solutions from both total normalities, to compare with the original system. Subsequently, all homoionic zeolites were prepared by exchange with the nitrate salt to discount any possibility of lead chloride precipitation.

To determine the pH at which precipitation of basic lead salt occurred several solutions of constant normality (0.1 equiv. dm^{-3}), but with varying proportions of the lead and sodium ions, were made up and titrated against dilute ammonia.

Overexchange in systems involving Pb^{2+} exchange could be investigated by comparing total cation recovery in the zeolite by direct analysis (Section 4.6) with the theoretical cation content based on the exchange capacity (i.e. aluminium content).

X-ray analysis (Section 4.10) and scanning electron microscopy (Section 4.11) were used to elucidate the nature of this overexchange.

4.9 KINETIC STUDIES

4.9.1 Inorganic Lead/Sodium Exchange

A limited study was carried out in order to investigate the rate of exchange of lead into the range of faujasites (Section 4.2). By varying the zeolite:solution ratio from 0.1 to 1% w/v, (see Table 4.3), one can determine the rate of removal of lead from solution for varying quantities of zeolite.

Table 4.3

weight of zeolite (grammes)	volume of 0.001M $Pb(NO_3)_2$ solution (ml)	zeolite:solution ratio (% w/v)
0.05	50	0.1
0.1	50	0.2
0.2	50	0.4
0.3	50	0.6
0.4	50	0.8
0.5	50	1.0

The sample of zeolite was added to 50 ml of 10^{-3} mol dm^{-3} lead nitrate solution. The solution was stirred mechanically and the concentration of Pb^{2+} monitored using an Orion Pb^{2+} ion selective electrode. The zeolite/solution mixture was then transferred to sealed polypropylene bottles, left to equilibrate and the two phases then separated (Section 4.5.1). The equilibrium concentration of Pb^{2+} in solution was determined using the ion selective electrode. Thus, the rate of removal of Pb^{2+} ions from solution and the fractional attainment of equilibrium (F.A.E.) was ascertained (when the concentration of Pb^{2+} in the equilibrium solution was too low to be measured by the ion selective electrode it was taken as 1×10^{-7} mol dm^{-3} for the purposes of determination of F.A.E.).

The electrode was calibrated before and after each run so that any electrode "drift" could be accounted for.

4.9.2 Trimethyllead/Sodium Exchange

The length of time needed to allow a Me_3Pb^+/zeolite system to attain equilibrium was studied by exchanging similar Me_3Pb^+/Na^+ solutions of constant total normality (T_N = 0.01 equiv. dm^{-3}) with NaX and NaY for up to 2 weeks.

Both the nitrate and chloride sodium salts were investigated which would also give information on the possible long term association of Me_3Pb^+ in a high chloride background (see Section 4.1)

4.10 X-RAY ANALYSES

The crystallinities of all zeolite samples were examined by powder X-ray diffraction using a Guinier camera and employing CuKα radiation.

4.11 ELECTRON MICROSCOPIC ANALYSES

Any gross crystal damage which may have occurred during ion exchange was examined for by scanning electron microscopy (S.E.M.) using a JEM/JOEL 100B electron microscope. S.E.M. was also used for the indication of precipitation of basic lead salt on the surface of the crystals during Pb^{2+} exchange. At the same time EDAX (Energy dispersive analysis by X-rays) was employed to obtain semi-quantitative analyses on a lead-exchanged sample of zeolite X.

4.12 PARTICLE SIZE

The particle size distribution of the range of faujasites (see Section 4.2) and zeolite A were determined by laser diffractometry using a Malvern Particle Sizer 3600D. Results were compared with those obtained by S.E.M. (see Section 4.11).

4.13 CRYSTAL PHASE SPECIATION OF LEAD FOLLOWING Me_3Pb^+/Na^+ EXCHANGE

The unambiguous determination of the species of lead in the zeolite following exchange with Me_3Pb^+ containing solutions was attempted using infra-red analysis and by DPASV (Section 4.7.3).

4.13.1 Infra-Red Analysis

Forms of zeolites X and Y exchanged with trimethyllead (Section 4.3.2) were analysed, using the KBr disc technique, on a Perkin Elmer 983G Infra-red spectrophotometer, and their infra-red patterns compared with those of their respective sodium forms, which were analysed similarly.

4.13.2 DPASV

A 0.3g sample of NaX was exchanged, as described in Section 4.3.2, with 100 ml of 0.01 N $(CH_3)_3PbCl$ solution. After 7 days the two phases were separated, the zeolite washed twice with 40 ml of distilled water, then re-exchanged with 100 ml of 0.01N sodium chloride solution. After a further 7 days the two phases were separated again.

The solution phase was analysed for the levels of Pb^{2+} by DPASV (Section 4.7.2) and for Me_3Pb^+ (Section 4.7.3).

4.14 INVESTIGATION OF HYDRONIUM EXCHANGE IN ZEOLITES

Hydronium exchange occurs concurrently as other exchange processes take place. A comparison of the total cation recovery in the zeolite by direct analysis (Section 4.6) with the theoretical cation content based on the exchange capacity (i.e. aluminium content), makes it possible to estimate the equilibrium level of hydronium exchange.

The mechanism by which hydronium exchange occurs has, as far as is known, received very little attention. Thus, as part of the overall study, a series of kinetic tests were carried out on the

exchange systems discussed in this thesis in order to investigate this phenomenon. A 0.3g sample of zeolite was added to 50 ml of exchange solution which was stirred mechanically, and the concentration of hydronium ions were monitored over the first five minutes of exchange using a pH electrode. The zeolite/solution mixture was then transferred to sealed polypropylene bottles, left to equilibrate, the two phases separated (Section 4.5.1) then the solution was filtered through membrane filters (0.45 μm) to remove zeolite fines. The pH of the equilibrium solution was measured and this solution phase analysed for aluminium (Section 4.7.5).

CHAPTER 5 - RESULTS

5.1 ANALYSIS OF ZEOLITES

Chemical analyses of the zeolites are shown in tables 5.1 - 5.3, whilst tables 5.4 and 5.5 present these results in terms of both their oxide formulae and unit cell compositions.

The cationic composition of NAT.CLI and F.EX.CLI given in tables 5.4 and 5.5 are the levels which were determined as being a true representation of the total number of apparently exchangeable cations (see Section 6.1.3.2).

For zeolites where the cation content was found to be less than the exchange capacity (as determined by the aluminium content), the difference was considered to be due to hydronium exchange. In table 5.5 therefore, the unit cell compositions show inferred levels of hydronium exchange. The proton contents of the acid treated clinoptilolites were determined similarly.

The results presented in tables 5.1 and 5.2 are averages of up to ten analyses per zeolite component. The difficulty in determining the silica content accurately was shown by the fact that individual analyses differed by up to 1% while for the alumina, cation and water contents the individual analyses only differed by up to 0.3%. The total analyses were low by as much as 3%, which is a reflection of the silica analyses as well as hydronium exchange.

Where two batches of the zeolite were prepared (i.e. NaZ1 (I and II) and NaZ5 (I and II)) the similarity between the batches was good, though the total analyses in the second batches were

greater, especially with NaZ1. This was probably due to improvements in analytical technique, together with greater care being taken to take into account the possibility of hydronium exchange.

No iron was detected in the faujasites or zeolite A.

Elemental analsyes for the data presented in table 5.3 were carried out by Laporte Industries, Widnes, using X-ray fluorescence spectrometry.

X-ray powder data for the various exchanged forms of the zeolites are presented in tables 5.6 - 5.29 and representative X-ray diffractograms are shown in Figures 5.1 - 5.3. Where diffractograms were similar, such as those for the sodium faujasites, only one figure is presented as illustration.

All original zeolite samples appeared to give standard diffraction patterns, and variations occurred in the peak positions and intensities as a result of variation in the cation composition. However, detailed analysis of the diffractograms was made difficult due to low peak intensities and poor resolution in some cases.

Particle size distributions of zeolite A and the faujasites, as determined by laser diffractometry, are presented in table 5.30. It is clear that the results are unlikely to represent crystal sizes, but rather the agglomeration of crystals. This was confirmed by electron microscopy, which revealed the mean crystallite sizes for zeolites A, X and the four Y-type zeolites to be approximately 2.1 and 0.2 microns respectively.

Attempts to break up the aggregates into their constituent crystals by ultrasonics proved unproductive, and indeed in the case of NaZ2 and NaA the particle sizes appeared to increase.

In the case of the faujasites it is interesting to note that the mean and size range of the aggregates increased as the Si:Al ratio was increased. However, the mean and size distribution of NaA aggregates were amongst the largest measured, yet zeolite A has the lowest Si:Al ratio.

Table 5.31(i) includes the relevant data necessary for calculation of the framework, and framework charge densities as well as the void fractions of the faujasites, which are presented in table 5.31 (ii). The framework density as g cm^{-3} (expression (a) : Table 5.31 (ii) is said to be equal to ten times the number of tetrahedra per unit volume of 1000 $\mathring{A}^3$ (Breck 1973(i)). This latter expression can be derived from a simple calculation involving the measured unit cell volume and number of tetrahedra per unit cell. Calculation of the void fractions was carried out based upon a "corrected equation" rather than that presented by Breck (1973(j)) (see section 6.1.2.3).

Based on one's aluminium and silicon analyses it is possible to calculate the unit cell diameter (Breck and Flanigen 1968). This is presented in table 5.32 and figure 5.4 is presented to illustrate the linear relationship between the unit cell diameter and number of aluminium atoms per unit cell for the synthetic faujasites and the analyses presented here when fitted to this derived expression.

Table 5.33 shows the alumina content of the acid treated clinoptilolite as estimated from the aluminium determination of

the 2N and 4N hydrochloric acid extracts. Figure 5.5 illustrates the change in alumina content of these clinoptilolite samples.

5.2 UPTAKE OF LEAD (II) BY THE FAUJASITES

A summary of the rate of uptake of Pb^{2+} ions by sodium faujasites is presented in Table 5.34 (experimental data presented in Appendix 1). It can be seen, for example, that for zeolite 2 at a concentration of 0.1% w/v the times taken to reach 70%, 80% and 90% of the equilibrium concentration are 70, 180 and 600 seconds respectively.

Data were not obtainable where the rate of exchange was much too rapid to measure (for example, zeolite 1 at a concentration of 0.2% w/v had reached over 90% of the equilibrium concentration by the first measurement at 5 seconds).

Figure 5.6 illustrates the effect of increasing the quantity of zeolite suspended in solution (i.e. % w/v), whilst figure 5.7 shows a comparison of the rate of Pb^{2+} ion uptake by the various faujasites for the same quantity of zeolite suspended in solution.

5.3 ION EXCHANGE OF LEAD (II) IONS IN ZEOLITES

5.3.1 Exchange of Lead (II) Ions in Synthetic Faujasitic Zeolites

5.3.1.1 Lead-sodium ion exchange in faujasites

Summaries of the equilibrium data in terms of E_{Pb} and $\bar{E}_{Pb}$ for exchanges at both total normalities are presented in tables 5.35 and 5.36 (experimental data, in order of increasing E_{Pb}, are presented in Appendix 2). Ion exchange isotherms (figures 5.8 -

5.17) illustrate both the very high selectivity for lead, and the over-exchange which was observed for all these systems.

The equivalent fraction of the ions in the solution (E_A and E_B) and in the crystal phase ($\bar{E}_A$ and $\bar{E}_B$) were normally calculated on the basis of the measured concentrations of the ions in the two phases (Equations 2.2 and 2.3). However, where the concentration of lead in the crystal phase was such that it was greater than the exchange capacity of the zeolite, then Equation 5.1 was used to evaluate $\bar{E}_{Pb}$, since under these conditions the use of equation 2.3 is misleading (since equation 2.3 makes $\bar{E}_{Pb}$ always to be less than 1):

$$\bar{E}_{Pb} = 2\bar{m}_{Pb}/\bar{Q} \qquad 5.1$$

where $\bar{Q}$ is the ion exchange capacity of the zeolite, based on the known frameowrk aluminium content. In such cases $\bar{E}_{Na}$ was determined similarly:

$$\bar{E}_{Na} = \bar{m}_{Na}/\bar{Q} \qquad 5.2$$

Non-stoichiometric exchange and irreversibility precludes rigorous thermodynamic treatment of the data, but selectivity data for the exchanges are conveniently represented by plots of the separation factor α against $\bar{E}_{Pb}$ (Figures 5.18(a) and (b)) where (Barrer and Klinowski 1974(a)):

$$\alpha = \bar{E}_{Pb} \; m_{Na} \; / \; \bar{E}_{Na} \; m_{Pb} \qquad 5.3$$

Note that the selectivity plot for Pb^{2+} ion exchange in NaA is also included in Figure 5.18(b). The relevant data for these plots are given in Tables 5.37 and 5.38.

Comparison of Pb^{2+}/Na^{+} exchanges in two homoionic sodium forms of zeolite 1 which were prepared respectively using sodium chloride and sodium nitrate are presented in table 5.39.

The pHs at which $Pb(OH)_2$ precipitation occurs in Pb^{2+}/Na^{+} exchange solutions at a total normality of 0.1g equiv. dm^{-3} are presented in table 5.40. Figure 5.19 illustrates the change in pH at which precipitation occurs as the concentration of lead in the exchange solution is increased.

Figure 5.20 shows the trends in total normalities of the solution phase after exchange, and figure 5.21 the trends in cation recovery. Cation recovery (%) is defined as $100 \times (2\,\bar{m}_{Pb} + \bar{m}_{Na})/Q$, and was determined by direct analysis of the zeolite phase after centrifugal separation of the phases. Data for these plots are presented separately in Appendix 2.

5.3.1.2 Lead-calcium ion exchange in zeolite X

The ion exchange isotherm in figure 5.22 illustrates the change in selectivity of the Pb/CaX system. The zeolite is highly selective for lead at low lead loadings, but a converse very strong preference for calcium is exhibited at high loadings. This is further exemplified in the corresponding selectivity plot presented in figure 5.23, which also compares the selectivies for lead of the sodium and calcium forms of both zeolites A and X. Table 5.41 contains the selectivity data for the Pb^{2+}/Ca^{2+} exchanges in these zeolites (data for the Pb^{2+}/Na^{+} exchanges were presented in table 5.38). Trends in cation recovery for Pb^{2+}/Ca^{2+} and Pb^{2+}/Na^{+} exchange in zeolites A and X are presented in figure 5.24 (relevant data presented in Appendix 2).

5.3.2 Exchange of Lead (II) Ions in Zeolite A

5.3.2.1 Lead-sodium ion exchange in zeolite A

The very rectangular lead-sodium ion exchange isotherm presented in figure 5.25 illustrates the very strong preference for lead over sodium over most of the isotherm. The selectivity for lead over sodium in A (i.e. a plot of the separation factor α against $\bar{E}_{Pb}$), is included in figure 5.18(b), which is intended to illustrate the effect of varying the silica:alumina ratio on the selectivity of zeolites for lead (see also table 5.38). The same selectivity plot is also found in figure 5.23, which compares the selectivities for lead of the sodium and calcium forms of zeolites A and X.

Figure 5.20 includes the trend in total normality of the solution phase after exchange for the Pb^{2+}/Na^{+} exchange in zeolite A, and figure 5.21 gives the trend in terms of the percentage cation recovery for the crystal phase. A similar plot is presented in figure 5.24, which compares cation recoveries for the different forms of zeolites A and X. Data for the illustrations are presented in Appendix 2: Table 12.

5.3.2.2 Lead-calcium ion exchange in zeolite A

The isotherm for the Pb/CaA system is shown in figure 5.26. Again, a high degree of selectivity for lead over calcium is observed, together with over-exchange. Table 5.41 contains the selectivity data for Pb^{2+}/Ca^{2+} exchange in zeolite A, and a plot of this data is presented in figure 5.23. Figure 5.24 includes the trend in crystal phase cation recovery for the Pb/CaA ion exchange system and compares it with the other cationic forms of

zeolites A and X (relevant data presented in Appendix 2: Table 13).

5.3.3 Exchange of Lead (II) Ions in Clinoptilolite

Comparisons of the crystal phase composition determined by (A) by acid dissolution of crystal phase and subsequent elemental analyses, and (B) computer calculations, based on the original cation composition and elemental analysis of the solution phase before and after exchange, are compared in table 5.42 for the unexchanged clinoptilolite material (NAT.CLI) and a "fully" sodium exchanged sample (F.EX.CLI). These data correspond to the materials after exchanging with a couple of lead/sodium solutions (T_N = 0.1g equiv. dm^{-3}).

Direct treatment of silica rich zeolites with strong acid results in the progressive replacement of the cation by hydronium ion, and eventually breakdown of the aluminosilicate framework. It can be seen from the data in table 5.42 that, in nearly all cases, method (A) gave lower cation recoveries than method (B). Whereas method (B) takes into account all the available cations for exchange, method (A) relies on recovering the exchangeable cations from the zeolite. It is clear that the acid treatment employed was insufficient to remove all the exchangeable cations from the framework. It was thought that since it was difficult to completely breakdown this highly siliceous zeolite, subsequent determination of crystal phase compositions by method (B) would be more appropriate.

The isotherms for lead exchange in both forms of the clinoptilolite (figures 5.27 and 5.28) demonstrate reasonably high

selectivity of this zeolite for the lead ion, but there are significant differences in selectivity between the two materials.

A plot of the selectivity data for these exchanges are presented in figure 5.29, and illustrate the comments made above. In a number of cases, after equilibration the concentration of counterion in solution was greater than that found for the original composition. In such instances, the crystal phase counterion content was designated as zero for the isotherm (Appendix 2: Tables 16 and 18), and an arbitrarily low value was inserted into the calculation, so that values for the separation factor were then meaningless (table 5.43). Such data were not plotted in figure 5.29.

5.4 ION EXCHANGE OF ORGANOLEAD IONS IN ZEOLITES

5.4.1 Analysis of Alkyllead Species

5.4.1.1 Analysis of Me_3Pb^+ by atomic absorption spectrophometry

Attempts to use inorganic lead solutions as calibrants to determine Me_3Pb^+ concentrations in solution by A.A.S. (one needs to take into account the difference in cationic weights) were found to be unsuitable. Low readings were observed for a standard Me_3Pb^+ ion calibration (table 5.44). Suitable acid pretreatments of the stock solution, from which the calibration solutions had been made, showed it to be of approximately the correct concentration (table 5.45), so that low readings had to be accounted for in some other way.

Interference of the analysis for the Me_3Pb^+ ion by A.A.S. which arose from high concentrations of background sodium, is illustrated in tables 5.46 and 5.47.

5.4.1.2 Me_3Pb^+ analysis by DPASV

A comparison of the DPASV technique using the standard (section 4.7.3) and modified procedures (table 5.48 and figure 5.30, and table 5.49 and figure 5.31 respectively) illustrate the improvement in reproducibility of successive analyses for the same standard addition which resulted from the use of increasing purge times. Figure 5.32 exhibits the non-linearity of the same standard calibrations.

The sensitivity changes which occur from one calibration run to the next are presented in table 5.50, and figure 5.33 shows how the sensitivity of the instrument appeared to decrease over a day.

On comparing the Me_3Pb^+/Na^+ ion exchange characteristics for solutions having a similar Me_3Pb^+ : Na^+ ratio, but using anions of differing complexing ability, viz. chloride, nitrate and perchlorate, there was no significant difference between the three exchanges (table 5.51). Incomplete exchange, and slow association of ions were both discounted when a comparison of exchanges, using the chloride and nitrate counter-anion systems, showed no significant difference between those carried out over 1 or 2 weeks (table 5.52).

5.4.2 Me_3Pb^+ - Na^+ Ion Exchange in Zeolites X and Y

The isotherms for Me_3Pb^+/Na^+ exchange in zeolites X and Y, which were shown to be reversible (figures 5.34 and 5.35: open circles represent reverse points) illustrate the high degree of

selectivity for sodium over trimethyllead exhibited by these zeolites. This is further exphasised by determination of the separation factor, α (table 5.53), and plots of these data are presented in figure 5.36 to compare the selectivities of the zeolites under examination. Any change in the selectivities of the zeolites is difficult to establish because of the scatter of data points. Trends in crystal phase cation recoveries are presented in figure 5.37, and not only illustrate the effect of hydronium exchange, but also reveal zeolite losses arising from multiple exchanges (relevant data presented in Tables 5 and 6: Appendix 3).

The predicted removal of low levels of Me_3Pb^+ from high salt backgrounds by analytical determination of the differences in solution of the concentration of the organolead ion before and after exchange, failed to agree with those levels obtained by direct determination of the crystal phase (tables 5.54 and 5.55). This illustrated the difficulty in analysing for very small changes in Me_3Pb^+ concentration. Crystal phase analysis served to demonstrate the low removal of Me_3Pb^+ at these levels, but showed that as $E_{Me_3Pb} \rightarrow 0$ there was a change in the selectivity exhibited by zeolite X, and the effect was greater in the lower salt background (tables 5.56 and 5.57, and figure 5.38).

5.4.3 Me_3Pb^+ - Na^+ Ion Exchange in Natural and Acid Treated Clinoptilolite

Table 5.58 shows isothermal data for similar Me_3Pb^+/Na^+ exchanges in both the natural and the two acid-treated forms of clinoptilolite. Data were not presented as an isotherm since the large scatter of points gave no clear trends.

A comparison of Me_3Pb^+ absorbance readings for solutions before and after exchange with the different forms of clinoptilolite is presented in table 5.59, which show that there was very little difference between absorbance readings. Indeed, the dilutions which were involved must have led to erroneous results.

5.5 HYDRONIUM ION EXCHANGE IN ZEOLITES

The proportion of aluminium released from zeolites, thought to result from hydrolysis subsequent to hydronium exchange in salt solutions and in water, are presented in table 5.60.

Figures 5.39 and 5.40 show the kinetic pH responses which occurred when 0.3g aliquots of the appropriate zeolites were added to 50 ml volumes of well-stirred distilled water. Examination of the kinetic pH responses of a further sample of clinoptilolite (white in colour, as compared to the green form used throughout the project) was also carried out. The unexchanged and "fully" sodium exchanged forms of this further clinoptilolite sample (hereafter referred to as NAT.CLI (II) and F.EX.CLI (II) respectively) were studied to compare with the clinoptilolite sample used in this project.

Hydronium ion exchange which occurs over the isotherms was studied by measuring the kinetic pH responses following immersion of the zeolites in the respective salt solutions (figures 5.41 - 5.48).

Table 5.1 Analyses of the sodium forms of zeolites A, X and Y

		Na-A	Na-Z1(I)	Na-Z1(II)	Na-Z2	Na-Z3	Na-Z4	Na-Z5(I)	Na-Z5(II)
SiO_2	%	32.74	35.06	34.29	37.42	40.69	43.13	46.03	45.64
	mol hg^{-1}	0.5448	0.5833	0.5706	0.6226	0.6770	0.7176	0.7659	0.7595
Al_2O_3	%	27.69	24.41	23.81	21.52	19.18	17.69	16.33	16.26
	mol hg^{-1}	0.2715	0.2393	0.2334	0.2110	0.1880	0.1734	0.1601	0.1594
Na_2O	%	16.56	13.10	14.31	12.12	11.44	10.61	9.57	9.65
	mol hg^{-1}	0.2671	0.2113	0.2308	0.1955	0.1845	0.1711	0.1544	0.1557
H_2O	%	22.26	24.94	26.43	26.31	25.72	26.00	26.16	26.79
	mol hg^{-1}	1.2367	1.3856	1.4683	1.4617	1.4289	1.4444	1.4533	1.4883
Total %		99.24	97.51	98.84	97.37	97.03	97.43	98.09	98.34
Si/Al		1.00	1.22	1.22	1.48	1.80	2.07	2.39	2.38
Cation exchange capacity (C.E.C.) /m equiv. g^{-1}		5.43	4.79	4.67	4.22	3.76	3.47	3.20	3.19

Table 5.2 Analyses of calcium forms of zeolite A and X

	Ca-A	Ca-X
%	31.33	33.76
SiO_2 mol hg^{-1}	0.5213	0.5617
%	27.23	23.48
Al_2O_3 mol hg^{-1}	0.2670	0.2302
%	15.18	12.69
CaO mol hg^{-1}	0.2711	0.2266
%	0.22	0.17
Na_2O mol hg^{-1}	0.0036	0.0027
%	25.25	29.02
H_2O mol kg^{-1}	1.4028	1.6122
Total %	99.21	99.12
Si/Al	0.98	1.22
C.E.C./m equiv. g^{-1}	5.34	4.60

Table 5.3 Analyses of clinoptilolite samples

		NAT.CLI	F.EX.CLI	2N CLI	4N CLI
SiO_2	%	64.87	66.77	69.53	70.22
	mol hg^{-1}	1.0776	1.1091	1.1588	1.1703
Al_2O_3	%	10.61	10.96	9.14	8.47
	mol hg^{-1}	0.1040	0.1075	0.0896	0.0831
K_2O	%	4.59	0.57	0.61	0.29
	mol hg^{-1}	0.0488	0.0061	0.0065	0.0031
Na_2O	%	2.98	5.71	3.17	3.05
	mol hg^{-1}	0.0481	0.0921	0.0512	0.0491
CaO	%	1.24	0.07	<0.01	<0.01
	mol hg^{-1}	0.0221	0.0013	<0.0001	<0.0001
MgO	%	0.30	0.19	0.10	0.11
	mol hg^{-1}	0.0074	0.0047	0.0005	0.0005
Fe_2O_3	%	0.77	0.73	0.59	0.57
	mol hg^{-1}	0.0048	0.0046	0.0037	0.0036
TiO_2	%	0.09	0.09	0.09	0.09
	mol hg^{-1}	0.0011	0.0011	0.0011	0.0011
BaO	%	0.03	0.01	<0.01	<0.01
	mol hg^{-1}	0.0002	0.0001	<0.0001	<0.0001
SrO	%	0.06	0.01	<0.01	<0.01
	mol hg^{-1}	0.0006	0.0001	<0.0001	<0.0001
H_2O	%	13.36	13.86	15.42	16.11
	mol hg^{-1}	0.7422	0.7700	0.8567	0.8950
Total %		98.90	98.97	98.65	98.91
Si/Al		5.18	5.16	6.47	7.05
C.E.C./m equiv. g^{-1}		2.08	2.15	1.79	1.66

Table 5.4 Oxide formulae of zeolite samples

Na-A	0.984	Na_2O.	Al_2O_3.	2.007	SiO_2.	4.555	H_2O			
Na-Z1(I)	0.883	Na_2O.	Al_2O_3.	2.438	SiO_2.	5.790	H_2O			
Na-Z1(II)	0.989	Na_2O.	Al_2O_3.	2.444	SiO_2	6.290	H_2O			
Na-Z2	0.927	Na_2O.	Al_2O_3.	2.951	SiO_2.	6.928	$H2_0$			
Na-Z3	0.981	Na_2O.	Al_2O_3.	3.601	SiO_2.	7.601	H_2O			
Na-Z4	0.986	Na_2O.	Al_2O_3.	4.138	SiO_2.	8.330	H_2O			
Na-Z5(I)	0.964	Na_2O.	Al_2O_3.	4.784	SiO_2.	9.078	H_2O			
Na-Z5(II)	0.977	Na_2O.	Al_2O_3.	4.765	SiO_2.	9.337	H_2O			
Ca-A	1.015	CaO.	0.014	Na_2O.	Al_2O_3.	1.952	SiO_2.	5.254	H_2O	
Ca-X	0.958	CaO.	0.012	Na_2O.	Al_2O_3.	2.440	SiO_2.	7.004	H_2O	
NAT.CLI	0.463	Na_2O.	0.469	K_2O.	Al_2O_3.	10.362	SiO_2.	7.137	H_2O	
F.EX.CLI	0.857	Na_2O.	0.057	K_2O.	Al_2O_3.	10.317	SiO_2.	7.163	H_2O	
2N CLI	0.571	Na_2O.	0.429	H_3O^+.	Al_2O_3.	12.933	SiO_2.	9.561	H_2O	
4N CLI	0.591	Na_2O.	0.409	H_3O^+.	Al_2O_3.	14.083	SiO_2.	10.770	H_2O	

Table 5.5 Unit cell compositions of zeolite samples

Na-A	$Na_{11.79}$	$H_{0.19}$	$(AlO_2)_{11.98}$	$(SiO_2)_{12.02}$ ·	27.29 H_2O
Na-Z1(I)	$Na_{76.41}$	$H_{10.13}$	$(AlO_2)_{86.54}$	$(SiO_2)_{105.47}$ ·	250.53 H_2O
Na-Z1(II)	$Na_{85.43}$	$H_{0.96}$	$(AlO_2)_{86.39}$	$(SiO_2)_{105.61}$ ·	271.75 H_2O
Na-Z2	$Na_{71.87}$	$H_{5.70}$	$(AlO_2)_{77.57}$	$(SiO_2)_{114.44}$ ·	268.66 H_2O
Na-Z3	$Na_{67.28}$	$H_{1.28}$	$(AlO_2)_{68.56}$	$(SiO_2)_{123.44}$ ·	260.54 H_2O
Na-Z4	$Na_{61.73}$	$H_{0.83}$	$(AlO_2)_{62.56}$	$(SiO_2)_{129.44}$ ·	260.55 H_2O
Na-Z5(I)	$Na_{54.59}$	$H_{2.02}$	$(AlO_2)_{56.61}$	$(SiO_2)_{135.40}$ ·	256.91 H_2O
Na-Z4(II)	$Na_{55.44}$	$H_{1.32}$	$(AlO_2)_{56.76}$	$(SiO_2)_{135.22}$ ·	264.98 H_2O
Ca-A	$Ca_{6.17}$	$Na_{0.16}$	$(AlO_2)_{12.14}$	$(SiO_2)_{11.86}$ ·	31.90 H_2O
Ca-X	$Ca_{42.57}$	$Na_{1.01}$	$H_{0.34}$ $(AlO_2)_{86.49}$	$(SiO_2)_{105.52}$ ·	302.85 H_2O
NAT.CLI	$Na_{2.69}$	$K_{2.73}$	$(AlO_2)_{5.83}$	$(SiO_2)_{30.18}$ ·	20.78 H_2O
F.EX.CLI	$Na_{5.01}$	$K_{0.33}$	$(AlO_2)_{5.85}$	$(SiO_2)_{30.16}$ ·	20.94 H_2O
2N CLI	$Na_{2.76}$	$H_{2.06}$	$(AlO_2)_{4.82}$	$(SiO_2)_{31.18}$ ·	23.05 H_2O
4N CLI	$Na_{2.65}$	$H_{1.83}$	$(AlO_2)_{4.48}$	$(SiO_2)_{31.52}$ ·	24.11 H_2O

Table 5.6 X-ray powder data of NaA

2θ	d(Å)	I_{meas}	I_{rel}
7.10	12.44	36.0	81.8
10.10	8.75	30.5	69.3
12.35	7.16	28.5	64.8
16.00	5.53	21.5	48.9
21.55	4.12	29.5	67.0
23.90	3.72	41.0	93.2
26.00	3.42	20.0	45.5
27.00	3.30	36.5	83.0
29.00	3.08	44.0	100.0
30.75	2.90	16.5	37.5
32.50	2.75	16.0	36.4
33.25	2.69	12.0	27.3
34.10	2.63	33.0	75.0
35.70	2.51	10.0	22.7
36.50	2.46	10.0	22.7
40.10	2.25	8.5	19.3
41.50	2.17	11.5	26.1
42.10	2.14	10.0	22.7
42.80	2.11	8.5	19.3
43.40	2.08	9.0	20.5
44.10	2.05	13.0	29.5
47.20	1.92	11.0	25.0
49.70	1.83	8.0	18.2
52.50	1.74	14.5	33.0
54.20	1.69	10.0	22.7
57.40	1.60	9.5	21.6
58.50	1.58	9.0	20.5

where I_{meas} = measured intensity

I_{rel} = relative intensity

Table 5.7 X-ray powder data of CaA

2θ	d(Å)	I_{meas}	I_{rel}
6.00	14.72	39.0	100.0
7.20	12.27	20.5	52.6
8.20	10.77	21.0	53.8
9.80	9.02	21.0	53.8
12.20	7.25	18.0	46.2
15.40	5.75	21.5	55.1
18.40	4.82	16.0	41.0
20.00	4.44	19.5	50.0
23.30	3.81	28.0	71.8
24.80	3.59	15.0	38.5
26.60	3.35	19.5	50.0
27.40	3.25	15.5	39.7
29.20	3.06	14.0	35.9
30.30	2.95	17.0	43.6
30.96	2.89	22.0	56.4
32.00	2.79	15.5	39.7
32.60	2.74	14.0	35.9
33.60	2.66	13.0	33.3
34.20	2.62	12.0	30.8
36.60	2.45	9.0	23.1
37.30	2.41	11.5	29.5
40.00	2.25	8.0	20.5
40.90	2.20	10.0	25.6
41.30	2.18	9.0	23.1
42.20	2.14	8.0	20.5
42.70	2.12	8.0	20.5
43.40	2.08	8.0	20.5
44.10	2.05	7.0	17.9
51.70	1.77	8.5	21.8
57.50	1.60	10.0	25.6

Table 5.8 X-ray powder data of PbA (exchanged from NaA)

2θ	d(Å)	I_{meas}	I_{rel}
7.10	12.44	24.5	98.0
8.50	10.39	21.0	84.0
9.60	9.20	20.0	80.0
11.60	7.62	20.0	80.0
14.30	6.19	20.0	80.0
16.00	5.53	18.5	74.0
20.30	4.37	16.5	66.0
21.50	4.13	19.5	78.0
22.70	3.91	15.0	60.0
23.60	3.77	16.0	64.0
23.95	3.71	16.0	64.0
24.95	3.57	17.5	70.0
27.00	3.30	17.5	70.0
28.00	3.18	16.0	64.0
29.80	3.00	25.0	100.0
30.70	2.91	15.0	60.0
32.45	2.76	20.0	80.0
34.10	2.63	13.5	54.0
35.70	2.51	13.5	54.0
36.30	2.47	11.5	46.0
37.80	2.38	11.0	44.0
39.30	2.29	12.0	48.0
41.40	2.18	15.5	62.0
42.10	2.14	12.0	48.0
43.10	2.10	11.0	44.0
47.20	1.92	10.0	40.0
49.50	1.84	10.0	40.0
52.50	1.74	11.5	46.0

Table 5.9 X-ray powder data of PbA (exchanged from CaA)

2θ	d(Å)	I_{meas}	I_{rel}
7.10	12.44	26.5	98.1
8.40	10.52	20.0	74.1
9.40	9.40	20.5	75.9
11.90	7.43	19.0	70.4
12.70	6.96	18.0	66.7
14.30	6.19	20.5	75.9
15.30	5.79	18.0	66.7
15.70	5.64	18.5	68.5
16.00	5.53	19.0	70.4
17.50	5.06	14.0	51.9
18.40	4.82	15.0	55.6
20.30	4.37	16.5	61.1
21.50	4.13	20.0	74.1
22.70	3.91	15.0	55.6
23.90	3.72	17.0	63.0
24.90	3.57	19.0	70.4
25.80	3.45	16.0	59.3
26.30	3.39	14.5	53.7
27.00	3.30	18.5	68.5
29.80	3.00	27.0	100.0
30.70	2.91	15.0	55.6
32.40	2.76	20.0	74.1
34.10	2.63	13.5	50.0
35.60	2.52	14.5	53.7
37.70	2.38	12.0	44.4
39.30	2.29	12.0	44.4
41.35	2.18	16.0	59.3
42.00	2.15	13.5	50.0
43.40	2.08	11.0	40.7
47.10	1.93	10.0	37.0
49.50	1.84	11.0	40.7
52.50	1.74	12.0	44.4

Table 5.10 X-ray powder data of NaZ1

2θ	d(Å)	I_{meas}	I_{rel}
6.10	14.47	54.0	100.0
9.95	8.88	28.0	51.9
11.70	7.56	25.0	46.3
12.40	7.13	19.0	35.2
15.40	5.75	30.0	55.6
17.60	5.03	15.0	27.8
18.40	4.82	17.0	31.5
20.10	4.41	21.5	39.8
22.50	3.95	17.5	32.4
23.30	3.81	38.0	70.4
25.40	3.50	14.0	25.9
26.00	3.42	13.5	25.0
26.70	3.34	39.0	72.2
29.20	3.06	16.5	30.6
30.30	2.95	23.0	42.6
31.00	2.88	42.5	78.7
32.00	2.79	25.0	46.3
32.70	2.74	14.0	25.9
33.60	2.66	23.5	43.5
34.20	2.62	15.0	27.8
35.20	2.55	11.0	20.4
37.40	2.40	15.5	28.7
40.90	2.20	14.0	25.9
41.30	2.18	13.0	24.1
42.70	2.12	12.5	23.1
43.40	2.08	9.5	17.6
51.70	1.77	10.5	19.4
53.20	1.72	13.5	25.0
57.50	1.60	12.5	23.1

Table 5.11 X-ray powder data of CaZl

2θ	d(Å)	I_{meas}	I_{rel}
6.30	14.02	20.0	58.8
6.90	12.80	25.0	73.5
7.10	12.44	34.0	100.0
7.50	11.78	23.0	67.6
8.30	10.64	22.5	66.2
10.10	8.75	26.0	76.5
12.50	7.07	25.0	73.5
13.40	6.60	18.0	52.9
14.40	6.14	19.5	57.4
15.60	5.67	16.0	47.1
16.10	5.50	19.5	57.4
17.60	5.03	14.5	42.6
18.70	4.74	14.5	42.6
20.30	4.37	14.0	41.2
21.70	4.09	24.0	70.6
22.80	3.90	14.5	42.6
23.20	3.83	14.5	42.6
24.00	3.70	25.0	73.5
24.60	3.62	15.0	44.1
26.10	3.41	19.5	57.4
27.20	3.28	27.0	79.4
29.40	3.04	13.0	38.2
30.00	2.98	28.0	82.4
30.90	2.89	15.0	44.1
31.60	2.83	12.5	36.8
34.30	2.61	23.5	69.1
35.80	2.51	11.0	32.4
36.60	2.45	11.0	32.4
40.20	2.24	8.0	23.5
41.60	2.17	11.0	32.4
42.90	2.11	10.0	29.4
44.30	2.04	8.5	25.0
47.50	1.91	8.0	23.5
52.70	1.74	12.0	35.3
54.40	1.68	7.5	22.1
57.70	1.60	8.0	23.5

Table 5.12 X-ray powder data of PbZ1 (exchanged from NaZ1)

2θ	d(Å)	I_{meas}	I_{rel}
6.00	14.72	27.0	83.1
8.00	11.04	20.0	61.5
8.40	10.52	20.0	61.5
9.90	8.93	21.0	64.6
11.60	7.62	21.5	66.2
12.20	7.25	17.0	52.3
12.80	6.91	18.0	55.4
15.40	5.75	15.0	46.2
17.30	5.12	15.5	47.7
18.30	4.84	16.5	50.8
20.10	4.41	15.0	46.2
21.20	4.19	19.0	58.5
23.20	3.83	32.5	100.0
23.40	3.80	29.0	89.2
25.30	3.52	15.5	47.7
26.50	3.36	14.5	44.6
27.20	3.28	18.0	55.4
28.40	3.14	17.0	52.3
29.30	3.05	21.5	66.2
30.10	2.97	17.0	52.3
31.80	2.81	14.5	44.6
32.40	2.76	22.5	69.2
33.50	2.67	11.0	33.8
34.00	2.63	20.0	61.5
35.55	2.52	14.5	44.6
36.40	2.47	14.0	43.1
37.00	2.43	12.5	38.5
39.80	2.26	10.0	30.8
40.60	2.22	18.5	56.9
41.15	2.19	16.0	49.2
42.40	2.13	11.5	35.4
46.30	1.96	13.0	40.0
50.90	1.79	12.0	36.9
51.40	1.78	12.0	36.9
51.90	1.76	13.0	40.0
57.20	1.61	13.5	41.5

Table 5.13 X-ray powder data of PbZl (exchanged from CaZl)

2θ	d(Å)	I_{meas}	I_{rel}
6.00	14.72	38.0	100.0
7.20	12.27	19.0	50.0
8.50	10.39	20.0	52.6
9.50	9.30	20.5	53.9
9.90	8.93	20.5	53.9
11.70	7.56	19.0	50.0
12.40	7.13	17.5	46.1
13.00	6.80	17.5	46.1
13.80	6.41	18.0	47.4
16.50	5.37	15.0	39.5
17.30	5.12	15.5	40.8
18.20	4.87	15.0	39.5
20.00	4.44	15.0	39.5
20.90	4.25	17.0	44.7
21.20	4.19	20.5	53.9
22.40	3.97	16.0	42.1
23.20	3.83	32.0	84.2
23.40	3.80	28.5	75.0
24.70	3.60	15.0	39.5
25.40	3.50	16.5	43.4
26.80	3.32	15.0	39.5
27.30	3.26	17.0	44.7
28.50	3.13	14.0	36.8
29.40	3.04	18.0	47.4
30.20	2.96	19.0	50.0
31.00	2.88	15.0	39.5
31.90	2.80	17.0	44.7
32.50	2.75	19.5	51.3
33.50	2.67	13.0	34.2
34.10	2.63	16.0	42.1
35.60	2.52	13.0	34.2
36.50	2.46	13.5	35.5
38.70	2.32	10.5	27.6
40.70	2.21	15.0	39.5
41.20	2.19	13.0	34.2
42.50	2.12	11.5	30.3
46.30	1.96	11.0	28.9
47.50	1.91	9.5	25.0
51.00	1.79	10.5	27.6
51.60	1.77	11.0	28.9
52.10	1.75	10.5	27.6
57.30	1.61	10.5	27.6

Table 5.14 X-ray powder data of Me_3PbZ1

2θ	d(Å)	I_{meas}	I_{rel}
6.00	14.72	33.0	100.0
7.40	11.93	21.0	63.6
8.30	10.64	21.0	63.6
9.70	9.11	21.5	65.2
10.60	8.34	19.0	57.6
11.70	7.56	20.0	60.6
12.40	7.13	18.5	56.1
15.40	5.75	21.5	65.2
16.40	5.40	16.0	48.5
17.20	5.15	14.5	43.9
17.90	4.95	14.5	43.9
18.30	4.84	16.0	48.5
20.00	4.44	17.5	53.0
21.60	4.11	14.0	42.4
22.40	3.97	16.0	48.5
23.20	3.83	29.5	89.4
23.40	3.80	24.0	72.7
25.30	3.52	14.0	42.4
26.60	3.35	23.5	71.2
27.20	3.28	15.0	45.5
28.70	3.11	12.0	36.4
29.10	3.07	15.0	45.5
30.40	2.94	17.0	51.5
30.90	2.89	25.0	75.8
32.00	2.79	19.5	59.1
33.60	2.66	16.5	50.0
34.10	2.63	14.0	42.4
35.10	2.55	12.0	36.4
37.40	2.40	11.0	33.3
40.80	2.21	11.0	33.3
41.20	2.19	10.0	30.3
42.70	2.12	10.0	30.3
43.50	2.08	8.0	24.2
45.70	1.98	8.0	24.2
46.40	1.95	9.5	28.8
50.90	1.79	8.0	24.2
51.60	1.77	9.5	28.8
53.20	1.72	9.5	28.8
57.40	1.60	8.0	24.2

Table 5.15 X-ray powder data of NaZ2

2θ	d(Å)	I_{meas}	I_{rel}
6.05	14.59	46.0	100.0
9.95	8.88	24.5	53.3
11.70	7.56	23.0	50.0
13.40	6.60	19.0	41.3
15.40	5.75	28.0	60.9
17.70	5.01	15.0	32.6
18.50	4.79	18.5	40.2
20.10	4.41	22.0	47.8
21.50	4.13	17.5	38.0
22.50	3.95	18.0	39.1
23.40	3.80	35.0	76.1
25.50	3.49	15.0	32.6
26.80	3.32	28.0	60.9
27.90	3.19	18.5	40.2
29.30	3.05	16.0	34.8
30.25	2.95	20.5	44.6
31.10	2.87	34.0	73.9
32.10	2.79	19.0	41.3
33.70	2.66	18.0	39.1
34.40	2.60	12.5	27.2
37.50	2.40	13.5	29.3
41.10	2.19	10.5	22.8
41.50	2.17	10.5	22.8
42.80	2.11	10.5	22.8
52.00	1.76	9.0	19.6
53.60	1.71	10.0	21.7
57.80	1.59	10.0	21.7

Table 5.16 X-ray powder data of PbZ2

2θ	d(Å)	I_{meas}	I_{rel}
6.00	14.72	28.5	100.0
8.00	11.04	20.0	70.2
8.40	10.52	20.0	70.2
9.90	8.93	20.0	70.2
11.70	7.56	20.0	70.2
12.40	7.13	17.0	59.6
14.20	6.23	16.0	56.1
14.80	5.98	16.0	56.1
15.20	5.82	15.0	52.6
16.40	5.40	14.5	50.9
17.20	5.15	15.0	52.6
18.30	4.84	15.0	52.6
21.20	4.19	18.0	63.2
23.20	3.83	26.0	91.2
23.50	3.78	24.0	84.2
25.30	3.52	15.0	52.6
27.25	3.27	19.0	66.7
28.40	3.14	15.0	52.6
29.30	3.05	20.0	70.2
30.20	2.96	18.0	63.2
31.90	2.80	12.0	42.1
32.50	2.75	19.0	66.7
33.50	2.67	11.0	38.6
34.10	2.63	16.5	57.9
35.60	2.52	13.0	45.6
36.50	2.46	14.5	50.9
39.90	2.26	9.0	31.6
40.70	2.21	14.5	50.9
41.20	2.19	15.0	52.6
42.40	2.13	11.5	40.4
46.30	1.96	11.0	38.6
50.90	1.79	12.0	42.1
51.50	1.77	12.0	42.1
51.90	1.76	11.5	40.4
57.20	1.61	11.5	40.4

Table 5.17 X-ray powder data of NaZ3

2θ	d(Å)	I_{meas}	I_{rel}
6.10	14.47	61.0	100.0
10.00	8.84	25.5	41.8
11.80	7.49	24.0	39.3
12.40	7.13	19.5	32.0
15.55	5.69	34.0	55.7
17.60	5.03	15.0	24.6
18.60	4.77	20.0	32.8
20.25	4.38	24.5	40.2
21.60	4.11	15.0	24.6
22.65	3.92	18.0	29.5
23.55	3.77	37.0	60.7
25.60	3.48	14.5	23.8
26.95	3.31	30.0	49.2
28.10	3.17	15.5	25.4
29.50	3.02	16.0	26.2
30.50	2.93	20.5	33.6
31.25	2.86	36.0	59.0
32.35	2.76	18.0	29.5
33.90	2.64	17.5	28.7
34.50	2.60	13.5	22.1
37.70	2.38	13.0	21.3
40.30	2.24	8.5	13.9
41.25	2.19	10.5	17.2
43.10	2.10	9.5	15.6
43.90	2.06	9.0	14.8
52.20	1.75	9.5	15.6
53.80	1.70	10.0	16.4
58.10	1.59	10.0	16.4

Table 5.18 X-ray powder data of PbZ3

2θ	d(Å)	I_{meas}	I_{rel}
6.05	14.59	33.5	100.0
8.05	10.97	19.5	58.2
8.35	10.58	21.0	62.7
9.80	9.02	20.0	59.7
11.70	7.56	20.5	61.2
12.30	7.19	19.0	56.7
14.70	6.02	16.0	47.8
15.20	5.82	16.0	47.8
17.30	5.12	16.0	47.8
18.40	4.82	16.0	47.8
20.00	4.44	16.0	47.8
20.80	4.27	17.0	50.7
21.20	4.19	20.0	59.7
21.80	4.07	16.0	47.8
23.30	3.81	32.0	95.5
23.50	3.78	25.0	74.6
25.40	3.50	17.0	50.7
27.40	3.25	20.0	59.7
28.50	3.13	17.5	52.2
29.40	3.04	19.5	58.2
30.30	2.95	20.0	59.7
31.10	2.87	15.0	44.8
32.00	2.79	14.5	43.3
32.60	2.74	20.5	61.2
33.60	2.66	13.0	38.8
34.20	2.62	16.5	49.3
35.70	2.51	12.0	35.8
36.65	2.45	15.0	44.8
40.85	2.21	15.0	44.8
41.30	2.18	14.5	43.3
42.60	2.12	12.0	35.8
46.50	1.95	11.5	34.3
51.10	1.79	12.0	35.8
51.70	1.77	12.5	37.3
52.10	1.75	12.5	37.3
57.50	1.60	11.5	34.3

Table 5.19 X-ray powder data of NaZ4

2θ	d(Å)	I_{meas}	I_{rel}
6.15	14.36	50.5	100.0
10.10	8.75	24.0	47.5
11.80	7.49	23.0	45.5
12.35	7.16	19.0	37.6
15.60	5.67	29.5	58.4
17.55	5.05	14.0	27.7
18.60	4.77	20.0	39.6
20.30	4.37	25.0	49.5
22.70	3.91	18.0	35.6
23.55	3.77	35.0	69.3
25.00	3.56	15.0	29.7
25.70	3.46	14.0	27.7
26.95	3.31	29.0	57.4
27.70	3.22	16.0	31.7
29.55	3.02	17.5	34.7
30.65	2.91	20.0	39.6
31.30	2.85	31.5	62.4
32.40	2.76	18.0	35.6
34.00	2.63	16.5	32.7
34.55	2.59	14.0	27.7
37.75	2.38	12.0	23.8
40.55	2.22	8.5	16.8
41.30	2.18	9.5	18.8
43.20	2.09	9.5	18.8
43.90	2.06	8.5	16.8
52.30	1.75	9.5	18.8
53.90	1.70	9.5	18.8
58.10	1.59	9.5	18.8

Table 5.20 X-ray powder data of PbZ4

2θ	d(Å)	I_{meas}	I_{rel}
6.05	14.59	30.0	100.0
8.00	11.04	22.0	73.3
8.40	10.52	22.5	75.0
9.40	9.40	20.5	68.3
11.70	7.56	20.0	66.7
12.30	7.19	19.0	63.3
14.20	6.23	17.0	56.7
14.90	5.94	16.0	53.3
15.10	5.86	16.0	53.3
18.50	4.79	17.0	56.7
20.10	4.41	18.5	61.7
21.10	4.21	17.5	58.3
21.40	4.15	18.5	61.7
23.40	3.80	29.3	97.7
23.60	3.77	24.0	80.0
24.70	3.60	16.0	53.3
25.50	3.49	16.5	55.0
26.80	3.32	17.5	58.3
27.55	3.23	19.5	65.0
28.70	3.11	17.0	56.7
29.55	3.02	17.0	56.7
30.50	2.93	18.0	60.0
31.10	2.87	16.0	53.3
32.20	2.78	15.0	50.0
32.80	2.73	17.0	56.7
33.75	2.65	14.5	48.3
34.40	2.60	17.0	56.7
35.90	2.50	12.0	40.0
36.90	2.43	13.0	43.3
37.50	2.40	12.0	40.0
41.00	2.20	15.5	51.7
41.50	2.17	14.0	46.7
42.80	2.11	13.0	43.3
46.70	1.94	11.5	38.3
51.30	1.78	11.0	36.7
52.10	1.75	12.0	40.0
57.80	1.59	11.5	38.3

Table 5.21 X-ray powder data of NaZ5

2θ	d(Å)	I_{meas}	I_{rel}
6.05	14.59	46.5	100.0
10.00	8.84	25.0	53.8
11.70	7.56	22.0	47.3
15.40	5.75	25.0	53.8
17.60	5.03	14.0	30.1
18.50	4.79	17.5	37.6
20.15	4.40	20.5	44.1
21.50	4.13	15.5	33.3
22.55	3.94	17.0	36.6
23.55	3.77	31.5	67.7
24.80	3.59	14.5	31.2
25.50	3.49	15.0	32.3
26.70	3.34	29.5	63.4
27.90	3.19	15.0	32.3
29.30	3.05	17.0	36.6
30.40	2.94	20.5	44.1
31.10	2.87	35.0	75.3
32.10	2.79	19.0	40.9
33.70	2.66	19.0	40.9
34.25	2.62	12.5	26.9
37.50	2.40	14.0	30.1
40.10	2.25	8.0	17.2
41.00	2.20	11.0	23.7
41.40	2.18	11.0	23.7
42.80	2.11	9.5	20.4
51.90	1.76	10.5	22.6
53.40	1.71	11.5	24.7
57.70	1.60	10.0	21.5

Table 5.22 X-ray powder data of PbZ5

2θ	d(Å)	I_{meas}	I_{rel}
6.05	14.59	25.0	96.2
7.90	11.18	21.5	82.7
8.45	10.45	22.5	86.5
9.60	9.20	21.5	82.7
11.70	7.56	19.5	75.0
12.30	7.19	19.0	73.1
15.50	5.71	17.5	67.3
16.70	5.30	16.5	63.5
17.50	5.06	16.5	63.5
18.50	4.79	16.5	63.5
20.20	4.39	17.5	67.3
21.60	4.11	16.0	61.5
23.50	3.78	26.0	100.0
23.70	3.75	21.5	82.7
25.20	3.53	15.5	59.6
26.90	3.31	17.5	67.3
27.60	3.23	16.0	61.5
28.70	3.11	14.5	55.8
26.90	3.01	14.5	55.8
30.50	2.93	16.0	61.5
31.20	2.86	17.0	65.4
32.30	2.77	14.0	53.8
33.00	2.71	14.0	53.8
33.80	2.65	12.5	48.1
34.50	2.60	15.5	59.6
36.50	2.46	11.0	42.3
37.50	2.40	11.0	42.3
41.30	2.18	11.5	44.2
43.00	2.10	11.0	42.3
50.40	1.81	8.5	32.7
52.20	1.75	10.0	38.5
58.00	1.59	9.0	34.6

Table 5.23 X-ray powder data of Me_3PbZ5

2θ	d(Å)	I_{meas}	I_{rel}
6.10	14.47	38.5	100.0
7.90	11.18	21.0	54.5
8.40	10.52	22.0	57.1
9.40	9.40	21.5	55.8
10.00	8.84	21.0	54.5
11.80	7.49	21.0	54.5
12.75	6.94	19.5	50.6
15.50	5.71	26.0	67.5
16.70	5.30	15.5	40.3
17.50	5.06	15.5	40.3
18.60	4.77	19.0	49.4
20.20	4.39	26.5	68.8
21.10	4.21	15.5	40.3
21.50	4.13	15.5	40.3
22.60	3.93	17.5	45.5
23.50	3.78	34.0	88.3
23.80	3.73	20.0	51.9
25.00	3.56	15.0	39.0
25.70	3.46	17.0	44.2
26.90	3.31	23.0	59.7
27.70	3.22	15.0	39.0
28.70	3.11	13.5	35.1
29.50	3.02	17.0	44.2
30.60	2.92	18.5	48.1
31.25	2.86	27.5	71.4
32.30	2.77	16.0	41.6
32.90	2.72	13.0	33.8
33.90	2.64	15.5	40.3
34.50	2.60	14.5	37.7
36.90	2.43	10.0	26.0
37.70	2.38	13.0	38.8
38.30	2.35	10.0	26.0
40.40	2.23	10.0	26.0
41.30	2.18	10.5	27.3
41.70	2.16	10.0	26.0
43.10	2.10	10.0	26.0
43.90	2.06	10.0	26.0
45.60	1.99	9.0	23.4
51.60	1.77	9.0	23.4
52.30	1.75	9.5	24.7
54.40	1.68	10.0	26.0

Table 5.24 X-ray powder data of NAT.CLI

2θ	d(Å)	I_{meas}	I_{rel}
5.80	15.22	21.5	71.7
8.40	10.52	22.0	73.3
10.00	8.84	28.0	93.3
11.10	7.96	22.0	73.3
13.00	6.80	20.0	66.7
13.70	6.46	17.0	56.7
14.20	6.23	17.5	58.3
14.80	5.98	17.0	56.7
15.20	5.82	17.0	56.7
15.70	5.64	15.0	50.0
17.20	5.15	19.0	63.3
18.20	4.87	15.0	50.0
19.00	4.67	16.5	55.0
20.40	4.35	16.0	53.3
22.35	3.97	30.0	100.0
22.65	3.92	27.5	91.7
24.40	3.64	15.0	50.0
24.90	3.57	15.0	50.0
26.00	3.42	20.5	68.3
26.80	3.32	16.0	53.3
27.30	3.26	12.5	41.7
28.15	3.17	18.0	60.0
28.60	3.12	15.5	51.7
28.95	3.08	15.0	50.0
29.95	2.98	23.0	76.7
31.95	2.80	16.5	55.0
32.75	2.73	13.0	43.3
33.40	2.68	10.0	33.3
35.00	2.56	10.0	33.3
36.90	2.43	11.5	38.3
39.48	2.28	10.0	33.3

Table 5.25 X-ray powder data of Pb-NAT.CLI

2θ	d(Å)	I_{meas}	I_{rel}
6.10	14.47	20.0	95.2
7.00	12.62	17.0	81.0
8.20	10.77	20.0	95.2
9.40	9.40	21.0	100.0
9.80	9.02	19.0	90.5
11.10	7.96	18.5	88.1
11.30	7.82	18.5	88.1
13.10	6.75	18.0	85.7
14.20	6.23	16.5	78.6
15.20	5.82	16.0	76.2
15.50	5.71	16.5	78.6
16.30	5.43	16.0	76.2
17.30	5.12	16.5	78.6
18.10	4.90	14.0	66.7
19.00	4.67	17.0	81.0
19.75	4.49	16.0	76.2
20.30	4.37	16.0	76.2
22.40	3.97	18.0	85.7
22.70	3.91	17.5	83.3
23.05	3.85	15.5	73.8
25.30	3.52	15.0	71.4
26.00	3.42	15.0	71.4
26.90	3.31	14.0	66.7
27.60	3.23	13.5	64.3
28.10	3.17	15.0	71.4
28.50	3.13	17.0	81.0
30.05	2.97	19.5	92.9
31.20	2.86	12.0	57.1
32.00	2.79	14.0	66.7
32.60	2.74	13.0	61.9
33.50	2.67	11.5	54.8
35.20	2.55	11.0	52.4
36.20	2.48	11.5	54.8

Table 5.26 X-ray powder data of F.EX.CLI

2θ	d(Å)	I_{meas}	I_{rel}
5.90	14.96	22.0	62.0
8.40	10.52	23.0	64.8
9.80	9.02	32.0	90.1
11.10	7.96	25.0	70.4
13.00	6.80	21.5	60.6
13.70	6.46	19.5	54.9
14.80	5.98	17.5	49.3
15.70	5.64	16.5	46.5
16.40	5.40	16.5	46.5
16.70	5.30	17.5	49.3
17.22	5.14	20.0	56.3
19.00	4.67	18.5	52.1
20.00	4.44	15.0	42.3
20.40	4.35	16.5	46.5
20.80	4.27	16.0	45.1
21.00	4.23	15.5	43.7
22.40	3.97	35.5	100.0
22.70	3.91	30.0	84.5
24.00	3.70	15.5	43.7
24.90	3.57	16.5	46.5
25.90	3.44	24.0	67.6
26.70	3.34	17.0	47.9
28.15	3.17	18.5	52.1
28.55	3.12	18.5	52.1
28.90	3.09	15.5	43.7
30.05	2.97	27.0	76.1
31.90	2.80	20.0	56.3
32.60	2.74	14.0	39.4
35.35	2.54	10.5	29.6
36.80	2.44	12.0	33.8

Table 5.27 X-ray powder data of Pb-F.EX.CLI

2θ	d(Å)	I_{meas}	I_{rel}
6.10	14.47	20.0	95.2
7.30	12.10	20.5	97.6
8.00	11.04	20.5	97.6
9.40	9.40	21.0	100.0
9.60	9.20	20.5	97.6
11.00	8.04	19.0	90.5
11.60	7.62	18.0	85.7
12.80	6.91	19.5	92.9
14.00	6.32	18.0	85.7
14.80	5.98	16.0	76.2
15.00	5.90	16.0	76.2
15.75	5.62	16.0	76.2
16.55	5.35	17.0	81.0
16.80	5.27	16.0	76.2
17.40	5.09	18.5	88.1
18.05	4.91	15.5	73.8
18.90	4.69	18.5	88.1
19.60	4.52	16.5	78.6
20.30	4.37	16.5	78.6
22.20	4.00	19.0	90.5
22.70	3.91	18.0	85.7
23.20	3.83	16.0	76.2
23.95	3.71	16.0	76.2
25.00	3.56	17.0	81.0
25.95	3.43	16.5	78.6
26.75	3.33	15.5	73.8
27.40	3.25	14.0	66.7
28.55	3.12	17.0	81.0
28.90	3.09	14.5	69.0
29.95	2.98	20.5	97.6
31.80	2.81	14.5	69.0
32.75	2.73	13.5	64.3
33.50	2.67	13.0	61.9
35.15	2.55	12.0	57.1
36.40	2.47	12.0	57.1

Table 5.28 X-ray powder data of 2N CLI

2θ	d(Å)	I_{meas}	I_{rel}
6.15	14.36	21.0	66.7
8.00	11.04	22.0	69.8
8.50	10.39	22.0	69.8
9.75	9.06	29.5	93.7
11.05	8.00	22.0	69.8
11.40	7.75	20.0	63.5
12.60	7.02	20.0	63.5
13.00	6.80	20.5	65.1
14.60	6.06	17.0	54.0
16.00	5.53	16.0	50.8
16.70	5.30	16.0	50.8
17.20	5.15	19.0	60.3
19.00	4.67	16.0	50.8
20.35	4.36	16.5	52.4
22.30	3.98	31.5	100.0
22.60	3.93	28.0	88.9
24.30	3.66	15.5	49.2
25.00	3.56	17.0	54.0
25.95	3.43	20.0	63.5
26.70	3.34	17.5	55.6
28.05	3.18	19.0	60.3
28.50	3.13	16.0	50.8
28.90	3.09	16.0	50.8
29.95	2.98	20.5	65.1
30.60	2.92	14.0	44.4
31.90	2.80	16.5	52.4
32.65	2.74	15.0	47.6
34.30	2.61	10.5	33.3
35.30	2.54	11.0	34.9
36.70	2.45	11.0	34.9

Table 5.29 X-ray powder data of 4N CLI

2θ	d(Å)	I_{meas}	I_{rel}
6.15	14.36	22.0	68.8
7.90	11.18	22.0	68.8
8.35	10.58	23.5	73.4
9.70	9.11	30.5	95.3
11.10	7.96	21.5	67.2
12.00	7.37	20.5	64.1
13.00	6.80	20.0	62.5
14.55	6.08	17.0	53.1
15.70	5.64	17.0	53.1
16.30	5.43	16.0	50.0
16.90	5.24	16.0	50.0
17.20	5.15	18.5	57.8
19.00	4.67	15.5	48.4
19.90	4.46	16.0	50.0
20.30	4.37	15.0	46.9
20.75	4.28	16.0	50.0
22.30	3.98	32.0	100.0
22.55	3.94	27.5	85.9
24.20	3.67	16.5	51.6
24.95	3.57	15.0	46.9
25.95	3.43	21.0	65.6
26.20	3.40	18.0	56.3
26.80	3.32	15.5	48.4
27.40	3.25	13.0	40.6
28.10	3.17	16.0	50.0
28.60	3.12	14.5	45.3
28.90	3.09	15.5	48.4
29.95	2.98	20.5	64.1
31.90	2.80	16.0	50.0
32.60	2.74	11.5	35.9
33.40	2.68	10.5	32.8
34.20	2.62	9.0	28.1
34.90	2.57	9.5	29.7
35.35	2.54	10.0	31.3
36.90	2.43	11.0	34.4

Table 5.30 The distribution and average particle sizes (μ) of the faujasites and zeolite A as determined by laser diffractometry

Zeolite	With Ultrasonics		Without Ultrasonics	
	Size range	Mean	Size range	Mean
NaA	1 → 46	18.38	1 → 28	14.89
NaZ1	1 → 6	3.51	1 → 8	4.37
NaZ2	1 → 10	4.19	1 → 7	4.03
NaZ3	1 → 16	8.17	1 → 16	8.41
NaZ4	1 → 18	8.74	1 → 18	9.32
NaZ5	1 → 29	13.49	1 → 31	15.34

Table 5.31(i) Data for calculation of framework densities, void fractions and framework charge densities of the faujasites

ZEOLITE	Unit cell diameter/A^{o} (a)	Unit cell volume/A^{3}	Number of AlO_2 units p.u.c.	Number of SiO_2 units p.u.c.	Number of tetrahedra p.u.c.
Z1	24.95	15531	86.5	105.5	192
Z2	24.86	15364	77.6	114.4	192
Z3	24.78	15216	68.6	123.4	192
Z4	24.74	15143	62.6	129.4	192
Z5	24.68	15033	56.6	135.4	192

(a) Data supplied by Unilever Research Limited (from x-ray data)

Table 5.31(ii) Framework densities[a], void fractions[b] and framework charge densities[c] of the faujasites[d]

ZEOLITE	Framework density		Void fraction	Framework charge density/C cm^{-3}
	Number of tetrahedra/1000A^3	g cm^{-3}		
Z1	12.36	1.22	0.525	892
Z2	12.50	1.24	0.519	809
Z3	12.62	1.25	0.515	722
Z4	12.68	1.26	0.512	662
Z5	12.77	1.27	0.509	603

(a) Framework density (g cm^{-3}) = (1.66 x formula weight of framework)/(unit cell volume)

(b) Void fraction (V_f) = 0.975 - ((framework density (d_f) as no. of tetrahedra per 1000 A^3)/26)

(c) Framework charge density (C cm^{-3}) = (no. of Al atoms p.u.c. x charge on electron)/(unit cell volume)

(d) These were calculated from the data presented in table 5.31(i)

Table 5.32 Relation between the unit cell diameter and aluminium density (number of Al atoms p.u.c.) for the faujasites

ZEOLITE	Number of Al p.u.c. (N_{Al})	Number of Si p.u.c. (N_{Si})	Unit cell diameter/Å	
			METHOD 1[(a)]	METHOD 2[(b)]
Z1	86.5	105.5	24.94	24.95
Z2	77.6	114.4	24.87	24.86
Z3	68.6	123.4	24.79	24.78
Z4	62.6	129.4	24.73	24.74
Z5	56.6	135.4	24.68	24.68

(a) Buckner (1958).

$$\text{Unit cell diameter } (a_o) = \frac{192(\text{slope})}{1+(N_{Si}/N_{Al})} + \text{intercept}$$

where slope = 0.00868

and intercept = 24.191

(b) Data supplied by Unilever Research Limited (from x-ray data)

Table 5.33 Effect of acid treatment on alumina content (mol hg^{-1}) of clinoptilolite

TREATMENT	2N HCl EXTRACT		4N HCL EXTRACT	
	Al_2O_3 removed/ mol hg^{-1}	Al_2O_3 content of remaining zeolite	Al_2O_3 removed/ mol hg^{-1}	Al_2O_3 content of remaining zeolite
Original Zeolite(0)	-	0.1040	-	0.1040
1	0.0102	0.0938	0.0103	0.0937
2	6.2×10^{-3}	0.0875	8.0×10^{-3}	0.0858
3	1.5×10^{-3}	0.0860	1.9×10^{-3}	0.0839
4	1.0×10^{-3}	0.0850	1.7×10^{-3}	0.0822

Table 5.34 Summary of rate of Pb^{2+} uptake by zeolites 1 - 5

	$t_{(F.A.E. = 70\%)}/s$			$t_{(F.A.E. = 80\%)}/s$			$t_{(F.A.E. = 90\%)}/s$		
w/v	0.1%	0.2%	0.4%	0.1%	0.2%	0.4%	0.1%	0.2%	0.4%
Zeolite									
1	<5	*	*	<10	*	*	35	<5	<<<5
2	70	*	*	180	*	*	600	<5	<<5
3	5	*	*	15	*	*	180	5	<<5
4	12	*	*	45	5	*	450	14	<5
5	30	<10	*	70	12	<5	240	30	<10

* data not obtainable

where $t_{(F.A.E. = 70\%)}/s$ is the time (seconds) to attain 70% of equilibrium

Table 5.35 Equilibria data for Pb^{2+}/Na^{+} exchanges at T_N = 0.05g equiv. dm^{-3}

Zeolite 1		Zeolite 2		Zeolite 3		Zeolite 4		Zeolite 5	
E Pb	$\bar{E}$ Pb	E Pb	$\bar{E}$ Pb	E Pb	$\bar{E}$ Pb	E Pb	$\bar{E}$ Pb	E Pb	$\bar{E}$ Pb
7.4E-6	0.099	2.8E-5	0.109	2.8E-5	0.104	7.0E-5	0.124	2.0E-4	0.152
3.7E-6	0.048	5.6E-5	0.053	2.1E-5	0.055	2.2E-5	0-062	6.8E-5	0.075
8.0E-6	0.048	8.4E-5	0.053	2.4E-5	0.057	2.6E-5	0.064	6.2E-5	0.073
8.9E-6	0.024	7.1E-5	0.029	1.3E-5	0.028	1.5E-5	0.031	3.0E-5	0.041
1.2E-5	0.199	5.5E-5	0.208	1.9E-4	0.262	2.1E-4	0.255	6.7E-4	0.341
2.3E-5	0.389	2.5E-4	0.413	4.9E-4	0.424	1.7E-3	0.505	7.4E-3	0.555
2.9E-5	0.558	1.3E-3	0.613	1.9E-3	0.628	0.013	0.741	0.034	0.701
1.1E-4	0.757	2.6E-3	0.821	0.026	0.842	0.082	0.819	0.139	0.758
2.7E-3	0.926	0.021	0.932	0.112	0.906	0.174	0.850	0.234	0.771
0.040	1.002	0.127	1.016	0.186	0.922	0.246	0.857	0.318	0.770
0.107	1.056	0.197	1.066	0.270	0.921	0.362	0.876	0.412	0.791
0.188	1.065	0.286	1.107	0.396	0.939	0.466	0.881	0.519	0.793
0.260	1.131	0.394	1.111	0.484	0.943	0.552	0.890	0.619	0.804
0.385	1.166	0.505	1.140	0.574	0.949	0.660	0.898	0.716	0.817
-	-	-	-	0.777	1.087	0.814	0.929	0.859	0.849
-	-	-	-	-	-	-	-	0.907	0.895
-	-	-	-	0.888	1.083	0.894	1.023	0.932	0.905
-	-	-	-	0.934	1.127	0.935	1.007	0.949	0.930
-	-	-	-	0.951	1.071	0.956	0.964	0.966	1.004
-	-	-	-	0.957	1.019	0.958	1.052	0.970	0.956

Table 5.36 Equilibria data for Pb^{2+}/Na^{+} exchanges at T_N = 0.1g equiv. dm^{-3}

Zeolite 1		Zeolite 2		Zeolite 3		Zeolite 4		Zeolite 5	
E Pb	$\bar{E}$ Pb	E Pb	$\bar{E}$ Pb	E Pb	$\bar{E}$ Pb	E Pb	$\bar{E}$ Pb	E Pb	$\bar{E}$ Pb
7.2E-6	0.192	2.5E-5	0.215	1.3E-4	0.236	5.4E-4	0.272	1.7E-3	0.318
7.2E-6	0.098	9.3E-6	0.107	4.6E-5	0.120	1.1E-4	0.137	5.6E-4	0.169
2.3E-6	0.097	1.1E-5	0.107	3.9E-5	0.112	1.0E-4	0.129	4.6E-4	0.162
4.0E-6	0.049	2.5E-5	0.053	2.1E-5	0.055	4.9E-5	0.068	1.9E-4	0.082
1.7E-5	0.394	1.1E-4	0.608	8.9E-4	0.454	3.0E-3	0.504	0.011	0.520
1.6E-4	0.735	4.2E-3	1.003	0.018	0.785	0.050	0.770	0.074	0.703
0.016	0.970	0.068	1.145	0.090	0.817	0.136	0.828	0.165	0.751
0.088	1.047	0.149	1.096	0.188	0.911	0.229	0.860	0.263	0.762
0.180	1.181	0.243	1.095	0.271	1.007	0.323	0.858	0.362	0.770
0.280	1.195	0.347	1.100	0.387	1.013	0.422	0.863	0.458	0.782
0.398	1.146	0.449	1.196	0.488	1.086	0.523	0.881	0.562	0.793
0.499	1.150	0.546	1.403	0.591	1.150	0.617	0.895	0.656	0.805
0.606	1.223	0.651	1.220	0.694	1.142	0.717	0.907	0.769	0.816
0.719	1.193	0.768	1.194	0.790	1.131	0.806	0.917	0.865	1.001
-	-	-	-	-	-	0.914	1.033	0.925	0.886
-	-	-	-	-	-	0.936	1.086	0.952	0.911
-	-	-	-	-	-	0.953	1.096	0.963	0.922
-	-	-	-	-	-	0.966	1.111	0.975	1.016
-	-	-	-	-	-	0.980	1.103	0.981	1.058
-	-	-	-	-	-	0.985	1.183	0.983	1.044

Table 5.37 Selectivity data for Pb^{2+}/Na^{+} ion exchange in the faujasites at T_N = 0.05g equiv. dm^{-3}

Z1		Z2		Z3		Z4		Z5	
$\bar{E}_{Pb}$	$\log_{10} \alpha$	$\bar{E}_{Pb}$	$\log_{10} \alpha$	$\bar{E}_{Pb}$	$\log_{10} \alpha$	$\bar{E}_{Pb}$	$\log_{10} \alpha$	$\bar{E}_{Pb}$	$\log_{10} \alpha$
0.024	3.739	0.029	2.928	0.028	3.635	0.031	3.641	0.041	3.454
0.028	3.484	0.030	3.131	0.055	3.741	0.062	3.776	0.073	3.404
0.048	4.106	0.053	3.124	0.057	3.699	0.064	3.718	0.075	3.738
0.048	4.430	0.053	3.294	0.064	3.503	0.124	3.607	0.078	3.174
0.054	3.937	0.058	3.259	0.078	3.555	0.255	3.510	0.150	3.193
0.059	3.973	0.062	3.315	0.104	3.927	0.505	3.080	0.152	3.245
0.099	4.468	0.109	3.937	0.116	3.489	0.741	2.631	0.341	3.185
0.110	4.366	0.125	3.721	0.262	3.569	0.819	2.006	0.555	2.522
0.199	4.627	0.208	3.977	0.424	3.477	0.850	1.733	0.701	2.122
0.389	4.753	0.413	3.751	0.628	3.253	0.857	1.565	0.758	1.588
0.558	4.941	0.613	3.402	0.842	2.605	0.876	1.395	0.770	1.157
0.757	4.762	0.821	3.553	0.906	2.188	0.881	1.231	0.771	1.342
0.926	3.969	0.932	3.101	0.922	2.015	0.890	1.116	0.791	1.033
1.002	3.217	1.016	2.577	0.921	1.800	0.898	0.959	0.793	0.852
1.065	3.053	1.066	2.456	0.939	1.667	0.929	0.678	0.804	0.704
1.131	2.983	1.107	2.366	0.943	1.548	0.964	0.391	0.817	0.550
1.166	2.759	1.111	2.210	0.949	1.439	1.008	0.607	0.849	0.267
		1.140	2.100	1.020	0.603	1.023	0.678	0.895	0.243
				1.071	0.761			0.905	0.140
				1.083	0.979			0.930	0.158
				1.087	1.182			0.956	0.127
				1.127	0.820			1.004	0.126

Table 5.38 Selectivity data for Pb^{2+}/Na^{+} ion exchange in zeolite A and the faujasites at T_N = 0.1g equiv. dm^{-3}

A		Z1		Z2		Z3		Z4		Z5	
$\bar{E}_{Pb}$	$\log_{10} \alpha$	$\bar{E}_{Pb}$	$\log_{10} \alpha$	$\bar{E}_{Pb}$	$\log_{10} \alpha$	$\bar{E}_{Pb}$	$\log_{10} \alpha$	$\bar{E}_{Pb}$	$\log_{10} \alpha$	$\bar{E}_{Pb}$	$\log_{10} \alpha$
0.044	3.862	0.049	4.409	0.053	3.657	0.055	3.740	0.065	3.476	0.075	2.919
0.090	4.368	0.055	4.315	0.107	4.326	0.065	3.706	0.068	3.474	0.082	2.964
0.091	4.848	0.097	4.975	0.107	4.410	0.112	3.810	0.129	3.463	0.136	2.797
0.167	4.335	0.098	4.479	0.117	4.028	0.138	3.747	0.134	3.446	0.149	2.860
0.514	5.323	0.108	4.801	0.126	4.158	0.236	3.675	0.135	3.370	0.162	2.926
0.641	4.663	0.110	4.891	0.215	4.341	0.269	3.790	0.137	3.455	0.169	2.861
0.921	3.277	0.192	4.815	0.248	4.332	0.454	3.273	0.272	3.137	0.283	2.716
0.963	2.724	0.221	5.000	0.608	4.465	0.785	2.610	0.303	3.108	0.318	2.733
0.975	2.564	0.394	4.892	1.002	3.337	0.817	1.957	0.504	2.832	0.520	2.302
1.003	2.154	0.735	4.527	1.096	1.606	0.911	1.950	0.770	2.106	0.703	1.773
1.011	2.351	0.970	3.595	1.096	1.773	1.007	1.815	0.828	1.784	0.752	1.487
1.014	0.695	1.047	3.320	1.100	1.381	1.012	1.677	0.858	1.403	0.763	1.253
1.018	2.455	1.146	2.772	1.144	2.032	1.087	1.563	0.860	1.615	0.770	1.071
1.021	2.312	1.150	2.664	1.194	0.862	1.131	1.250	0.863	1.236	0.782	0.930
1.033	2.049	1.181	3.132	1.196	1.375	1.142	1.362	0.881	1.131	0.793	0.777
1.047	0.647	1.194	2.348	1.220	1.243	1.150	1.442	0.895	1.024	0.805	0.636
1.061	1.694	1.195	2.889					0.908	0.889	0.816	0.426
1.120	0.595	1.222	2.519					0.917	0.728	0.886	0.097
								1.030	0.557	0.911	0.013
								1.086	0.464	0.922	-0.041
								1.096	0.462	1.001	0.320
								1.103	-0.256	1.016	-0.071
								1.111	0.310	1.044	-0.032
								1.183	0.044	1.058	-0.022

Table 5.39 Pb^{2+}/Na^{+} exchanges in NaZ1 samples prepared with NaCl and $NaNO_3$

		Cl^-	NO_3^-	Cl^-	NO_3^-	Cl^-	NO_3^-	Cl^-	NO_3^-
Sol. Phase Conc/	Pb^{2+}	6.84×10^{-5}	6.61×10^{-5}	0.628	0.625	0.081	0.155	2.672	2.732
($\times 10^{-2}$ mol. dm^{-3})	Na^+	4.746	4.723	3.578	3.467	9.958	9.733	3.472	3.667
T_N/(10^{-2} equiv. dm^{-3})		4.746	4.723	4.834	4.717	10.012	9.962	8.816	9.131
Crystal Phase Conc/	Pb^{2+}	1.271	1.321	2.706	2.734	2.258	2.200	2.926	2.900
(equiv. kg^{-1})	Na^+	2.018	1.899	0.032	0.039	0.141	0.191	0.023	0.032
Total/equiv. kg^{-1}		4.560	4.541	5.444	5.507	4.657	4.591	5.875	5.832
Percentage recovery		95.27	94.80	113.74	114.97	97.30	95.85	122.75	121.75
Isotherm	E_{Pb}	2.88×10^{-5}	2.80×10^{-5}	0.260	0.265	0.016	0.023	0.606	0.598
data	$\bar{E}_{Pb}$	0.558	0.582	1.131	1.150	0.970	0.958	1.223	1.212

Table 5.40 Precipitation limit of $Pb(NO_3)_2$ in the presence of $NaNO_3$. T_N = 0.1g. equiv. dm^{-3}

m_{Pb}	E_{Pb}	m_{Na}	E_{Na}	pH at point of precipitation
0.005	0.1	0.09	0.9	7.50
0.01	0.2	0.08	0.8	6.55
0.02	0.4	0.06	0.6	6.08
0.03	0.6	0.04	0.4	5.89
0.04	0.8	0.02	0.2	5.89
0.05	1.0	0.00	0.0	5.89

Table 5.41 Selectivity data for Pb^{2+}/Ca^{2+} ion exchange in zeolites A and X at T_N = 0.1g equiv. dm^{-3}

Pb/CaX		Pb/CaA	
$\bar{E}_{Pb}$	$\log_{10}\alpha$	$\bar{E}_{Pb}$	$\log_{10}\alpha$
0.120	3.355	0.097	3.225
0.184	3.833	0.098	3.185
0.121	3.705	0.177	3.489
0.237	3.375	0.198	3.528
0.429	2.790	0.452	4.127
0.714	2.196	0.829	4.505
0.739	2.137	0.918	2.975
0.804	1.667	1.014	2.436
0.830	1.410	1.052	2.330
0.847	1.236	1.076	2.262
0.847	0.976	1.048	2.567
0.848	0.827	1.058	2.831
0.851	0.667	1.068	2.624
0.850	0.451	1.069	*
0.847	0.239	1.123	*
0.852	-0.465	1.203	*
0.853	-0.775	1.187	*
0.883	-2.589	1.226	*
0.885	-2.570		
0.957	-2.073		
0.959	-2.053		
1.027	-2.451		
1.040	-2.495		

* $\bar{E}_{Ca}$ too low to be analysed accurately

Table 5.42 Crystal phase composition (mol kg^{-1}) determination of lead exchanged forms of clinoptilolite

	NAT.CLI(1)		NAT.CLI(2)		F.EX.CLI(1)		F.EX.CLI(2)	
Element	A	B	A	B	A	B	A	B
Pb^{2+}	0.794	0.768	0.833	0.911	0.888	1.796	0.966	2.247
Na^{+}	0.251	0.602	0.148	0.265	0.294	0.493	0.192	0.271
K^{+}	0.351	0.436	0.352	0.436	0.075	0.094	0.072	0.092
Ca^{2+}	0.151	0.197	0.156	0.195	0.023	0.013	0.033	0.013
Mg^{2+}	0.050	0.069	0.060	0.069	0.041	0.046	0.046	0.046
TOTAL	1.597	2.072	1.549	1.876	1.321	2.442	1.309	2.669

A - crystal phase determination by acid dissolution

B - computer derivation of crystal phase composition following analysis of solution phase

Table 5.43 Selectivity data for inorganic lead ion exchange in natural and "fully" exchanged forms of clinoptilolite at T_N = 0.1g equiv. dm^{-3}

NAT.CLI		F.EX.CLI	
$\bar{E}_{Pb}$	$\log_{10}\alpha$	$\bar{E}_{Pb}$	$\log_{10}\alpha$
0.107	2.891	0.107	2.762
0.200	2.146	0.198	2.697
0.202	2.347	0.203	2.812
0.328	1.918	0.340	2.326
0.429	0.966	0.535	1.824
0.463	1.547	0.577	1.332
0.491	0.793	0.621	1.060
0.590	0.775	0.660	0.925
0.641	0.686	0.721	0.864
0.649	0.526	0.760	0.785
0.662	0.384	0.800	0.728
0.715	0.310	0.844	0.675
0.816	0.334	0.859	0.495
0.840	0.042	1.000	3.532
0.896	-0.021	1.113	4.968
0.921	-0.256	1.117	5.302
0.987	0.332	1.560	4.486
1.103	3.499	1.677	3.576
1.253	3.388	1.870	4.135
1.658	3.281	2.200	4.355

Table 5.44 Me_3Pb^+ analysis by atomic absorption using a Pb^{2+} calibration

Me_3Pb^+ standard solutions/(ppm)	Reading as Pb^{2+}/(ppm)	Apparent Me_3Pb^+[(a)] concentration/(ppm)	Recovery/%[(b)]
5	2.943	3.582	71.64
10	6.019	7.326	73.26
15	9.350	11.381	75.87
20	12.417	15.114	75.57

(a)

$$(Me_3Pb^+)/ppm = (Me_3Pb^+) \text{ as ppm } Pb^{2+} \times \frac{\text{Cationic weight of } Me_3Pb^+}{\text{Atomic weight of } Pb^{2+}}$$

(b)

Recovery (%) = (Apparent concentration / standard solution) x 100

Table 5.45 Effect of pretreatment on the determination of a standard 10 ppm Me_3Pb^+ solution by atomic absorption

Treatment	Reading as Pb^{2+}/(ppm)	Apparent Me_3Pb^+ concentration/(ppm)
1	6.272	7.634
2	7.801	9.495
3	7.973	9.705

where 1 = no pretreatment

2 = 5 ml HNO_3 acid added

3 = 5 ml HNO_3 acid added and warmed for 15 minutes

Table 5.46 Effect of 0.1 mol dm^{-3} NaCl background on Me_3Pb^+ analysis by atomic absorption

Me_3Pb^+ standard solutions/(ppm)	Me_3Pb^+ (ppm)[a] only	Recovery/(%)[b]	Me_3Pb^+ (ppm)[a] in 0.1 mol dm^{-3} NaCl	Recovery/(%)[b]	Increase in recovery (%)
5	3.582	71.64	4.584	91.68	20.04
10	7.326	73.26	8.872	88.72	15.46
15	11.381	75.87	13.717	91.45	15.58
20	15.114	75.57	18.056	90.28	14.71

(a) derived Me_3Pb^+ concentration from Pb^{2+} calibration and correction for difference in cationic weight

(b) Recovery (%) = (Derived concentration/standard solution) X 100

Table 5.47 Effect of varying background concentration of NaCl on lead absorption signal

Concentration of background NaCl/(mol dm^{-3})	Absorption signal for lead	Derived Me_3Pb^+ concentration/(ppm)
0	21	3.582
10^{-6}	21	3.582
10^{-5}	21	3.582
10^{-4}	21	3.582
10^{-3}	21	3.582
10^{-2}	23	4.083
10^{-1}	25	4.584

Table 5.48 Me_3Pb^+ calibration by standard procedure (a)

Standard addition	Peak height (mm)			Average peak height/(mm)	Peak height increase/(mm)
	Scan 1	Scan 2	Scan 3		
(b) 0	2	-	-	2	-
20	43	44	45	44	44
40	88	90	92	90	46
60	139	141	143	141	51
80	201	204	207	204	63

(a) see section 4.7.3

(b) when small and consistent this can be disregarded (see section 6.4.2.2)

Table 5.49 Improvement in Me_3Pb^+ analysis by increasing purge times

Standard addition	Peak height (mm)			Average peak height/(mm)	Peak height increase/(mm)
	Scan 1	Scan 2	Scan 3		
0	2	-	-	2	-
20	33	33	-	33	33
40	70	70	-	70	37
60	113	113	-	113	43
80	163	164	163	163	50

Table 5.50 Sensitivity changes in Me_3Pb^+ calibration

Standard addition/ppb	Average peak height /(mm)							
	1A	1B	1C	2A	3A	3B	3C	3D
0	4	2	<2	3	4	6	3	2
20	53	33	15	54	76	185	50	37
40	117	71	44	120	158	(a)195	105	77
60	190	117	78	195	(a)124	-	163	125
80	(a)135	173	118	276	(a)174	-	(a)116	185

(a) sensitivity reduced to 10μA

1A - 1C refer to 3 successive calibrations carried out on the same day, whilst 2A and 3A - 3D refer to subsequent days

Table 5.51 Me_3Pb^+/Na^+ exchange at T_N = 0.01 equiv. dm^{-3} using anions of sodium of differing complexing ability (1 week exchange)

Solution number	Counter-anion	Z1(II)		Z5(II)	
		E_{Me_3Pb}	$\bar{E}_{Me_3Pb}$	E_{Me_3Pb}	$\bar{E}_{Me_3Pb}$
I	Cl^-	0.093	2.941×10^{-3}	0.099	5.964×10^{-3}
II	Cl^-	0.222	0.015	0.289	0.022
III	Cl^-	0.369	0.030	0.431	0.039
IV	Cl^-	0.469	0.047	0.565	0.069
I	NO_3^-	0.095	2.904×10^{-3}	0.101	6.015×10^{-3}
II	NO_3^-	0.228	0.016	0.295	0.021
III	NO_3^-	0.367	0.033	0.427	0.038
IV	NO_3^-	0.465	0.050	0.571	0.071
I	ClO_4^-	0.096	2.425×10^{-3}	0.097	5.572×10^{-3}
II	ClO_4^-	0.229	0.015	0.287	0.022
III	ClO_4^-	0.364	0.030	0.433	0.040
IV	ClO_4^-	0.450	0.047	0.554	0.071

Table 5.52 Me_3Pb^+/Na^+ exchange at T_N = 0.01 equiv. dm^{-3} using anions of sodium of differing complexing ability (1 and 2 week exchanges)

Exchange time(days)	Solution number	Counter-anion	Z1(II)		Z5(II)	
			E Me_3Pb	$\bar{E}$ Me_3Pb	E Me_3Pb	$\bar{E}$ Me_3Pb
7	V	Cl^-	0.360	0.044	0.462	0.051
7	VI	Cl^-	0.487	0.071	0.632	0.093
7	V	NO_3^-	0.365	0.040	0.490	0.048
7	VI	NO_3^-	0.495	0.067	0.673	0.092
14	V	Cl^-	0.376	0.043	0.474	0.050
14	VI	Cl^-	0.492	0.072	0.641	0.093
14	V	NO_3^-	0.368	0.045	0.449	0.050
14	VI	NO_3^-	0.504	0.075	0.638	0.088

Table 5.53 Selectivity data for Me_3Pb^+ ion exchange in NaX and NaY at T_N = 0.01g equiv. dm^{-3}

NaX		NaY	
$\bar{E}_{Me_3Pb}$	$\log_{10}\alpha$	$\bar{E}_{Me_3Pb}$	$\log_{10}\alpha$
2.941×10^{-3}	-1.542	5.964×10^{-3}	-1.261
9.632×10^{-3}	-1.300	0.014	-1.233
0.015	-1.278	0.022	-1.257
0.023	-1.268	0.031	-1.234
0.030	-1.271	0.039	-1.268
0.043	-1.228	0.045	-1.068
0.046	-1.015	0.056	-1.244
0.047	-1.253	0.069	-1.243
0.056	-1.258	0.077	-1.101
0.064	-1.016	0.081	-1.269
0.070	-1.220	0.098	-1.260
0.077	-1.218	0.113	-1.302
0.100	-1.201	0.131	-1.376
0.123	-1.220	0.165	-1.413
0.169	-1.171	0.190	-1.437
0.222	-1.109	0.234	-1.404
0.263	-1.111	0.274	-1.417
0.334	-1.083	0.318	-1.478
0.342	-1.140	0.360	-1.475
0.384	-1.289	0.393	-1.537
0.476	-1.558	0.475	-1.691
0.506	-1.891	0.522	-1.879
0.879	-1.108	0.626	-1.991
0.939	-0.803	0.688	-1.566
0.948	-0.778	0.717	-1.546

Table 5.54 Removal of low Me_3Pb^+ levels (1-100 ppm) from high salt background (T_N = 0.01g equiv. dm^{-3})

Solution concentration (ppm) of Me_3Pb^+		Crystal phase concentration (ppm) of Me_3Pb^+	
Exchange solution	Equilibrium solution	Expected[a]	Observed[b]
0.89	0.89	0	19.71
1.77	1.77	0	8.33
4.94	4.59	59.44	7.40
9.91	9.38	89.71	8.17
19.83	18.74	186.0	11.78
47.25	43.68	952.3	39.27
100.5	82.35	3047	141.5

(a) calculated from the difference between the exchange and equilibrium solutions

(b) derived Me_3Pb^+ concentration from D.P.A.S.V. analysis for Pb^{2+} and correction for difference in cationic weights

Table 5.55 Removal of low Me_3Pb^+ levels (1-100 ppm) from high salt background (T_N = 0.1g equiv. dm^{-3})

Solution concentration (ppm) of Me_3Pb^+		Crystal phase concentration (ppm) of Me_3Pb^+	
Exchange solution	Equilibrium solution	Expected[a]	Observed[b]
0.84	0.84	0	7.19
1.96	1.94	0	7.04
5.02	5.02	0	9.76
9.97	9.97	0	11.64
18.96	18.63	54.76	14.36
49.39	44.09	901.0	60.21
99.13	92.00	1201	164.7

(a) calculated from the difference between the exchange and equilibrium solutions

(b) derived Me_3Pb^+ concentration from D.P.A.S.V. analysis for Pb^{2+} and correction for difference in cationic weights

Table 5.56 Crystal phase determination of the removal of low Me_3Pb^+ levels (1-100 ppm) from high salt background (T_N = 0.01g equiv. dm^{-3})

Me_3Pb^+ concentration/(ppm)			
Exchange solution	Crystal phase	Quantity removed	Percentage removed
0.89	19.71	0.121	13.60
1.77	8.33	0.049	2.77
4.94	7.40	0.044	0.89
9.91	8.17	0.049	0.50
19.83	11.78	0.069	0.35
47.25	39.27	0.230	0.49
100.5	141.5	0.840	0.84

Table 5.57 Crystal phase determination of the removal of low Me_3Pb^+ levels (1-100 ppm) from high salt background (T_N = 0.1 g equiv. dm^{-3})

Me_3Pb^+ concentration/(ppm)			
Exchange solution	Crystal phase	Quantity removed	Percentage removed
0.84	7.19	0.042	5.00
1.96	7.04	0.043	2.19
5.02	9.76	0.058	1.16
9.97	11.64	0.067	0.67
18.96	14.36	0.089	0.47
49.39	60.21	0.354	0.72
99.13	164.7	0.978	0.99

Table 5.58 Isotherm data for Me_3Pb^+/Na^+ ion exchange in natural and acid treated clinoptilolite samples

Zeolite	Solution number	E_{Me_3Pb}	$\bar{E}_{Me_3Pb}$
NAT CLI	1	0.092	3.97×10^{-3}
NAT CLI	2	0.183	0.010
NAT CLI	3	0.354	0.023
NAT CLI	4	0.440	0.038
NAT CLI	5	0.612	0.042
NAT CLI	6	0.695	0.060
NAT CLI	7	0.864	0.070
2N CLI	1	0.113	0
2N CLI	2	0.222	8.07×10^{-3}
2N CLI	3	0.434	0
2N CLI	4	0.527	0.020
2N CLI	5	0.693	0.106
2N CLI	6	0.791	0.093
2N CLI	7	0.952	0.160
4N CLI	1	0.111	3.25×10^{-3}
4N CLI	2	0.272	8.31×10^{-3}
4N CLI	3	0.422	0.038
4N CLI	4	0.521	0.021
4N CLI	5	0.700	0.068
4N CLI	6	0.791	0.097
4N CLI	7	0.951	0.121

Table 5.59 Me_3Pb^+ absorbance readings of exchange and equilibrium solutions

Solution number	Dilution factor	Absorbance reading			
		Exchange solution	Equilibrium solutions		
			NAT.CLI	2N CLI	4N CLI
1	x20	52	50	52	51
2	x50	42	40	41	41
3	x100	42	40	42	40
4	x100	52	49	51	51
5	x100	72	69	67	69
6	x200	42	40	40	40
7	x200	52	50	49	50

Table 5.60 Proportion of aluminium removed from sodium and calcium forms of zeolites of different densities after immersion in various salt solutions or water

Salt solution / Zeolite	Percentage aluminium removed							
	Distilled water	0.1N $NaNO_3$	0.095N Na^+: 0.005N Pb^{2+}	0.05N Na^+: 0.05N Pb^{2+}	0.1N $Pb(NO_3)_2$	0.01N $Pb(NO_3)_2$	0.01N NaCl	0.01N Me_3PbCl
NaZ1	0.55	0.22	0.15	0.58	1.06	0	-	-
NaZ1	0.13	0	0	4.39	6.45	0	0.13	0
NaZ2	0	0	-	3.95	4.97	-	-	-
NaZ3	0	0	-	1.64	2.41	-	-	-
NaZ4	0	0	-	0.45	1.06	-	-	-
NaZ5	0	0	0	0.19	0.62	0	0	0
CaA	0	0	0	-	1.29	0	-	-
CaX	0	0	0	-	3.16	0	-	-

Figures5.1 X-ray diffraction patterns of zeolite A

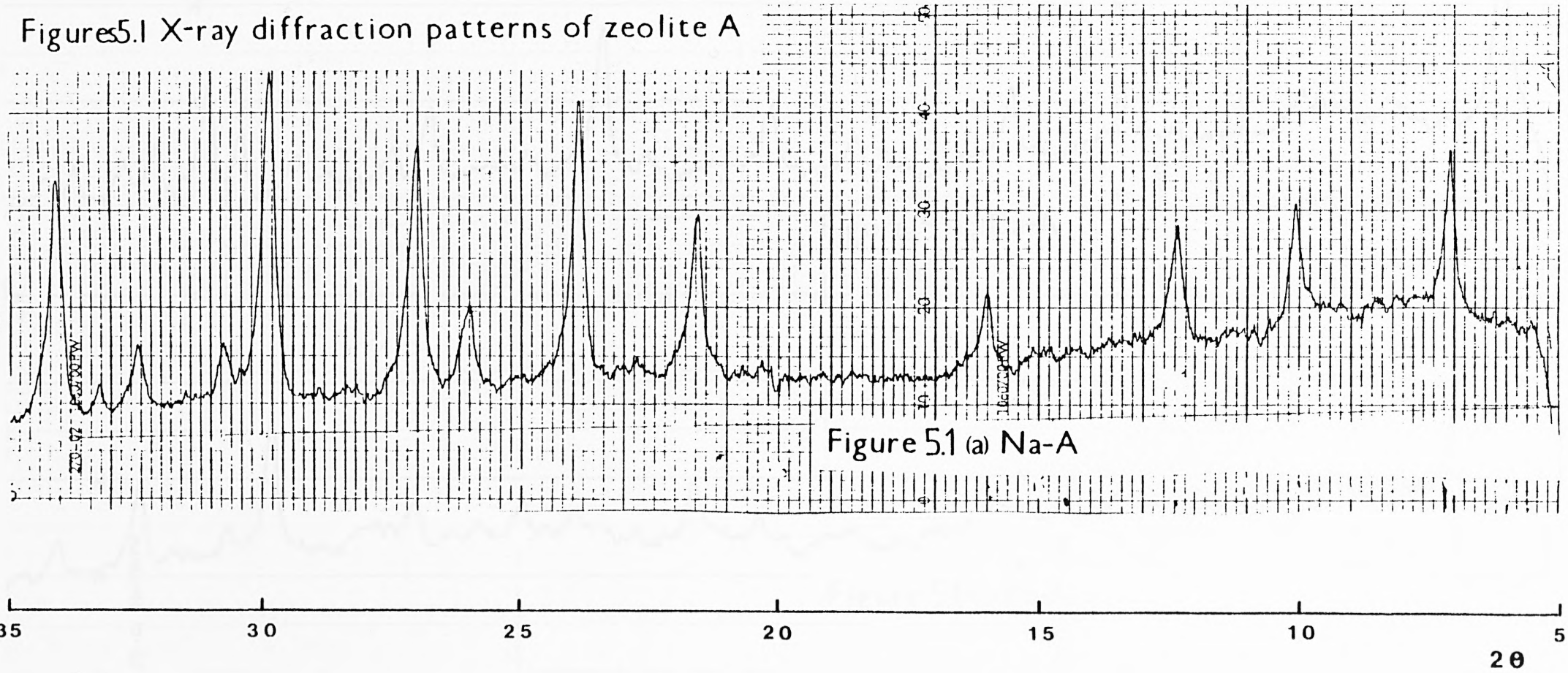

Figure 5.1 (a) Na-A

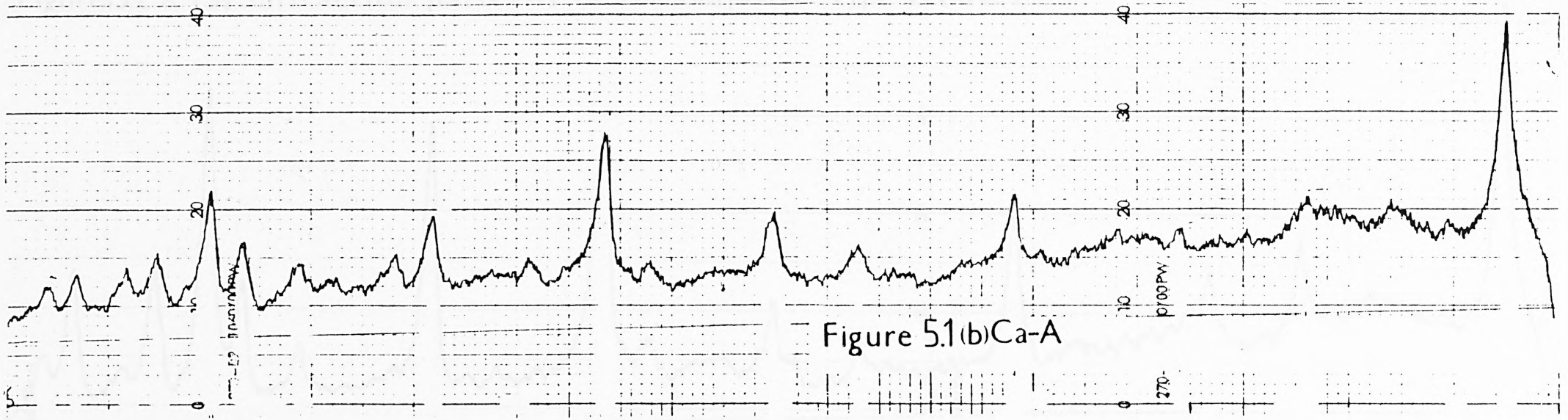

Figure 5.1(b)Ca-A

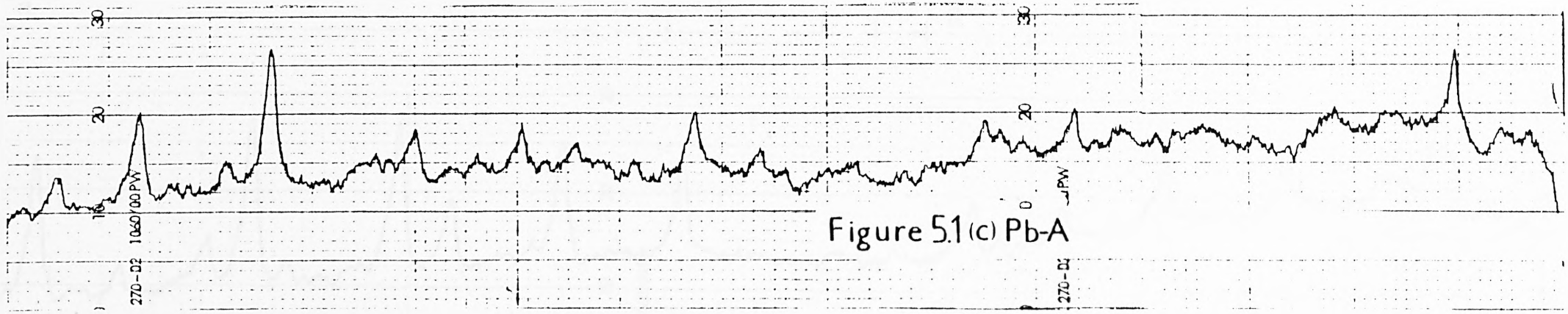

Figure 5.1(c) Pb-A

Figures5.2 X-ray diffraction patterns of the faujasite-type zeolites

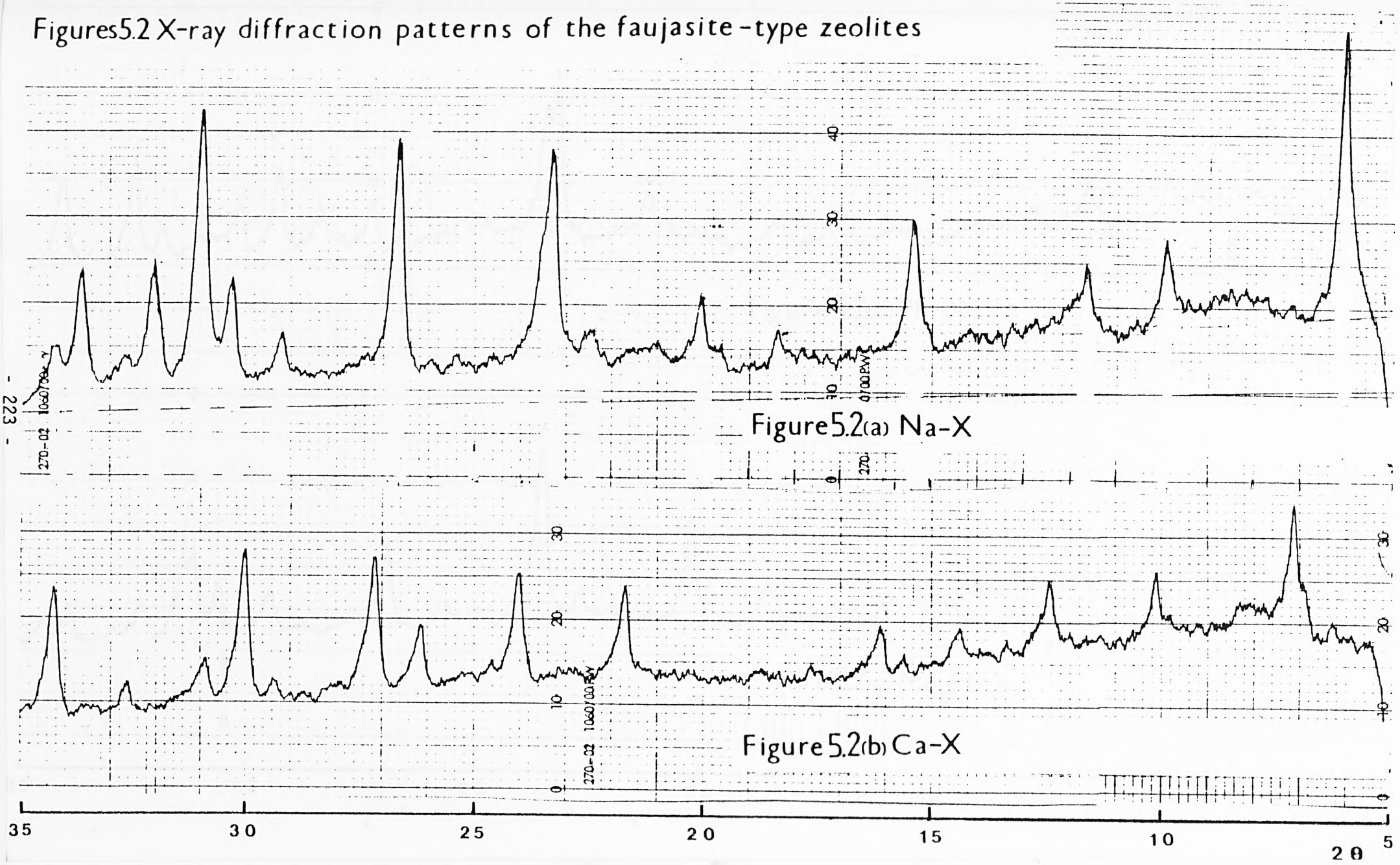

Figure5.2(a) Na-X

Figure 5.2(b) Ca-X

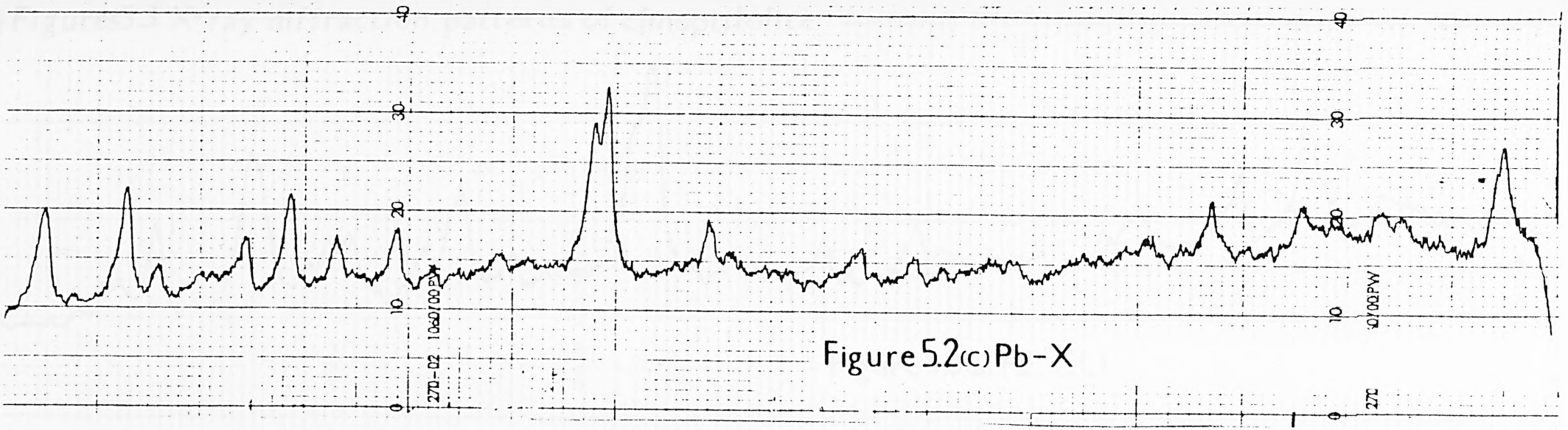

Figure 5.2(c) Pb-X

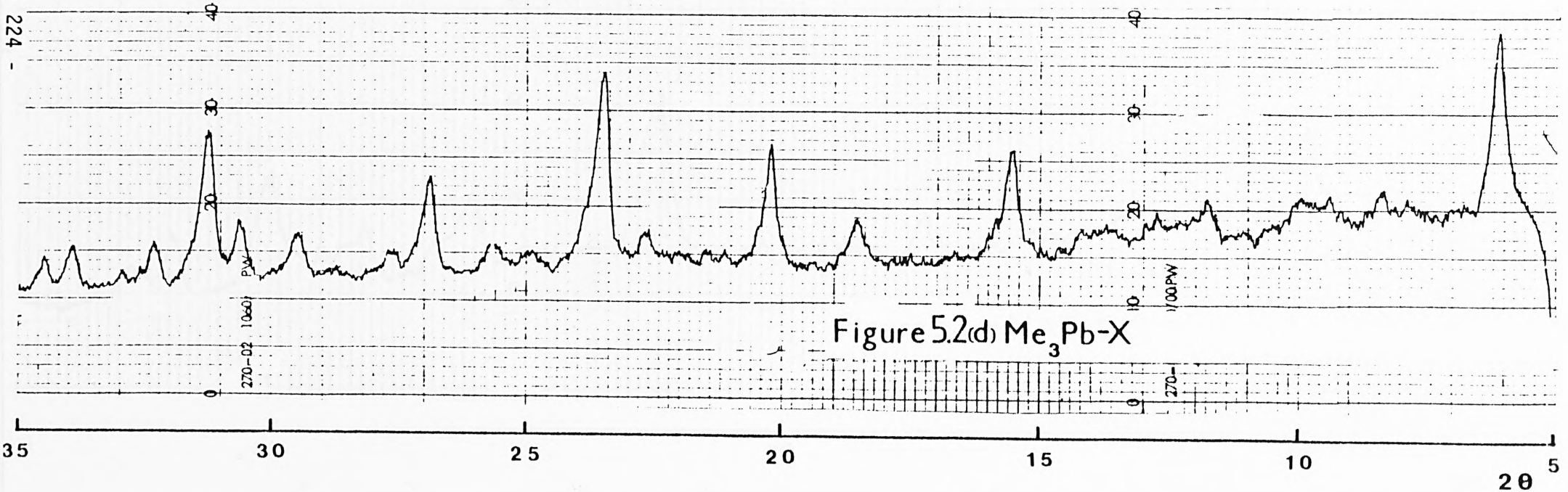

Figure 5.2(d) Me_3Pb-X

Figures5.3 X-ray diffraction patterns of clinoptilolite

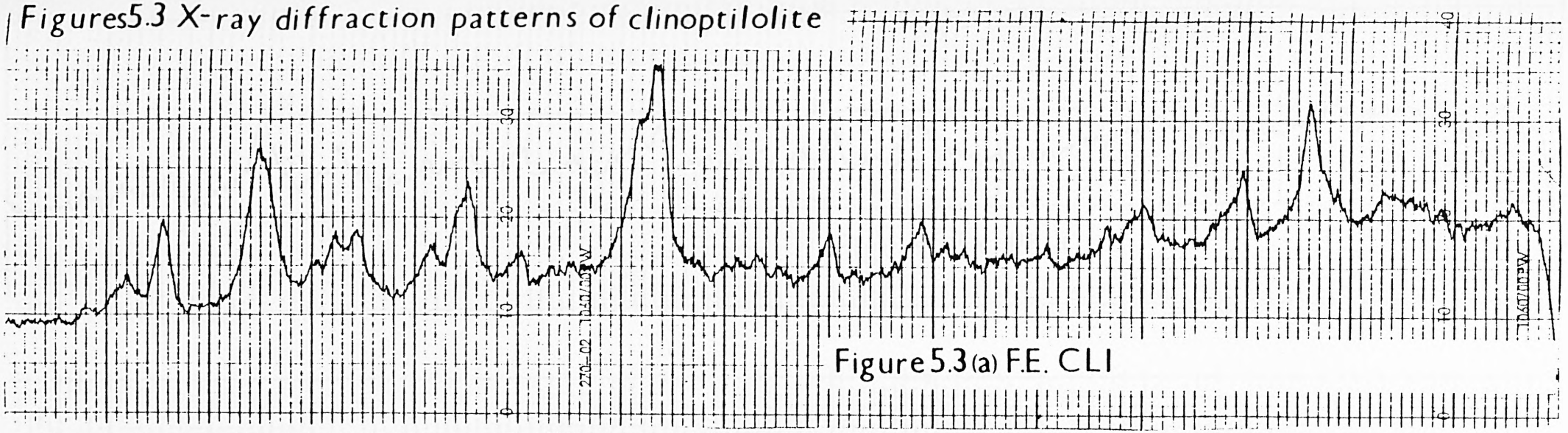

Figure 5.3 (a) F.E. CLI

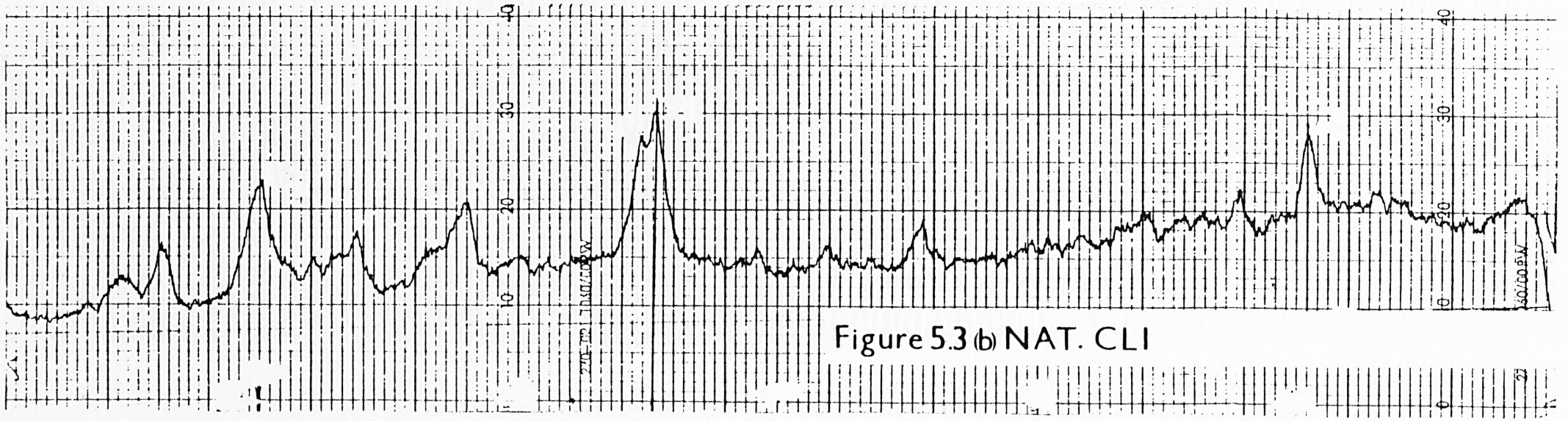

Figure 5.3 (b) NAT. CLI

35 30 25 20 15 10 5

2θ

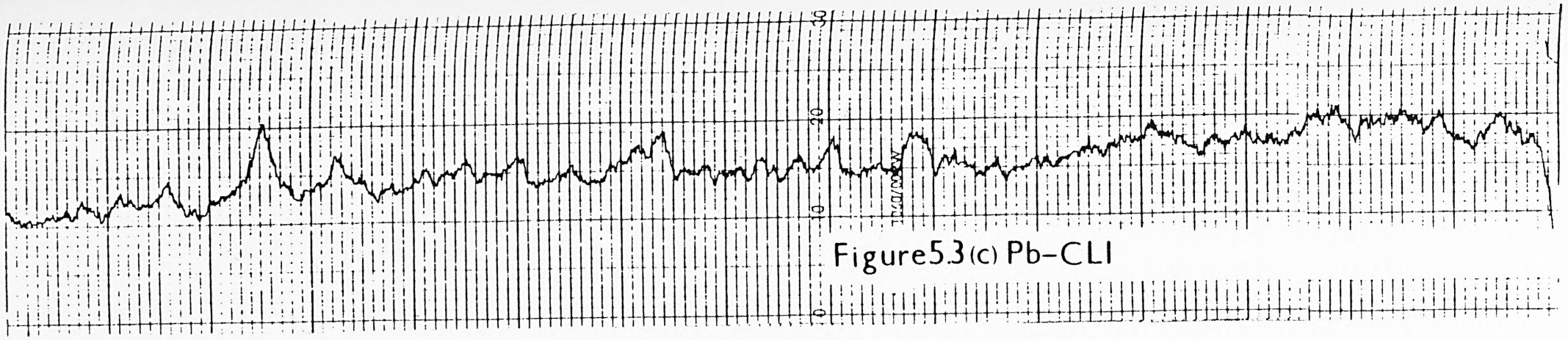

Figure 5.3 (c) Pb–CLI

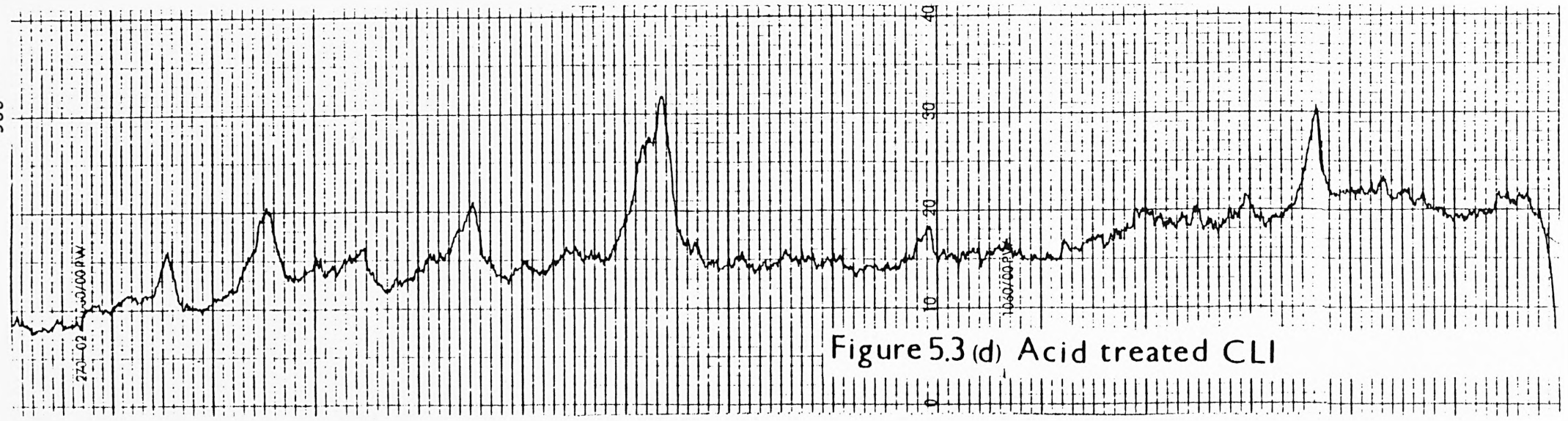

Figure 5.3 (d) Acid treated CLI

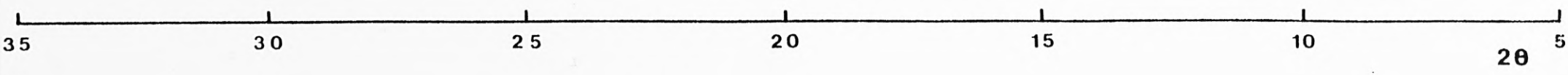

Figure 5.4 Relation between the unit cell volume (a_o) and aluminium atom density (N_{Al}) in number per unit cell

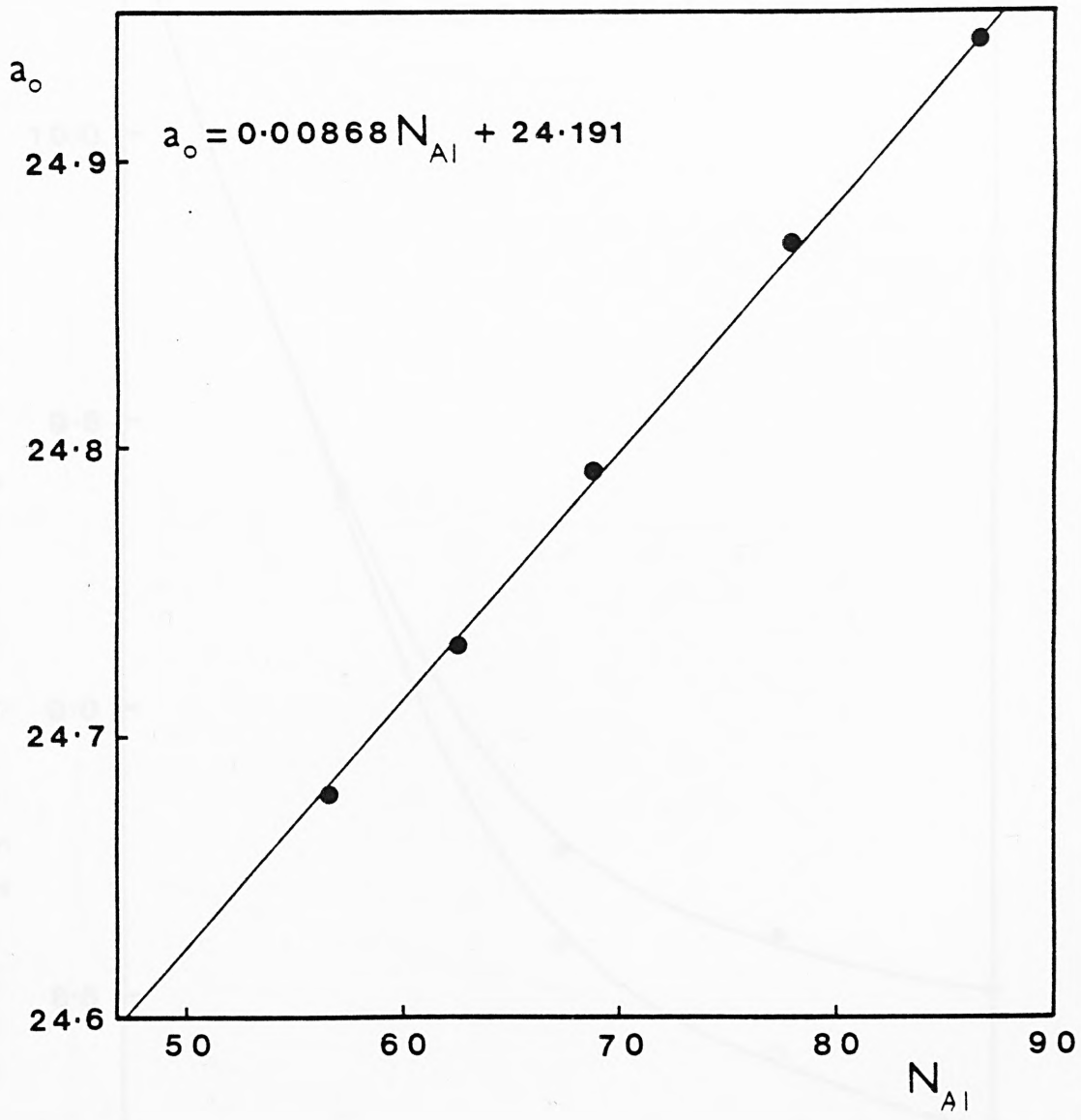

Figure 5.5 Alumina content of clinoptilolite following successive acid treatments

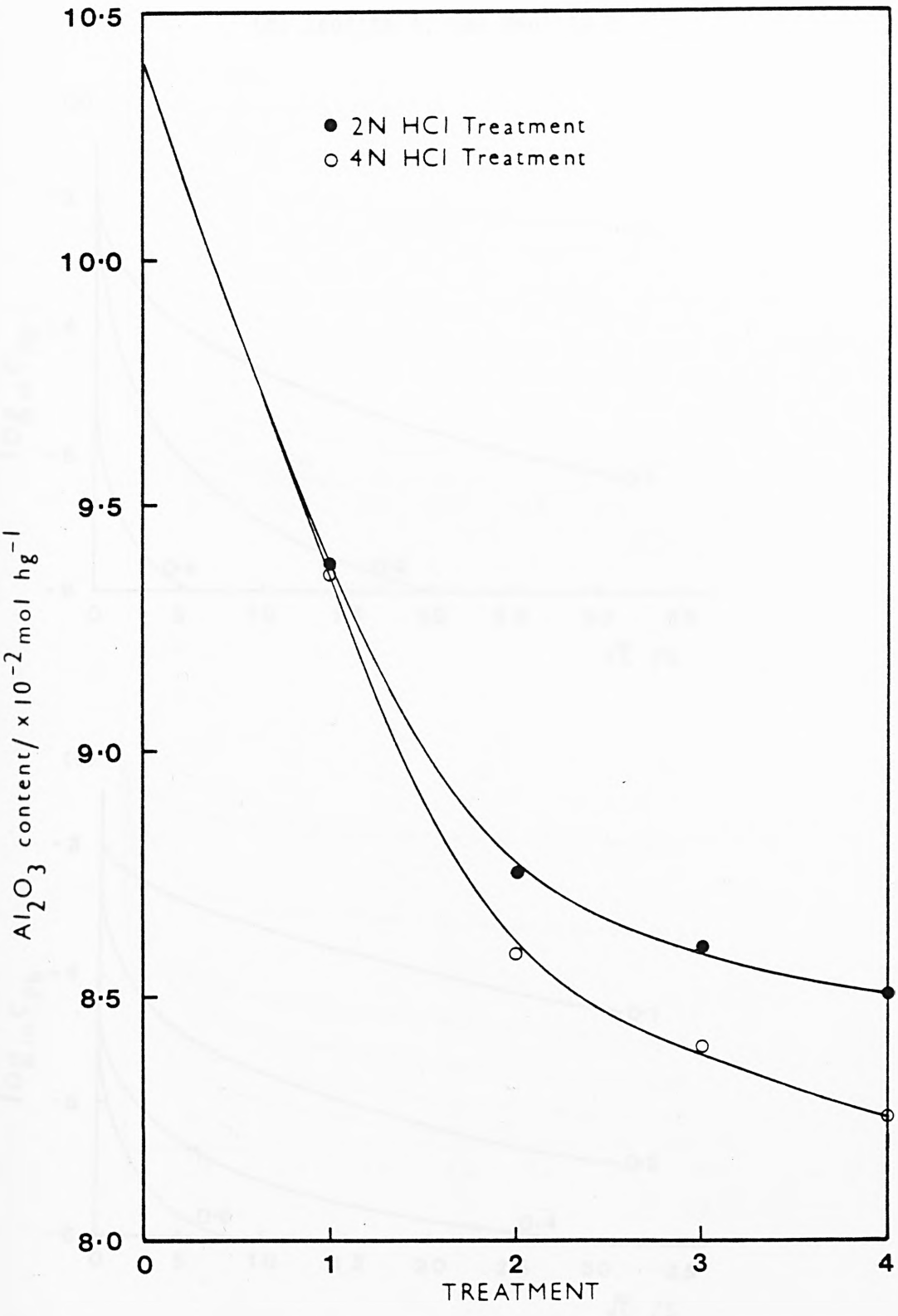

Figure 5.6 Pb^{2+} uptake by faujasites at varying quantities suspended in solution (% w/v).
(a) zeolite 1; (b) zeolite 2; (c) zeolite 3;
(d) zeolite 4; (e) zeolite 5

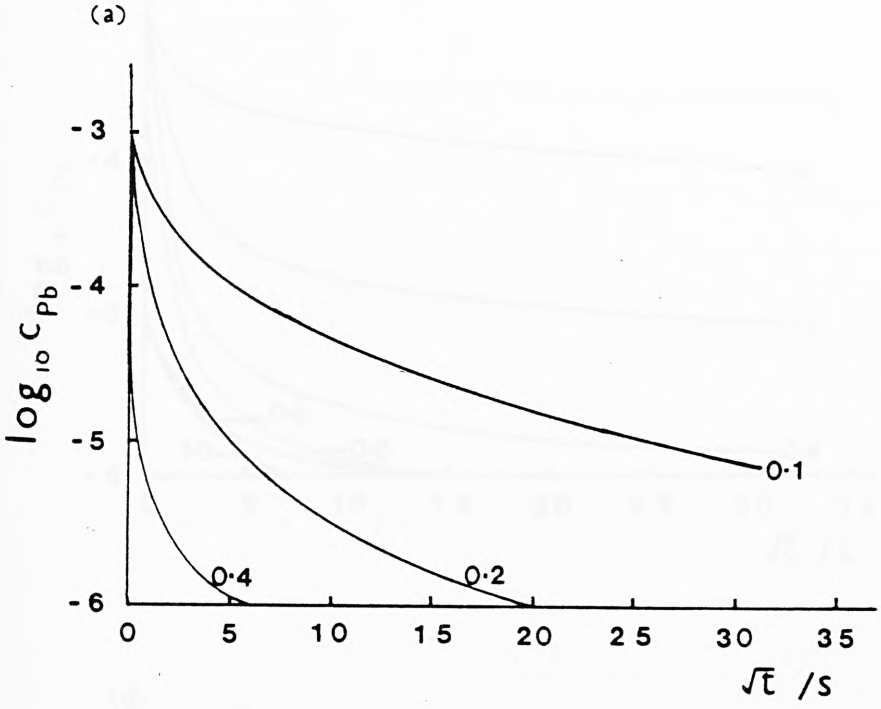

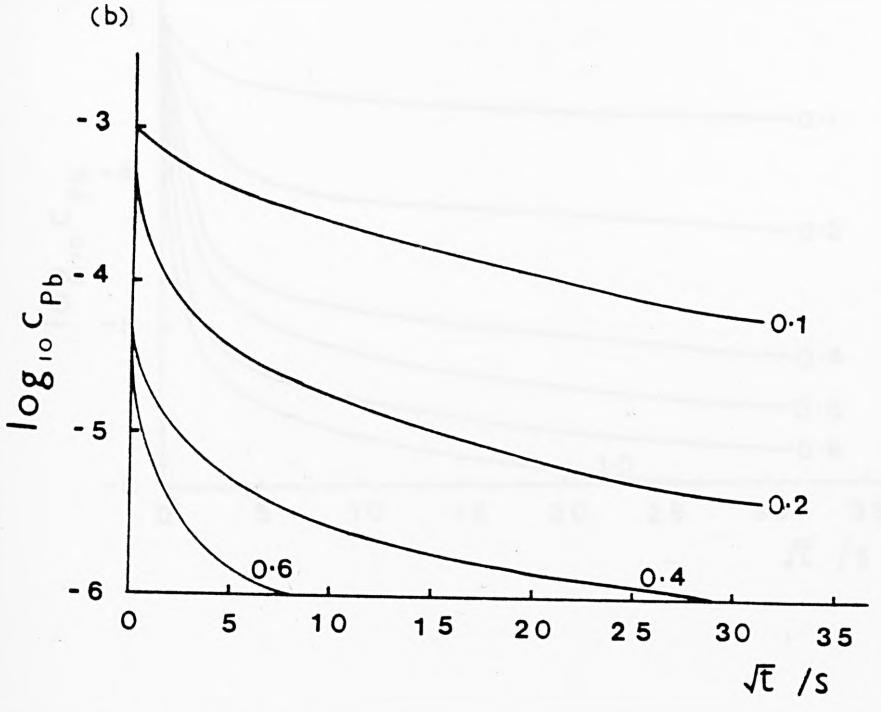

Figure 5.6 (continued)

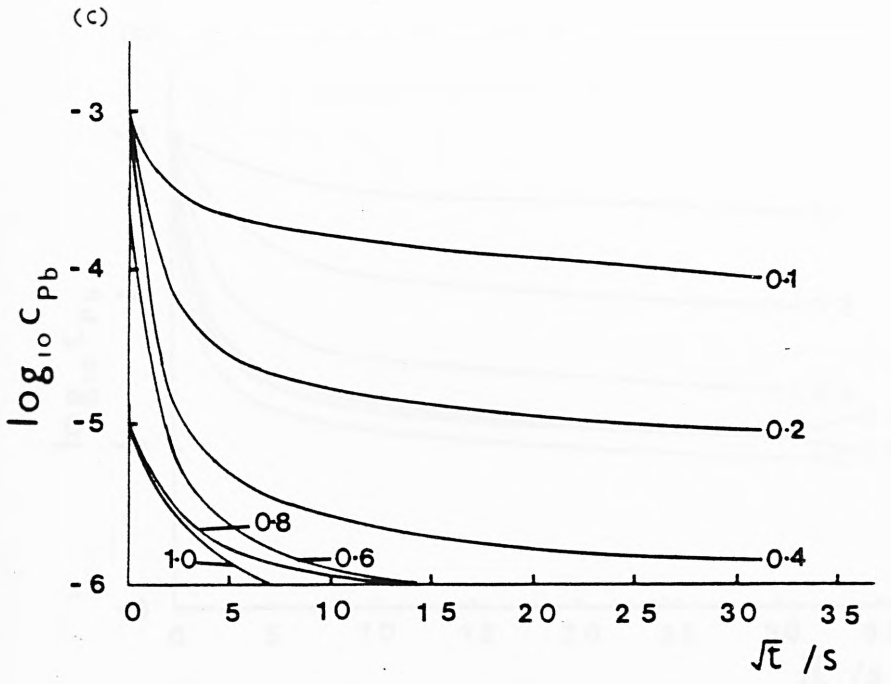

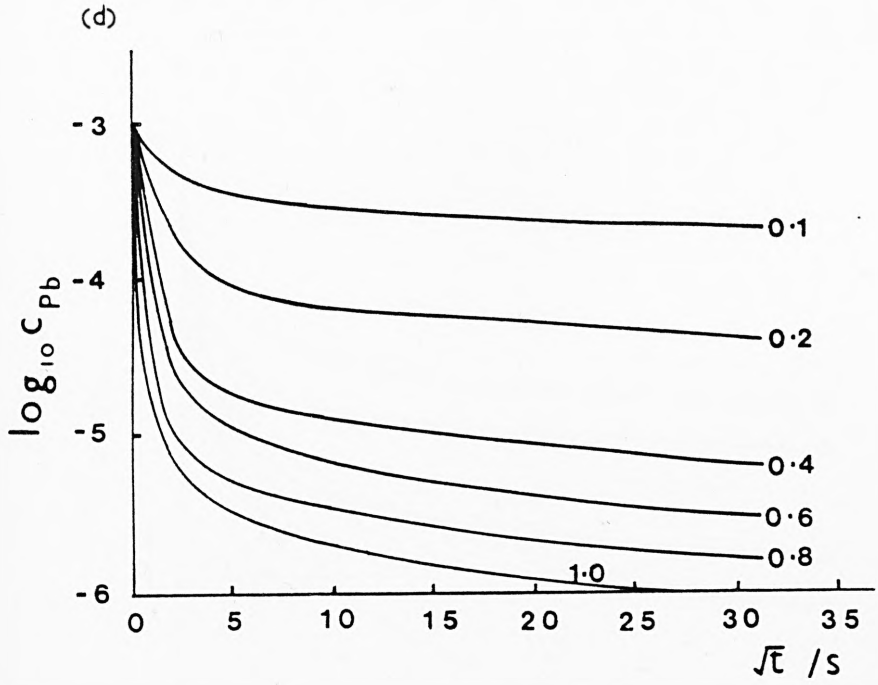

Figure 5.6 (continued)

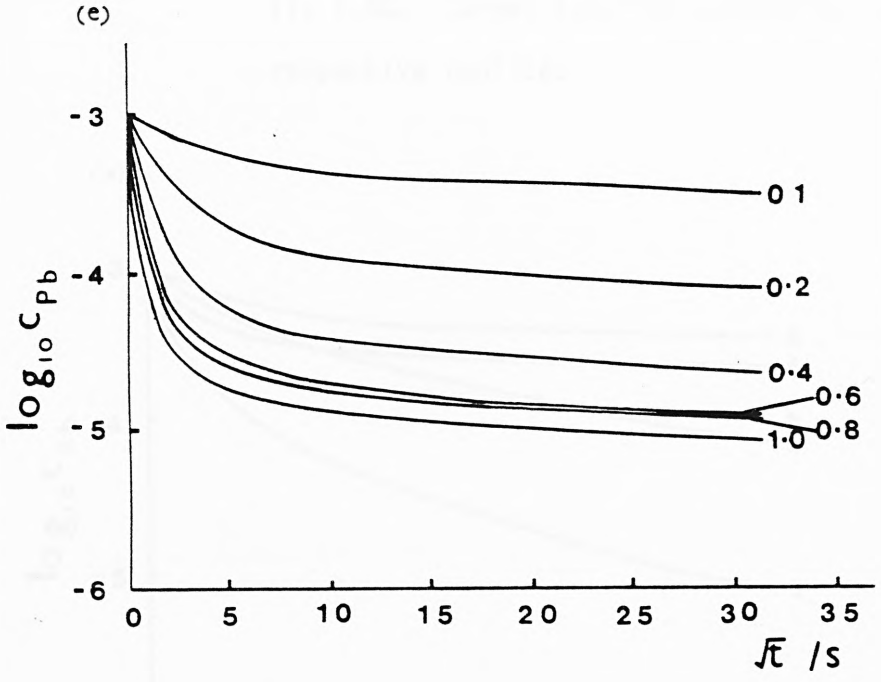

Figure 5.7 Comparison of Pb^{2+} uptake by faujasites for varying quantities suspended in solution (% w/v). (a) 0.1%; (b) 0.2%; (c) 0.4%; (d) 0.6%; (e) 0.8%; (f) 1.0%. Curves labelled according to the respective zeolites

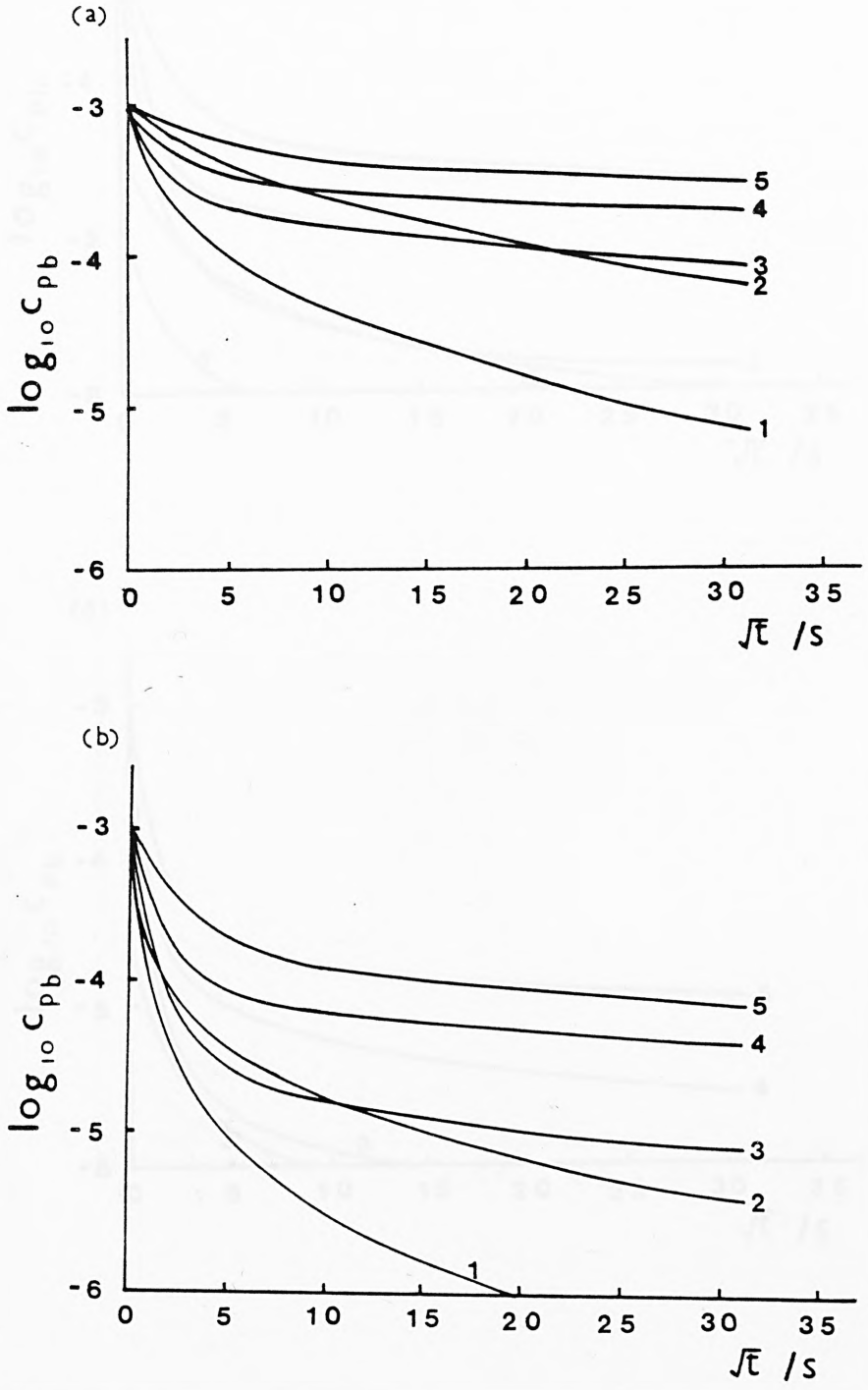

Figure 5.7 (continued)

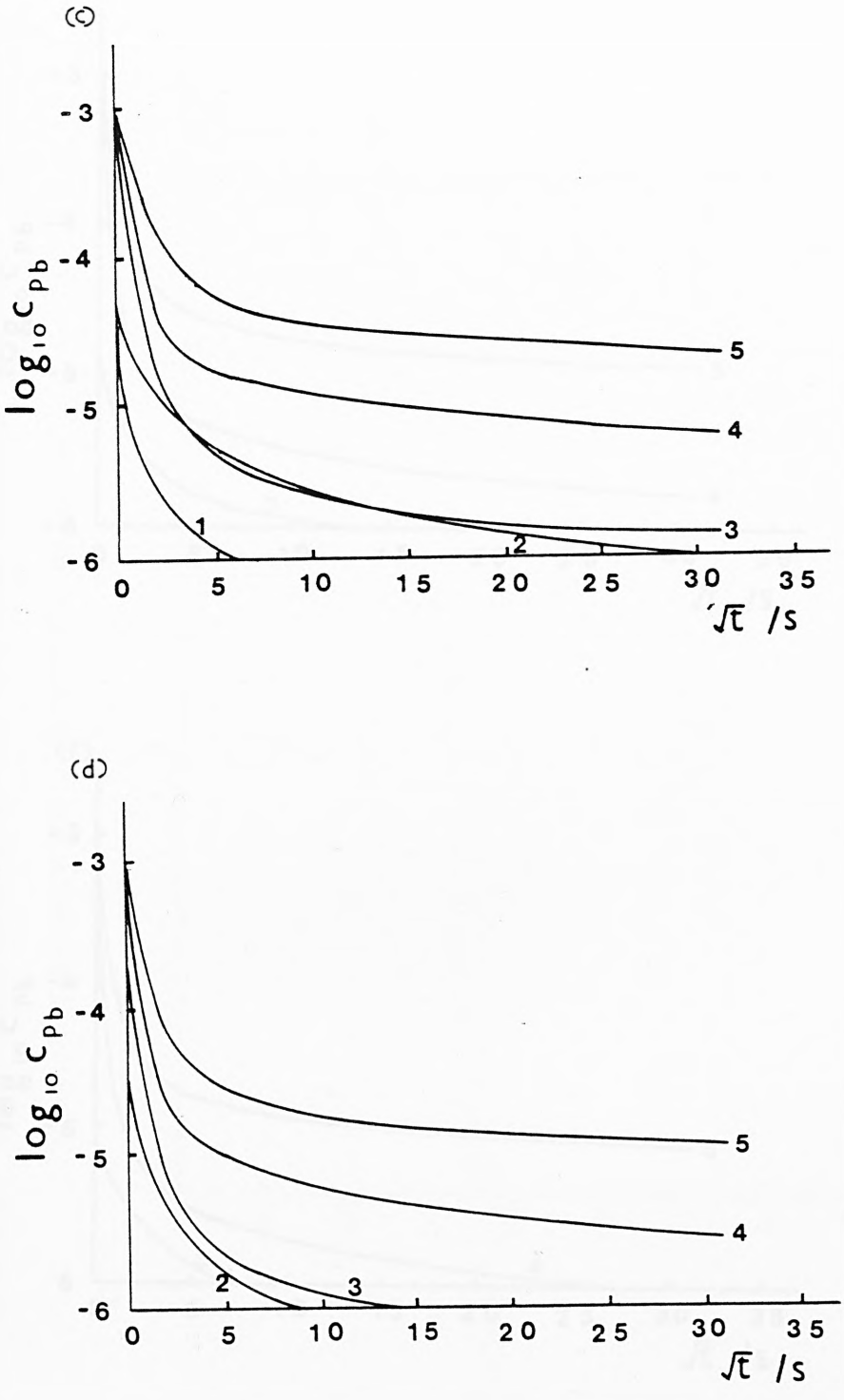

Figure 5.7 (continued)

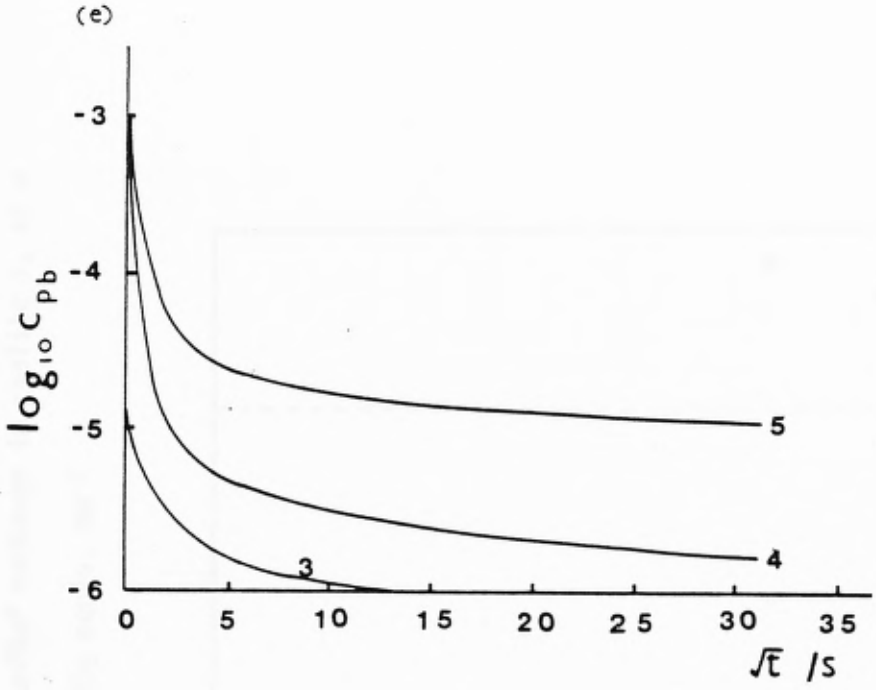

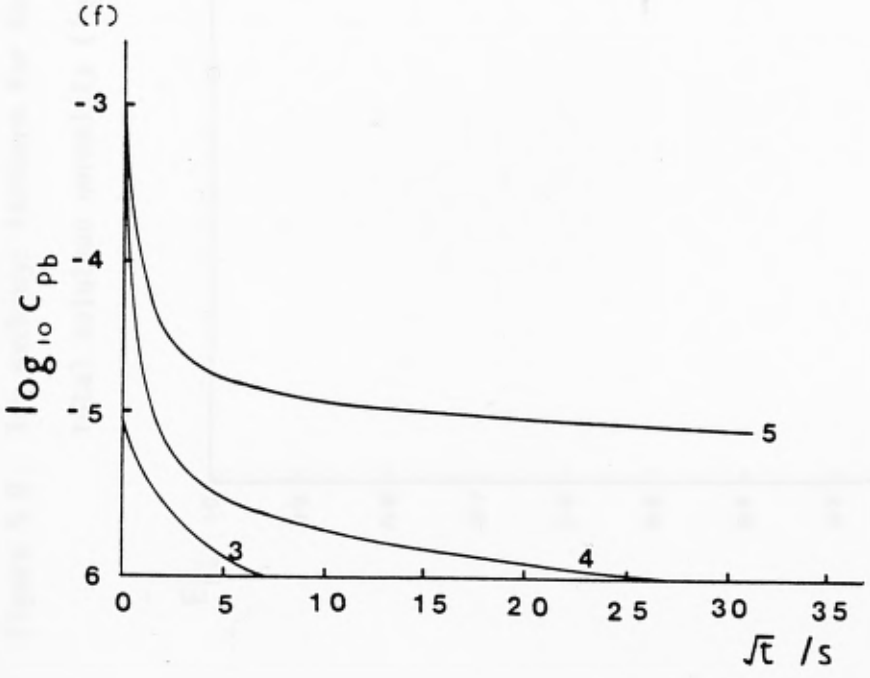

Figure 5.8 Ion exchange isotherm for the $Pb^{2+} \rightleftharpoons 2Na^{+}$ exchange in zeolite 1, at a total solution normality (T_N) of 0.05g equiv. dm^{-3}

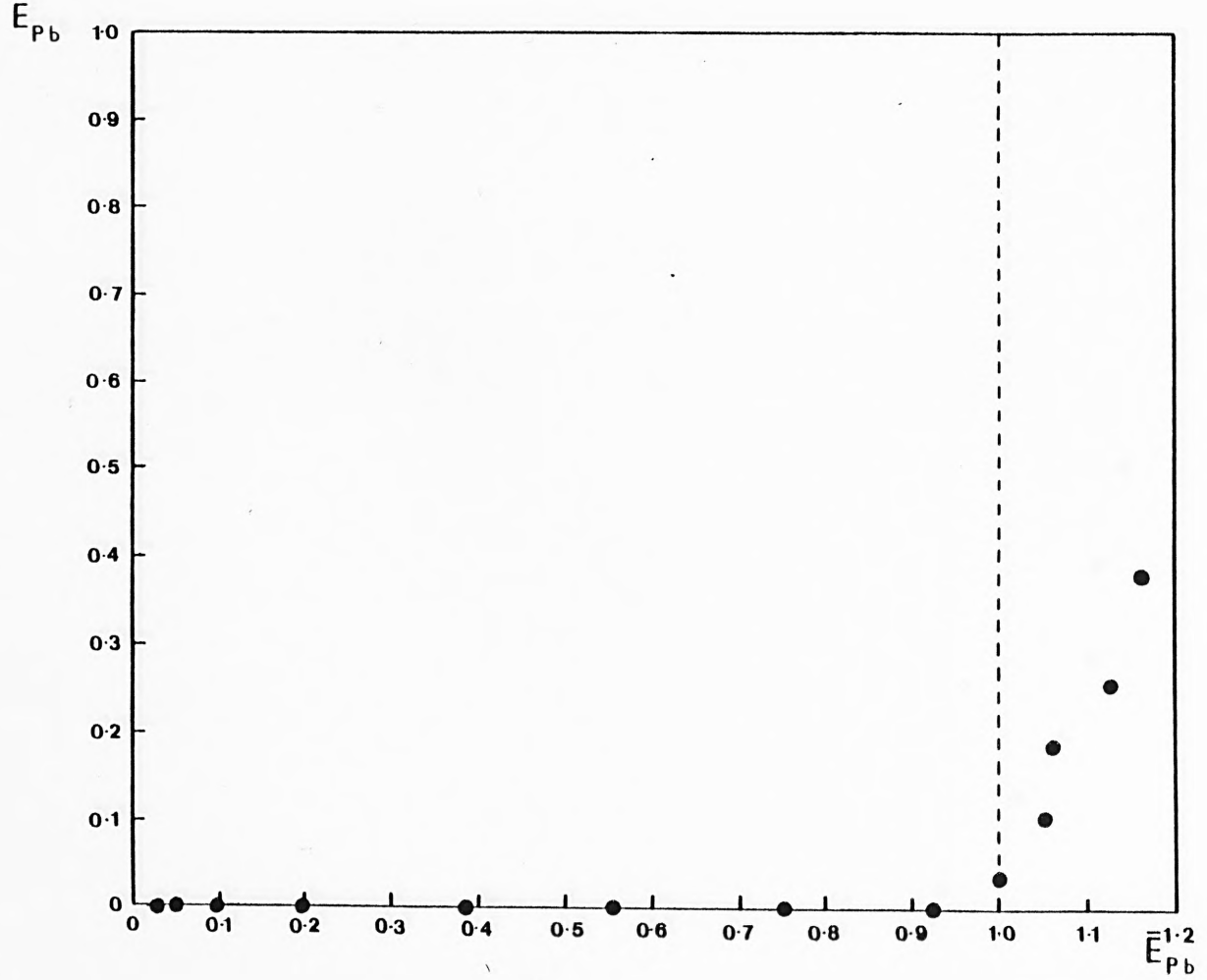

Figure 5.9 Ion exchange isotherm for the $Pb^{2+} \rightleftharpoons 2Na^{+}$ exchange in zeolite 2, at a total solution normality (T_N) of 0.05g equiv. dm^{-3}

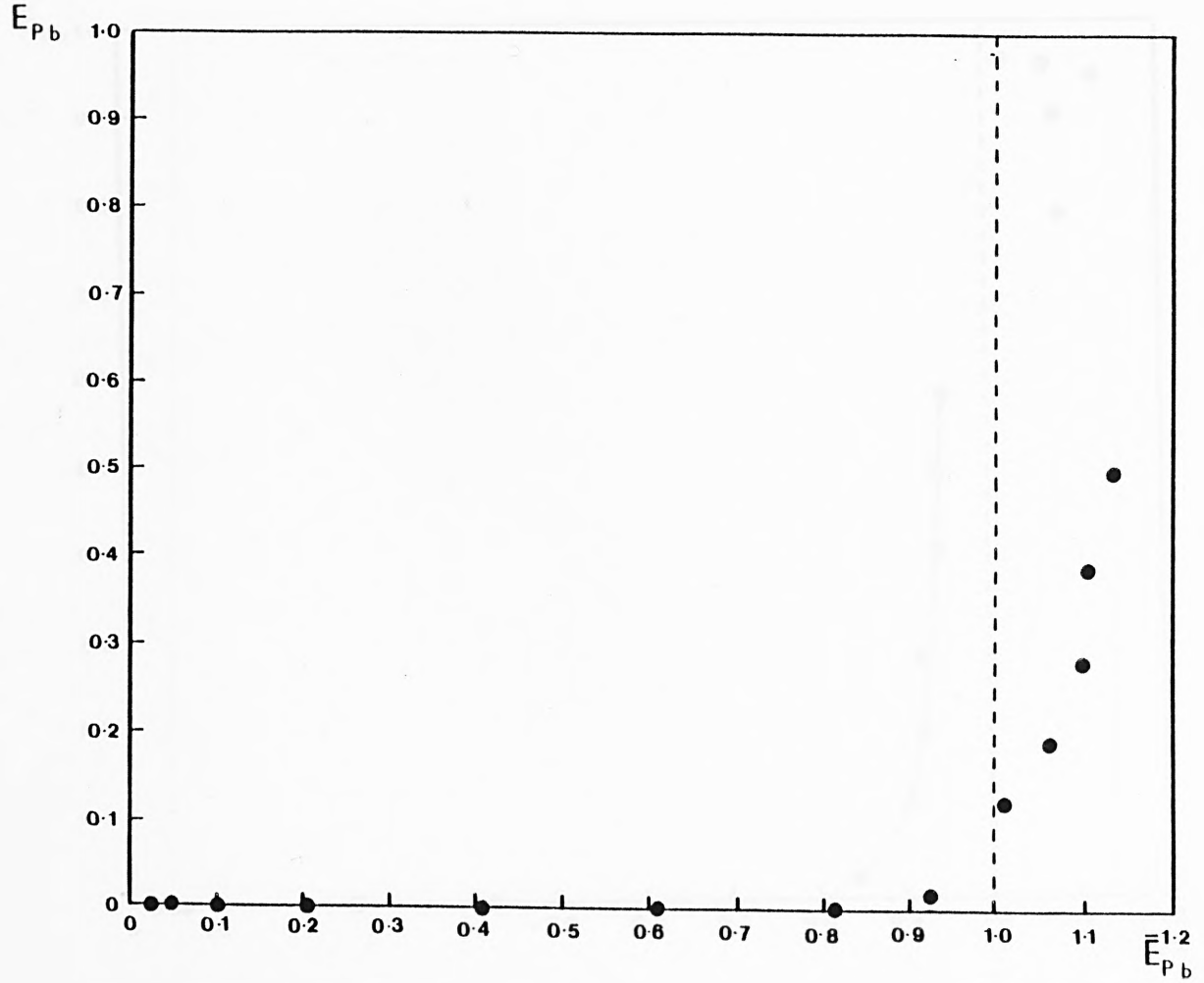

Figure 5.10 Ion exchange isotherm for the $Pb^{2+} \rightleftharpoons 2Na^{+}$ exchange in zeolite 3, at a total solution normality (T_N) of 0.05g equiv. dm^{-3}

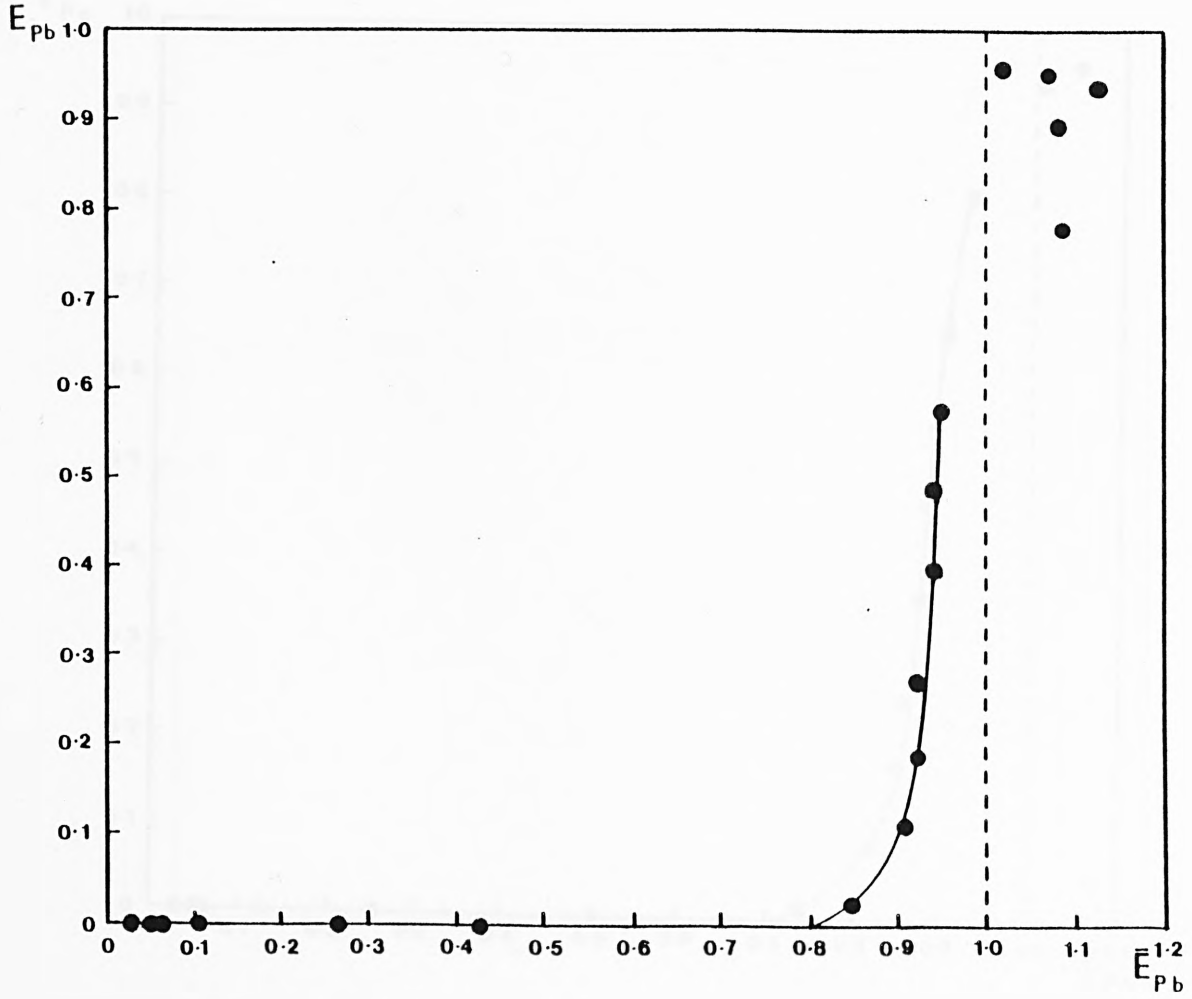

Figure 5.11 Ion exchange isotherm for the $Pb^{2+} \rightleftharpoons 2Na^{+}$ exchange in zeolite 4, at a total solution normality (T_N) of 0.05g equiv. dm^{-3}

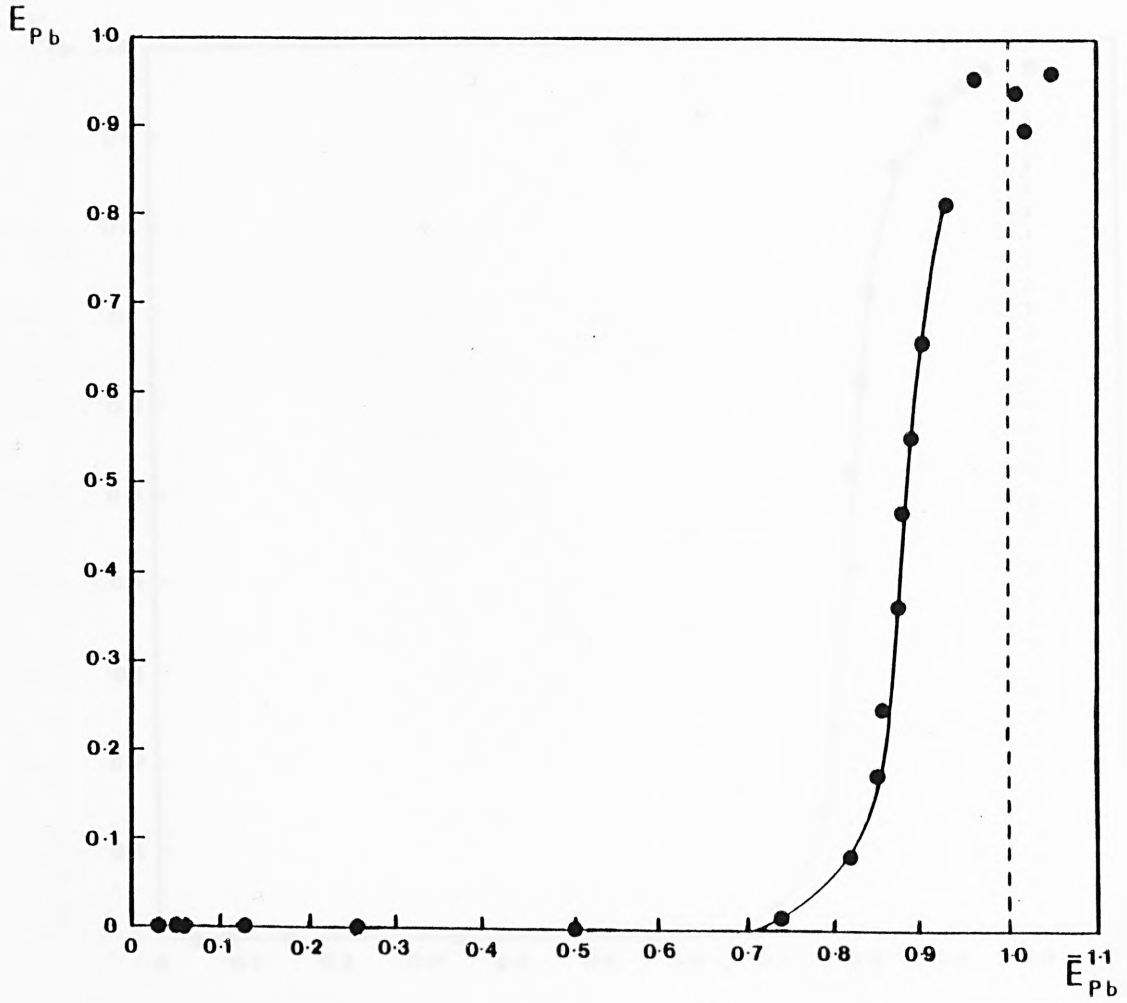

Figure 5.12 Ion exchange isotherm for the $Pb^{2+} \rightleftharpoons 2Na^{+}$ exchange in zeolite 5, at a total solution normality (T_N) of 0.05g equiv. dm^{-3}

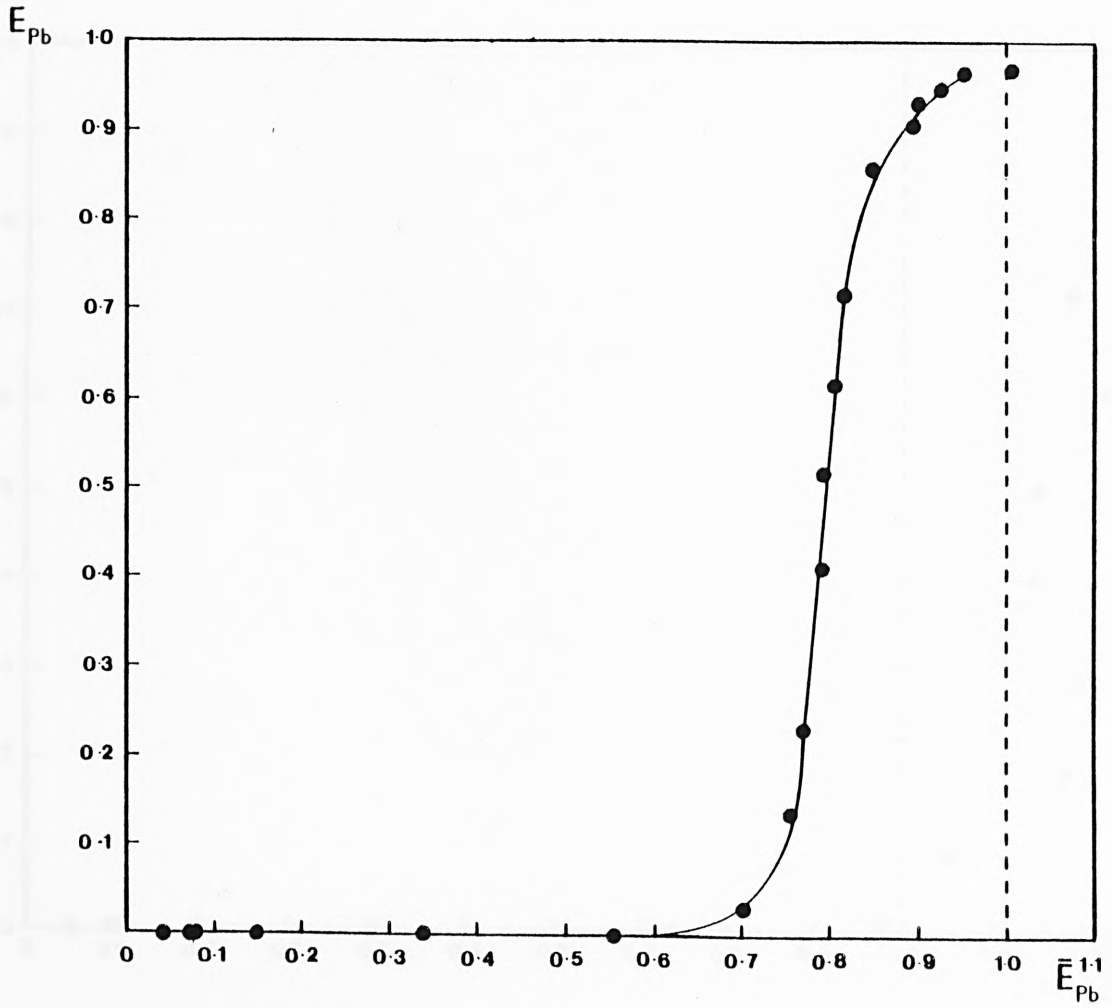

Figure 5.13 Ion exchange isotherm for the $Pb^{2+} \rightleftharpoons 2Na^{+}$ exchange in zeolite 1, at a total solution normality (T_N) of 0.1g equiv. dm^{-3}

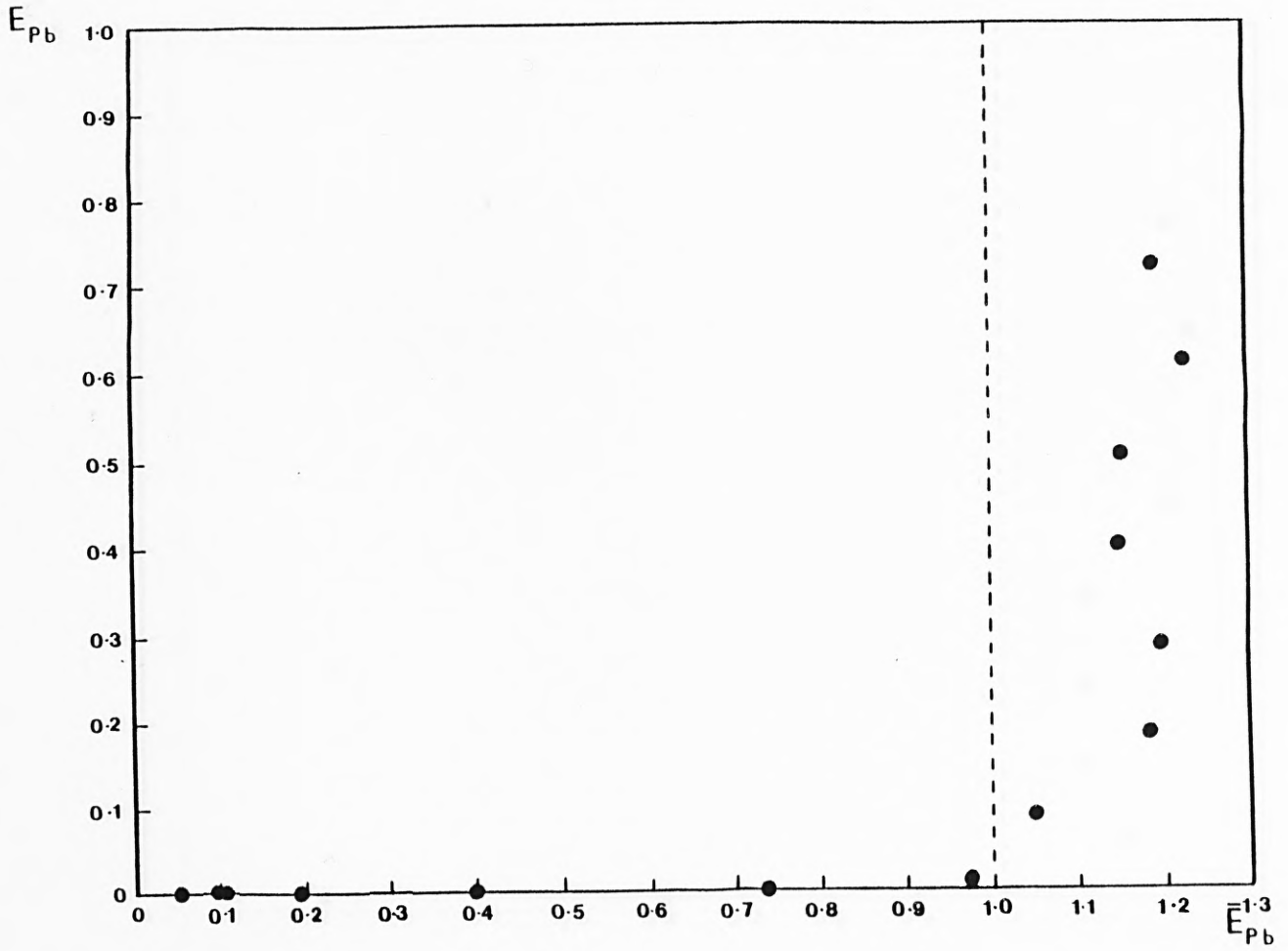

Figure 5.14 Ion exchange isotherm for the $Pb^{2+} \rightleftharpoons 2Na^{+}$ exchange in zeolite 2, at a total solution normality (T_N) of 0.1g equiv. dm^{-3}

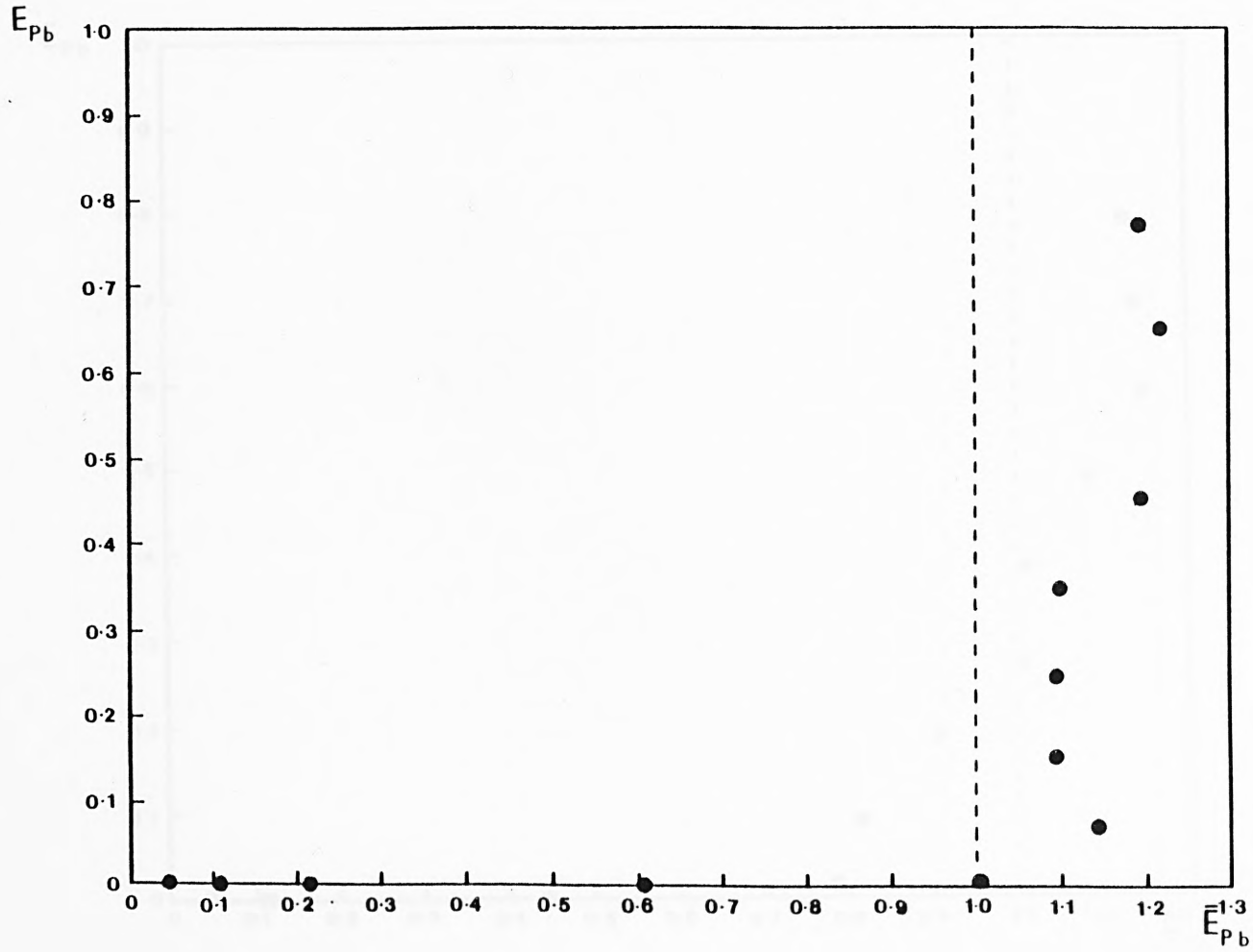

Figure 5.15 Ion exchange isotherm for the $Pb^{2+} \rightleftharpoons 2Na^{+}$ exchange in zeolite 3, at a total solution normality (T_N) of 0.1g equiv. dm^{-3}

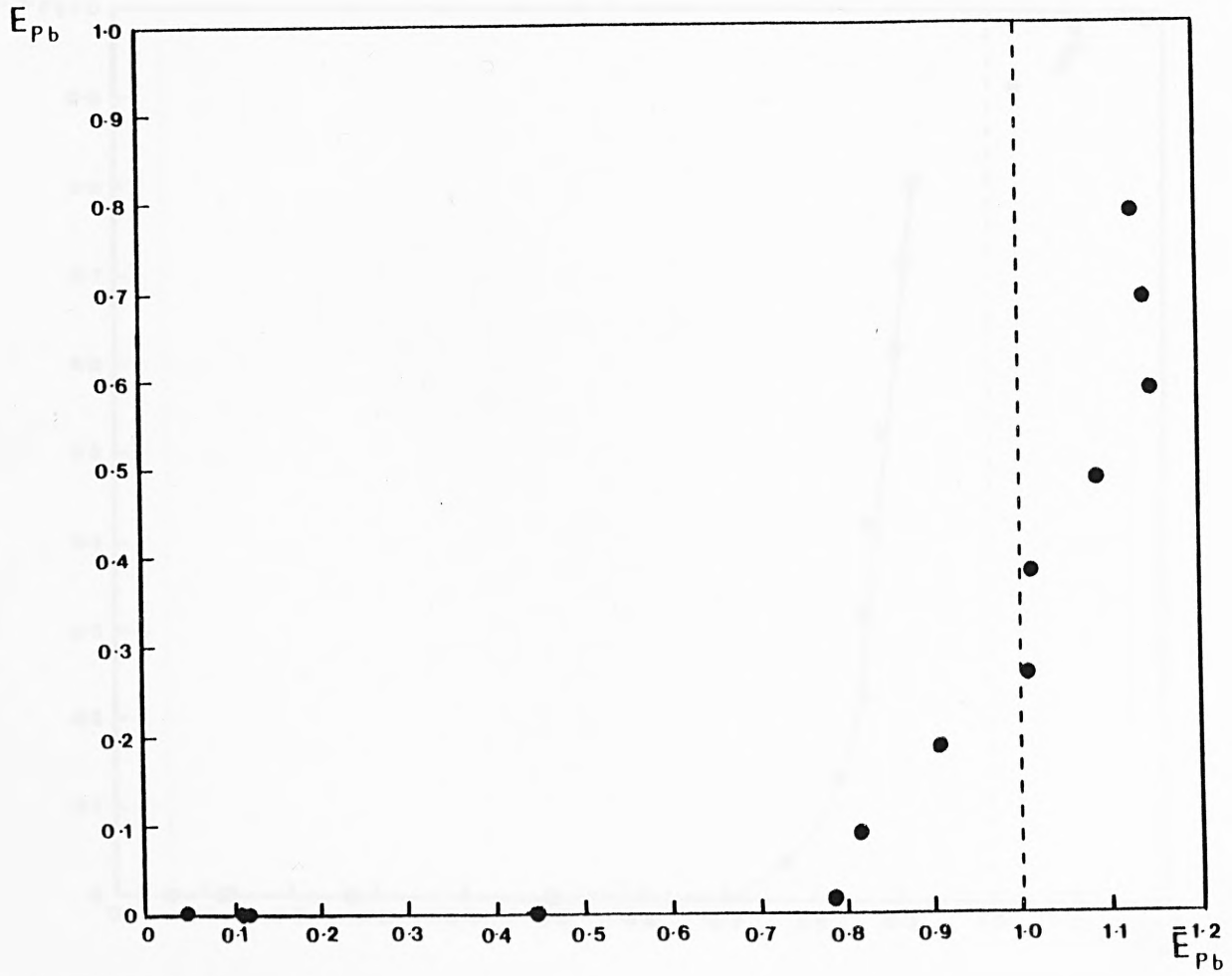

Figure 5.16 Ion exchange isotherm for the $Pb^{2+} \rightleftharpoons 2Na^{+}$ exchange in zeolite 4, at a total solution normality (T_N) of 0.1g equiv. dm^{-3}

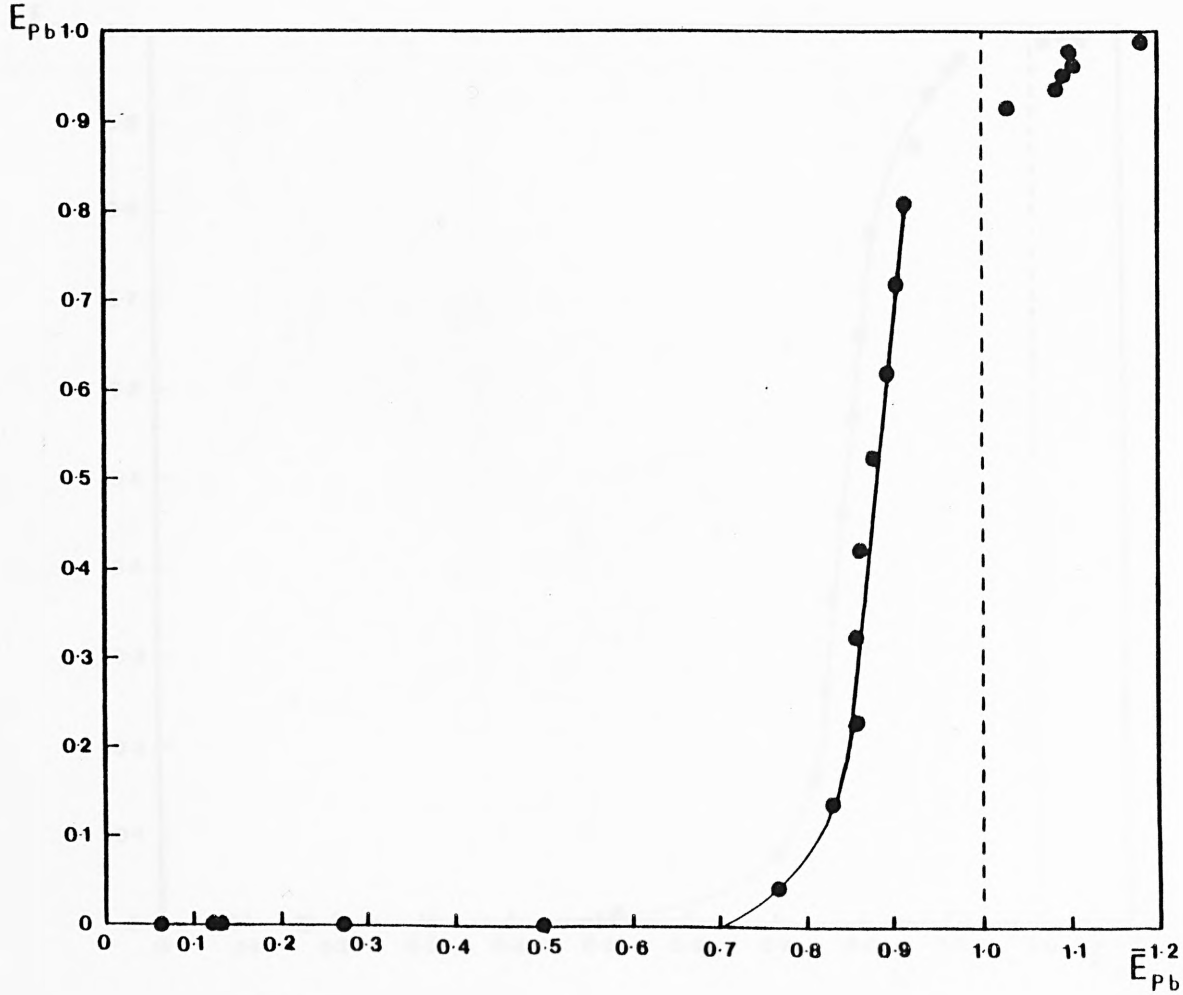

Figure 5.17 Ion exchange isotherm for the $Pb^{2+} \rightleftharpoons 2Na^{+}$ exchange in zeolite 5, at a total solution normality (T_N) of 0.1g equiv. dm^{-3}

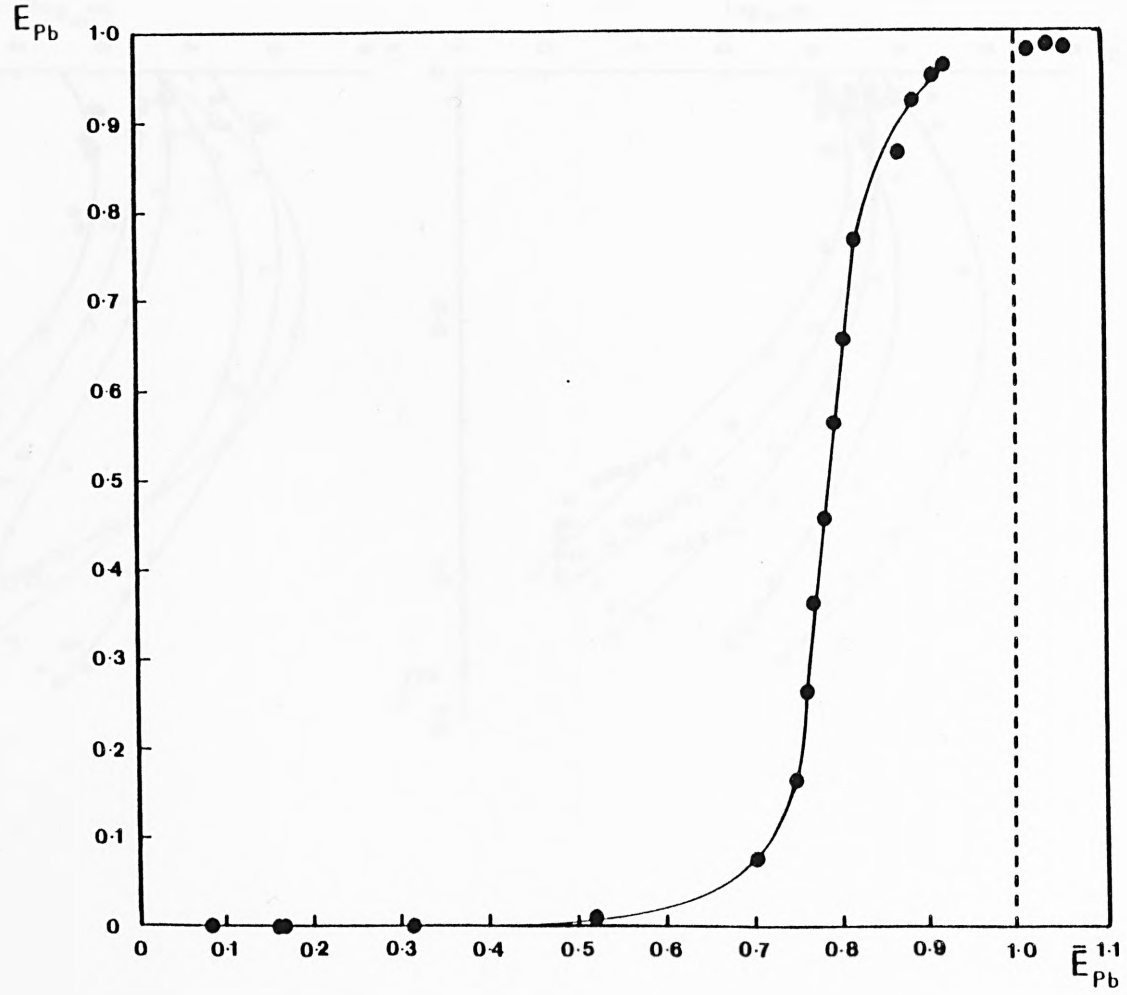

Figure 5.18 Selectivity plots for lead exchange in zeolite A and zeolites 1-5 as a function of equivalent fraction of lead in the crystal phase. Data for (○) A; (▲)1; (▽)2; (×)3; (□)4; (◆)5.

(a) T_N = 0.05g equiv. dm^{-3}.

(b) T_N = 0.1g equiv. dm^{-3}

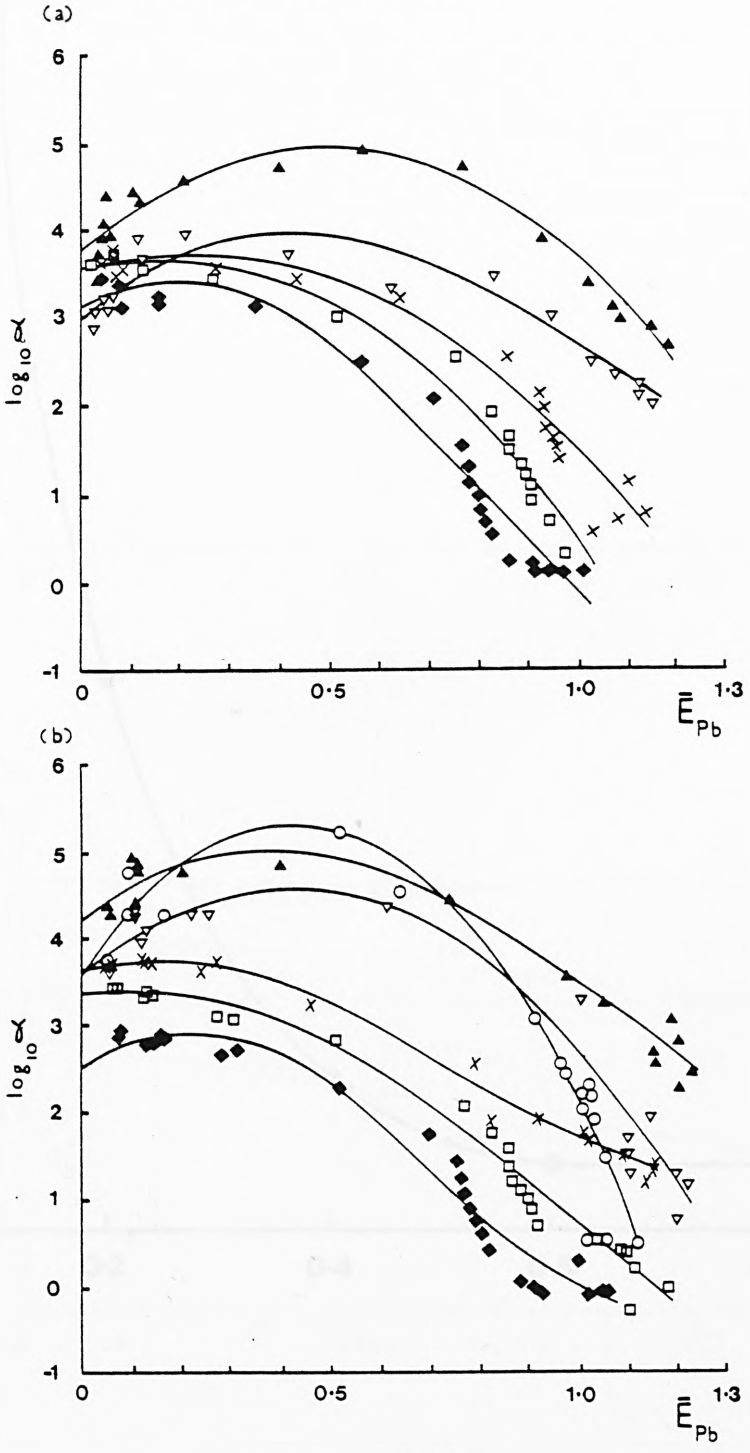

Figure 5.19 Precipitation limit of $Pb(NO_3)_2$ in the presence of $NaNO_3$, depicted as a plot of pH against equivalent fraction of Pb^{2+} ion in solution.
T_N = 0.1g equiv. dm^{-3} for all solutions.

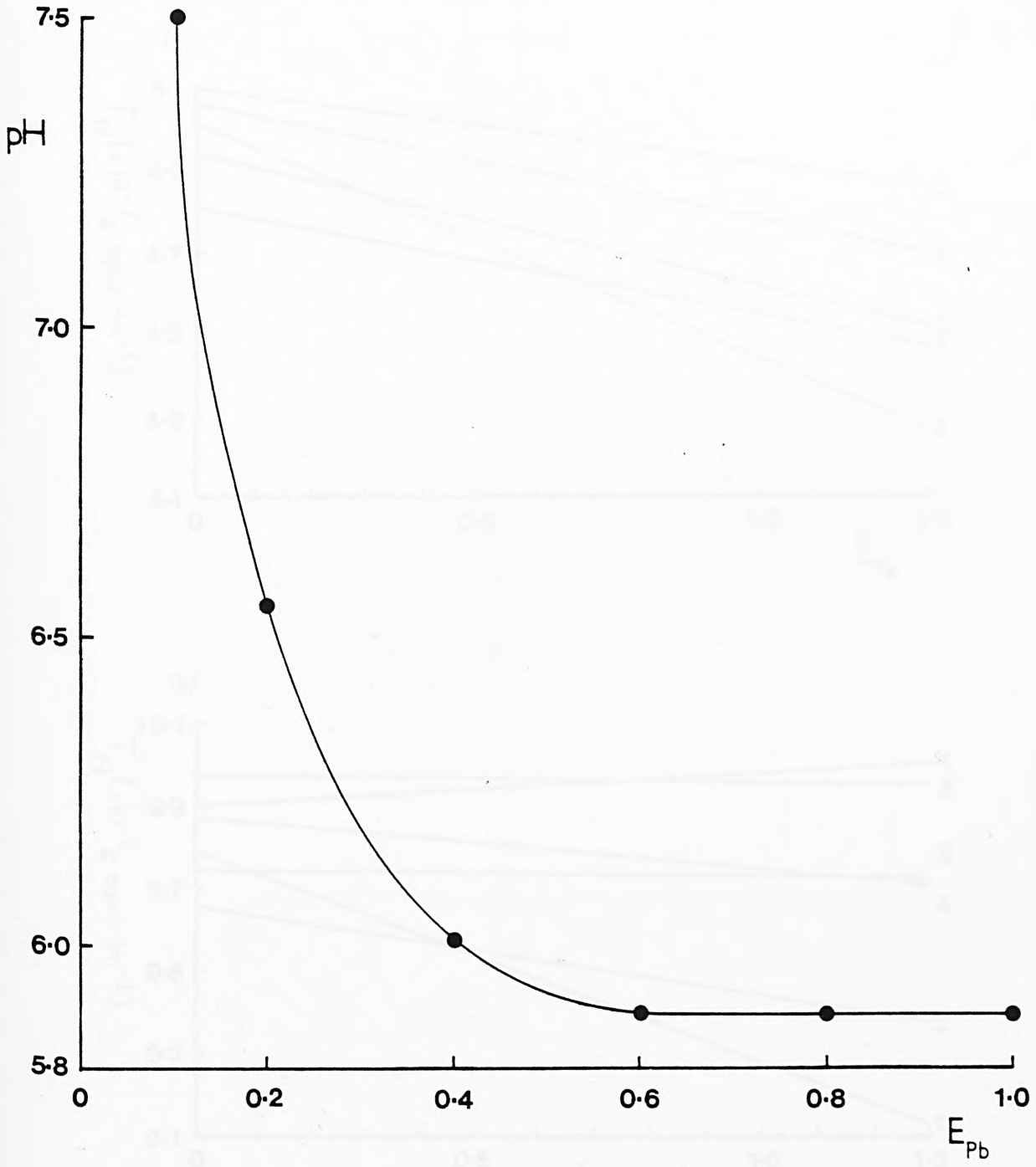

Figure 5.20 Plots showing trends in total normalities of solution phase as a function of equivalent fraction of lead in the zeolite.

(a) T_N = 0.05g equiv. dm^{-3}

(b) T_N = 0.1g equiv. dm^{-3}

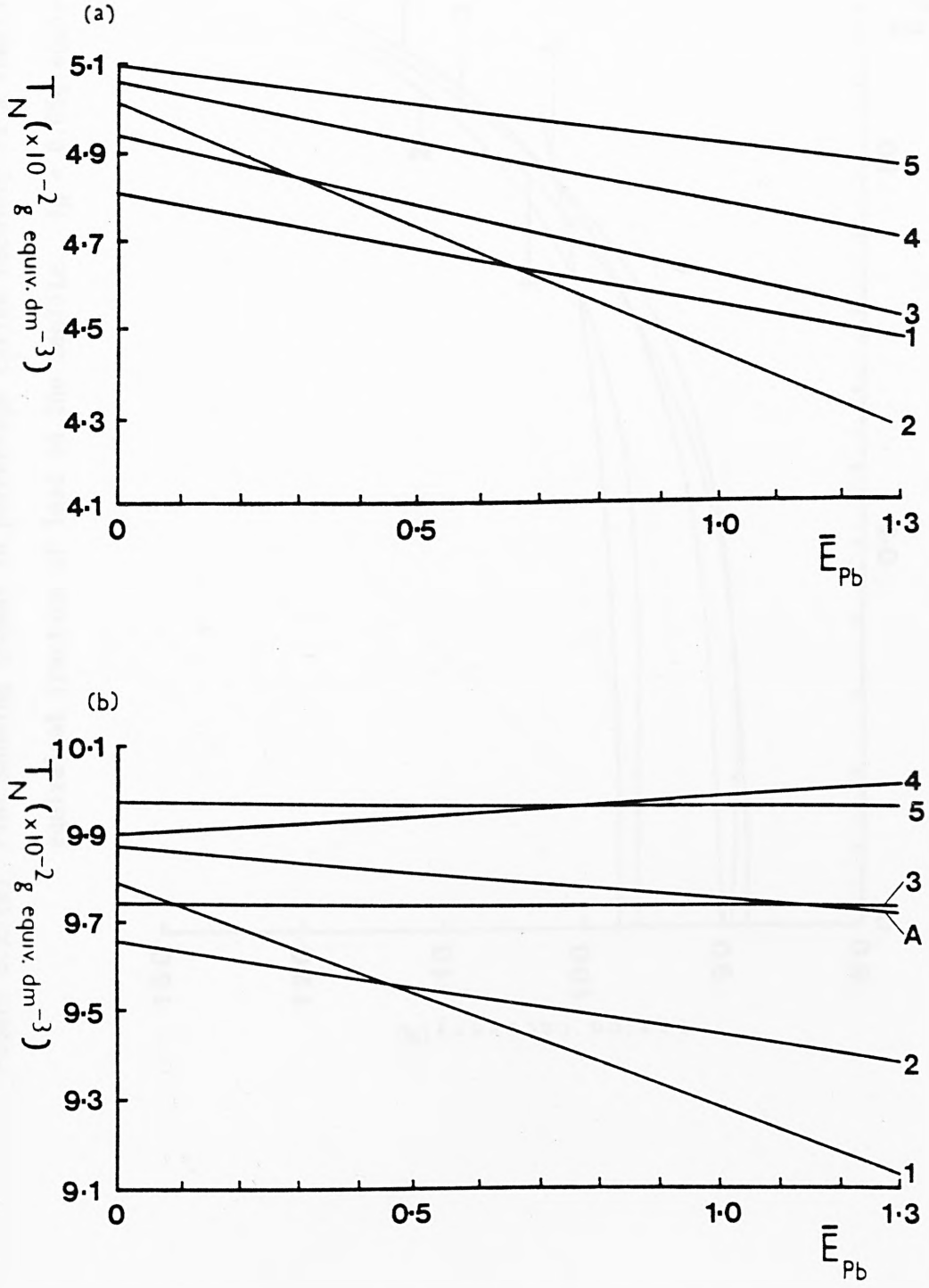

Figure 5.21(a) Plot showing trends in percentage cation recovery as a function of equivalent fraction of lead in the zeolite. T_N = 0.05g equiv. dm^{-3}

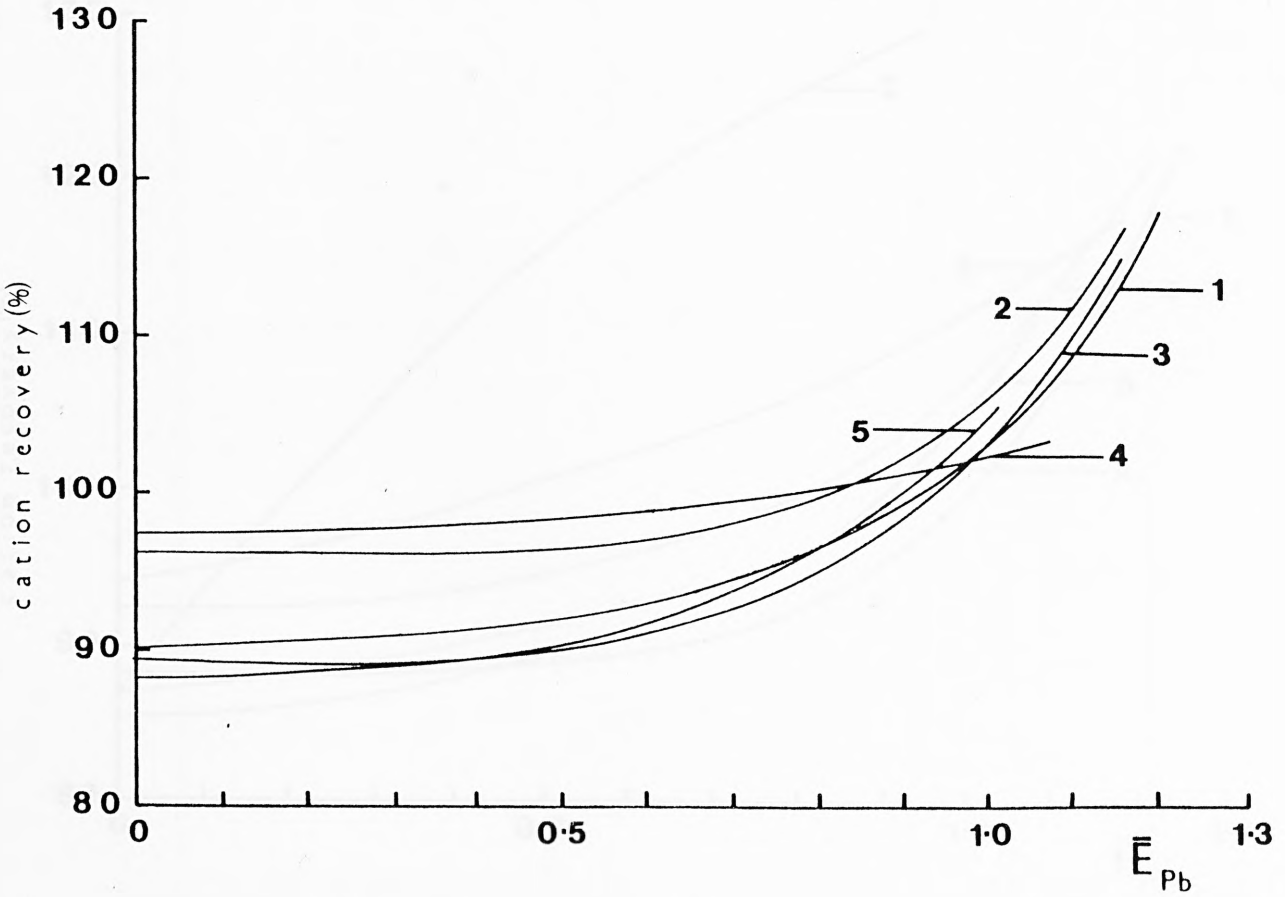

Figure 5.21(b) Plot showing trends in percentage cation recovery as a function of equivalent fraction of lead in the zeolite. T_N = 0.1g equiv. dm^{-3}

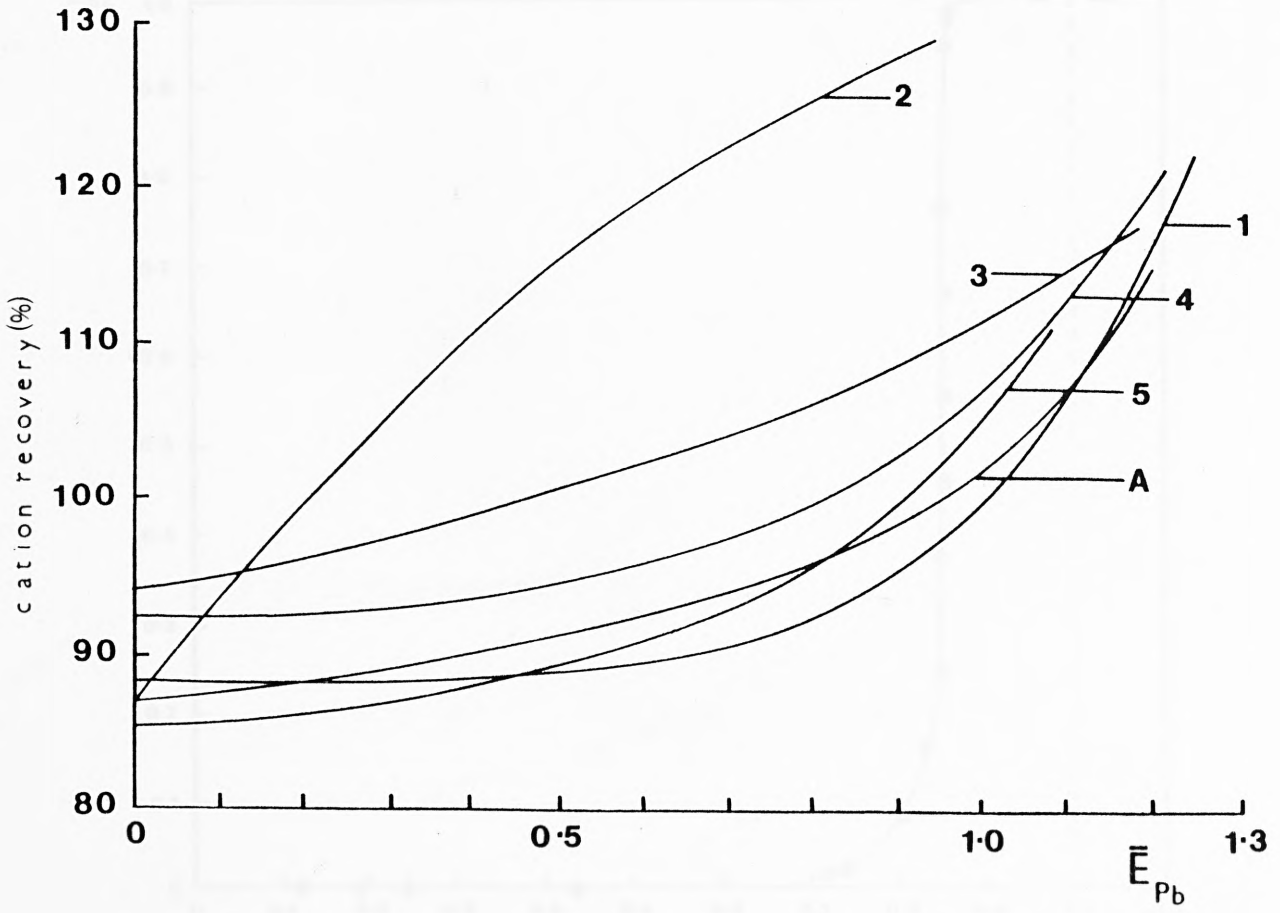

Figure 5.22 Ion exchange isotherm for the $Pb^{2+} \rightleftharpoons Ca^{2+}$ exchange in zeolite X, at a total solution normality (T_N) of 0.1g equiv. dm^{-3}

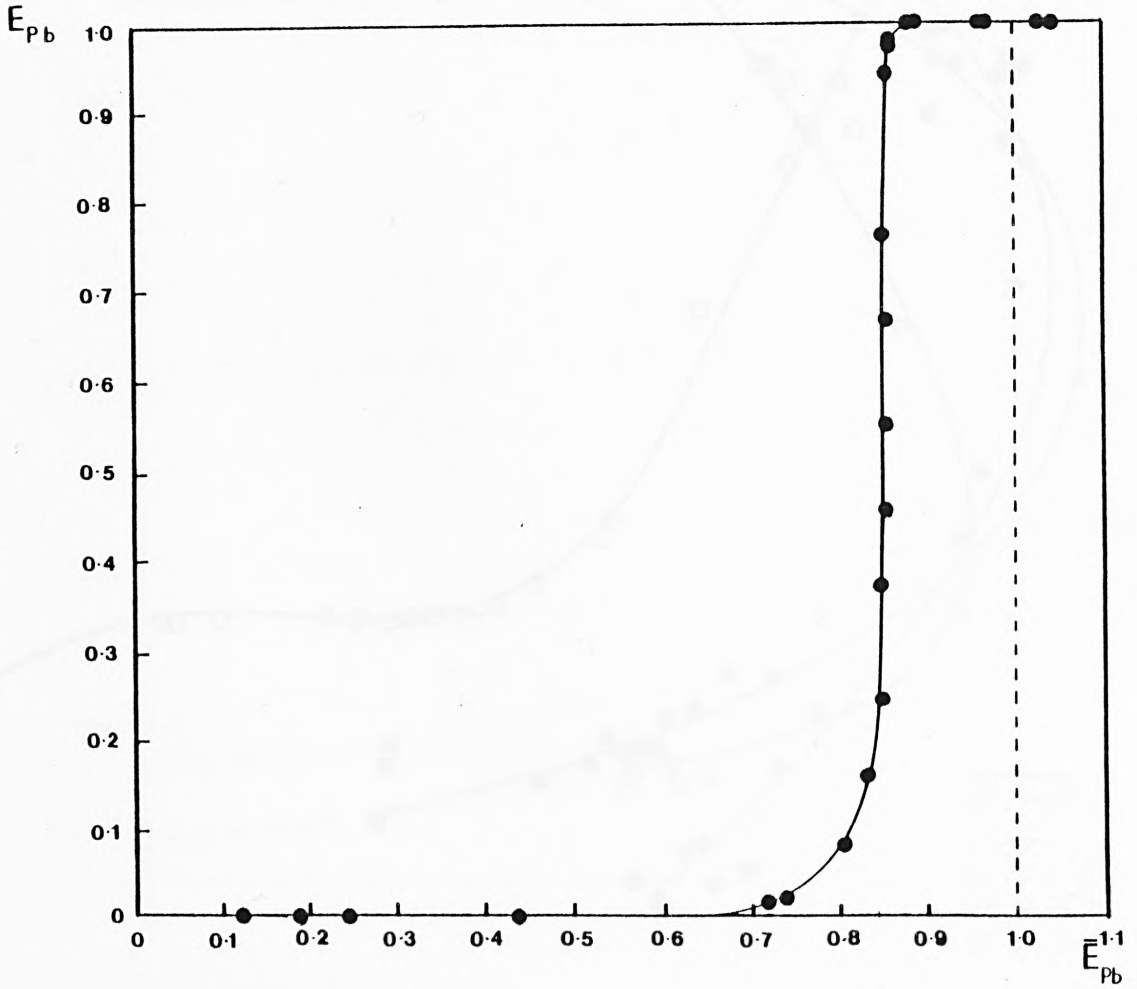

Figure 5.23 Selectivity plots for lead exchange in sodium and calcium forms of zeolites A and X as a function of equivalent fraction of lead in the crystal phase. T_N = 0.1g equiv. dm^{-3}

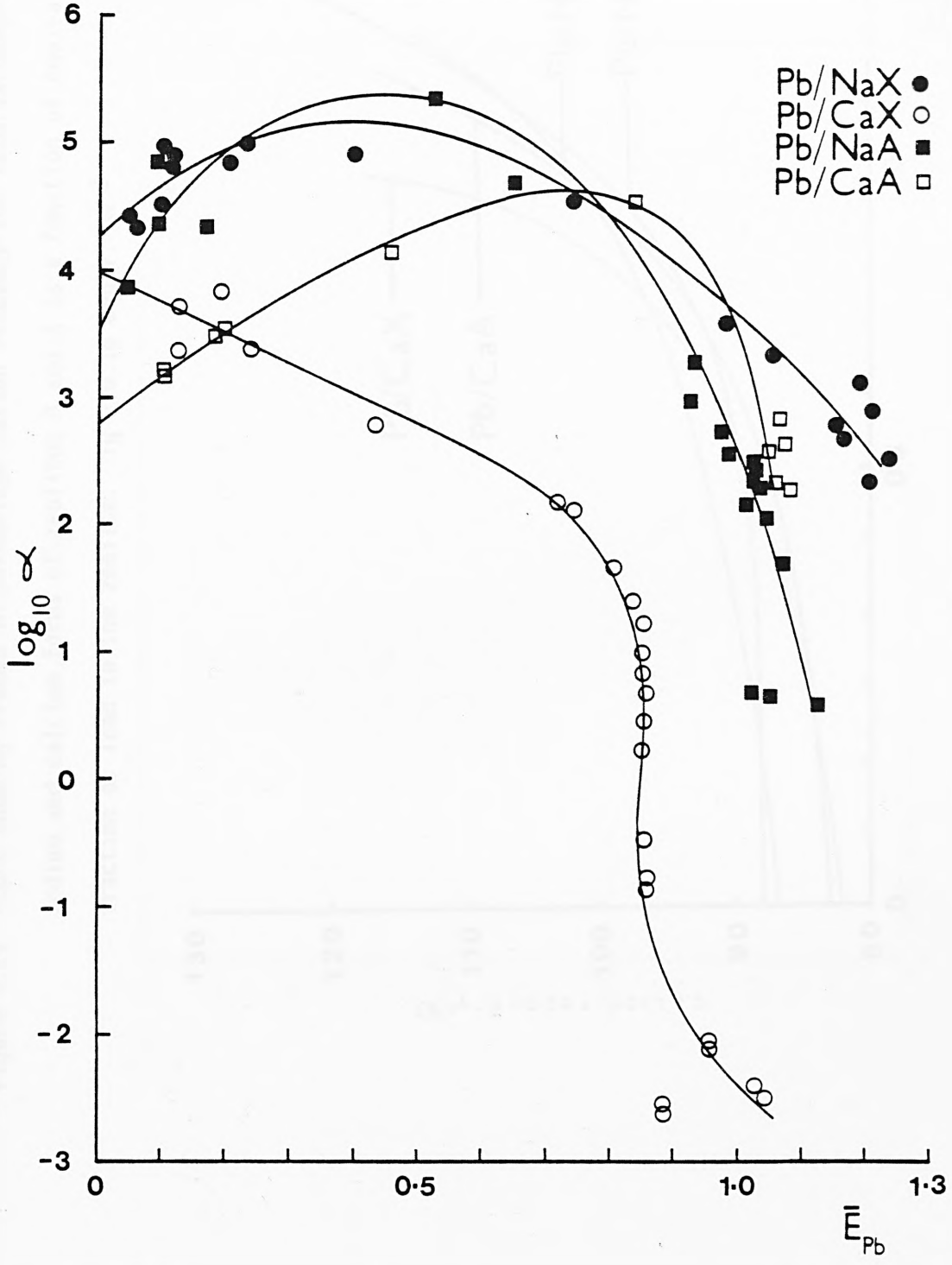

Figure 5.24 Plots showing trends in percentage cation recovery for lead exchange with sodium and calcium forms of zeolites A and X as a function of equivalent fraction of lead in the zeolite. T_N = 0.1g equiv. dm^{-3}

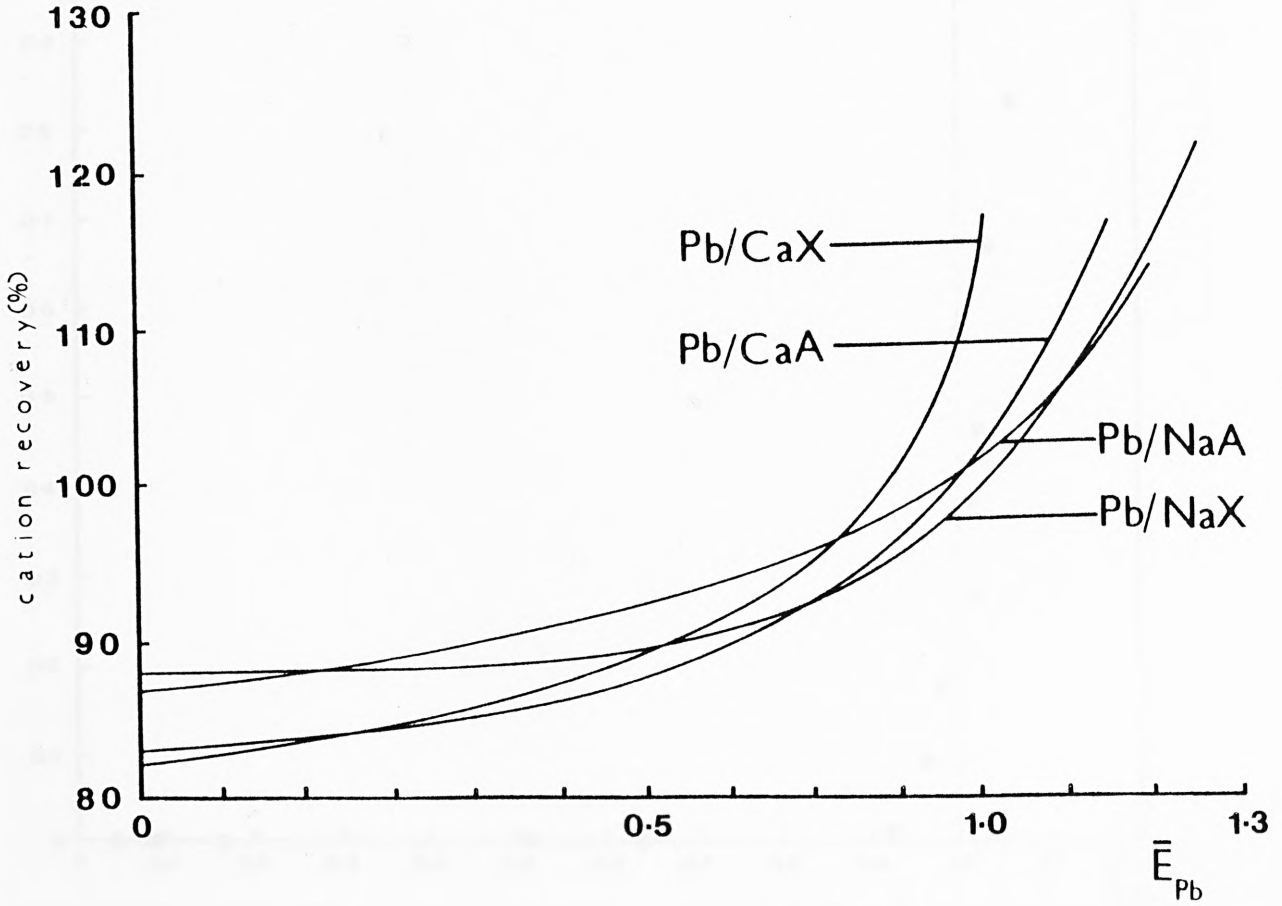

Figure 5.25 Ion exchange isotherm for the $Pb^{2+} \rightleftharpoons 2Na^{+}$ exchange in zeolite A, at a total solution normality (T_N) of 0.1g equiv. dm^{-3}

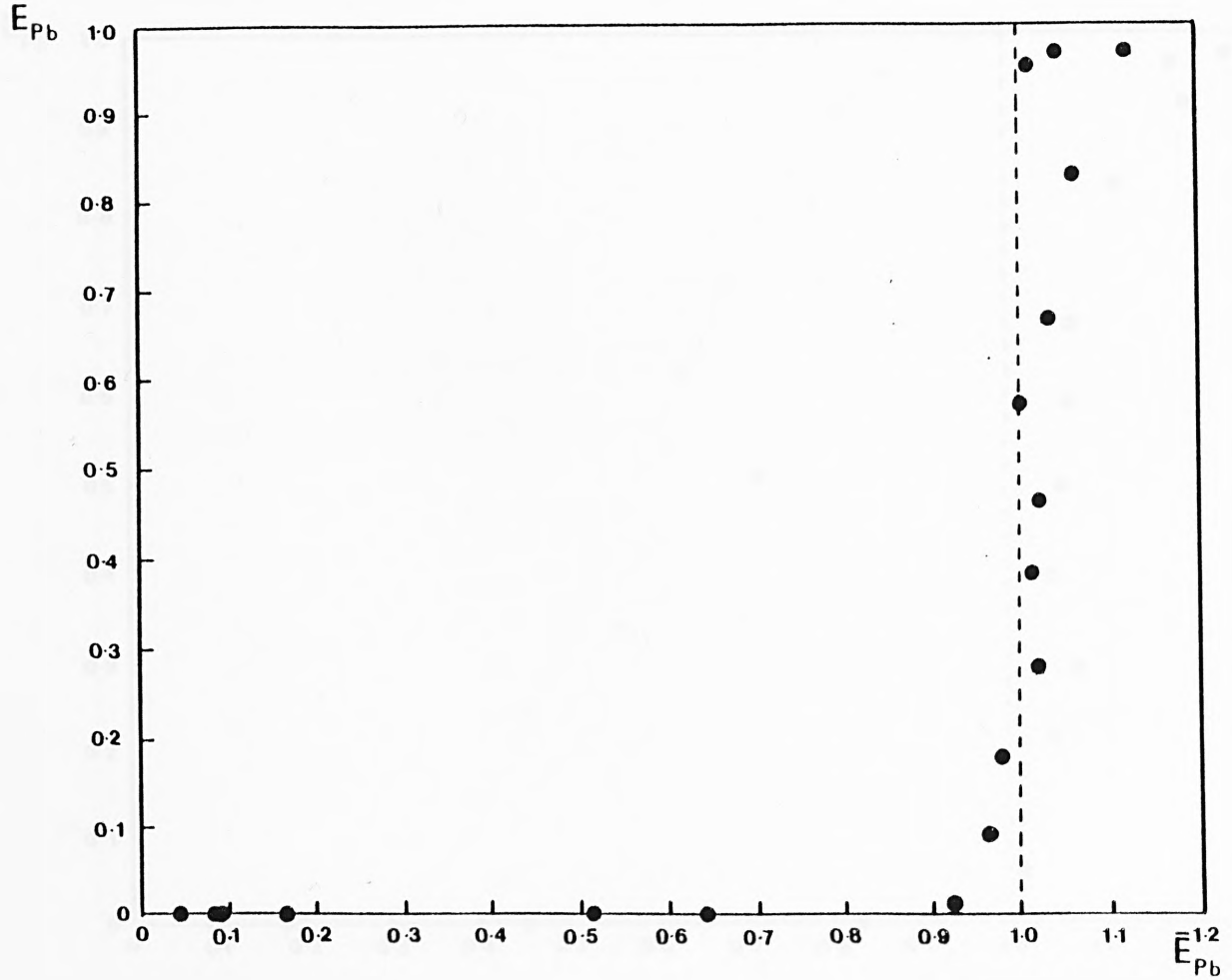

Figure 5.26 Ion exchange isotherm for the $Pb^{2+} \rightleftharpoons Ca^{2+}$ exchange in zeolite A, at a total solution normality (T_N) of 0.1g equiv. dm^{-3}

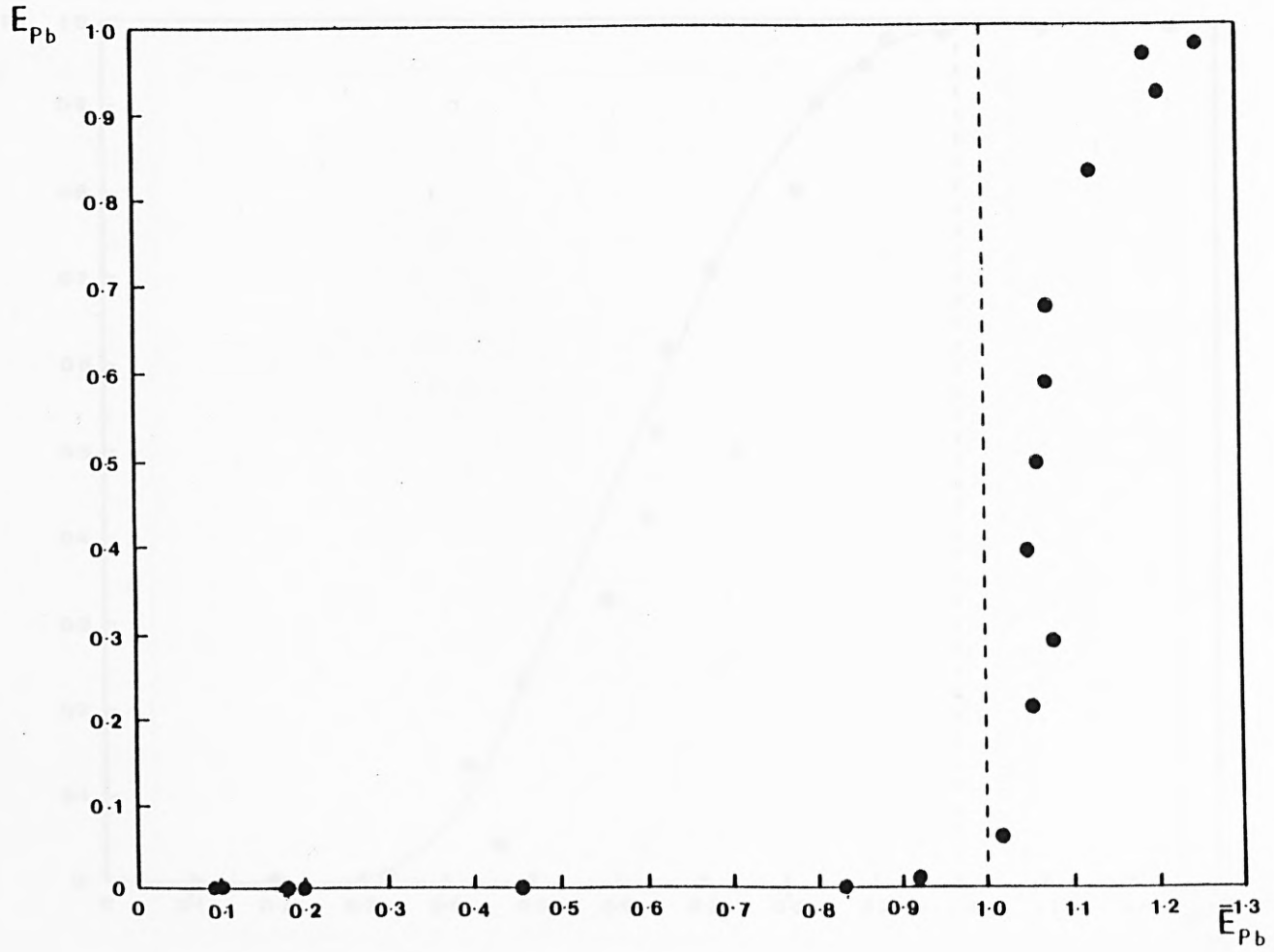

Figure 5.27 Ion exchange isotherm for lead exchange in natural clinoptilolite (NAT.CLI) at a total solution normality (T_N) of 0.1g equiv. dm^{-3}

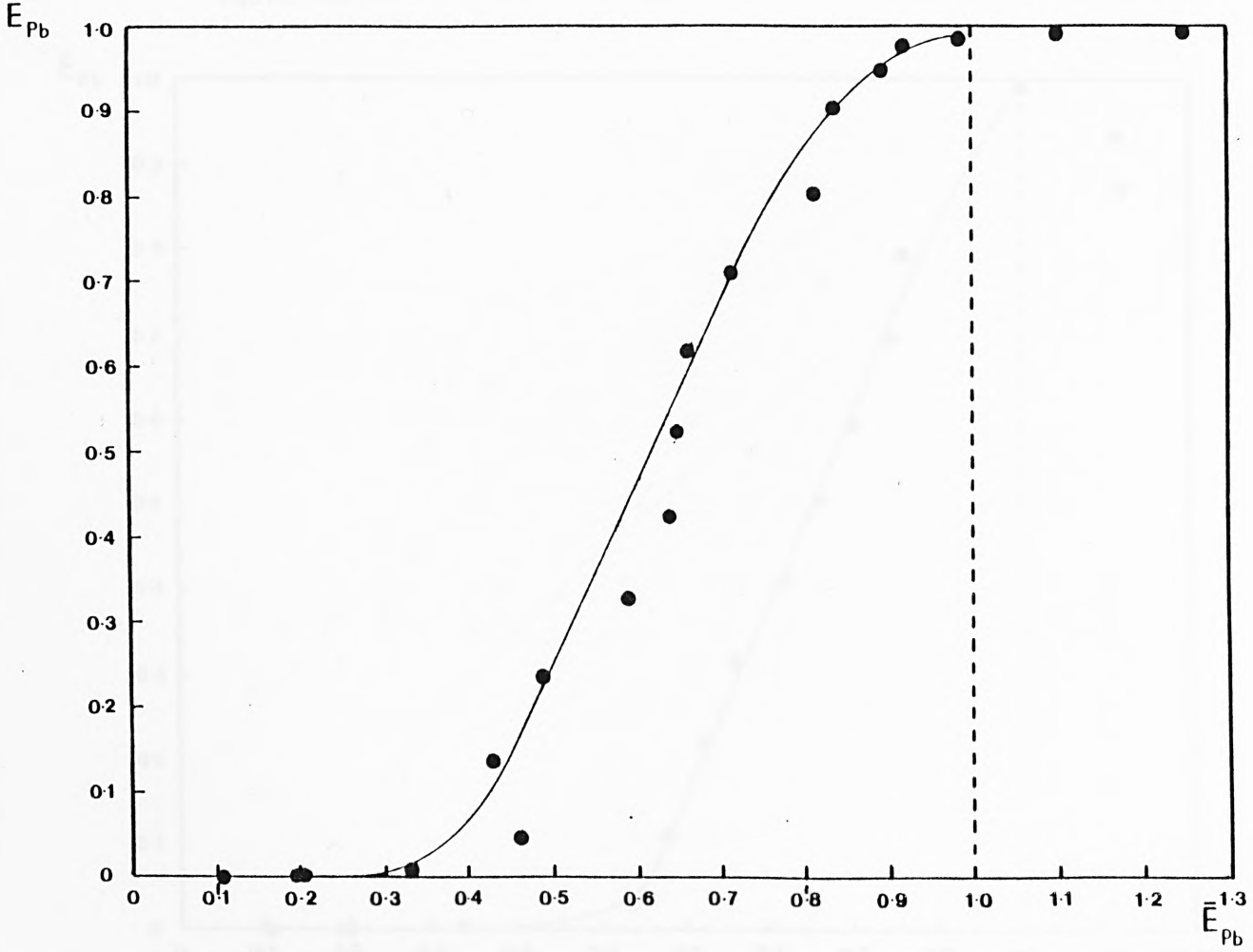

Figure 5.28 Ion exchange isotherm for lead exchange in "fully" sodium exchanged clinoptilolite (F.EX.CLI) at a total solution normality (T_N) of 0.1g equiv. dm^{-3}

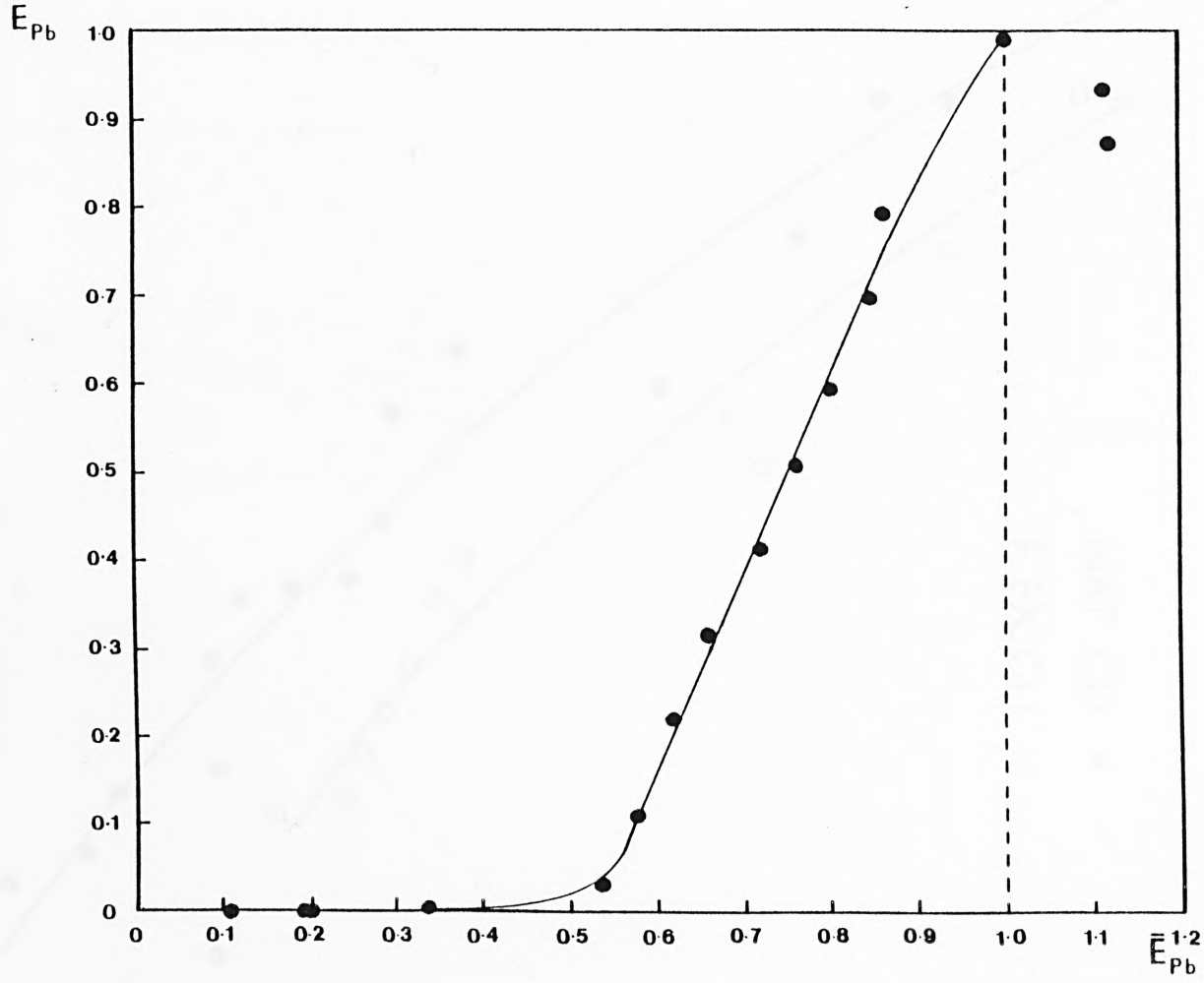

Figure 5.29 Selectivity plots for lead exchange in natural and sodium forms of clinoptilolite as a function of equivalent fraction of lead in the crystal phase. T_N = 0.1g equiv. dm^{-3}

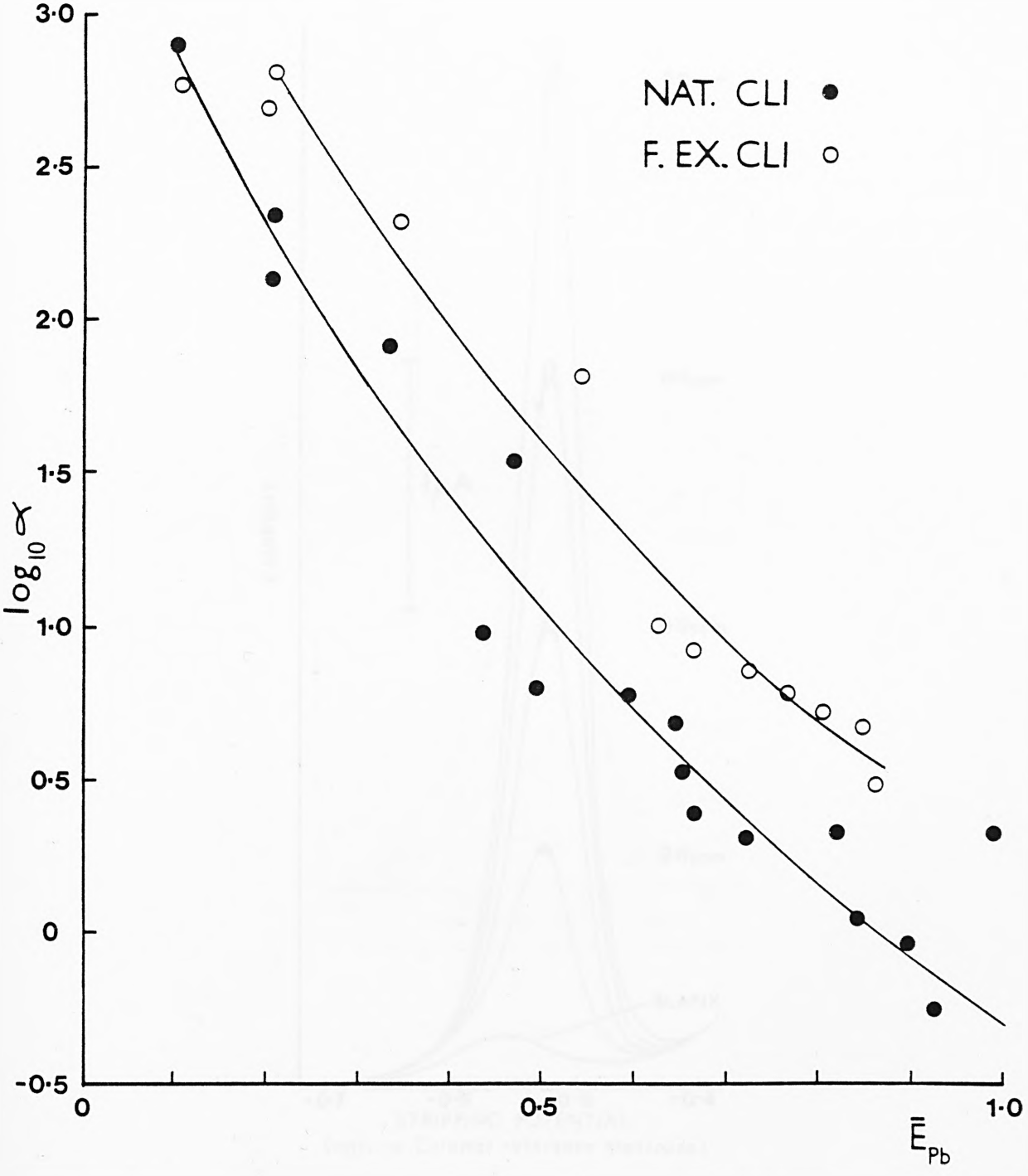

Figure 5.30 Me_3Pb^+ calibration by standard D.P.A.S.V. procedure (12 minutes initial nitrogen purge; 1 minute purge following a standard addition and 30 seconds between successive scans on same addition).

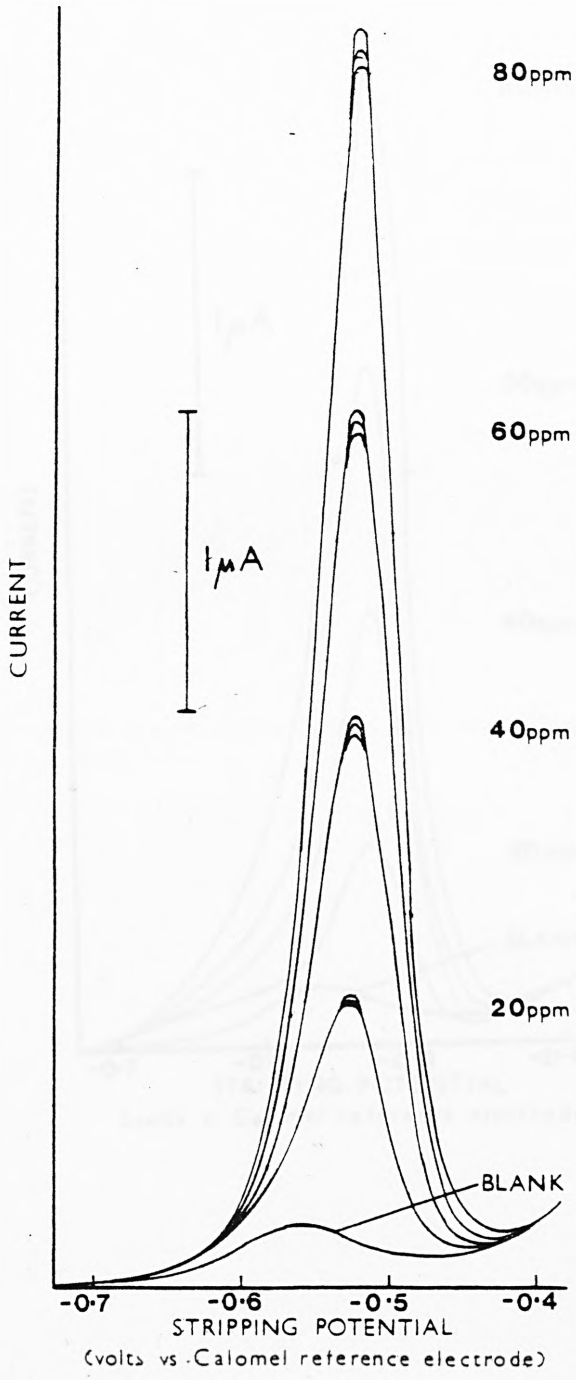

Figure 5.31 Me_3Pb^+ calibration by modified D.P.A.S.V. procedure (12 minutes initial nitrogen purge; 2 minute purges following a standard addition and between successive scans on same addition).

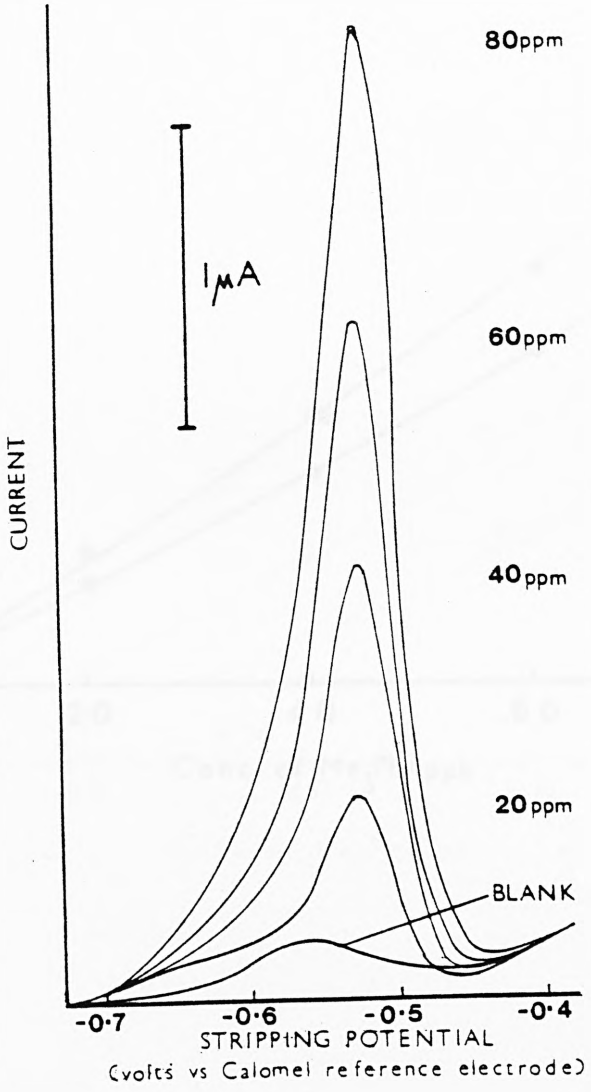

Figure 5.32 Non-linear Me_3Pb^+ calibrations obtained by the standard (1), and modified (2), D.P.A.S.V. procedures

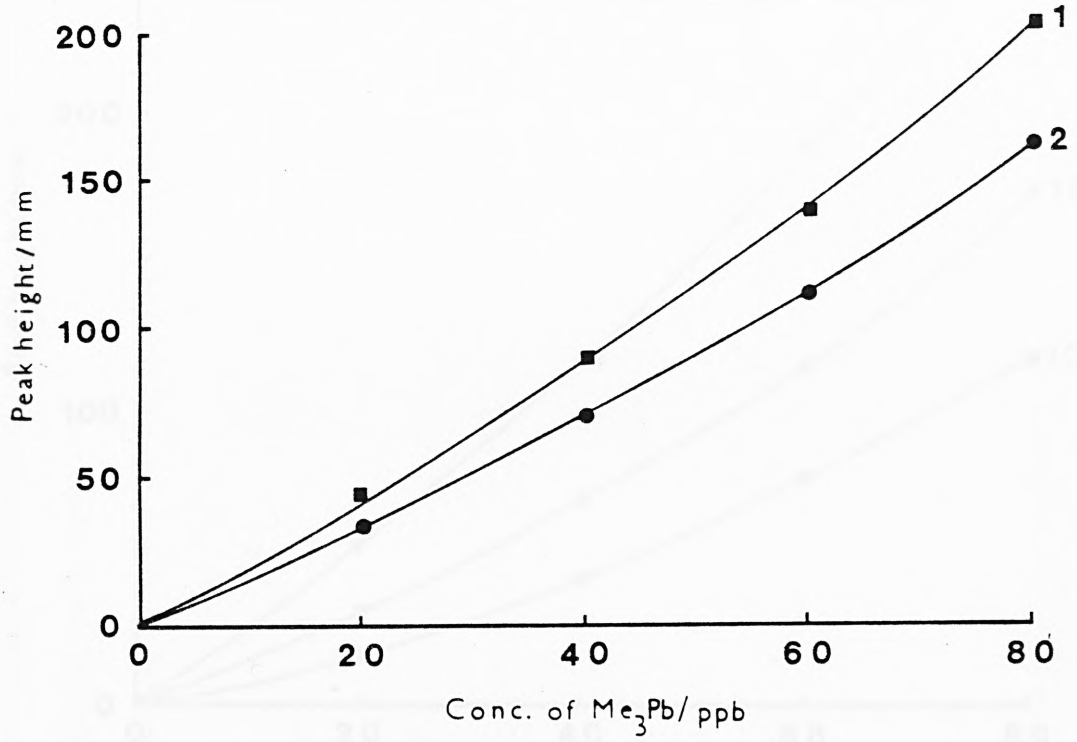

Figure 5.33 Change in the sensitivity of Me_3Pb^+ calibrations obtained over a day.

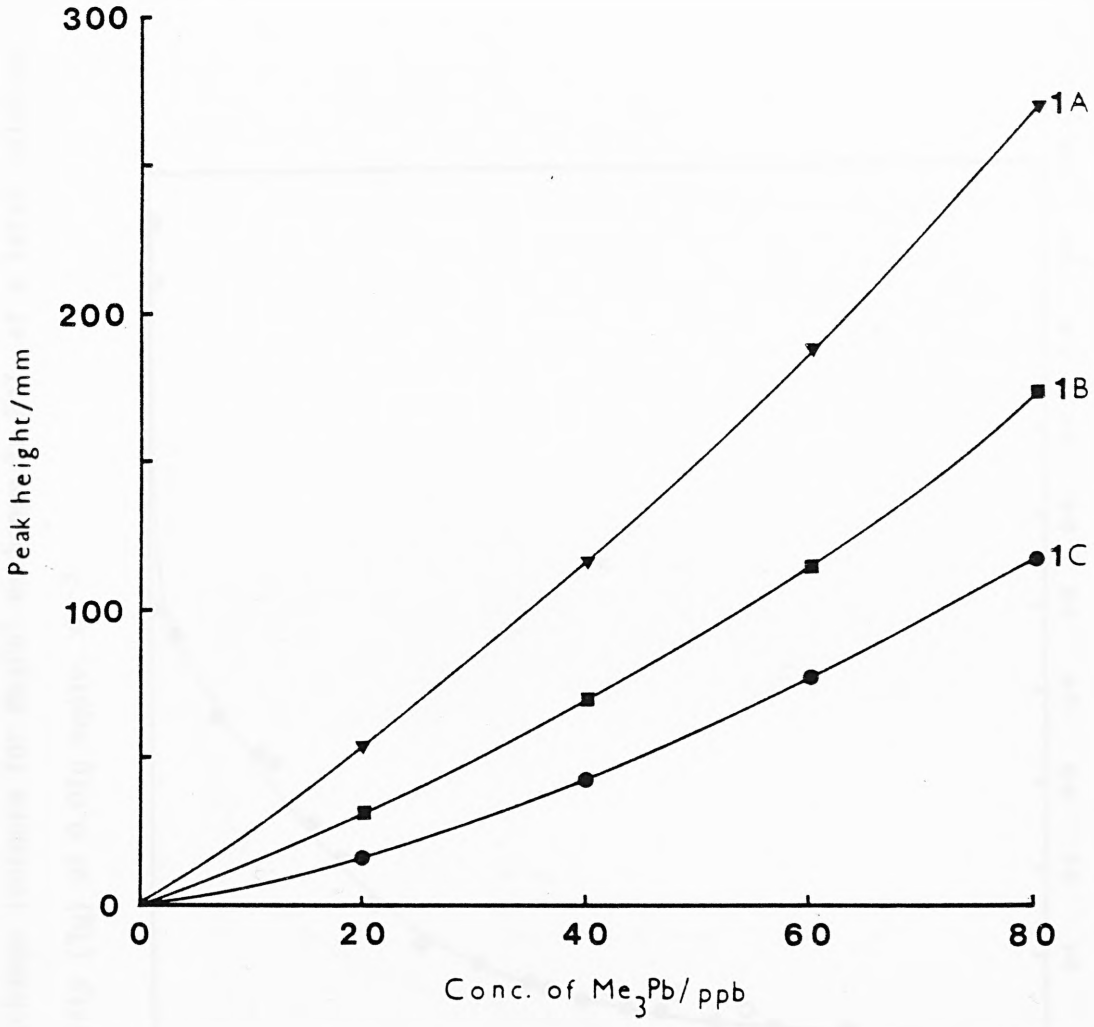

Figure 5.34 Ion exchange isotherm for Me_3Pb^+ exchange in NaX, at a total solution normality (T_N) of 0.01g equiv. dm^{-3}

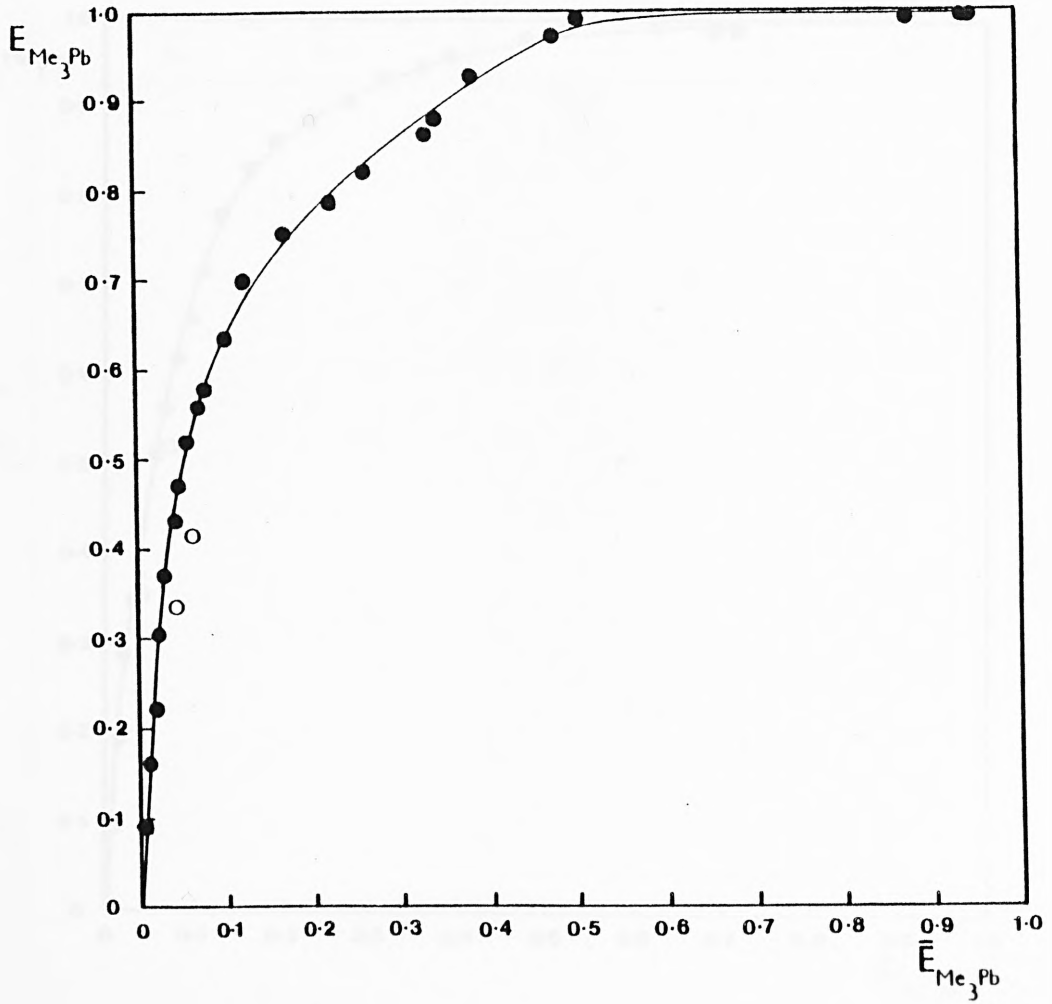

Figure 5.35 Ion exchange isotherm for Me_3Pb^+ exchange in NaY, at a total solution normality (T_N) of 0.01g equiv. dm^{-3}

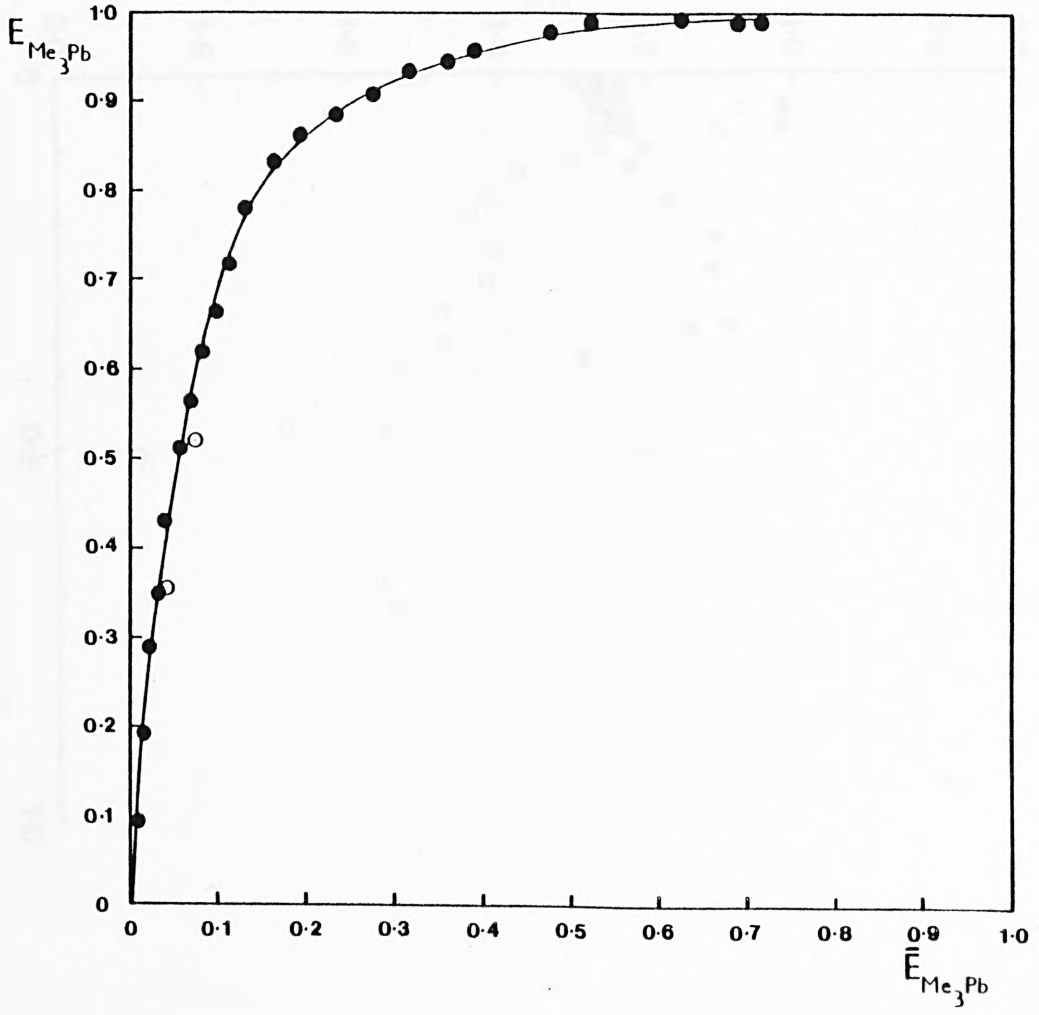

Figure 5.36 Selectivity plots for Me_3Pb^+ exchange in NaX and NaY as a function of equivalent fraction of Me_3Pb^+ in the crystal phase.

Data for (●) Me_3Pb^+/NaX; (□) Me_3Pb^+/NaY

T_N = 0.01g equiv. dm^{-3}

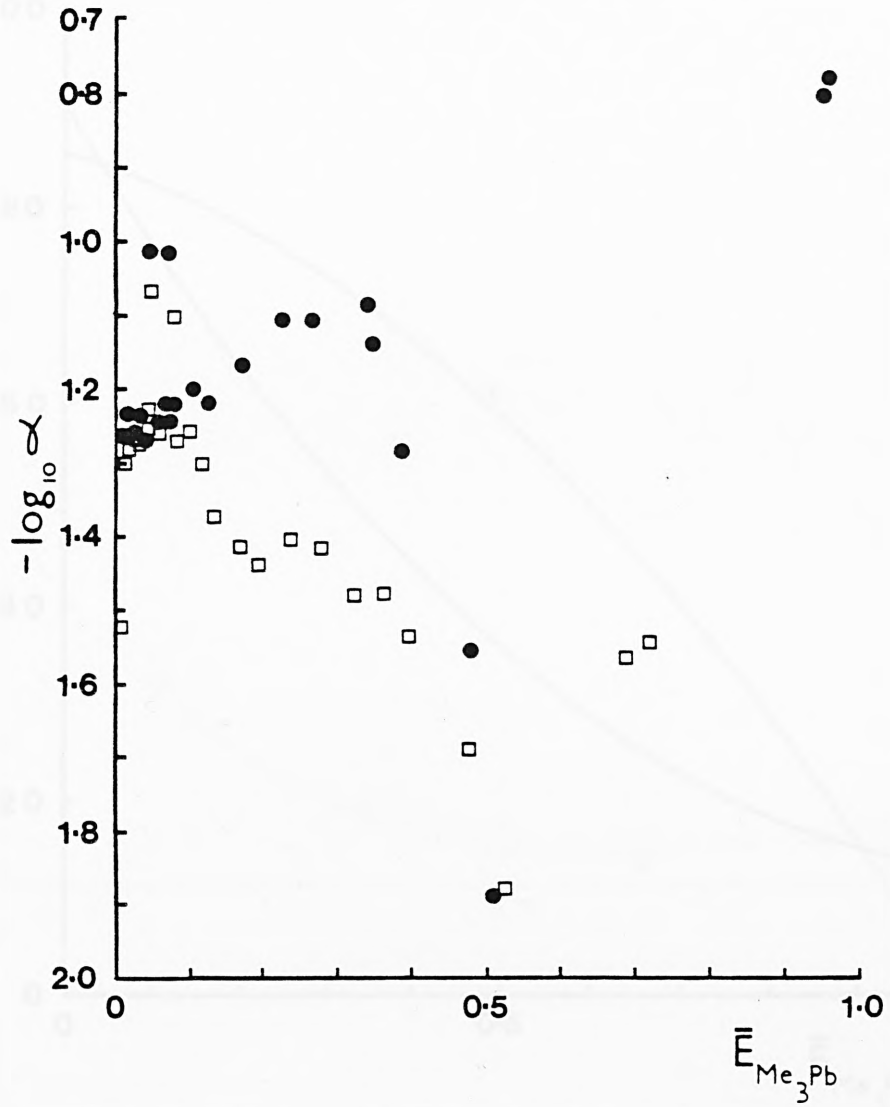

Figure 5.37 Plots of trends in percentage cation recovery for Me_3Pb^+ exchange in zeolites X and Y as a function of equivalent fraction of Me_3Pb^+ in the zeolite. T_N = 0.01g equiv. dm^{-3}

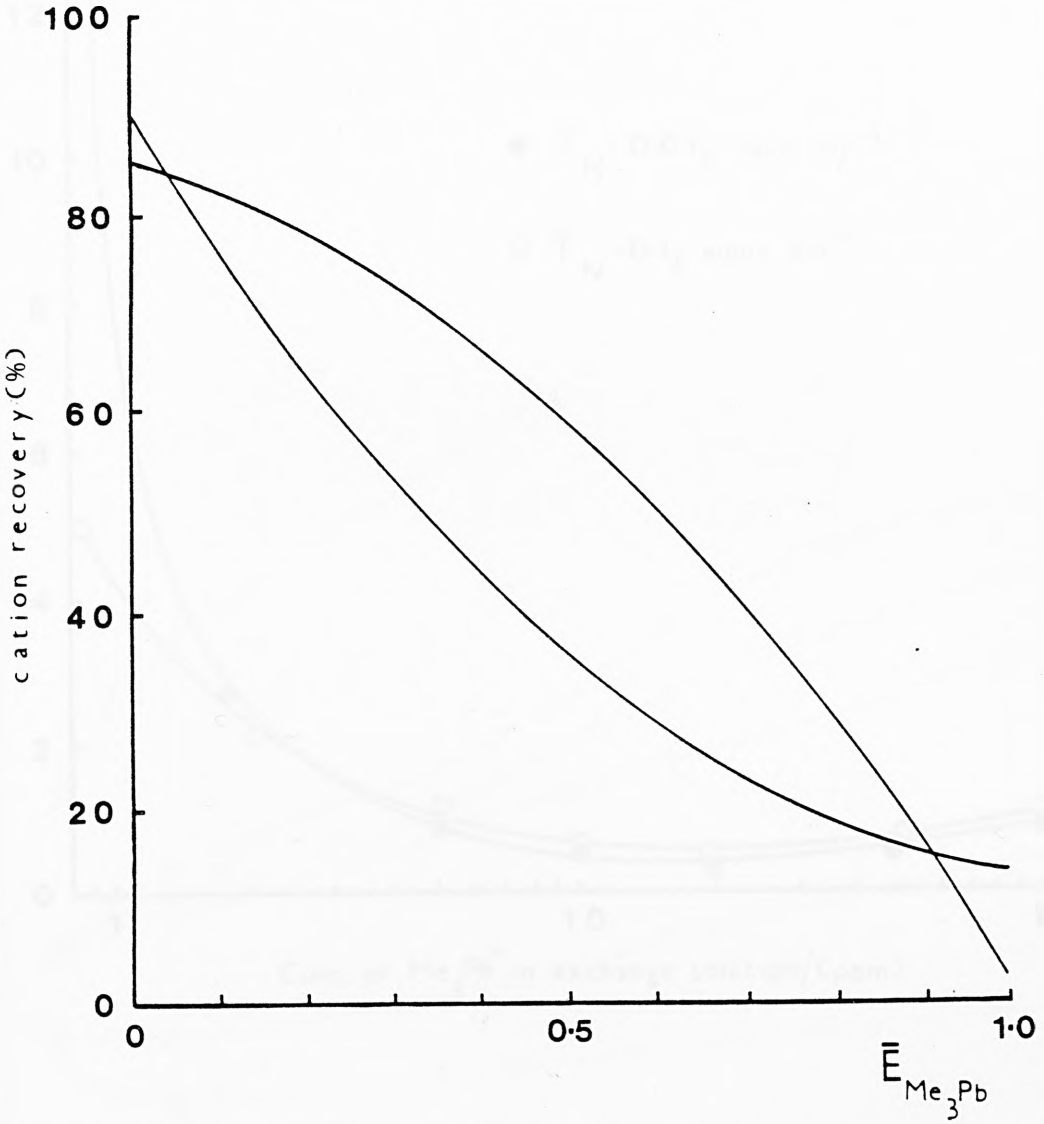

Figure 5.38 Percentage removal of low levels of Me_3Pb^+ from high salt backgrounds

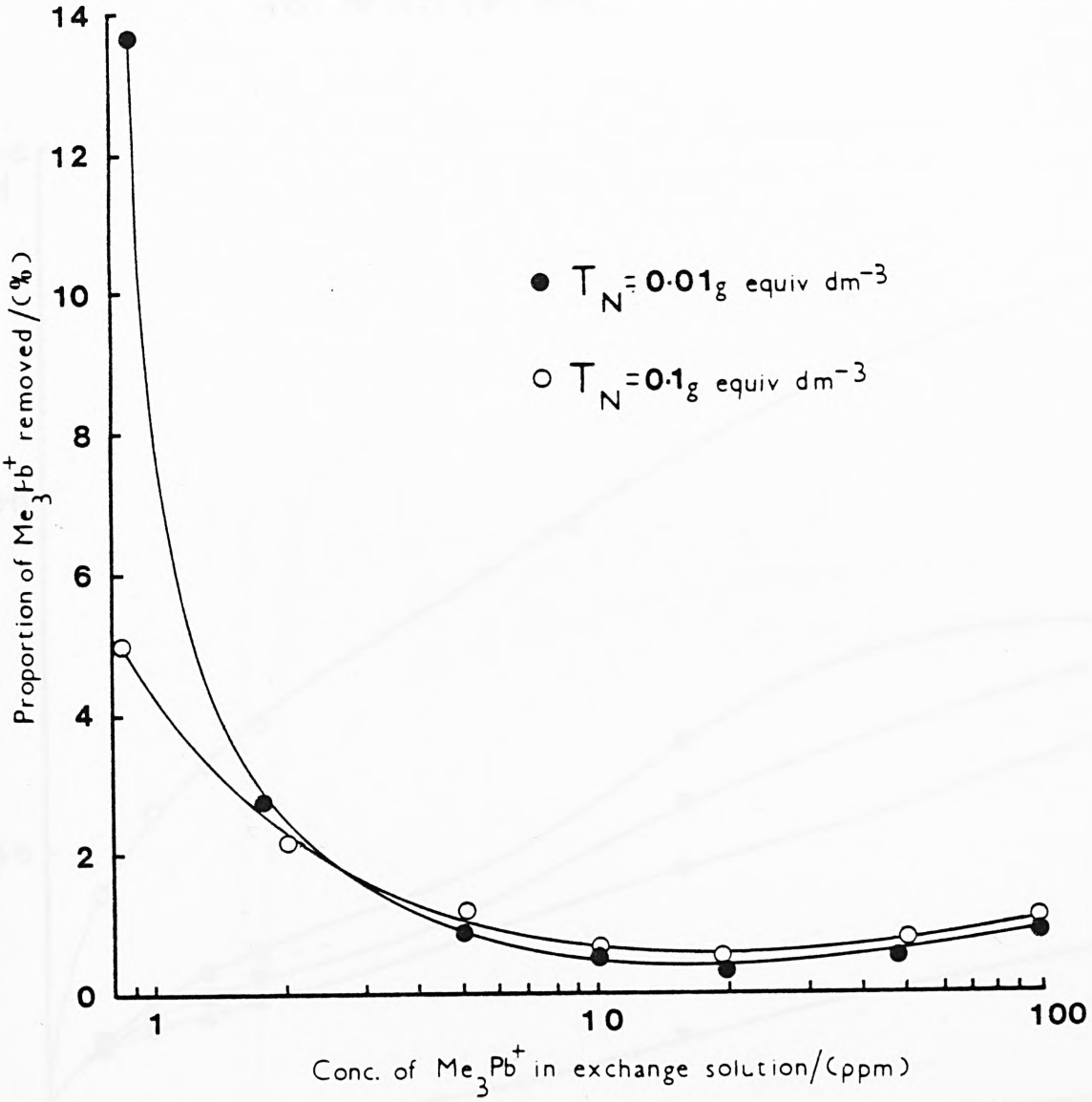

Figure 5.39 Kinetic pH responses of various clinoptilolite forms after immersion in distilled water.
Data for (◇) NAT.CLI; (■) F.EX.CLI;
(✡) NAT.CLI (II); (✱) F.EX.CLI (II);
(✪) 2N CLI; (▼) 4N CLI

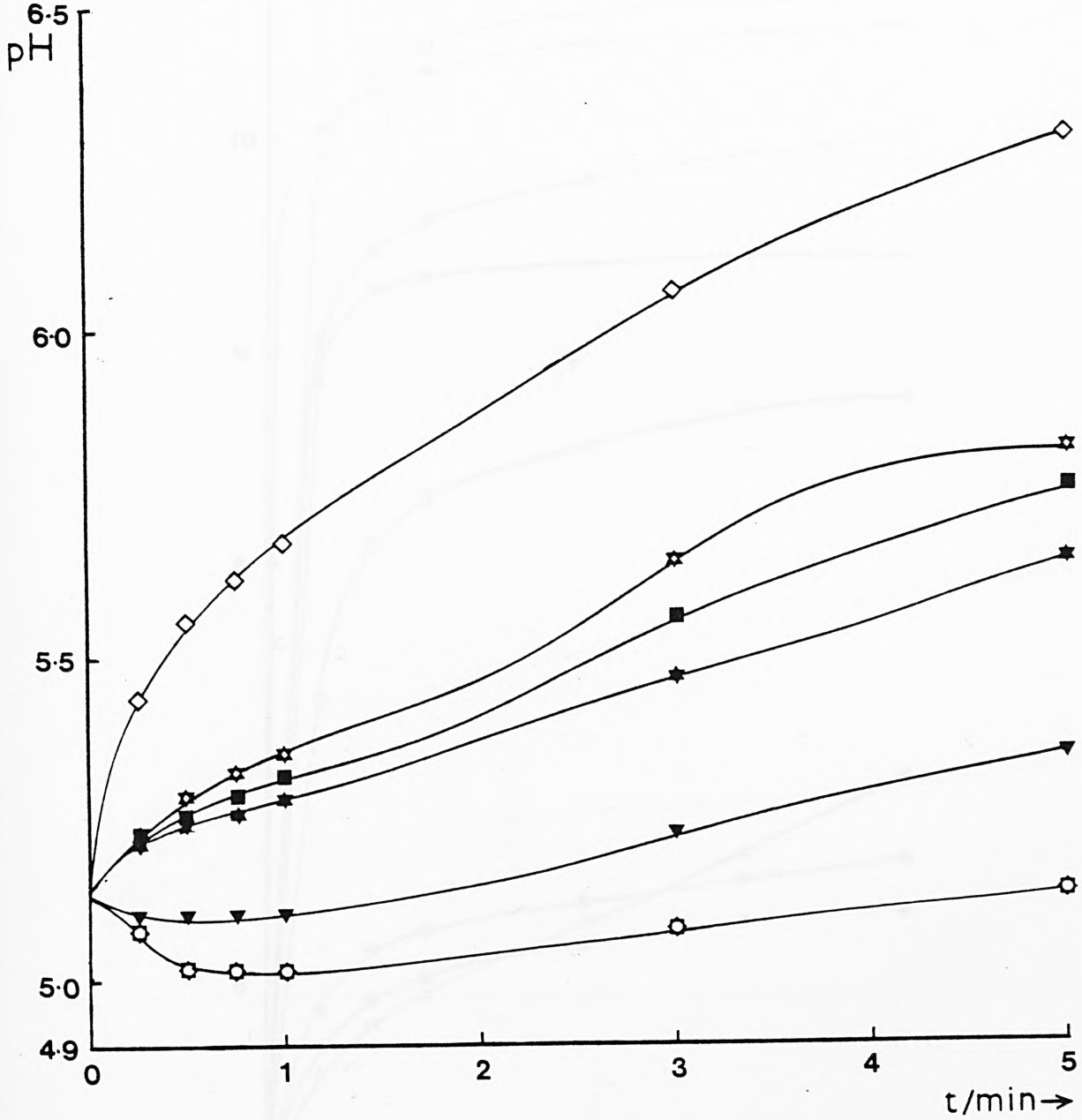

Figure 5.40 Kinetic pH responses of sodium and calcium forms of synthetic zeolites of different framework density after immersion in distilled water. Data for (○) NaA; (▲) NaZ1; (▽) NaZ2; (×) NaZ3; (□) NaZ4; (◆) NaZ5; (△) CaA; (●) CaX

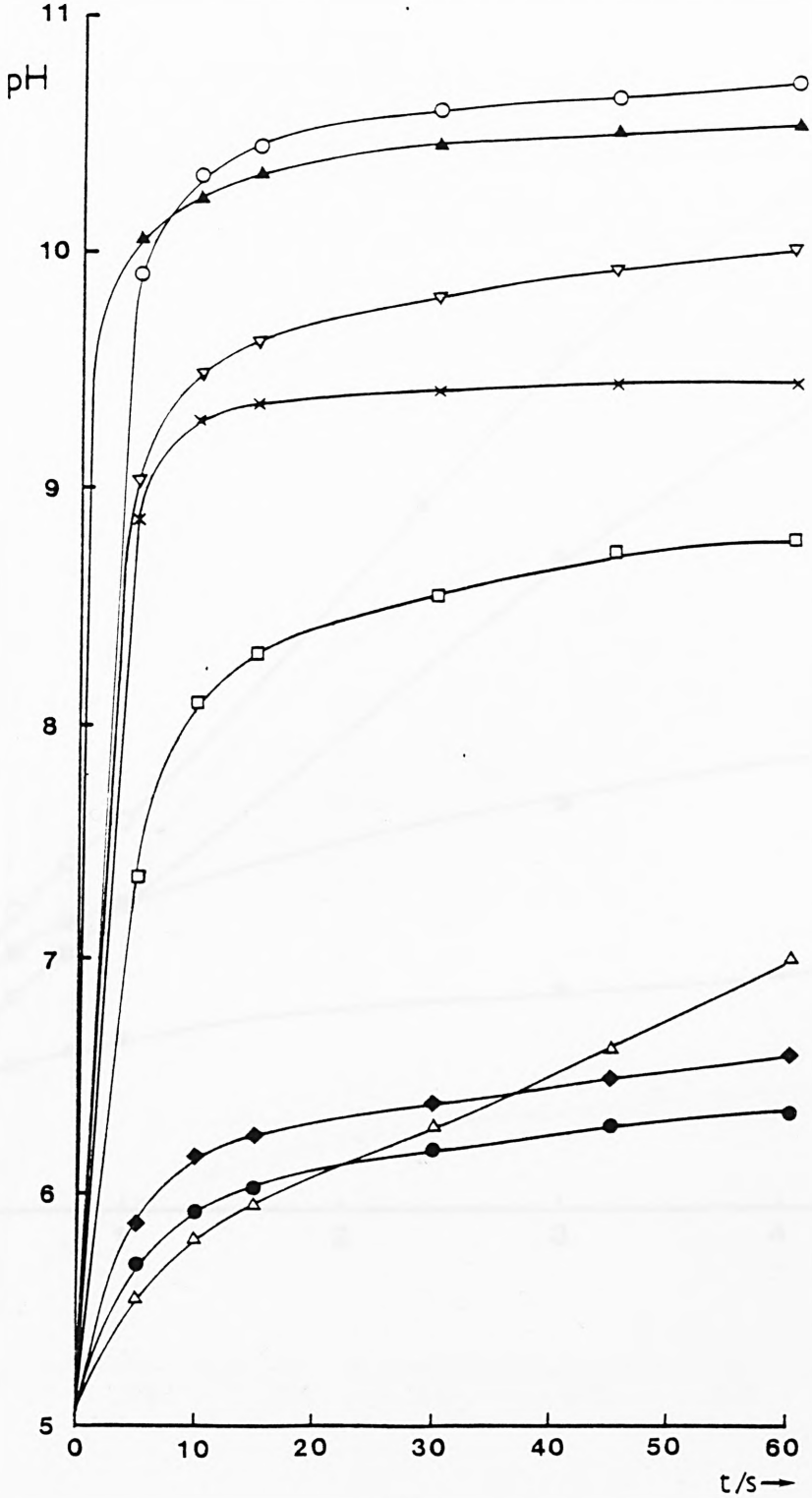

Figure 5.41 Kinetic pH responses of various clinoptilolite forms after immersion in 0.1N $NaNO_3$. Data for (◇) NAT.CLI; (■) F.EX.CLI; (✡) NAT.CLI (II); (✱) F.EX.CLI (II)

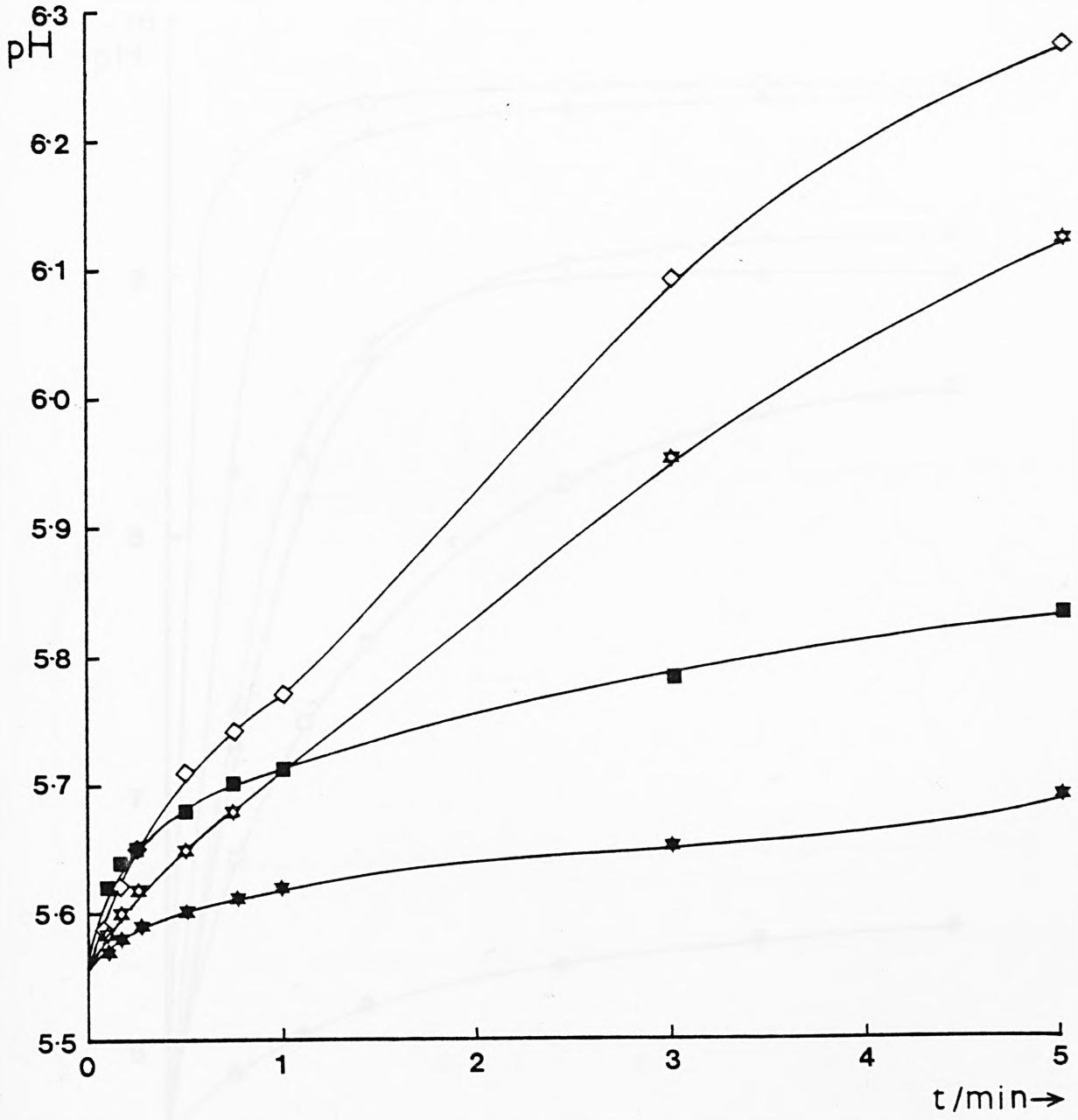

Figure 5.42 Kinetic pH responses of sodium forms of synthetic zeolites of different framework density after immersion in 0.1N $NaNO_3$. Data for (○) NaA; (▲) NaZ1; (▽) NaZ2; (×) NaZ3; (□) NaZ4; (◆) NaZ5

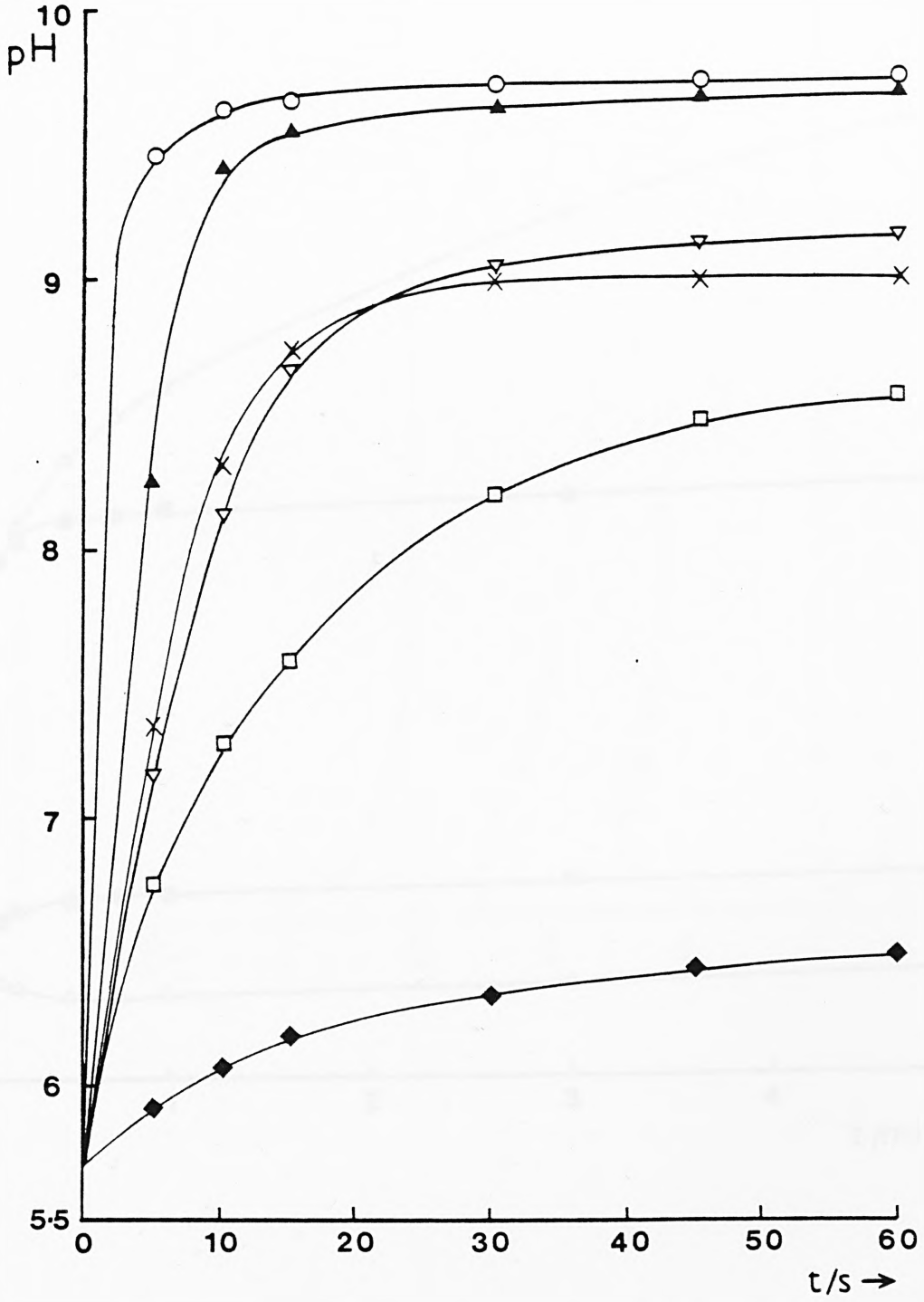

Figure 5.43 Kinetic pH responses of calcium forms of zeolites A and X after immersion in either (i) 0.1N $Ca(NO_3)_2$ or (ii) 0.1N $Pb(NO_3)_2$

Data for (△) CaA; (●) CaX

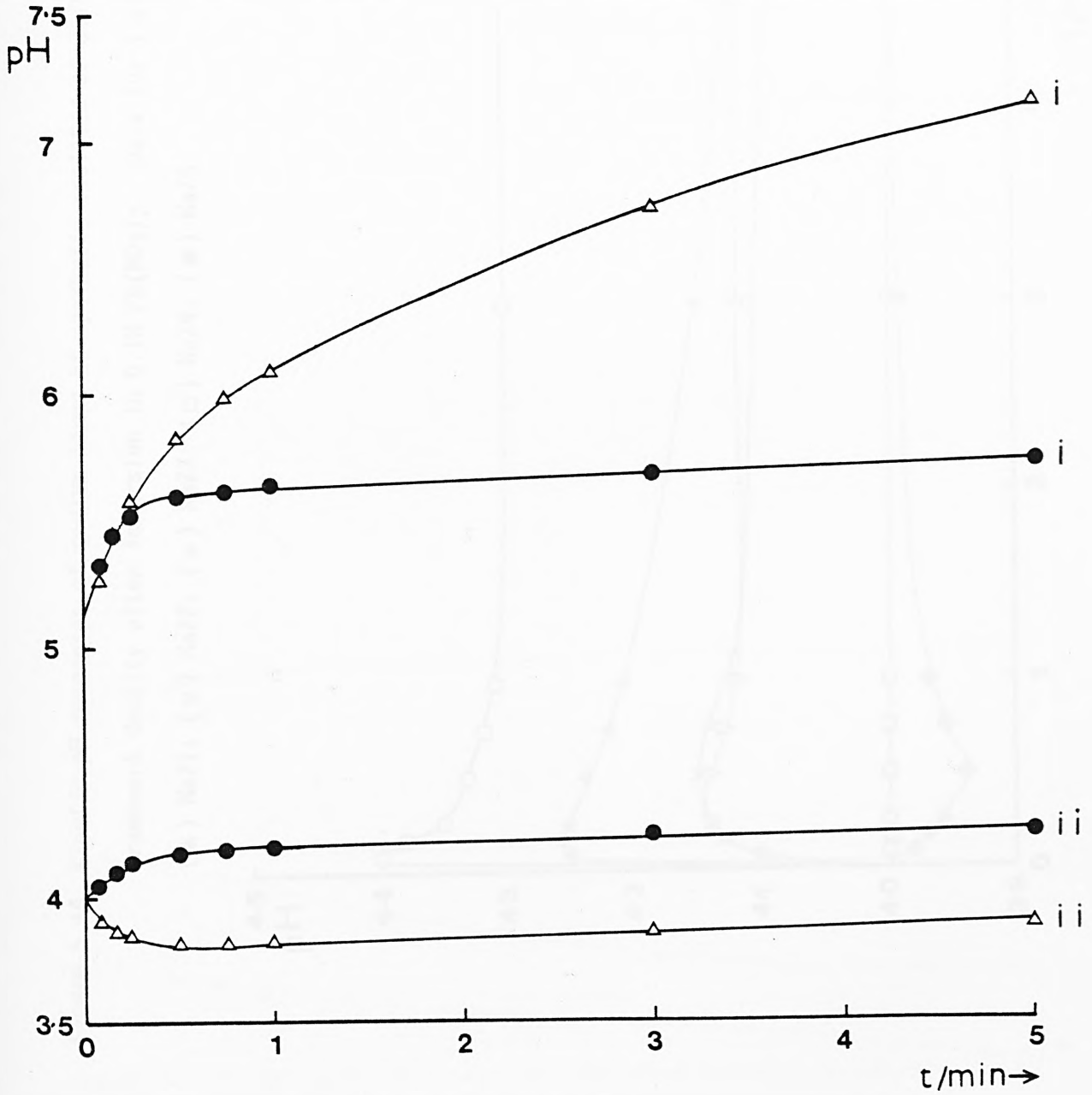

Figure 5.44 Kinetic pH responses of sodium forms of synthetic zeolites of different framework density after immersion in 0.1N $Pb(NO_3)_2$. Data for (○) NaA; (▲) NaZ1; (▽) NaZ2; (×) NaZ3; (□) NaZ4; (◆) NaZ5

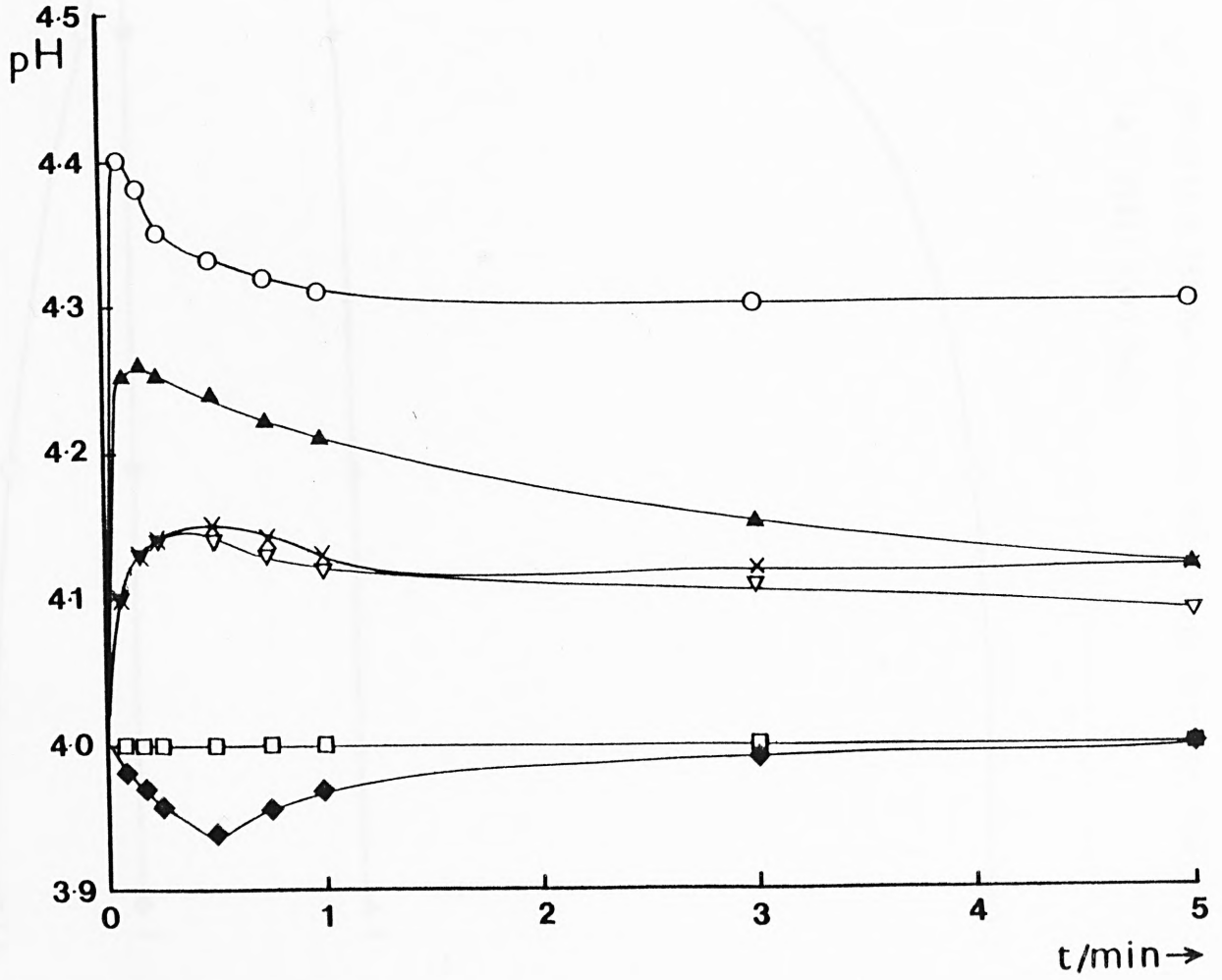

Figure 5.45 Kinetic pH responses of sodium forms of synthetic zeolites of different framework density after immersion in solutions containing either (i) 0.095N Na^+ : 0.005N Pb^{2+}, or (ii) 0.05N Na^+ : 0.05N Pb^{2+}. Data for (○) NaA; (▲) NaZ1; (◆) NaZ5.

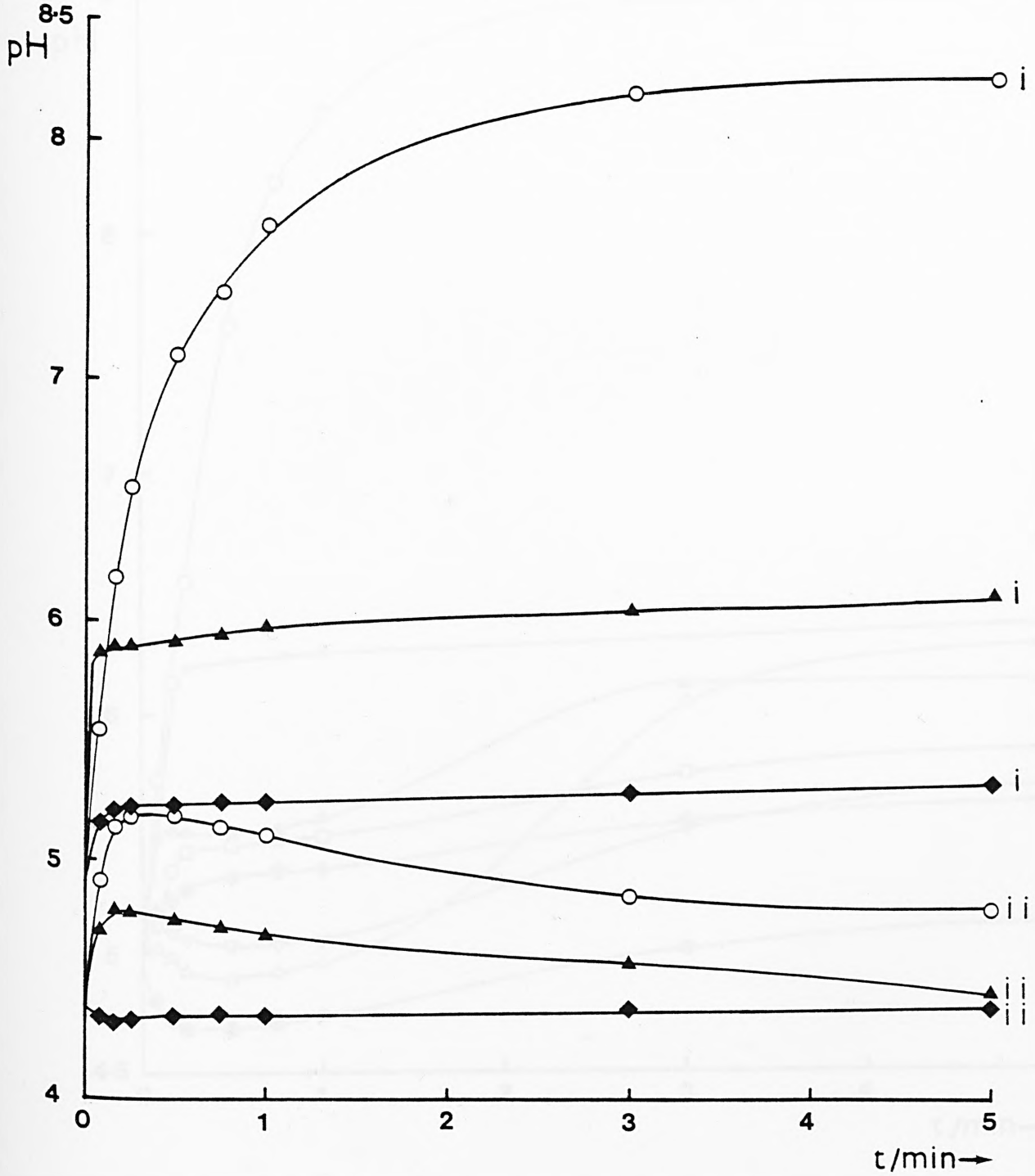

Figure 5.46 Kinetic pH responses of sodium and calcium forms of synthetic zeolites of different framework density after immersion in 0.01N $Pb(NO_3)_2$. Data for (○) NaA; (▲) NaZ1; (▽) NaZ2; (×) NaZ3; (□) NaZ4; (◆) NaZ5; (△) CaA; (●) CaX

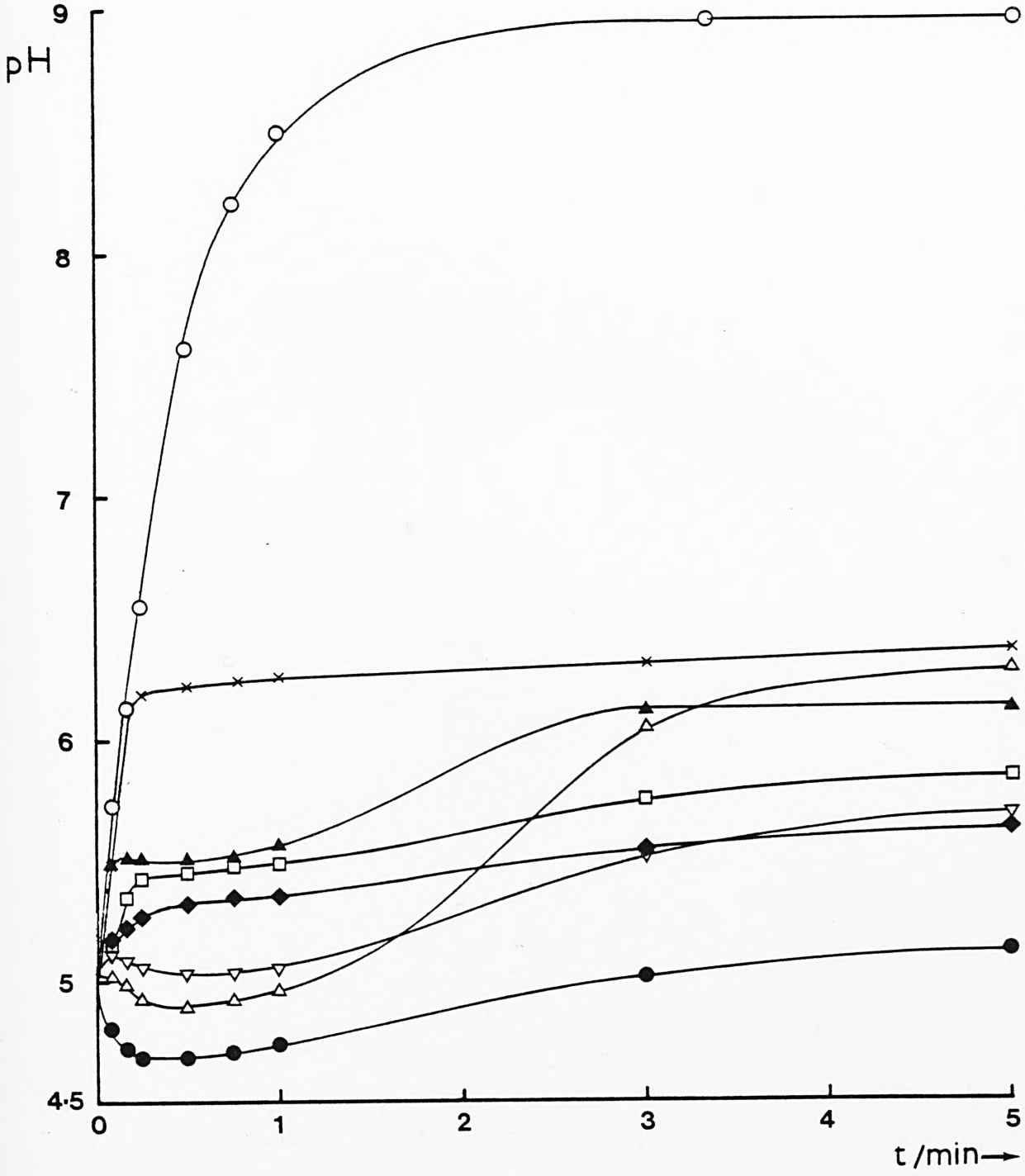

Figure 5.47 Kinetic pH responses of sodium forms of zeolites X and Y after immersion in either (i) 0.01N NaCl or (ii) 0.01N $(CH_3)_3PbCl$. Data for (▲) NaZ1; (◆) NaZ5

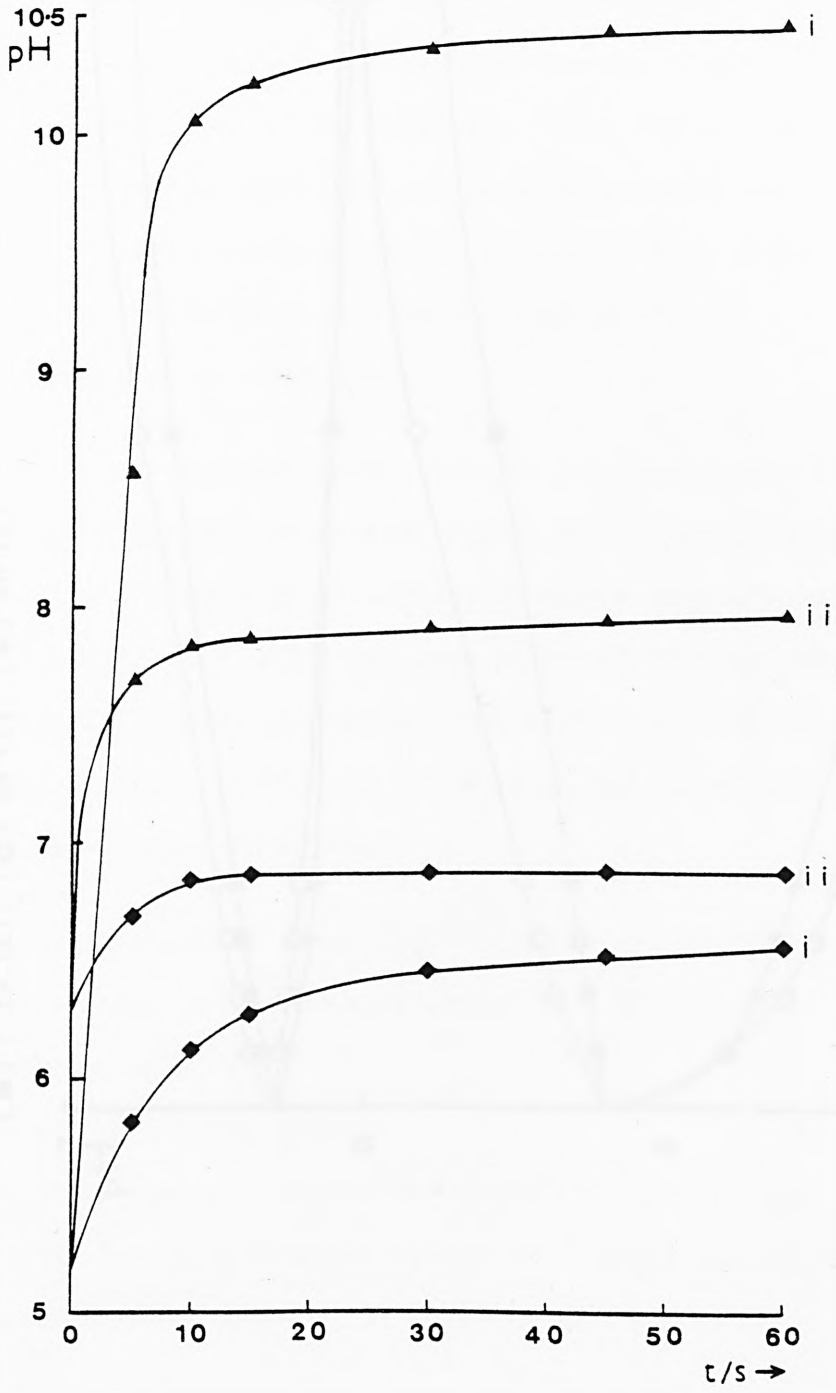

Figure 5.48 Kinetic pH responses of various clinoptilolite forms after immersion in either (i) 0.01N NaCl or (ii) 0.01N $(CH_3)_3PbCl$. Data for (◇) NAT.CLI; (■) F.EX.CLI; (✿) 2N CLI; (▼) 4N CLI

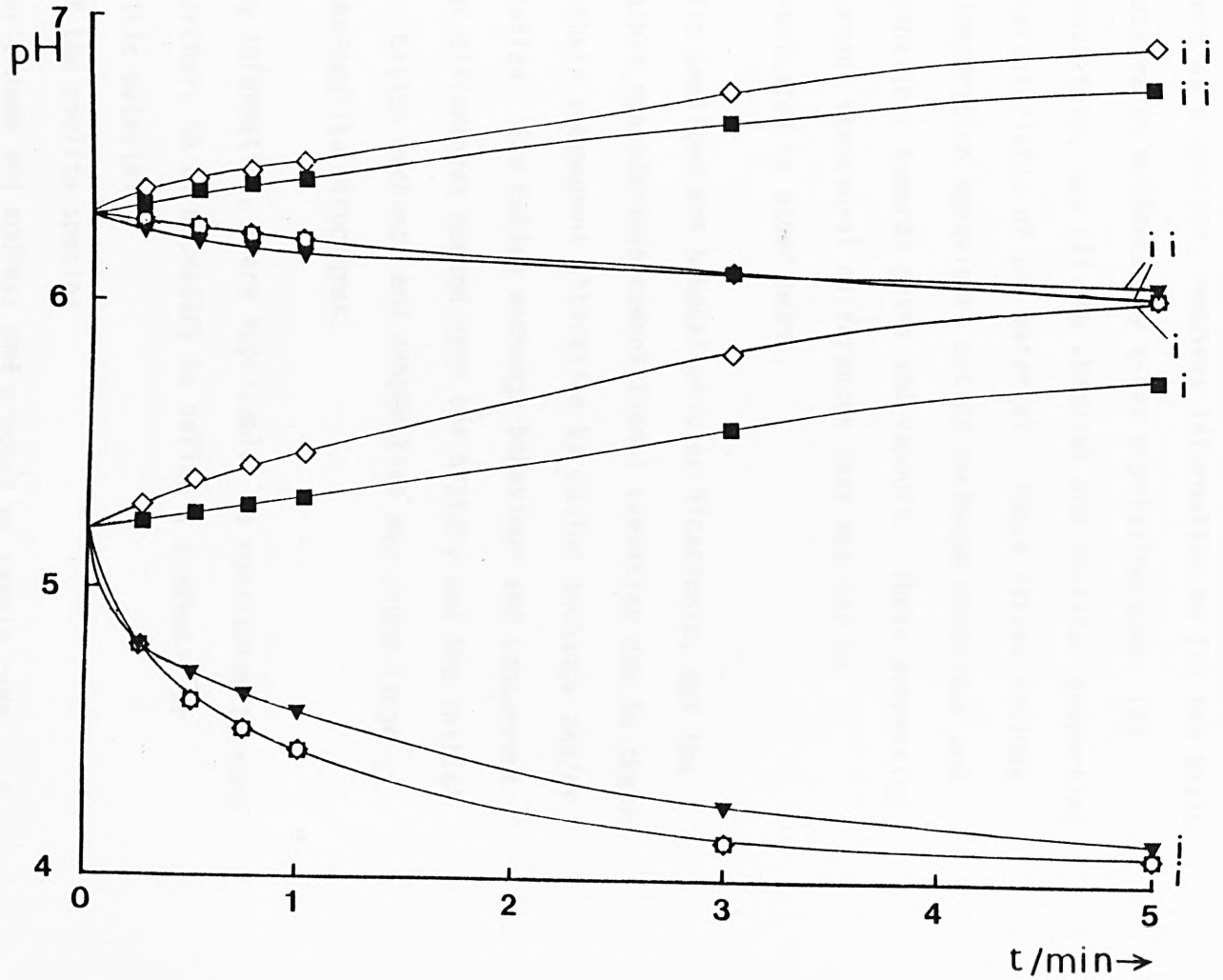

CHAPTER SIX - DISCUSSION

6.1 ANALYSIS OF ZEOLITES

The characterisation of a previously unknown mineral or synthetic material, such as a zeolite, requires information on (1) the basic crystal structure as evidenced by x-ray crystallography, (2) chemical composition, and (3) the chemical and physical properties which are characteristic of the material. These latter include stability, dehydration behaviour, cation exchange behaviour and adsorption behaviour towards gases and vapours. These properties reflect important structural differences that may not be adequately indicated by other means.

Most synthetic zeolites are homocationic or dicationic, but the minerals exhibit considerable compositional variation due to their genesis and their subsequent alteration by cation exchange and/or recrystallisation. The cation exchange behaviour and concurrent compositional differences depend upon the history and the initial composition. Cation exchange and dehydration may cause large changes in the zeolite structures.

The following information, where applicable, is considered by many zeolite researchers to be necessary to define a synthetic or mineral zeolitic material:

(1) name of the zeolite species

(2) supplier's name and address and product or sample code. Some companies have more than one source for a given zeolite or zeolitic material, and the code is keyed to each source or deposit.

(3) location of the mineral zeolite deposit as to the country,

and town from which the mineral was mined, because the exact source of the zeolitic material is then specified.

(4) mesh or particle size of the zeolitic material should be reported because particle size influences some properties of the zeolite, such as the extent and rapidity of cation exchange.

(5) mineralogical composition of the zeolitic material. Analysis by x-ray powder diffraction is generally adequate to estimate the purity of the sample, and to identify common impurities such as clay minerals, silica minerals, other zeolites, and feldspars.

(6) chemical composition of the zeolitic material, which in the case of most natural zeolite species is variable.

(7) homogeneity of the zeolitic material. In the case of natural zeolites inhomogenous mixing of impurities of other mineral fragments with the zeolite may affect the reproducibility of experiments.

(8) the crystallite size (as opposed to mesh size) of the zeolite should be reported because the size may affect certain properties such as rate of sorption of gases, and the extent and rapidity of cation exchange.

(9) cation exchange and/or adsorption properties. These properties are affected by the chemistry of the zeolite, by the abundance of zeolite mineral in the rock, and by the kind and amount of impurities in the zeolite rock, so it is not surprising that both properties vary from zeolite to zeolite, and for a particular mineral zeolite from deposit to deposit.

(10) modifications of the zeolitic material will probably affect the experimental results and any modification of the material should be reported. Modifications are defined as any physical or

chemical treatment such as increasing the zeolite content of a mineral mixture, thermal treatment, acid/base treatment, or cation exchange.

Modern x-ray diffraction instrumentation has led to improvements in detection limits, analysis time, and quantitative analysis. However it is still the case that one must rely upon the operator for sampling, sample preparation and effective use of the equipment for the production of high quality patterns to identify the crystalline compounds present. Interpretation thereafter depends very much on the analyst.

In some cases, it may be difficult to assign a particular x-ray powder diffraction pattern to a certain species because variations do occur in the x-ray pattern. A slight shift in d-spacings of the main diffraction lines may be due to slightly different Si:Al ratios, or to different cation compositions. Intensity measurements are not only difficult to make accurately, but they are subject to variation because of other factors such as orientation and size of crystallites and also because of chance coincidence with other lines in a mixture of phases. Therefore, it is not surprising that different workers have found slightly different diffraction patterns for the same synthetic zeolite e.g. zeolite NaA-Milton (1959(a)) and Gramlich and Meier (1971), especially as one would expect that the conditions of synthesis for a particular zeolite from different suppliers are never quite identical.

Assigning a specific set of x-ray powder data to a natural zeolite is a problem since variations, due to their mode of formation, are evident between deposits e.g. clinoptilolite - Wyoming, U.S.A,

(Wise, Nokleburg, and Kokinos 1969); San Bernadino, California, U.S.A. (Sheppard and Gude 1969); and Agoura, U.S.A. (Koyoma and Takeuchi 1977).

Measurements of the properties of sedimentary zeolite minerals are most in doubt because sedimentary zeolite crystals are very small, and they contain a proportion of mineral impurities which are not readily separated. Analysis by x-ray diffraction is generally adequate to estimate the abundance of the zeolite and to identify common impurities such as clay minerals (such as kaolinite and illite), silica minerals (such as quartz), and other zeolites and feldspars. Although some zeolite deposits are nearly uniform, many show extreme variations in mineralogy either vertically or laterally (Sheppard and Gude 1968). Although several tens of thousands of tons of high-grade zeolite are present in the immediate vicinity of the mine site, zeolitic material obtained from different areas of the same tuff deposit can have significantly different mineralogical compositions and, hence, may affect the reproducibility of an experiment.

Zeolite minerals which occur in igneous rocks as well developed single crystals are commonly several millimeters in size, but those zeolites which are found to occur in sedimentary deposits as fine grained crystals have generally a size range of 0.1 - 30 μm. Synthetic zeolites are crystallised from the typical aqueous hydrogels or other aluminium silicates such as kaolin, and are produced as crystalline powders with particle sizes up to 10μm. Determination of particle size distribution using a photographic technique such as electron microscopy is well established, but nowadays a much quicker method involves the use of a complete

measurement tool such as those measuring the diffraction pattern of laser light caused by solids in a liquid suspension. However, the weight distribution obtained from such an instrument does not provide information on the aggregation of the particles under examination. In addition to providing information on individual crystal sizes electron microscopy is used extensively to study crystal shape and surface topography of zeolites. Thus, crystals may show well developed faces or appear as irregular aggregates, and indication of amorphous and crystalline impurities in zeolites is possible.

The formation of synthetic zeolite crystals might be expected to produce a range of chemical compositions in a given specimen, particularly if the zeolite itself can exhibit a range in compositions, such as that observed for zeolite Y. The chemical composition of a powder specimen may vary from crystal to crystal, and possibly within individal crystals. Thus a chemical analysis of the bulk specimen represents an average chemical composition of all of the crystals. A particular physical property, as it is related to composition, could not show discontinuity since the property would be an average of the bulk specimen.

In most instances the properties of zeolite minerals have been determined on a variety of mineral specimens which do not have well documented chemical compositions. Measurements of the properties of sedimentary zeolite minerals are most in doubt because sedimentary zeolite crystals are very small, their chemical composition may vary, and they may contain a relatively large proportion of mineral impurities which are not readily separated. Ideally, it would be useful to know not only the

chemical composition of the bulk zeolitic material used, but also the chemical composition of the principal zeolite mineral present. An analysis of the zeolite must usually be obtained by an instrumental technique which could identify and subsequently analyse zeolite particles in a mineral mixture. X-ray fluorescence spectrometry is accepted as a standard method for the analysis of a very wide range of materials. It is often regarded as a technique for analysis of major constituents, but has been used quite successfully for the analysis of less than 0.01% of many elements. For some studies, it is useful to know the contents of the minor and trace elements, as well as the major elements, and thus electron probe microanalysis is a very sensitive technique (allows detection of parts per million levels of elements) which is becoming increasingly popular in this area. It should be recognised that although the analysis of bulk zeolitic material used may list many trace elements, most of these elements are bound in insoluble silicate materials and are not removable by exchange. In general, only those species in cation-exchange positions in the zeolite mineral or soluble minerals, such as carbonates, will be removable.

The character of water in hydrated zeolite crystals varies in behaviour from what is best described as the normal liquid, to water which is associated strongly with the cations and the framework oxygens. Relative quantities are dependent to some extent upon the free space or the size of the cavity that is available.

When zeolites which are stable and do not undergo appreciable dimensional change upon dehydration are dehydrated, the free space

is available for occupancy by other molecular species. The capacity of the zeolite for sorption is usually related to the free space or void volume as determined by the quantity of contained water when fully hydrated.

The framework density of a zeolite, expressed as the number of structural framework tetrahedra per unit volume of 1000A^3, for various zeolites of known structure may be related to the void fraction. Zeolites which contain the larger polyhedral units and double 6-rings have void fractions greater than 0.3 and corresponding values of the framework density of less than 17 tetrahedra/1000A^3(Breck 1973(j)). In filling space the packing of the double 6-units or double 4-units, in conjunction with larger polyhedral units, results in a framework with a framework density of less than 17 tetrahedra/1000A^3.

The most open zeolite structures known are the zeolites of groups 3 and 4. These are based upon the double 6-ring units and truncated octahedral units, or β cages. Of the zeolites known to date, the largest observed void fraction is 0.5 as found in the zeolites related structurally to faujasite.

If the methods and materials of an investigation are the same, the results of controlled experiments ought to agree at least within experimental error. If the results are not in agreement one must conclude that either the methods or materials differ. The researcher must recognise that the results have only limited application unless the zeolitic materials are characterised to the fullest extent. Therefore, where applicable, the previously described criteria were used for the complete characterisation of the synthetic and natural samples used in this research programme,

bearing in mind the comments made with regard to the various techniques involved.

6.1.1 Analysis of Zeolite A

6.1.1.1 X-ray diffraction data

If after crystallisation, during synthesis, zeolite A remains in contact with the mother liquor (~ 1N NaOH) recrystallisation to the more stable zeolite P may occur and the P zeolite will in time transform further to a hydrated hydroxysodalite (Breck 1973(k)). Electron micrograph investigations indicate that in many instances the P phase crystallises on the surface of the A crystals (Breck 1973(l)).

As stated previously (section 5.1 and 6.1) it was difficult to assign peaks from the relatively poor x-ray diffractograms obtained, especially with the shift in d-spacings and variations in intensity measurements one might expect from sample to sample and from one trace to another. Many of the d-spacings for zeolite P are coincidental with those of zeolite A, but from the x-ray powder data for NaA (Table 5.6) it can be seen that the major peak obtained was that with a d-spacing of 3.08. This could be construed to be that corresponding to a d-spacing of 3.18 from zeolite P (von Ballmoos 1984) and/or that corresponding to the d-spacing of 2.99 from zeolite A. Since electron microscopy failed to reveal spheroids of zeolite P growing from the original cubic crystals of zeolite A, one must assume that the sample was a pure zeolite A.

In some cases, it is difficult to assign a particular x-ray powder diffraction pattern because variations do occur in the x-ray

pattern as a result of slightly different Si:Al ratios or variation in the exchange cation composition. This is illustrated in Table 5.7 where it appears that the powder data of CaA may vary from a "standard" pattern (Breck 1973(m)) by as much as 0.5 degrees 2θ but it can be seen from figure 5.1(b) that reduction in intensity of the CaA pattern makes interpretation difficult. The most surprising result is the position of the major peak at 6.0 degrees 2θ which, should this peak correspond to the peak at 7.2 degrees 2θ in the "standard" pattern of Breck (1973(m)), would mean a shift of over 1 degree 2θ. This could be explained by the supposition that, instead of the trace beginning at 5 degrees 2θ it was started at approximately 6 degrees, in which case all the peak positions would be increased by 1 degree 2θ . However, this would alter the good agreement which many of the peaks have with the standard pattern.

Inspection of Tables 5.8 and 5.9 show that the powder patterns for PbA exchanged from both NaA and CaA are quite similar, hence only one figure (5.1(c)) is presented as illustration. Comparison of the x-ray data for the different cationic forms of clinoptilolite reveal that the line intensity depends markedly on the size and charge of the exchange cations, whereas the interplanar spacings are practically constant (Chelishchev, Berenshtein and Martynova 1975). When sodium, or indeed calcium, is replaced by certain heavy metals, including lead, there is a considerable decrease in intensity of all the lines, particularly the strongest ones. As well as the high absorption coefficient for CuK_{α} radiation of lead, this effect is attributable to the high stresses in the aluminium-silicon-oxygen matrix of the zeolite, due to incorporation of large and heavy cations in the intracrystal space

of the zeolite. Chelishchev and his co-workers (1974) noted that the clinoptilolite crystal structure did not rupture, and, when the zeolite reverted to the Na form, the intensity of the lines was completely restored. This would seem to have been confirmed when electron micrographic studies of PbA did not show any apparent crystal damage.

6.1.1.2 Particle size

Examination of Table 5.30 indicates a wide range of crystal sizes for zeolite A from 1 μm up to 46 μm. As expected, however, scanning electron microscopy (S.E.M.) showed this to represent aggregations rather than individual crystal sizes; the latter were measured as averaging around 2 μm diameter. Using ultrasonics to break up these crystal aggregates unexpectedly produced an apparent increase in the mean size and distribution of the particles in solution.

6.1.1.3 Chemical analyses

It can be seen from Tables 5.1 - 5.5 that the sample of NaA was of typical composition (i.e. Si:Al=1), but that the CaA sample had a Si:Al ratio of slightly less than 1. This may reflect problems in the silica analysis (see section 5.1).

The sodium form appears to be a little under-exchanged while the calcium form was slightly over-exchanged. Analyses showed that about 1.3% of the sodium initially in NaA could not be removed by exhaustive exchange with calcium. It is interesting to note that Barri and Rees (1980) and Franklin and Townsend (1985) found a slightly higher, but similar amount of non-exchangeable sodium in Laporte NaA which may have been locked in the sodalite cages

(Barri and Rees 1980). Such a cation composition may go some way to explaining the difference between the diffraction pattern obtained here (Table 5.7) as compared to the "standard" pattern of Breck (1973(m)).

The number of water molecules per unit cell is seen to increase when sodium is replaced by calcium. Since the total void space must remain constant within the rigid crystal, the volume occupied by various cations will affect the number of water molecules that can subsequently be added. The water content increases with decreasing ionic radius. Thus although there is little difference in the size of the Na^+ and Ca^{2+} ionic radii, 0.97 and 0.99 $\mathring{A}$ respectively, the number of water molecules per unit cell increases from 27.3 to 31.9 because CaA zeolite contains only half the number of ions.

6.1.2 Analysis of the Faujasitic Zeolites Z1-Z5

6.1.2.1 X-ray diffraction data

In zeolite synthesis the temperature, the nature of the gel structure as influenced by the reactants, and the concentration of the reacting components in the initial mixture are all very important in determining the species produced. Zeolite P is more readily formed from gels of higher silica content than zeolites A or X, though zeolite P (which forms readily as the equilibrium phase at elevated temperatures) does not crystallize readily at the lower temperatures. At ambient temperature, the composition field is dominated by zeolites Y, A and X, but above 150°C, zeolite P is the dominant phase along with zeolite A (Breck 1973(n)).

As with the analysis of the diffractograms for zeolite A (section 6.1.1) it was difficult to assign peaks with very great accuracy. However, it was obvious from the x-ray powder data that "standard" diffraction patterns for the faujasites NaZ1-NaZ5, were obtained (see Tables 5.10 - 5.23). There was no evidence of impurities (e.g. zeolites A or P) in NaX (see Table 5.10). In the case of the four Y-type zeolites (Z2-Z5) a peak at approximately 28 degrees 2θ was evident which would seem to indicate the presence of traces of zeolite P. For NaZ2 this peak was particularly marked (see Table 5.15). Scanning electron microscopy failed however to reveal visible evidence of this impurity.

Examination of Table 5.11 shows that this x-ray powder data varies somewhat from the "standard" pattern of Milton (1959(b)). This is hardly surprising when one considers that the CaX sample of Milton had Si:Al and Ca:Al ratios of 1.25 and 0.84 respectively, whilst those for this sample were 1.22 and 1.02 with approximately 1.3% unexchangeable sodium present.

The major peak for CaX at a d-spacing of 12.44 (i.e. 7.1 degrees 2θ) is approximately 1 degree 2θ higher than that of Miltons (1959(b)) pattern. In the unlikely event that the trace actually began at 4 degrees 2θ this would cause all subsequent peaks to be displaced by 1 degree 2θ. However, by adjusting each of the major peaks accordingly and comparing with the "standard" pattern, the fit was not improved. Thus one must assume that differences in the traces obtained is due to genuine differences in the samples analysed.

Inspection of the x-ray powder data for the lead exchanged faujasites show that they are all fairly similar, hence only one diffractogram is presented as illustration (Figure 5.2(c)). The major peaks of the original forms are seen to be retained, but there is a considerable decrease in the intensity of all the lines which has been explained previously (see section 6.1.1). Particularly characteristic of the lead forms was the presence of two well-defined peaks at approximately 23.5 degrees 2θ separated by only 0.2 degrees.

The diffractograms for the trimethyllead forms of X and Y (Tables 5.14 and 5.23) are similar, and Figure 5.2(d) is shown as illustration. The strongest lines of the original sodium forms were retained, but once again there is a decrease in the intensity of these lines, presumably due to the presence of heavy metal ions as dicussed earlier (section 6.1.1). As for the inorganic lead forms of these zeolites, the characteristic peaks at approximately 23.5 degrees 2θ were again evident. In these organic lead forms, rather than there being well defined peaks, less conspicuous but distinct shoulders on the main peak were seen.

6.1.2.2 Particle size

The distribution and average particle sizes of the faujasites (Table 5.30) as determined by laser diffractometry were seen to increase with increasing Si:Al ratio. However S.E.M. again showed that this technique indicated the degree of aggregation of the individual zeolite crystals. By S.E.M. the crystal sizes were estimated at 1 μm for zeolite X and the four samples of Y were all highly aggregated, containing crystals of approximately 0.2 μm diameter.

With the exception of zeolite Z2, ultrasonics succeeded in breaking up the aggregates to a certain degree, so that the mean size and distribution of the particles was reduced.

6.1.2.3 Chemical analyses

It is apparent from the analytical data (Tables 5.1 - 5.5) that all the univalent cation forms of the faujasites did not contain a total cation equivalency. A deficiency in the metal cation balance has been indicated and confirmed by several investigators (Angell and Schaffer 1965; Ward 1968). This has been attributed to partial hydrolysis of the cation and replacement by hydronium ion (H_3O^+) during the preparation and washing of the zeolites, as manifest by the alkaline pH which was seen to develop in slurries of the sodium forms of the zeolites, a phenomenon which has been observed elsewhere (Wiers, Grosse and Cilley 1982; Cook, Cilley, Savitsky and Wiers 1982; Drummond, De Jonge and Rees 1983). Exchangeable cations in some silica-rich zeolites may be replaced by hydrogen or hydronium ions using a strong acid (see section 6.1.3). However, treatment of a zeolite with a strong acid may result in direct attack on the aluminosilicate framework and consequent dealumination. Zeolites with a Si:Al ratio of around one are more subject to mild hydrolysis and instability as a result of hydrolysis than are the more silicious zeolites. In general therefore, hydrolysis of the exchangeable cation appears to be more likely in the alumina-rich zeolites, and indeed the degree of hydronium exchange was greatest with the most aluminous faujasite - NaZ1(I). However, the analytical data show that the Na:Al ratio for NaA is 0.98:1, which suggests that the method of preparation of the zeolite also determines the degree of hydronium

exchange i.e. the more times the zeolite is washed the greater the degree of exchange (Drummond, De Jonge and Rees 1983). This is confirmed when greater care was taken over preparation of the second batches of zeolites X and Y. The degree of hydronium exchange was much reduced in X (NaZ1(II) contains 9 sodium atoms per unit cell more than NaZ1(I)), and (as one might expect in Y) in the most siliceous faujasite there was a much smaller increase, from 54.6 and 55.4 sodium atoms per unit cell, since it is much less prone to hydronium exchange. Therefore, the Na:Al ratio seems to depend upon the composition of the starting material before preparation, the method of preparation and the Si:Al ratio of the zeolites.

The water content of NaZ1 and NaZ5 is shown (Table 5.5) to increase when greater care was taken over the preparation of these zeolites. Considering the fact that in both such cases the sodium content per unit cell was increased, this is difficult to explain.

The total cation exchange capacity of NaZ1 was found to be lower in the second batch (Table 5.1) which appears odd bearing in mind that the sodium content was greater. The cation exchange capacity was based upon the theoretical capacity i.e. the known aluminium content, and not on the cation content because of the problem of hydronium exchange. The proportion of aluminium was ostensibly lower in the second batch which accounts for a similarly smaller cation exchange capacity.

The calcium form of zeolite X was seen to contain a small amount (about 1.3%) of sodium which could not be removed after exhaustive exchange with calcium. Replacement of the 16 Site I Na^+ ions per unit cell in the sodalite cages of zeolite X by Ca^{2+} ions has been

shown to be difficult (Barrer, Rees and Shamsuzzoha 1966; Sherry 1968; Barrer, Davies and Rees 1969(b); Dyer, Gettins and Brown 1970). The hydrated Ca^{2+} ion is too large to diffuse through the 2.5Å, 6-oxygen window from the supercages to the sodalite cages and energy must be supplied to strip the hydration shell of the Ca^{2+} ion. However, complete replacement, at 25°C, has been recorded on a number of occasions. (Barrer, Rees and Shamsuzzoha 1966; Sherry 1968; Barrer, Davies and Rees 1969(b)) and in fact has been accomplished on a similar sample of zeolite X (Fletcher, Townsend and Loizidou 1983). This is a similar amount of residual sodium to that observed in CaA (see section 6.1.1), but whereas similar levels of unexchangeable sodium had been noted elsewhere for CaA (Barri and Rees 1980; Franklin and Townsend 1985), for CaX this particular observation is not in accord with other reports.

The small degree of under-exchange (i.e. $H_{0.34}$) in Table 5.5 is well within experimental error.

The number of water molecules per unit cell is seen to increase on going from the sodium to the calcium form of zeolite X and is as expected (see section 6.1.1.).

One would expect that isomorphous substitution of aluminium for silicon would lead to an increase in unit cell volume since Al_2O_3 units would be replacing SiO_2 units, and this is confirmed in Tables 5.3 (a) and (b). In addition, since the number of tetrahedra per unit cell remains the same, obviously the framework density decreases, while the void fraction and framework charge density increases as the Si:Al ratio decreases.

The relationship between void fraction (V_f) and framework density (d_f) has been expressed by Breck (1973(j)) as:

$$V_f = (d_f/26) + 1 \qquad 6.1$$

It is clear that this equation assumes a positive gradient, but this is not representative of the data shown (Breck 1973(j)) in which the gradient is clearly negative. By extrapolating Breck's data the intercept on the ordinate at $d_f = 0$ is $V_f = 0.975$. Although this cannot actually be true, it is a consequence of the best linear fit to the data shown. Probably the best fit is not strictly linear, but is in fact a very slightly concave curve (quadratic fit). The "correct equation" (i.e. the best linear fit) is therefore:

$$V_f = 0.975 - (d_f/26) \qquad 6.2$$

and it is this equation which was used to calculate the void fractions. This data confirms the faujasites as the most open known zeolite structures with the largest observed void fraction of 0.5 (Breck 1973(j)).

Values obtained, for the unit cell diameter, from the derived expression of Breck and Flanigen (1968) are in excellent agreement with the data supplied by Unilever, which is based on x-ray studies (Table 5.32). This demonstrates the overall accuracy of the aluminium and silicon analyses, bearing in mind the problems mentioned previously (section 5.1) with regard to the silicon analysis. Figure 5.4 shows the analyses obtained when fitted to this derived expression.

6.1.3 Analysis of the Clinoptilolite Samples

6.1.3.1 X-ray diffraction data

In the case of mineral zeolites, where the diffraction pattern is that of a mixture of phases, the identification of the unknown impurities demands more information than can be provided by the powder diffraction data alone. If the analyst can make an "educated guess" about the unknown he can then go to the alphabetical index of the powder diffraction file (P.D.F.) and check with the three strongest lines there.

Due to their mode of genesis it is possible to make initial conjectures as to the identity of those minerals that may accompany clinoptilolite. For example, various feldspars, clays and micas as well as calcite, gypsum and quartz have been identified in different zeolite deposits. However, often there are multiple entries for each pattern in the P.D.F. and of course not all the standard patterns are of the same quality with regard to accuracy of d-values, resolution of closely spaced lines and measurement of intensities.

The task of identification of a mixture of phases in this clinoptilolite sample (Table 5.24) was made more difficult when the diffractograms showed low peak intensities and had poor resolution. However, by identifying the distinctly recognisable peaks and accounting for those which may be assigned to clinoptilolite from various "standard" patterns (Sheppard and Gude 1969; Wise, Nokleburg and Kokinos 1969; Koyama and Takeuchi 1977) a number of peaks remained to be ascribed to the impurities.

The peak with a d-value of 15.22 can probably be assigned to a montmorillonite clay (typical composition - $Na_{0.66}(Al_{3.34}Mg_{0.66}Si_8O_{20})(OH)_4$). A number of standard montmorillonite samples have been shown to show similar interplanar spacings at d-values in the range 15-15.3. Other major peaks are coincident with those of clinoptilolite.

The unassigned peak at a d-value of 10.52 may be attributable to any of the various illite clays (typical composition - $KAl_2(Si_3AlO_{10})(OH)_2$) all of which have their most intense peak at d-values of approximately 10. Ascribing this particular peak is ambiguous however, since various mica samples (typical composition of biotite - $H_4K_2Mg_6Al_2Si_6O_{24}$) also have their strongest line at about the same value.

It is probable that the unidentified peak at d=3.26 indicates the presence of orthoclase/microcline (typical composition - $KAlSi_3O_8$). A number of analyses have shown the d-value for the major peak to lie in the region 3.24-3.26. One would normally expect another line for orthoclase at about d=4.22. After examining the trace, once again, it it possible that the presence of a peak at this value confirms the presence of orthoclase, but the low intensity and poor resolution make it difficult to be certain.

The presence of calcite in natural zeolite samples would not be unexpected. Amongst the strongest lines of a typical calcite powder pattern are those with d values of 3.57 and 2.81 which again are coincidental with those of this clinoptilolite sample. However, closer examination of the diffractogram (Figure 5.3(b)

reveals a distinct shoulder, at 29.5 degrees 2θ, on the main peak, which corresponds to the most intense line (d=3.03) of calcite.

Other minerals such as anthorthite (typical composition - $CaAl_2Si_2O_8$), kaolinite (typical composition - $Al_2Si_2O_5(OH)_4$) and gypsum cannot be discounted, but their major peaks are coincidental with those of clinoptilolite, and identification of lesser peaks is difficult due to the low overall intensity of the trace.

Ideally, identification of a mixture of phases requires a high quality pattern, and thorough analysis by an expert to identify and quantify the impurities therein. However, even the partial information obtained from these traces can be helpful when combined with knowledge of the chemical composition of the material.

On comparing the diffractograms of the "fully exchanged" clinoptilolite sample (Figure 5.3(a)) with that of the original form (Figure 5.3(b)) it can be seen that, generally, the trace for F.EX.CLI appears more intense and of greater resolution. Exchanging many times with a sodium solution has the same effect of "cleaning" the original material that was carried out in the past before exchange studies (Barrer and Townsend 1976(b); Loizidou 1983). Less dense material than clinoptilolite is floated off from the zeolite and soluble impurities, such as calcite, are gradually dissolved. The remaining material has a proportionally greater content of zeolite and gives a better diffraction pattern.

Tables 5.25 and 5.27 show that the powder patterns for Pb-CLI exchanged from both NAT.CLI and F.EX.CLI are similar, hence just one figure (5.3(c)) is presented as illustration. As discussed previously (section 6.1) there is a considerable decrease in the intensity of all the lines, but this effect seems to be more pronounced for clinoptilolite than zeolites A, X or Y. Comparison of the X-ray data for the various cationic forms of clinoptilolite obtained by Chelishchev and his co-workers (1975) confirm that the particularly weak x-ray pattern for the lead-form is normal.

Aluminium can be extracted, at least in part, from certain zeolite structures without the collapse of the crystalline framework. Barrer (1968) described the essentially complete removal of aluminium from $Na_{1.0}(Al_{1.0}Si_{4.65})$ clinoptilolite without loss of crystalline structure by treatment with 2N HCl. He characterised several variously dealuminated clinoptilolites by their carbon dioxide and krypton adsorption. The cation originally associated with the removed aluminium was, of course, also removed, leading eventually to a crystalline silica having no ion exchange character.

$$Si_{4.65}O_{7.3}(OH)_{4.0}.n\ H_2O$$

Similarly, comparison of the x-ray data for different cationic forms of clinoptilolite, prepared by Chelishchev and his co-workers (1975), showed that the sample of H-clinoptilolite had interplanar spacings practically identical with those of the sodium form. No chemical analysis data were presented for their H-clinoptilolite, which was prepared by treating natural clinoptilolite with 0.1N HCl at room temperature.

Tables 5.28 and 5.29 show the x-ray diffraction patterns for acid-treated clinoptilolite samples to be similar, hence just one figure (5.3(d)) is presented as illustration. The findings agree with those of Barrer and Makki (1964), Barrer and Coughlan (1968) and Chelishchev, Berenshtein and Martynova (1975) in that there was no loss in crystallinity compared with the natural form (Table 5.24 and Figure 5.3(b) when the clinoptilolite was subjected to treatment with strong acid.

6.1.3.2 Chemical analyses of natural and "fully exchanged" clinoptilolite

For synthetic zeolites the exchange capacity can be safely based on the aluminium content under normal conditions. However, when dealing with natural zeolites it is difficult to decide what the true exchange capacity may be because some of the aluminium is likely to be present in impurities. Determination of the exchange capacity of a natural zeolite based on the measurement of cations can also be difficult. Certain cations are not easy to replace either because they are chemically bound to the aluminosilicate framework or because they are present, along with aluminium, in associated impurities.

The difficulty in measuring cation exchange capacities of many zeolites is illustrated by the work of Martin (1982). More than 100 bed volumes of 2N sodium chloride applied at a very slow flowrate were needed to convert a sample of Anaconda 1010A clinoptilolite to the sodium form. The zeolite, as mined, probably contained a mixture of Na^+, K^+ and Ca^{2+} ions in exchangeable positions in its structure, and by the inherent selectivity of that zeolite for different cations (Ames 1960)

small amounts of K^+ and Ca^{2+} would be released very slowly even in the presence of such high concentrations of sodium. A great deal of the variations reported in the literature for the cation exchange capacities of certain natural zeolites may stem from just such problems.

Barrer and his co-workers (1967) concluded that, since the sodium present was almost entirely exchangeable and that the only known impurity that could influence exchange was a trace of montmorillonite, it was permissible to determine the ion exchange capacity by determining the sodium content of the clinoptilolite, made homoionic with respect to sodium by prolonged treatment with sodium chloride solution. Based on the above assumption the exchange capacity for sodium clinoptilolite was 1.83 m equiv. g^{-1} (this agreed with that determined from the nitrogen content of the fully exchanged NH_4^+ form). Following this assumption, Barrer and Townsend (1976(b)) obtained the exchange capacity of their purified clinoptilolite in the ammonium form to be 2.14 m equiv. g^{-1}. The figure is higher that that obtained in the previous work because the attempt to remove impurities was more rigorous. Figures for sodium forms of 1.90 m equiv. g^{-1} (Loizidou 1983) and 2.02 m equiv. g^{-1} (Araya 1979) have also been reported for clinoptilolite from the same location (Hector, California), and differences may arise from the techniques used to determine this value.

Comparisons of the analytical data for NAT.CLI and F.EX.CLI (Table 5.3) show that BaO, TiO_2 amd Fe_2O_3 contents hardly change as the zeolite is exchanged, and therefore these can be regarded as non-exchangeable components. In F.EX.CLI the sum for

K_2O,CaO,SrO,MgO and Na_2O contents of 0.1043 mol hg^{-1} is in reasonable agreement with the Al_2O_3 content, but this does not validate an assumption that this therefore represents the exchange capacity of the zeolite. There may be insoluble feldspars present such as anorthite ($CaAl_2Si_2O_8$) or orthoclase ($K\ AlSi_3O_8$). The sum for the same ions in the original material was 0.1270 mol hg^{-1} which suggests the presence of a soluble material. By regarding the CaO content (0.0221 mol hg^{-1}) to comprise mainly soluble calcite or gypsum (which is reasonable when one considers that there was a 94% decrease in CaO content) a figure of 0.1049 mol hg^{-1} for the remaining cations components is in good agreement with the sum obtained for F.EX.CLI.

It seems likely that since Ca^{2+} is present mainly as non-exchangeable cations the same is also true for Mg^{2+}. However, the much smaller decrease in MgO content (only 36%) indicates that magnesium forms part of an insoluble impurity, as well as $MgCO_3$. The K_2O content of F.EX.CLI (0.0061 mol hg^{-1}) is a similar value to the MgO content of 0.0047 mol hg^{-1}. It is possible that potassium and magnesium are present in a clay such as montmorillonite or even in a mica such as biotite (see previous notes in this section).

The decrease in K_2O content in the "purified" clinoptilolite was due to the ion exchange process producing an apparent homoionic clinoptilolite with respect to sodium. It is also true that the decrease in CaO and MgO contents will be in some way due to exchange of Ca^{2+} and Mg^{2+} ions which are resident cations associated with the zeolite framework.

For the oxide formulae and unit cell compositions (Tables 5.4 and 5.5) the total analysed potassium has been assigned to clinoptilolite. Bearing in mind the previous comments, it is highly unlikely that this is in fact the case, however, the difficulty lies in deciding the proportion of potassium arising from impurities (see section 6.3.3.1).

In his estimation of the chemical composition of clinoptilolite, Minato (1980) assumed that the analysed aluminium content was from the zeolite only. This is particularly erroneous unless one can be assured that there are indeed no impurities present.

Based on a number of assumptions, including that the homoionic form of the clinoptilolite was produced and that all exchangeable cations were contained in the zeolitic part of the exchanged material, the oxide formula and the percentage impurities by weight were derived (Barrer, Papadopoulos and Rees 1967; Barrer and Townsend 1976(b)). In this study, by assuming that all the exchangeable sodiums (0.0921 mol hg^{-1}) were contained in the zeolite, the Al_2O_3 contribution from impurities would be 0.0154 mol hg^{-1}. However, the combined CaO, MgO and K_2O content is only 0.0121 mol hg^{-1}. This suggests that a certain proportion of the supposed Al_2O_3 impurity is actually zeolitic, which in turn indicates that the zeolite is not fully sodium exchanged. This was found also to be true for the sodium form used by Barrer, Papadopoulos and Rees (1967) where the Al_2O_3 impurity was 0.0271 mol hg^{-1} and the combined Na_2O, CaO and K_2O content was only 0.0181 mol hg^{-1}; however this was not commented upon. The ammonium form of Barrer and Townsend (1976(b)) was apparently free of Na^+ and K^+ ions so that excess aluminium (0.007 mol hg^{-1}) was

thought to be due to anorthite ($CaAl_2Si_2O_8$). Their analysed CaO content of (0.0276 mol hg^{-1}) was accounted for by balancing the charges in anorthite, with the remainder as calcite (0.0206 mol hg^{-1}). This is a reasonable assumption when one considers that any Ca^{2+} ions should be replaced by NH_4^+ ions. In the case of sodium clinoptilolite, Na^+ do not appear to exchange readily with Ca^{2+} ions, and even less so for K^+ ions. These observations are in line with the known selectivity sequence for clinoptilolite (Ames 1960).

A figure of 1.84 m equiv. g^{-1} for the exchange capacity of the F.EX.CLI, based on the sodium analysis, is in good agreement with that of Barrer, Papadopoulos and Rees (1967), and Loizidou (1983) i.e. 1.83 and 1.90 m equiv. g^{-1} respectively. The figure for the sodium form of Araya (1979) of 2.02 m equiv. g^{-1} was obtained on a sample that had undergone a more rigorous purification procedure. Barrer and Townsend (1976(b)) not only subjected their sample to a similar rigorous purification procedure, but also exchanged with NH_4^+ ions, for which clinoptilolite has a much greater selectivity than Na^+, to obtain the highest figure of 2.14 m equiv. g^{-1}. Hence, it appears that one can only hypothesise as to the composition of clinoptilolite material, and the subsequent exchange capacity based on the cation content.

For practical reasons (as in the case of the use of zeolites for pollution purposes) it is convenient to base the exchange capacity on their aluminium content.

For the production of ion exchange isotherms (in this work), the crystal phase composition after exchange was based on the cation composition of the clinoptilolite before exchange and the change

in solution phase composition. Only when the cation content of the crystal phase was greater than the exchange capacity (i.e. aluminium content) does the definition of exchange capacity come into question. As will be seen later, basing the exchange capacity on total aluminium content is not a problem, and in no way affects the results.

The amount of water present in the samples was determined by the loss in weight when the samples were heated up to 1000°C. However, this loss in weight was not due only to the loss of zeolitic water, because there must be a loss in weight due to the evolution of carbon dioxide within this temperature from carbonate impurities.

The amount of zeolitic water in the sample could be determined by subtracting the amount of carbon dioxide evolved from the total loss in weight up to 1000°C. It may be possible to estimate the amount of carbon dioxide evolved by assigning a certain proportion of the oxides of calcium and magnesium as carbonates, based on the derivation of zeolite composition (Barrer and Townsend 1976(b)). Alternatively a series of the isothermal thermogravimetric analyses may also provide the weight loss due to carbon dioxide, since breakdown of the carbonates is unlikely at less than 500°C (Liptay 1971) (this would also provide an estimation of the proportion of carbonates present).

In this case, the weight loss for the UNEX.CLI must be ascribed to both loss of water and loss of carbon dioxide. That of F.EX.CLI may be expected to consist mainly of water, since there should be little, if any, soluble carbonates present after a large number of exchanges.

When Na^+ ions replace larger cations such as K^+, Ca^{2+} or Mg^{2+} ions one might expect that the intracrystalline volume available to water would increase. This would seem to be confirmed by the fact that F.EX.CLI contained a greater amount of water than UNEX.CLI.

Although the water contents of the lead exchanged clinoptilolite samples were not determined in this case it is interesting to note the findings of Chelishchev and his co-workers (1975).

Lead exchanged clinoptilolite would apparently contain half the number of cations compared with the sodium form, yet the water content of the lead form was lower. When one considers that the ionic radius of Pb^{2+} ion is 1.32Å compared with 0.99Å for the Na^+ ion this result appears strange because the intracrystalline space occupied by water is increased from 28.8% to 32.1%.

Analysis of the infra-red spectra of the different cationic forms of the clinoptilolite revealed that the relative amount of water associated with the aluminium-silicon-oxygen framework varies with the size, atomic weight and charge of the exchange cations as a result of the reaction of the latter with the unshared pair of electrons of the oxygen atom of the water molecule. Such observations may also apply to lead forms of zeolites A, X and Y.

6.1.3.3 Chemical analyses of acid-treated clinoptilolite

The aluminosilicate zeolites have limited stability in acid media because of the solubility of aluminium away from the structure. Hydrated alumina becomes appreciably soluble at a pH of about 4, but in the presence of hydrated silica, the solubility of aluminium is suppressed to a slightly lower pH (McDaniel and Maher 1976). The zeolites are chemically similar in nature to other

aluminosilicate minerals and to the hydrated amorphous silica-aluminas. They are especially susceptible to acid attack because, in most cases, their aluminium is essentially all surface aluminium and receives little or no protection by being buried or inaccessible. Some clays, for example, resist acid leaching of the aluminium because the aluminium atoms are largely located between silicate layers and are therefore inaccessible to the aqueous phase. Zeolites, by their nature, are extremely open structures and their aluminiums are consequently subject to acid attack.

There are very little quantitive data in the literature concerning the stability of zeolites to acid attack. Nevertheless, it is possible to distinguish three categories of behaviour concerning their acid stability:

(1) Those that cannot be put into the acid form without collapse of the crystalline framework (e.g. zeolites A and X).

(2) Those that can be put into the acid form by a conventional ion exchange process with an acidic solution. Undoubtedly some removal of aluminium is involved, the amount being dependent on the acid used, its concentration, etc. (e.g. mordenite and clinoptilolite).

(3) Those that can be conveniently put into the acid form only by an indirect method wherein an ion exchange is performed with some ion such as ammonium, which upon subsequent heating will decompose, leaving the zeolite in the acid form (e.g. zeolite Y).

Direct treatment of silica-rich zeolites with strong acid results in the progressive replacement of the cation by hydronium ion.

This is illustrated schematically for the zeolite mordenite by the reaction

$$Na_8((AlO_2)_8(SiO_2)_{40}).24\ H_2O$$

$$\downarrow n\ H_3O^+ \qquad 6.3$$

$$Na_{8-n}(H_3O^+)_n((AlO_2)_8(SiO_2)_{40}).m\ H_2O + nNa^+ + (24-m)H_2O$$

Replacement of all the original cations by hydronium ions has been carried out in mordenite (Barrer and Peterson 1964) and clinoptilolite (Barrer and Makki 1964; Barrer and Coughlan 1968). Further treatment with strong acid removes the framework aluminium ions, which are probably replaced by four hydroxyl groups (Barrer and Makki 1964):

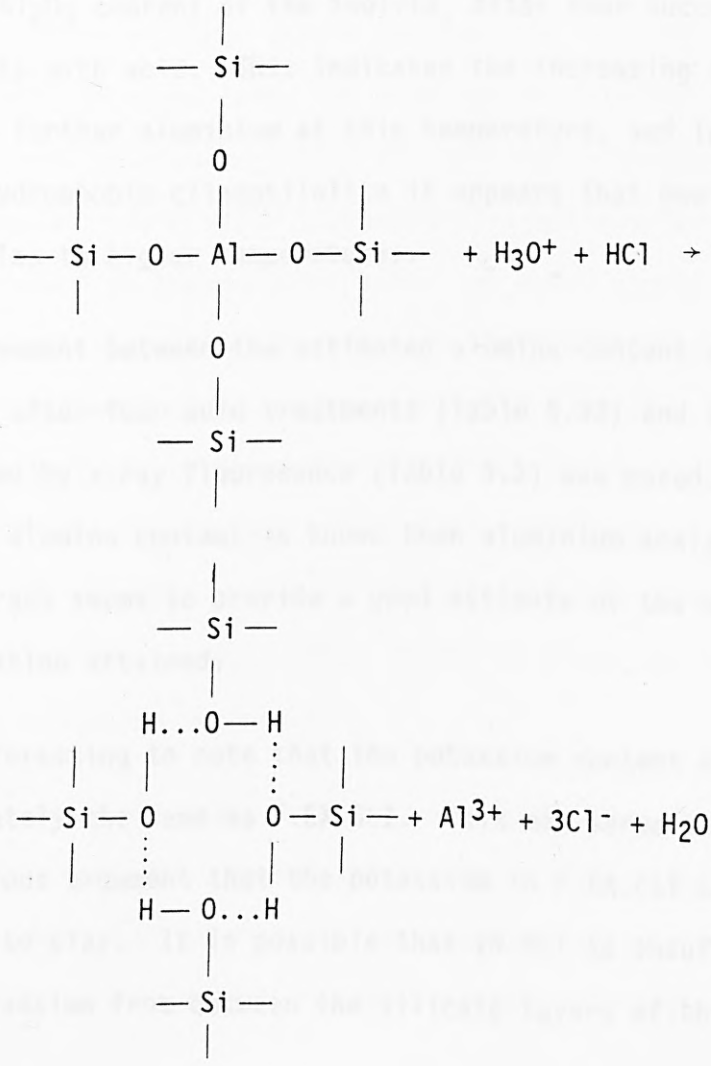

6.4

Barrer and Makki (1964) showed that, by refluxing samples of clinoptilolite for 4 hours at a temperature of about 100°C with hydrochloric acid solutions of varying strengths from 0.25N to 30N, 82% of the aluminium could be removed with 2N acid and complete dealumination occurred with 5N acid. Barrer and Coughlan (1968) went on to show that treatment with 2N HCl was sufficient to yield a completely dealuminated form which retained crystallinity. This is in contrast to the results in Table 5.3 which showed that treatment with 2N and 4N HCl at room temperature, resulted in samples whose Al_2O_3 content had been reduced by only 14% and 20% respectively.

Table 5.33 and figure 5.5 show that a plateau is almost attained, for the Al_2O_3 content of the zeolite, after four successive treatments with acid. This indicates the increasing difficulty of removing further aluminium at this temperature, and in order to obtain hydrophobic clinoptilolite it appears that one must subject the samples to higher temperatures.

Good agreement between the estimated alumina content of the zeolites after four acid treatments (Table 5.33) and that determined by x-ray fluoresence (Table 5.3) was noted. If the original alumina content is known then aluminium analysis of the acid extract seems to provide a good estimate of the degree of dealumination attained.

It is interesting to note that the potassium content of 2N CLI was approximately the same as F.EX.CLI. This may serve to strengthen the previous argument that the potassium in F.EX.CLI can be assigned to clay. It is possible that 2N HCl is insufficient to leach potassium from between the silicate layers of the clay,

whereas increasing the strength of the acid to 4N is sufficient to reduce the potassium content by half.

For the oxide formulae and unit cell compositions (Tables 5.4 and 5.5) it was assumed that, apart from sodium which had been re-exchanged into the zeolite, all exchangeable cations had been removed from the zeolite. The degree of hydronium exchange was determined by difference between Na_2O and Al_2O_3 contents.

Chelishchev and his co-workers (1974) noted that on treating natural clinoptilolite with 0.1N solutions of various cations, apart from the lithium form, the largest water content measured was that for the sample treated with 0.1N hydrochloric acid. This might be expected since the intracrystalline space available to water increases as other larger cations are replaced. Barrer and Makki (1964) observed that, for a series of clinoptilolite samples refluxed with hydrochloric acid of different strengths up to 30N, the volume of sorbed water increased to a maximum for the sample treated with 0.5N hydrochloric acid. It would appear that treatment of clinoptilolite with acid up to 0.5N results in hydronium exchange and a certain degree of aluminium removal, hence the increase in the intracrystalline space available to water. Treatment with hydrochloric acid of 1N and above results in increased aluminium removal, and although the intracrystalline space also increases, the number of cation sites and hence the degree of hydration decreases.

It can be seen from Table 5.3 that samples treated with 2N and 4N hydrochloric acid had greater water contents than the natural form, the water content increasing with increasing concentration of acid. It is convenient to note that the SiO_2:Al_2O_3 ratio of 2N

CLI (12.9:1) is the same as that of the 0.5N hydrochloric acid refluxed samples of Barrer and Makki (1964) which was shown to adsorb the maximum volume of water of those samples studied. Increasing the acid strength to 4N causes increased aluminium removal (SiO_2:Al_2O_3 ratio is 14.1:1), but is such that the water content increases. Thus the water content of acid treated samples seems to depend on the number of cation sites and the intracrystalline space available, so that by obtaining the right balance between the two would result in a sample with the maximum water content attainable.

6.2 RATE OF UPTAKE OF INORGANIC LEAD BY THE FAUJASITES

The extremely rapid removal of Pb^{2+} ions from solution by all the faujasites is clearly evident from Table 5.34. For example, zeolite 1 using a suspension of 0.1% w/v, took only 35 seconds to reach 90% of the equilibrium concentration. On doubling the zeolite quantity to 0.2% w/v the same level of removal occurred in less than 5 seconds.

Obviously as one increases the quantity of zeolite the rate of removal increases (Figure 5.6). Uptake by zeolite 1 at greater than 0.4% w/v and by zeolite 2 at greater than 0.6% w/v was so fast that it was not possible to measure the rate of removal using the ion selective electrode.

From table 5.34 and figure 5.7 it can be seen that as the Si:Al ratio increases the rate of removal decreases. However, for suspensions containing lower quantities of zeolites, zeolites 3 and 4 were seen to remove Pb^{2+} ions more rapidly than zeolite 2 in the initial stages of exchange. This anomalous behavious is

difficult to explain, but it is possible that the zeolite P impurities in zeolite 2 discussed previously (see section 6.1.2.1) may account for this.

As time proceeded, zeolite 2 was observed to remove more Pb^{2+} ions from solution than zeolites 3 or 4 because of its greater exchange capacity (Figure 5.7). At a zeolite concentration of 0.6% w/v the anomalous behavious is removed (figure 5.7(e)), probably because the rate of removal by zeolite 2 is so rapid at this concentration that it overcomes any non-analogous behaviour of any impurities.

6.3 ION EXCHANGE OF LEAD (II) IONS IN ZEOLITES

6.3.1 Exchange of Lead (II) Ions in Synthetic Faujasitic Zeolites

6.3.1.1 Non-stoichiometry of exchange

Previously it was thought that treatment of zeolites with sufficiently concentrated lead solutions would lead to an exchange level of 100%. Tables 5.35 and 5.36, and figures 5.8 - 5.17 show that the equivalent fraction of lead in the zeolite was greater than one (*see note at bottom of page) for all exchanges at both

* *Where the concentrations of lead in the crystal phase were such that they were greater than the exchange capacity of the zeolite, then equation* 6.5 *was used to evaluate* $\bar{E}_A$*, since under these conditions equation* 2.3 *is misleading:*

$$\bar{E}_A = z_A \ \bar{m}_A \ / \ \bar{Q} \qquad 6.5$$

where $\bar{Q}$ *is the ion exchange capacity of the zeolite, based on the known framework content. In such cases* $\bar{E}_B$ *would be determined similarly:*

$$\bar{E}_B = z_B \ \bar{m}_B \ / \ \bar{Q} \qquad 6.6$$

total normalities when the zeolites were treated with sufficiently concentrated lead solutions.

The high degree of selectivity for Pb^{2+} ions exhibited by the faujasites is illustrated by calculating the separation factor. The α values are usually >> 1 (Tables 5.37 and 5.38) and the selectivity increases as the SiO_2:Al_2O_3 ratio decreases (figures 5.18(a) and (b)).

As the selectivity manifested by a zeolite for lead increases, the point at which precipitation occurs (i.e. the concentration of lead in the exchange solution) is seen to decrease, and the extent of precipitation for exchange solutions of similar concentrations is greater in these cases (Tables 5.35 and 5.36 and Figures 5.8 - 5.17).

When over-exchange was noted in the first systems studied - (Pb^{2+}/Na^+Z1 exchange at 0.05N and 0.1N) precipitation due to the presence of residual chloride ions adsorbed on the zeolite was thought to be responsible. However, when a sample of the sodium zeolite prepared using sodium chloride solutions was rigorously shaken in distilled water, separated, and a chloride test carried out on the supernatant, no chloride was detected. Also the oxide formula of the analysed zeolite (Table 5.4) showed that there was a deficiency of sodium in the structure (0.95 Na_2O:Al_2O_3), indicating that there was no residual sodium chloride. By comparing exchanges carried out on similar Pb^{2+}/Na^+ exchange solutions using chloride and nitrate salts of sodium (Table 5.39) it can be seen that there was good agreement between the equilibrium data for the two forms, and that precipitation occurred just as readily in the nitrate prepared form as in the

chloride prepared form. Subsequently, exchanges at both total normalities for all the zeolites prepared by exchanging with sodium nitrate, all showed over-exchange.

For zeolite A, it has been shown that, as a result of hydronium exchange highly alkaline pH's may develop in exchange solutions (Drummond, De Jonge and Rees 1983). Thus, the possibility arises that it is the precipitation of lead hydroxide from solution which accounts for the excess lead in the crystal phase.

It can be seen from figure 5.19 that (as one would expect) the pH at which $Pb(OH)_2$ precipitation occurs decreases as the concentration of Pb^{2+} ion in solution increases up to a point (pH5.9) where it becomes constant.

For precipitation to occur in a solution containing 0.01N Pb^{2+}:0.09N Na^+ a pH of approximately 7.5 is needed, whereas for a solution containing 0.06N Pb^{2+}:0.04N Na^+ a pH of approximately 5.9 only is required (Table 5.40).

One must take into account the rate of removal of lead from solution, as well as the degree and rate of pH change of that solution. It has been shown (section 6.2) that, at the zeolite concentrations used in most of the isotherm work (0.3g/50 ml = 0.6%), the exchanges have reached 95% of the equilibrium value within the first 5 seconds. For $E_{Pb} \rightarrow 0$ this means that the concentration of Pb^{2+} ion in solution is reduced to 10^{-5} - 10^{-7} mol dm^{-3}, depending on the selectivity of the zeolite. As the SiO_2:Al_2O_3 ratio decreases, the pH change increases (section 6.5.2.1) but at the same time the rate of removal of Pb^{2+} ion increases (section 6.2). Thus for zeolite A, which may be

expected to exhibit the greatest pH change in solution (section 6.5.2.1), the high degree of selectivity for Pb^{2+} ion (Hertzenberg and Sherry 1980) ensures that the concentration of Pb^{2+} ion in solution is reduced so rapidly that precipitation is unlikely.

In the study of Semmens and Seyfarth (1978) into the selectivity of clinoptilolite for heavy metals, including lead, the increase in solution pH measured during their equilibrium study, caused by leaching of basic impurities from clinoptilolite into solution, led them to suggest carbonate precipitation in solution. In contrast to their findings, analysis of the total normalities of solutions after exchange (Figure 5.20) revealed that the final total cation concentrations were generally lower than the initial concentration (either 0.05N or 0.1N) and that generally recoveries decreased as $E_{Pb} \rightarrow 1$. Similarly the percentage cation recoveries for the crystal phase (Figure 5.21) increased in the same direction. (Figures 5.20 and 5.21 are discussed in more detail in section 6.5.2.1 in relation to hydronium exchange and precipitation). In contrast to the previous study these results suggest that precipitation has occurred within the zeolite. In their studies, Semmens and Seyfarth (1978) decanted and acidified their solutions after exchange, before analysis. Thus they argued that the measured solution concentrations represented the sum of metal as precipitate and metal in true solution. However it may equally be argued that the clinoptilolite fines which remained in solution following simple decanting (and which they comment upon as clearly visible) upon acidification released bound ions from the zeolite particles, and that this was the cause of a greater cation recovery for the solution phase after exchange.

Scanning electron microscopy (S.E.M.) was used in these studies in order to investigate the possibility of surface precipitation. A sample of zeolite X that had been treated with a sufficiently high concentrated lead solution so as to cause precipitation was examined. Simultaneous x-ray fluoresence (X.R.F.) examination confirmed the sample to be 10% over-exchanged. The resolution of the S.E.M. technique is such that particles greater than 10nm on the surface of 1μm crystals of zeolite X would have been clearly distinguishable. Although a slight "softening" of the crystal features in PbX was noticeable, no evidence of clumping of particles on the surface was seen. This does not absolutely preclude precipitation on the outer surface of the crystallites since the precipitate is likely to be present as an even distribution over the surface of the crystals. Despite S.E.M. being inconclusive, X.R.F. did however confirm over-exchange.

Evidence has been given for the existence of other surface hydroxylated species such as Cu(II) in both NaX and NaY (Dyer and Barri 1977, Schoonheydt and Velghe 1976), $CdOH^+$ (McClusker and Seff 1978) and $Cd_2(OH)^{3+}$ (Abe and Sudoh 1980; McCusker and Seff 1978) have been suggested elsewhere as the hydroxyl species involved in cadmium over-exchange in both zeolite A and in crystalline antimonic (V) acid (C-SbA), but significant precipitation in the Cd/NaX system has not been observed (Gal and Radovanov 1975; Fletcher and Townsend 1985).

Since the most aluminous zeolite used here (X) is less aluminous than zeolite A, these observations contradict literature reports regarding near-stoichiometric lead exchange in zeolite A (Hertzenberg and Sherry 1980; Cook, Cilley, Savitsky and Wiers

1982; Wiers, Grosse and Cilley 1982), although Hertzenberg and Sherry (1980) noted some Pb^{2+} and Cd^{2+} over-exchange, but accounted for it in terms of the presence of small amounts of aluminium occluded in the sodalite cages.

Data from the literature (Smith and Martell 1976) can be obtained for the association constants of lead in aqueous solution, which indicate the ease with which this ion will form basic salts. At 298K, the decadic logarithms of the association constants (Fletcher and Townsend 1985) for the formation of the species $Pb(OH)_n^{(2-n)+}$ are respectively 7.8 (n=1), 10.9 (n=2), 13.9 (n=3), and 16.3 (n=4). The intracrystalline environment of a zeolite is clearly different from a purely aqueous environment and this analogy with the aqueous acidic reaction must not be held too rigorously, but comparison with other metal ions show that stoichiometric exchange of lead in zeolites X and Y must be difficult, if not impossible (Fletcher and Townsend 1985). Indeed, over thirty years ago a mechanism was proposed by Barrer and Hinds (1953) to account for apparent over-exchange of lead in analcite, in which it was suggested that lead entered the crystal as the univalent complex $PbOH^+$. More recently, adsorption of the tetra-nuclear species $Pb_4(OH)_4^{4+}$ was used to explain the additional capacity which was observed over the theoretical value in the exchanger C-SbA (Abe and Sudoh 1981).

The presence of hydroxylated species in zeolites and other inorganic ion-exchangers to explain over-exchange seems logical, but adsorption into the zeolite of a species as large as $Pb_4(OH)_4^{4+}$ seems improbable, and precipitation of basic salts within the channels (Semmens 1981) seems the most feasible

explanation for over-exchange in this instance, especially since the precipitation problem was greatest with zeolites having the highest aluminium content.

6.3.1.2 Exchange selectivities

Examination of the isotherms of Pb^{2+}/Na^{+} exchanges in the faujasites (Figures 5.8 - 5.17) shows the very high selectivity exhibited by these zeolites for lead over sodium at low sodium loading. For zeolites 1 and 2 this high preference for lead over sodium extends over the complete isotherm. For example, for zeolite 1 at T_N = 0.05 g equiv. dm^{-3}, at $\bar{E}_{Pb}$ = 0.926, E_{Pb} has a value of only 2×10^{-3}; and for zeolite 2 at the same concentration, at $\bar{E}_{Pb}$ = 0.932, E_{Pb} has a value of only 0.021. As the silica:alumina ratio increases several of the isotherms indicate a reversal in selectivities at low E_{Na}. In the case of zeolites 4 and 5 (Figures 5.11, 5.12, 5.16 and 5.17) approximately the last 30% of Na^{+} ions were more difficult to remove, and this presumably corresponds to some or all of the sodium ions present in the hexagonal prisms.

It has been shown (Sherry 1969) that as the anionic field strength (number of AlO_4^{-} tetrahedra per unit volume) varies the selectivity patterns exhibited by zeolites can also change. The effect of varying anionic site density while maintaining almost constant water content is vividly demonstrated by the faujasites. As a result of it's high aluminium content, NaX exhibits selectivity patterns characteristic of high field strength exchangers, whereas NaY exhibits the weak field strength pattern. For Pb^{2+}/Na^{+} exchanges Eisenman's (1962) model predicts that zeolite Y should prefer lead, but that zeolite X should prefer

sodium. However this model is only an approximation and changes in water content and entropy of ions in the zeolite phase could also be factors in determining selectivity (Sherry 1969) (see section 6.3.1.3).

The exchange of thallium for sodium in zeolites X and Y (Sherry 1966) provides a good analogy to the Pb^{2+}/Na^{+} exchanges observed here. NaX exhibits a high selectivity for thallium over the whole course of the exchange reaction. This is consistent with the high polarisability of the thallium ion - 3.9×10^{-24} cm^3 (Phillips and Williams 1965), and indicates strong binding by anionic sites (lattice oxygens) in both the supercages and the small cages. However, thallium did not replace 16 cations per unit cell in NaY. Based on the silicon and aluminium analyses of Sherry (1966) it was possible to calculate (Breck and Flanigen 1968) a unit cell diameter for the X and Y samples of Sherry as 24.94Å and 24.65Å respectively, compared to 24.95Å and 24.68Å (Table 5.32) for the samples of X and Y used in this study. The lattice contraction which occurs when SiO_2 isomorphously replaces AlO_2^- in the framework prevents thallium (ionic radius of 1.40Å) from passing through the windows from the supercages into the smaller cages. Although the reduction in unit cell size is not sufficient to exclude lead ions (ionic radius of 1.20Å) from entering the smaller cages, it appears to be more difficult in zeolite Y than in X, with a reversal in selectivity when all the sodium ions had been removed from the supercages.

For a given zeolite, comparisons of selectivities for lead over sodium at the two different solution normalities should show that the selectivity increases for the divalent ion as the total

concentration of ions in the external solution is decreased (Rees 1980). However this 'valence concentration effect' (Rees 1980) is not apparent from figure 5.18, possibly because of greater precipitation at the higher total normalitity. Note that the huge selectivities seen for lead in all cases (Figures 5.8 - 5.18) make the accurate evaluation of α as $\bar{E}_{Pb} \rightarrow 0$ quite difficult. Previously, selectivity trends have been discussed using dielectric theory (Barrer and Davies 1969; Barrer and Townsend 1976; Fletcher and Townsend 1981(a)); in its simplest form the following equation for ΔG^{θ} holds:

$$\Delta G^{\theta} = \frac{Ne^2}{8\pi} \left[\left(\frac{2}{r_{Pb}} - \frac{1}{r_{Na}}\right)\left(\frac{1}{\bar{\varepsilon}} - \frac{1}{\varepsilon}\right)\right] \quad 6.7$$

where N is the Avagadro constant, e is the charge on the electron, r_{Pb} and r_{Na} the 'bare' ionic radii of lead and sodium respectively, and $\bar{\varepsilon}$ and ε the appropriate (macro) permittivities of the zeolite and solution phases. Since $\bar{\varepsilon} < \varepsilon$ (Barrer, Rees and Shamsuzzoha 1966) and $r_{Pb} < 2r_{Na}$ equation 6.7 predicts that the standard free energy change for the exchange reaction should be positive for all zeolites.

In addition, it has been shown (Fletcher and Townsend 1981(a)) that simple dielectric theory leads to the conclusion that if the same exchange reaction is observed in two zeolites of differing framework charge density, then:

$$\left|\Delta G^{\theta}(hc)\right| < \left|\Delta G^{\theta}(lc)\right| \quad 6.8$$

where the subscripts (hc) and (lc) refer to zeolites having high and low charge densities respectively. Thus, if (as is the case here) dielectric theory predicts that ΔG^{θ} should be positive for

the exchange of lead in zeolites, then the theory also implies that ΔG^{θ} should be less positive for the zeolite of higher framework charge. On the basis of the framework charge densities presented in table 5.31, affinity sequences for exchange in these zeolites may be predicted in terms of these assumptions to be:

$$\text{Zeolite } 1 > 2 > 3 > 4 > 5 \qquad 6.9$$

Also, the relationship between ΔG^{θ} and the mass action quotient K_m for the exchange reaction:

$$Pb^{2+} + 2\overline{Na}^{+} \rightleftharpoons 2Na^{+} + \overline{Pb}^{2+} \qquad 6.10$$

is given by (Fletcher and Townsend 1980(b)):

$$\Delta G^{\theta}/RT = -\ln K_a = 1 - \int_0^1 \ln\Gamma d\bar{E}_{Pb} - \int_0^1 \ln K_m d\bar{E}_{Pb} \qquad 6.11$$

where Γ is the correction factor allowing for the non-ideality of the solution phase. For reaction 6.10 the relationship between α (equation 3.9) and K_m is:

$$K_m = \alpha(m_{Na}/\bar{E}_{Na}) \qquad 6.12$$

and therefore:

$$\Delta G^{\theta}/RT = 1 - \int_0^1 \ln\Gamma d\bar{E}_{Pb} - \int_0^1 \ln\alpha d\bar{E}_{Pb} - \int_0^1 \ln(m_{Na}/\bar{E}_{Na}) d\bar{E}_{Pb} \qquad 6.13$$

It is obvious that the contribution of the last integral of equation 6.13 can only increase the selectivity trend shown in the α values (Figure 5.18) and therefore provided the value of the first integral is similar for the exchanges in all five zeolites, then the ΔG^{θ} values must follow a trend in qualitative agreement with the α values. For exchanges where the selectivities change

markedly, the value of $\int_0^1 \ln\Gamma d\bar{E}_A$ can be substantially different for different exchangers (Fletcher and Townsend 1980(b)); however this is not the case here. It is therefore reasonable to conclude (especially if total solution normalities are the same) that trends in selectivites will be reflected qualitatively by a trend in affinities in the same direction (Barrer and Townsend 1976). Thus the affinity trends produced using dielectric theory (equation 6.9) do indeed agree with the observed selectivity trends in figure 5.18.

Typical values for the Γ function of equation 6.13 vary from 1.601 to 1.709 across the isotherm at T_N = 0.05g equiv. dm^{-3}. Similarly, at T_N = 0.1g equiv. dm^{-3} they vary from 1.875 to 2.021. The α values are usually >>1 (Figure 5.18) and the same is true for the ratio $(m_{Na}/\bar{E}_{Na})$ given in equations 6.12 and 6.13. Thus, taking equation 6.12 as a whole, it is obvious that the measured ΔG^θ values for each system shown in figure 5.18 must all be strongly negative. However, dielectric theory leads to the prediction that the ΔG^θ values be positive (equation 6.7 et sequens) which is not in accord with the data of figure 5.18 and equation 6.13.

Previously it has been shown that the assumption that the macropermittivity $\bar{\varepsilon}$ for a given zeolite hardly changes when different ions are exchanged is dubious if the exchanging ions are highly polarizable (Fletcher and Townsend 1981(a)). The lead ion is reported (Phillips and Williams 1965) as having a substantially higher polarizability than the sodium ion, so once more, as in the case of silver exchanges in faujasite and mordenite (Fletcher and Townsend 1981(a)), simple dielectric theory is seen to be at least

partly deficient. The results shown in figure 5.18 are the first example therefore of a prediction, made previously (Fletcher and Townsend 1981(a)), that if in fact $\bar{\varepsilon}_A > \bar{\varepsilon}_B$, even the sign may be predicted incorrectly. Dielectric theory is seen therefore to have limited utility in estimating selectivity trends in zeolites of different framework charge (O'Connor and Townsend 1985).

6.3.1.3 Prediction of ΔG^θ for the Pb/NaX exchange

Simple dielectric theory predicts that for the exchange reaction:

$$Pb^{2+} + 2\bar{Na}^{+} \rightleftharpoons 2Na^{+} + \bar{Pb}^{2+} \qquad 6.10$$

the standard free energy of exchange (ΔG^θ) should be positive, whilst the data of figure 5.18 and equation 6.13 show that the ΔG^θ must be strongly negative (section 6.3.1.2). However, over-exchange discussed in section 6.3.1.1 and probably due to precipitation, precludes direct and accurate evaluation of the thermodynamic function using equation 6.13. Thus application of the "triangle rule" (Barrer and Falconer 1956) to the systems - Pb/NaX, Pb/CaX and Ca/NaX, was considered, in order to predict a value of ΔG^θ for the Pb/NaX system. Investigation of the Pb/CaX ion exchange system would enable a prediction of ΔG^θ, since the Ca/NaX reaction had already been studied on a similar sample of NaX (Fletcher and Townsend 1985). However, a number of interesting points arose when the Ca^{2+}/Na^{+} isotherm and the respective $Ca^{2+} \rightleftharpoons Na^{+}$ Kielland plot obtained for a similar sample of zeolite X (Fletcher and Townsend 1985) were compared to other reported measurements on calcium exchange in NaX (Barrer, Rees and Shamsuzzoha 1966, Sherry 1968; Wolf, Ceacareanu and Pilchowski 1973).

The sigmoidal character of the Ca/NaX isotherms obtained by these studies is probably due to the equilibrium constant for exchange into the supercages being greater than unity, while the corresponding one for the exchange into the sodalite cages (see following discussion) would be less than unity (Sherry 1968). However, on comparison of their respective Kielland plots a number of differences were observed which would account for disagreement in the values obtained for the standard free energy of exchange. Sherry (1968) and Wolf and his co-workers (1973) observed smooth decreases in their Kielland plots with increasing loading of alkaline earth cations, whereas Fletcher and Townsend (1985) noted a change in selectivity for calcium at high calcium loadings. This was accounted for in terms of the difficulty in obtaining precise measurements at the isotherm extrema - the high selectivity of zeolite X for Ca^{2+} ion makes it very difficult to obtain accurate isotherm points at the extrema, so that small experimental errors caused large variations in computed values of K_c (Fletcher and Townsend 1980(b)). Thus, the acquisition of precise data at either end of the isotherm is a necessary prerequisite to determination of accurate values of K_c.

The standard free energy of exchange obtained for various examinations of the Ca/NaX exchange system are shown overleaf:

Study	ΔG^{θ}_{298}/KJ equiv.$^{-1}$	silica:alumina ratio of sample
Ames (1964)	-2.09	2.40
Barrer, Rees and Shamsuzzoha (1966)	-0.67	2.44
Sherry (1968)	-1.34	2.52
Wolf, Ceacareanu and Pilchowski (1973)	-1.36	2.29
Fletcher and Townsend (1985)	-1.46	2.54

All the samples of zeolite X shown above had almost the same silica:alumina ratio and therefore in principle very nearly the same number of exchangeable cations. They may however have differed somewhat in the number of Na^+ ions which had been initially replaced by hydronium ions as a result of hydrolysis (see section 6.3.2). One obvious difference which may be of importance is that Ames (1964) used bonded pellets of zeolite X, while in the other investigations the pure crystal powder was employed. In general equilibrium will take longer to be established in pellets than in the stirred crystal powder. This factor, together with the presence of binder impurities in the pellets, could account for any difference in the shape of isotherms. However, Ames (1966) published neither the isotherm nor the raw data, but only the derived thermodynamic data, so simple comparisons are not possible.

In summary, the derived standard free energies of exchange are seen to show wide variation becase (1) at low values of $\bar{E}_{Ca}$, K_c is very sensitive to small errors in the experimental measurements, (2) fundamental differences in the selectivity of the zeolites exist due to varying degrees of hydronium exchange (see section 6.3.2), and (3) the physical state in which the zeolites were used for exchange differed.

Previously it has been shown that the 25°C isotherm for the Ca/NaX system using a 24 hour equilibration time indicated that only 82% of the Na^+ ions were replaced by the divalent ions (Sherry 1968), and that 4 days was required to attain 100% exchange. It was concluded that the 18% of Na^+ ions that were difficult to replace represents the 16 Na^+ ions per unit cell that are in hexagonal prisms of hydrated NaX. It was also concluded that the slow rate of Ca^{2+} ion exchange in the network of small cavities in NaX was primarily attributable to the large hydration energy of the Ca^{2+} ion. Based on the ionic radius, Ca^{2+} ion should diffuse quite freely into the hexagonal prisms of NaX, since calcium and sodium have approximately the same Pauling radius - 0.99$\mathring{A}$ and 0.95$\mathring{A}$ respectively (Pauling 1960). It does not do so because the hydrated ion is too large to diffuse through the 2.5$\mathring{A}$ entrances to the small cages, and energy must be supplied to at least partially strip the primary hydration shell of Ca^{2+} ions. The hydration energy is 140.2 kcal/g-ion (Rosseinsky 1965) and even if only part of this energy must be supplied, the potential energy barrier to Ca^{2+} ion diffusion from the α into the small cages would be large.

It is immediately obvious that the exchange of Pb^{2+} ions with CaX (Figure 5.22) is quite different to that observed for the Pb/NaX system (Figure 5.13). The Pb/CaX exchange system shows a strong preference for lead over calcium at low lead loading (at $\bar{E}_{Pb}$ = 0.121, E_{Pb} has a value of only 2.701×10^{-5}) but it is apparent from figure 5.23 that NaX has a greater preference for Pb^{2+} ions in this range. From this same plot it is obvious that over the whole isotherm CaX is the least selective for lead of those studied. Clearly a selectivity sequence of $Pb^{2+} > Ca^{2+} > Na^{+}$ exists for this zeolite, which one might have predicted from the relevant isotherm data (Ca^{2+}/Na^{+}, Pb^{2+}/Na^{+} and Pb^{2+}/Ca^{2+} exchanges in zeolite X).

Analysis of the total normalities of the solutions after exchange revealed that in accord with the Pb/NaX system, the final total concentrations were generally lower than the initial concentration (0.1 g equiv. dm^{-3}). This suggests that precipitation, as might be expected from the association constants of lead (see section 6.3.1.1), has occurred within the zeolite in this case also. In accord with this assumption, as lead loading increases non-stoichiometric exchange is observed i.e. $2\bar{m}_{Pb} + 2\bar{m}_{Ca} > \bar{Q}$ (Figure 5.24), though in contrast to Pb^{2+}/Na^{+}, exchange in zeolite X, the concentration of lead in the crystal phase did not exceed the exchange capacity i.e. $2\bar{m}_{Pb} > \bar{Q}$.

Overexchange in the Pb/CaX system precludes the determination of ΔG^{θ} for this reaction, thus application of the triangle rule (Barrer and Falconer 1956) to estimate ΔG^{θ} for the Pb^{2+}/Na^{+} exchange system was not possible.

As the loading of calcium decreases the preference for lead decreases until at high lead loadings a strong preference for calcium over lead exists i.e. $\alpha<1$ (Table 5.41 and Figure 5.23). This selectivity reversal occurs at a calcium concentration ($\bar{m}_{Ca}$) of approximately 0.40 mol kg^{-1} (Appendix 2: Table 12) which is about 18% of the total number of Ca^{2+} ions present in zeolite X. 18% of the Ca^{2+} ions in CaX represents close to 8 Ca^{2+} ions per unit cell, and it must be concluded that the 8 Ca^{2+} ions that are in the hexagonal prisms of hydrated CaX, and which experienced difficulty in replacing the Na^{+} ions initially present (see above), are similarly very difficult to remove with Pb^{2+} ions. Exhaustive exchange with lead eventually resulted in the removal of a small amount of the remaining calcium in the crystal phase (approximately 2 Ca^{2+} ions per unit cell), but even in samples where $\bar{E}_{Pb} > 1$ calcium was still in evidence.

The selectivity reversal can be readily understood in terms of Eisenman's model (1962) which showed that the specificity of a surface containing fixed charges for alkali metal ions can be accounted for in terms of ion hydration and electrostatic bond energies. Sherry (1969) extended this model to divalent ions. According to the model, if a cation exchanger such as a zeolite is placed in a solution containing several different metal salts, the preference of the exchanger for one metal over another depends on whether the difference in their hydration free energy, or in their free energy of electrostatic interaction with fixed anionic exchange sites predominates.

For the di-divalent exchange:

$$A^{2+} + \bar{B}^{2+} \rightleftharpoons \bar{A}^{2+} + B^{2+} \qquad 6.14$$

the free energy ΔF^{θ}_{AB} of this reaction is given by (Sherry 1969):

$$\Delta F^{\theta}_{AB} = \tfrac{1}{2}(\bar{F}^{el}_{A} - \bar{F}^{el}_{B}) - \tfrac{1}{2}(\bar{F}^{hyd}_{A} - \bar{F}^{hyd}_{B}) \qquad 6.15$$

where $\bar{F}^{el}$ refers to the free energy of electrostatic interaction between the cations and the anionic sites and F^{hyd} refers to the free energy of hydration.

The electrostatic contribution to the free energy of exchange partly depends on the anionic field strength of the ion exchanger. If this quantity is small compared to the free energy of hydration of the ions in the aqueous solution, the hydration term in equation 6.15 predominates. This is the weak-field case, and the least hydrophilic ion is preferred by the exchanger. Alternatively, if the anionic field strength is high, the electrostatic contribution to the free energy of exchange is large compared to the hydration term in equation 6.15. This is the strong-field case, and the ion with the smallest ionic radius is most preferred because it interacts most strongly with the anionic field in the exchanger.

Zeolite X is considered to exhibit selectivity patterns characteristic of high field strength exchangers (Sherry 1969), so that one would expect the ion with the smallest ionic radius to be preferred throughout the zeolite. However, in the open network of the large cavities in zeolite X lead ions can exchange with the readily accessible calcium ions, and lead is preferred to calcium probably as a result of the greater polarisability of the Pb^{2+} ion compared to that of the Ca^{2+} ion (Phillips and Williams 1965). This allows greater ion-pair formation, which frees water of hydration ("free" intracrystalline water should possess more entropy than water co-ordinated to cations) and results in an

increase in entropy of the system (Sherry 1969). In contrast, one might postulate that ion-pair formation involving the smaller Ca^{2+} ions (0.99Å compared to 1.20Å for lead) in the relatively high anionic strength field of the small cages, together with the energy requirement (357.8 kcal/g-ion: Rosseinsky (1965)) necessary to strip the hydration shell of the Pb^{2+} ion for entry into the small cages, makes Pb^{2+}/Ca^{2+} exchange in these cages extremely difficult.

Since the relationship between $\bar{\varepsilon}$ and ε (the macro permittivities of the zeolite and solution phases respectively) is $\bar{\varepsilon} < \varepsilon$ (Barrer, Rees and Shamsuzzoha 1966) and $r_{Pb} > (z_{Pb}/z_{Ca})\, r_{Ca}$ simple dielectric theory predicts (equation 6.7) that the standard free energy change for the Pb^{2+}/Ca^{2+} exchange reaction should be negative for all zeolites.

The activity coefficient ratio (Γ) of 1.325 is constant throughout the isotherm, but the α values range from $>> 1$ to $<< 1$ (Table 5.41). Thus, taking equation 6.13 as a whole, it is difficult to predict the relative sign for ΔG^{θ} from the selectivity data, and dielectric theory predictions can neither be confirmed nor denied.

6.3.2 Lead Exchange in Sodium and Calcium Forms of Zeolite A

Precipitation was found to be a common problem with lead exchanges in the faujasites, especially when there were high lead concentrations in the zeolite, and the problem increased as the high alumina content of the zeolite was raised. Since the most aluminous zeolite used (zeolite X) was less aluminous than zeolite A this observation contradicts some literature reports regarding lead exchange in zeolite A (Hertzenberg and Sherry 1980; Cook,

Cilley, Savitsky and Wiers 1982; Weirs, Grosse and Cilley 1982) and an examination of the Pb/NaA system proved necessary in order to confirm that precipitation occurs as a result of the alkaline intracrystalline environment of the zeolites.

It has been asserted by various investigators that overexchange did not occur in their studies of lead exchange in either sodium or calcium forms of zeolite A (Hertzenberg and Sherry 1980; Cook, Cilley, Savitsky and Wiers 1982; Wiers, Grosse and Cilley 1982). Should this have proven correct the accuracy of the results obtained in this study could be tested by application of the 'triangle rule' (Barrer and Falconer 1956) to the systems Pb/NaA, Pb/CaA and Ca/NaA, since the Ca/NaA ion exchange system had been studied on a similar sample of zeolite A (Franklin 1984). Thus examination of the Pb/CaA system was necessary to check the literature data, and to complete an overall study of Pb^{2+} ion exchange as a function of silica:alumina ratio.

6.3.2.1 Lead exchange in NaA

Examination of the isotherm for Pb^{2+}/Na^{+} exchange in zeolite A (Figure 5.25) shows the high selectivity for lead exhibited by this zeolite over sodium for much of the isotherm, and especially at low lead loading (at $\bar{E}_{Pb} = 0.091$, E_{Pb} has a value of only 3×10^{-6}). At high lead loading there is evidence of a selectivity reversal beginning at approximately $\bar{E}_{Pb} = 0.9$ (Figure 5.25 and Table 5.38).

The total normalities of the solution after exchange (Figure 5.20) show that the final total concentrations were generally lower than the initial concentrations (0.1 g equiv. dm^{-3}), and that generally

recoveries decreased as $E_{Pb} \rightarrow 1$. This suggests that precipitation had occurred which was confirmed by over-exchange of the crystal phase (Figures 5.21 and 5.24). Precipitation of lead in the alkaline intracrystalline environment of zeolite A is in accord with observations recorded for lead exchange in the faujasites, even though there is no clear relationship between silica:alumina ratio and degree of precipitation (Figures 5.20 and 5.21).

It was shown in section 6.3.1.2 that for the Pb^{2+}/Na^{+} exchange dielectric theory (Barrer, Rees and Shamsuzzoha 1966; Barrer and Davies 1969; Barrer and Townsend 1976; Fletcher and Townsend 1981(a)) predicts a positive value for the standard free energy of exchange. In addition it was shown that if the same exchange reaction is observed in two zeolites of differing framework charge then the standard free energy of exchange should be less positive for the zeolite of higher framework charge (Fletcher and Townsend 1981(a)). One would naturally expect the framework charge density of zeolite A to be greater than that for zeolite X, so the affinity sequence presented in equation 6.9 can be extended to include zeolite A:

$$\text{zeolite A} > 1 > 2 > 3 > 4 > 5 \qquad 6.16$$

Provided that the value of $\int_0^1 \ln\Gamma d\bar{E}_{Pb}$ is similar for exchanges in all these zeolites, then the ΔG^{0}_{θ} values must follow a trend in qualitative agreement with the α values, since the contribution of the last integral in equation 6.13 serves to increase the selectivity trend shown in the α values. The value of $\int_0^1 \ln\Gamma d\bar{E}_{Pb}$ is not substantially different for the exchange involving zeolite A compared to that for the faujasites, so trends in selectivities

will be reflected qualitatively by a trend in affinities in the same direction (Barrer and Townsend 1976). However it is unclear from figure 5.18 whether the selectivity sequence observed with the faujasites extends to the selectivity observed for NaA, thus the affinity trends produced using dielectric theory (equation 6.16) cannot be confirmed.

Typical values for the Γ function of equation 6.13 vary from 1.875 to 2.020 across the isotherm. The α values are usually >> 1 (Figure 5.18) and the same is true for the ratio $(m_{Na}/\bar{E}_{Na})$ given in equations 6.12 and 6.13. Thus, taking equation 6.13 as a whole, the measured ΔG^{θ} values for the Pb/NaA system must be strongly negative. However, as for the faujasites, dielectric theory predicts that ΔG^{θ} values be positive (equation 6.7 et sequens) which is again not in agreement with the data of figure 5.18 and equation 6.13. Once again (see section 6.3.1.2) it has been shown that the failure of dielectric theory to take into account the polarizabilities of different ions can lead to the sign of ΔG^{θ} being predicted incorrectly (Fletcher and Townsend 1981(a)).

The Na^{+} ions in NaA are all thought to be located in the large cages (Broussard and Shoemaker 1960). However, the Na^{+} ions fall into two groups, the group of 8 cations co-ordinated directly to lattice oxygen in rings of six tetrahedra that separate supercages from the sodalite cages and the group of 4 ions that are presumed to be fully hydrated in occluded water in the supercages. The sigmoidal shape of the alkaline earth-sodium isotherms (Sherry and Walton 1967) have been accounted for in terms of the presence of these two crystallographically distinct kinds of Na^{+} ions.

According to Eisenman's model (1962) one would expect NaA to exhibit selectivity patterns characteristic of high field strength exchangers (i.e. the ion with the smallest ionic radius to be preferred because it interacts most strongly with the anionic field in the exchanger). However, diffferences arise because the simple model of Eisenman (1962) fails to take into account changes in water content and entropy of ions in the zeolite phase. The Pb^{2+}/Na^{+} exchange observed here may be explained in similar terms to that of the Ca/NaA system of Sherry and Walton (1967). Thus, extensive ion-pair formation of highly polarisable Pb^{2+} ions with the anionic framework releases water of hydration and leads to an increase in entropy of the system. Evidence of a selectivity reversal at high lead loading was probably due to the difficulty in removing the few remaining Na^{+} ions co-ordinated to lattice oxygens in the rings of six tetrahedra.

Crystal structures of zeolite A exchanged with Pb^{2+} at pH 4.3, 5.2 and 6.0 showed that the extent of exchange depends on pH (Ronay 1984; Ronay and Seff 1985). In all cases more metal ions than were needed to balance the anionic charge of the zeolite framework entered the zeolite, together with anions from solution, so that more than 6 Pb^{2+} ions (the stoichiometric number) were found per unit cell. At pH = 5.2 and 6.0, 9 Pb^{2+} ions were found per unit cell, and at pH 4.3, 6.3 Pb^{2+} ions were seen.

X-ray diffraction studies suggest that a small fraction of the lead ions present in zeolite A (following a flow-through technique at a constant pH of 3.9) are present as $PbOH^{+}$ which occupies an 8-ring site. In these positions the Pb^{2+} ion could co-ordinate to framework oxygens and its co-ordinated OH^{-} ion could hydrogen-bond

to oxygen(s) on the opposite side of the same 8-ring (Stamovlasis and Seff 1985).

In their study of lead and cadmium exchange in NaA, Hertzenberg and Sherry (1980) accounted for over-exchange in terms of the presence of small amounts of occluded aluminium in the sodalite cages, whilst McCusker and Seff (1978) thought that $CdOH^+$ present in acidic $CdCl_2$ exchange solution could explain their observed over-exchange. Wiers, Grosse and Cilley (1982) explained these previous non-stoichiometric observations in terms of the exchange of hydrolysed lead and cadmium cations which occur in the alkaline pH developed in NaA slurries, whereas in their work Pb^{2+} and Cd^{2+} cations exist predominantly under the less alkaline conditions of CaA slurries. However, this argument cannot apply to flow through techniques (Stamovlasis and Seff 1985), and Wiers, Grosse and Cilley (1982) failed to recognise that the presence of only a relatively small amount of lead ion is sufficient to buffer the pH change (section 6.5.2.1), and as the concentration of lead in the original exchange solutions decreases ($E_{Pb} \rightarrow 0$) the selectivity of zeolite A is such that the concentration of lead is reduced to ppm levels within seconds in these exchange solutions, so that formation of hydrolysed species is unlikely. The association constants of lead in solution indicated that stoichiometric exchange of this ion in zeolites X and Y must be difficult if not impossible (Fletcher and Townsend 1985). It is not surprising then that in zeolite A, the most aluminous of the zeolites, the higher internal metal concentrations and high internal pH lead to hydroxide precipitation within the zeolite.

A PbA sample was prepared from the calcium form by Cook and his co-workers (1982) in which the Pb/Al mole ratio was claimed to be 0.50. A Pb/CaA isotherm had also (apparently) been shown to be completely reversible (Wiers, Grosse and Cilley 1982), which enabled a value of log K (3.66) to be estimated for the Pb/NaA exchange, based on the application of the triangle rule to the Ca/NaA and Pb/CaA systems. However, it is difficult to understand how stoichiometric exchange was observed for the Pb/CaA system when it is the alkaline crystalline environment of the zeolite rather than the original cationic form which is responsible for overexchange.

Examination of the Pb/CaA system was therefore considered necessary in order to check the literature and, if stoichiometric exchange is observed, to estimate a value for ΔG^{θ} for the Pb/NaA system.

6.3.2.2 Lead exchange in CaA

The Ca/NaA ion exchange system studied on a similar sample of zeolite A (Franklin and Townsend 1985) showed a strong preference for calcium over sodium, especially at low calcium loadings. The isotherm showed thermodynamic reversibility and its shape agreed well with previously reported isotherms (Barrer, Rees and Ward 1963; Ames 1964; Wolf and Furtig 1965; Sherry and Walton 1967; Barri and Rees 1980; Wiers, Grosse and Cilley 1982).

Experimental selectivities for calcium over sodium were quantified using the separation factor α. This showed that at high sodium loading calcium was greatly preferred, but as the loading of sodium decreased the preference for calcium also decreased. As

was discussed in the previous section this may be accounted for by the presence of sodium ions in two crystallographically distinct sites.

The simple model of Eisenman (1962) predicts that NaA should exhibit selectivity patterns characteristic of high field strength exchangers. However a combination of ion-pair formation and the subsequent release of water of hydration leads to an increase in the entropy of the Ca^{2+}/Na^{+} exchange in zeolite A. Hence, calcium is preferred over sodium.

Despite the agreement with the literature regarding shape of the isotherm, the standard free energies of exchange are seen to show wide variation:

Investigators	ΔG^{θ}_{298}/kJ equiv.$^{-1}$
Barrer, Rees and Ward (1963)	-0.59
Ames (1964)	-2.27[a]
Wolf and Furtig (1965)	-1.12[bc]
Sherry and Walton (1967)	-3.08
Barri and Rees (1980)	-2.69
Wiers, Grosse and Cilley (1982)	-2.15
Franklin and Townsend (1985)	-2-83

a re-calculated by Wiers, Grosse and Cilley (1982)

b ΔG^{θ}_{293}

c calculated from selectivity data

On comparison of the respective Kielland plots used to calculate these standard free energies, it was seen that large differences occur at low calcium loading of the zeolite. As explained earlier (section 6.3.1.3), in this region K_c is very sensitive to small

errors in experimental measurements, and in fact Rees (1980) accounted for the large difference between the ΔG^{θ} values of Barrer, Rees and Ward (1963) and Barri and Rees (1980) in terms of the error in measurement of E_{Ca} at low values of $\bar{E}_{Ca}$ in the earlier study.

Smaller differences between the plots at higher values of $\bar{E}_{Ca}$ may not be entirely due to experimental scatter, but may be due to fundamental differences in selectivity due to the cation content of the starting material (section 6.3.1.3) or to the different methods of preparation. Wiers, Grosse and Cilley (1982) showed that the cation recovery of the crystal phase was lower than the exchange capacity of the zeolite, and that the recovery decreased as $\bar{E}_{Na}$ increased. This low cation recovery was observed in the Ca^{2+}/Na^{+} exchange carried out on a similar sample of zeolite A (Franklin and Townsend 1985), but the trend across the isotherm was not observed. Similar low retrieval of cations as $\bar{E}_{Na \to 1}$ have been observed in all those systems previously investigated in this thesis. (Figures 5.21 and 5.24). Wiers, Grosse and Cilley (1982) accounted for this in terms of hydronium exchange, and this was supported by Drummond, De Jonge and Rees (1983) who observed rapid hydronium exchange when zeolite A was placed in water. As will be seen later (section 6.5) rapid hydronium exchange occurs in 0.1 mol dm^{-3} sodium solutions, and the level of exchange depends on the experimental conditions (weight of zeolite, volume of solution, atmospheric conditions). The Na:Al ratio of the starting material will depend upon the composition of the starting material before preparation and the method of preparation. Since the level of hydronium exchange will affect the preference of the zeolite for other exchanging ions, then isotherms measured under

different conditions not surprisingly show differences in selectivity.

The isotherm for Pb^{2+}/Ca^{2+} exchange in zeolite A (Figure 5.26) once again shows the high selectivity for lead exhibited by this zeolite over calcium throughout the isotherm, and especially at low lead loading (at $\bar{E}_{Pb} = 0.097$, E_{Pb} has a value of only 6×10^{-5}). As in the Pb/NaA system, at high lead loading ($\bar{E}_{Pb} = 0.92$) there is the possibility of selectivity reversal being evident. The downward trend in selectivity values at high lead loading (Figure 5.23) tends to agree with this observation, but values for the separation factor (>>1) still indicate the high degree of selectivity for the ingoing ion (Table 5.41). In fact a point was reached at which the concentration of calcium in the crystal phase was so low that it could not be analysed accurately (Table 5.41), and hence α values could not be determined.

Thus, it is clear that in this exchange system lead ions readily exchanged for the calcium ions which are all located in the large cages of zeolite A, whereas in the Pb/CaX exchange system (section 6.3.1.3) there was a reversal in selectivity when all but the calcium ions present in the small cages were replaced.

With zeolite A having a high anionic field strength (Sherry 1969), one might have predicted, using Eisenman's model (1962), that it would prefer calcium to lead. However, the highly polarisable lead ion (Phillips and Williams 1965) is preferred to calcium, probably because the entropy of the system is larger in the lead form (see section 6.3.1.3).

The total normalities of the solutions after exchange were lower than the initial concentration (0.1g equiv. dm^{-3}) but in contrast to other systems studied, recoveries increased as $E_{Pb} \rightarrow 1$ (Appendix 2: Table 13). This could be explained if the total normalities of the exchange solutions were incorrect (specifically the concentration of calcium solution from which the exchange solutions were made up being lower than anticipated). However, the solutions used for these exchanges were from the same batch as those used for the Pb/CaX system where no such observation was made, so this anomolous behaviour is difficult to explain.

Precipitation of lead in the zeolite was confirmed by cation recoveries in the crystal phase (Figure 5.24), but there does not appear to be any clear relationship between silica:alumina ratio and cation recovery.

It is difficult to ascertain from figure 5.23 the relative selectivities for lead of the different cationic forms of zeolite A at high lead loading. At low lead loading the sodium form appears to be more selective for lead than is the calcium form and this would confirm a selectivity sequence for this zeolite of $Pb^{2+} > Ca^{2+} > Na^{+}$, which one might have predicted from the relevant isotherm data (Ca^{2+}/Na^{+}, Pb^{2+}/Na^{+} and Pb^{2+}/Ca^{2+} exchanges in zeolite A).

As shown in section 6.3.1.3 simple dielectric theory predicts that the standard free energy change for the Pb^{2+}/Ca^{2+} exchange reaction should be negative for all zeolites. In addition it has been shown (Fletcher and Townsend 1981(a)) that if the same exchange reaction is observed in two zeolites of differing framework charge then the standard free energy of exchange should

be less negative for the zeolite of higher framework charge. One would naturally expect the framework charge density of zeolite A to be greater than that for zeolite X, so one would expect CaX to have a greater affinity for lead than CaA.

The activity coefficient ratio of 1.325 is constant throughout the isotherm, the α values are >>1 (Figure 5.23 and Table 5.41) and the same is true for the ratio $(m_{Na}/\bar{E}_{Na})$. Thus, taking equation 6.13 as a whole, the measured ΔG^{θ} value for the Pb/CaA system must be strongly negative, which is in agreement with simple dielectric theory.

It follows from equation 6.13, that if the ion exchange properties of these zeolites are being compared for the same pair of ions and the solution strengths are the same, (so that the activity coefficient ratio for di-divalent exchange Γ is the same i.e. 1.325, and invariant with $\bar{E}_{Pb}$: see Rees (1980)), then if the α values obtained with one zeolite over the isotherm are higher than the corresponding α values for the second zeolite, the free energy of exchange will also be more negative with the first zeolite. It is clear from figure 5.23 and Table 5.41 that the α values for Pb^{2+}/Ca^{2+} exchange in zeolite A are greater than those for zeolite X over most of the isotherm, so one would expect the free energy of exchange to be more negative for zeolite A, which is not in accord with dielectric theory. The reasons for this failure must be as discussed earlier (see section 6.3.1.2).

Following comments made in the previous section, it was not surprising to have observed precipitation in this system considering the association constants of lead in solution (Fletcher and Townsend 1985), and a combination of high internal

metal concentrations with the highest internal pH possible for a zeolite.

Exchange of hydrolysed lead ion species, proposed by Wiers, Grosse and Cilley (1982) has been questioned (section 6.3.2.1) on the grounds that the very presence of any lead is sufficient to buffer the pH change necessary to form these complex species, and that the selectivity exhibited by the zeolite is such that Pb^{2+} ions are removed so rapidly that they are not present in solution long enough to form these species. It is only after the Pb^{2+} ions have been exchanged, and as such the inherent buffering agent has been removed, that the solution pH is allowed to rise (see section 6.5.2.1). Overexchange, and identification of $PbOH^{+}$ species, in zeolite A samples treated using flow-through techniques, in which 0.1M $Pb(NO_3)_2$ solution was held at constant acidic pH values, serve to strengthen the argument that solution pH is not responsible for the production and subsequent exchange of hydrolysed lead ion species in this zeolite (Ronay 1984, Ronay and Seff 1985; Stamovlasis and Seff 1985).

It is difficult to comprehend how Cook and his co-workers (1982) were able to obtain a sample of PbA, in which the Pb/Al mole ratio was 0.50, by exhaustive exchange with 0.05M $Pb(NO_3)_2$ solution. Equally incomprehensible must be the thermodynamically reversible Pb/CaA isotherms reported by Wiers, Grosse and Cilley (1982).

In conclusion, the results obtained in this study indicate it is wrong even to estimate a ΔG^{θ} value for the Pb/NaA system by appliciation of the triangle rule (Barrer and Falconer 1956) on the systems Pb/NaA, Pb/CaA and Ca/NaA.

6.3.3 Lead Exchange in Clinoptilolite

Clinoptilolite is a cheap readily available material, known for its high selectivity for a number of polluting ions. A number of investigations into Pb^{2+}/Na^{+} exchange in samples from various sources have revealed differences in metal selectivity, and the problem of precipitation had been suspected to occur in some natural zeolites (Barrer and Hinds 1953; Semmens and Seyfarth 1978; Semmens 1981). A study of the Pb^{2+}/Na^{+} ion exchange system in a raw unexchanged clinoptilolite material (NAT.CLI) and a "fully sodium exchanged" sample (F.EX.CLI) was thought necessary to clarify the behaviour of this zeolite, and to complete an overall study of Pb^{2+} exchange as a function of silica:alumina ratio.

6.3.3.1 Crystal phase composition determination

Initially, attempts were made to determine the crystal phase composition directly by acid dissolution and subsequent cation analyses, but the disparity of the results obtained showed this technique to be inappropriate. Subsequently, the crystal phase composition after exchange was derived from the initial composition (based on the X.R.F. analyses supplied by Laporte) and analysis of the solution phase before and after exchange. Comparison of the results obtained, for a couple of solutions exchanged with both forms of clinoptilolite, using either direct acid dissolution or calculations based on differences before and after exchange are shown in Table 5.42. It is obvious that recoveries determined by acid dissolution are less than those obtained by calculation based on the solution phase composition, and although the zeolite samples were treated in exactly the same

manner the cation recoveries were inconsistent. This reflects the difficulty in completely breaking down highly siliceous zeolites (see section 5.3.3).

An interesting point to note from table 5.42 is that the X.R.F. analysis provided a calcium content of 0.013 mol kg^{-1} for the F.EX.CLI sample Table 5.3), yet acid dissolution gave results of 0.023 and 0.033 mol kg^{-1} even after exchange with lead containing solutions.

When the solution phases of those exchanges involving F.EX.CLI were analysed, not only sodium, but measurable quantities of potassium, calcium and magnesium were discovered. The presence of potassium in solution is hardly surprising when one considers that clinoptilolite is more selective for this ion that it is for sodium. Only after subsequent exchange with lead solution, for which clinoptilolite is far more selective, is the remaining potassium removed. Similarly it is quite likely, even after exhaustive exchange with sodium, that traces of exchangeable calcium and magnesium may still be present within the zeolite. However, the concentration of these ions (approximately 10^{-4} mol dm^{-3} for potassium, and 10^{-6} mol dm^{-3} for calcium and magnesium) are such that they were not significant in the derivation of $\bar{E}_{Pb}$ and $\bar{E}_{Na}$.

Since the potassium content of those solutions exchanged with F.EX.CLI was insignificant in the subsequent determination of crystal phase composition, the K_2O content of F.EX.CLI must be regarded as essentially non-exchangeable (see section 6.1.3.2). It was interesting to note that a similar amount of potassium was determined in the sample treated with 2N hydrochloric acid (Table

5.3). This is consistent with comments made previously (section 6.1.3.3) regarding the difficulty in acid-leaching of clays. It is only when the clinoptilolite is treated with 4N hydrochloric acid that the potassium content is reduced still further. This may be further evidence that this potassium is contained in a clay component and is not available for exchange. Thus, it was decided that the potassium content of NAT.CLI after exchange should realistically be based on the analysed content minus the unexchangeable component i.e. 0.0488-0.0061 = 0.0427 mol hg^{-1} (Table 5.3).

As one would have expected, analyses of the solution phases of those exchanges involving NAT.CLI revealed that, not only sodium and potassium, but also calcium and magnesium were detected. Although it is evident that these ions must take part in the ion exchange reaction, their contents in solution (approximately 10^{-4} and 10^{-5} mol dm^{-3} for calcium and magnesium respectively) were such that they were not significant in the derivation of $\bar{E}_{Pb}$, $\bar{E}_{Na}$ and $\bar{E}_{K}$. Analyses of the results showed this to be correct because lead uptake by the zeolite was almost exactly equal to the sodium and potassium released, and this has been confirmed elsewhwere (Loizidou 1983). Thus, the exchange was essentially a binary one, and subsequent data were derived on this basis (for example, derivation of separation factors).

At higher values of $\bar{E}_{Pb}$, it was found that the amount of sodium or potassium removed from the crystal phase was actually greater than that reported to be present in the analysed original composition. This is a drawback of the X.R.F. technique, in that the material is non-homogenous, and unless a sufficient number of scans are

carried out to produce an accurate overall analysis, a misleading picture ensues. In such cases an arbitarily low value for the relative counter ion concentration was inserted into the programme to allow subsequent derivation of the crystal phase composition, but values for the separation factor are meaningless in such instances (Table 5.42).

Normally $2\bar{m}_{Pb} < \bar{Q}$, and $\bar{E}_{Pb}$ was based on the original cation composition derived from equations 2.2 and 2.3. Only when $2\bar{m}_{Pb} > \bar{Q}$ do equations 6.5 and 6.6 apply and the question then arises as to what the exchange capacity then is. One must decide either to base the exchange capacity on what one concludes is the exchangeable cation content (i.e. the exchangeable Na^+ and K^+ ion content of NAT.CLI and the exchangeable Na^+ content of F.EX.CLI), or on the maximum theoretical exchange capacity (i.e. aluminium content). In both forms of the zeolite the cation content has been shown to be less than the aluminium content (for NAT.CLI exchangeable $Na^+ + K^+ : Al^{3+} = 0.87:1$; for F.EX.CLI exchangeable $Na^+ : Al^{3+} = 0.86:1$), but this is because the total aluminium analysed consists of both zeolitic aluminium and that belonging to the impurity component of the material. It is obvious that when $2\bar{m}_{Pb} > \bar{Q}$, $\bar{E}_{Pb}$ would be slightly lower by using the theoretical exchange capacity in equation 6.5, and similarly for $\bar{E}_{Na}$ and $\bar{E}_K$ by applying equation 6.6 in these circumstances.

This illustrates the major problem in researching natural materials; they are not pure products but rather contain a variety of impurities such as calcite, unaltered glass, clays etc., which were occluded during the formation of the zeolite. The exchange capacity of a weighed sample for any particular isotherm point is

based on the weight of material used for that point, hence it is more than likely that the cation recovery ($100.(2\bar{m}_{Pb} + \bar{m}_{Na} + \bar{m}_{K})/Q$) will be less than the supposed capacity, since the original weighed sample contains impurities. It might be expected that as $E_{Pb} \rightarrow 0$ one would observe recoveries of less than 100%. As E_{Pb} increases, and precipitation of lead occurs in the crystal phase, one would observe an increase in recoveries until eventually they are greater than 100%. In the following section it will be shown that by using the aluminium content as the exchange capacity ($\bar{Q}$) in equation 6.5, cation recoveries follow this trend, whereas using the exchangeable cation content as $\bar{Q}$, recoveries of greater than 100% would be derived for all exchanges. Considering the trend in cation recoveries, together with the fact that the only difference between the two conventions is that $\bar{E}_{Pb}$ would be slightly lower using the theoretical exchange capacity when $2\bar{m}_{Pb} > \bar{Q}$, for practical reasons it was convenient to base the exchange capacity on the aluminium content.

6.3.3.2 Lead exchange in natural and "sodium forms" of clinoptilolite

The exchange isotherm in NAT.CLI (Figure 5.27) is highly sigmoidal, showing a strong preference for lead over sodium and potassium at low lead loadings (at $\bar{E}_{Pb} = 0.107$, E_{Pb} has a value of only 3×10^{-4}), and a converse strong preference for sodium and potassium at high lead loadings. The exchange isotherm for F.EX.CLI (Figure 5.28) also demonstrates the high selectivity for lead exhibited by this zeolite (at $\bar{E}_{Pb} = 0.107$, E_{Pb} has a value of only 4×10^{-4}). However, the isotherm for F.EX.CLI is further to

the right than that of NAT.CLI, indicating a somewhat greater selectivity.

The experimental selectivities for lead over sodium and potassium, quantified using the separation factors, α, show the normal pattern, in that as $E_{Pb} \rightarrow 0$ lead is greatly preferred, while as the sodium and potassium loading decreases the preference for lead decreases (Figure 5.29 and Table 5.42). This plot also shows that F.EX.CLI is more selective for Pb^{2+} ions than NAT.CLI over the entire isotherm.

Differences in the selectivity of various clinoptilolite samples have been accounted for in terms of mineralogical differences (Semmens 1981), but the only difference between these samples is the cationic content before exposure to lead. These results can be explained in terms of the fact that following exhaustive exchange with a sodium solution there would be (1) an improved accessibility of the exchange sites to the large, hydrated heavy metal due to the removal of soluble and other extraneous impurities; and (2) a substantial removal of other competing ions.

The first point is demonstrated by the fact that the isotherm points for the exchange in F.EX.CLI fit the curve more closely. When one weighs out a sample of NAT.CLI it has to be appreciated that this sample contains varying amounts of extra-zeolitic material, so that on subsequent derivation of the crystal phase this will be reflected in a scatter of isotherm points. On extensive treatment with sodium solution one will have removed a large amount of the soluble impurities, and also decanted off impurities which are less dense than clinoptilolite and which float (see Loizidou 1983).

The second point, above, explains the difference in selectivities between the two forms of the clinoptilolite, and can be interpreted in terms of Eisenman's (1962) simple model for ion specificity. Since the silica:alumina ratio in clinoptilolite is relatively high, and the volumetric capacity is correspondingly low, the anionic field within the zeolite structure is relatively weak, and the electrostatic contributions are not expected to be as important as hydration effects. The metals with the largest free energy of hydration should therefore prefer to remain in the solution phase where their hydration requirements are better satisfied. According to hydration energies (Rosseinsky 1965) the selectivity series, for the ions of interest in clinoptilolite, should be $Pb^{2+} > K^{+} > Na^{+}$, and indeed the selectivity of this zeolite for potassium is well known (Ames 1960). Thus, it is more difficult for lead to replace potassium in clinoptilolite than it is to replace sodium, and the mixed sodium/potassium natural form exhibits a lower selectivity for lead. These observations are illustrated by other studies of lead exchange in clinoptilolite. For instance, Chelishchev and his co-workers (1974) obtained a highly sigmoidal isotherm for lead exchange in their mixed sodium/potassium/calcium natural form, whereas other workers have obtained rectangular isotherms for the same exchange in "homoionic" forms (Semmens and Seyfarth 1978; Loizidou 1983). Loizidou (1983) is the only study in which a maximum exchange level of less than 100% was observed (80%), however this was considered to be the result of the reported exchange capacity (2.188 mol kg^{-1}) and the comment was made that by using the exchange capacity (1.80 mol kg^{-1}) reported by Semmens and Seyfarth (1978) the maximum level of exchange was similar.

In comparison to previous studies in which lead overexchange has been observed, the final solution cation concentrations were relatively constant, except where overexchange occurred. Crystal phase cation recoveries for exchanges involving NAT.CLI were constant, and generally lower than those involving F.EX.CLI, which is not unexpected considering previous comments on the relative quantities of impurities. However, there was no particular trend in cation recoveries, and only after treatment with a sufficient concentration of lead was overexchange clearly observed.

The intracrystalline environment of clinoptilolite is less alkaline than that encountered in zeolites A, X and Y and as such precipitation is clearly less likely. However, the results obtained confirm the possibility of lead precipitation in clinoptilolite, which has been noted before (Semmens and Seyfarth 1978), and other natural zeolites (Barrer and Hinds 1953).

Although the situation is more complicated in natural zeolites, in essence the exchange systems can be regarded as consisting of lead exchange for sodium in F.EX.CLI, and since lead uptake by NAT.CLI almost exactly equalled sodium and potassium released this system was regarded as essentially binary (see previous section). In the former case it has been shown (section 6.3.1.2) that for Pb^{2+}/Na^{+} exchange dielectric theory predicts a positive value for ΔG^{θ}. In the latter case the system is no different since where lead exchanges for potassium in the crystal $r_{Pb} < 2r_{K}$ and once again a positive value for ΔG^{θ} is predicted. It was also shown that if the same exchange reaction is observed in two zeolites of differing framework charge then ΔG^{θ} should be more positive for the zeolite of lower framework charge (Fletcher and Townsend

1981(a)). The framework charge density is obviously lower than that in zeolite Y, so the affinity sequence presented in equation 6.16 can be once again extended to include clinoptilolite:

$$\text{zeolite A} > 1 > 2 > 3 > 4 > 5 > \text{clinoptilolite} \qquad 6.17$$

Values for the Γ function of equation 6.13 are similar for Pb^{2+}/Na^{+} exchange in all these zeolites, thus the ΔG^{θ} values must follow a trend in qualitative agreement with the α values. It is clear from figures 5.18(b) and 5.29, and their respective data presented in tables 5.38 and 5.43 that the α values for clinoptilolite are lower than for all other zeolites, so one would expect the ΔG^{θ} value to be more positive for clinoptilolite, which is in accord with dielectric theory.

Since Γ varies from 1.875 to 2.023 across the isotherm and values for α and the ratio $(m_B/\bar{E}_B)$ are usually greater than one, equation 6.13 provides a value for ΔG^{θ} for lead exchange in clinoptilolite which is negative. This is yet another example to show that dielectric theory has a limited utility in estimating selectivity trends in zeolites of different framework charge (Fletcher and Townsend 1981(a)).

6.3.4 Concluding Remarks on Ion Exchange of Lead (II) Ions in Zeolites

A study of the selectivity of a variety of zeolites of varying silica:alumina ratios for Pb^{2+} ions in the presence of different counterions was carried out. Precipitiation of lead in all the zeolites was a serious problem, contrary to indications in some of the literature reports (Hertzenberg and Sherry 1980; Cook, Cilley, Savitsky and Wiers 1982; Wiers, Grosse and Cilley 1982). This

non-stoichiometric exchange precludes rigorous thermodynamic treatment of the data, and simple dieletric theory was shown to have serious limitations. Sherry's (1969) extension of the simple model of Eisenman (1962) can account for the ion exchange behaviour of all the systems studied.

6.4 ORGANOLEAD ION EXCHANGE IN ZEOLITES

6.4.1 Rationale for Studies in Zeolites X and Y

Considering the size of an ion such as Me_3Pb^+ it was thought that the most open zeolites, the faujasites, might be capable of accepting such an ion. These zeolites are relatively cheap, readily available and have been shown to have a high selectivity for inorganic lead ions. Although the same might be true of zeolite A, one might expect this zeolite to be more susceptible to decomposition and hence studies on the adsorption of the organolead species were concentrated on the faujasites.

The studies on the equilibrium selectivity characteristics of the ternary exchange system $PbR_3^+/Pb^{2+}/Na^+$ were initiated by concentrating on the PbR_3^+/Na^+ binary system in NaX and NaY in order to clarify the influences that silica:alumina ratio, ion size and shape may have on the exchange properties of these zeolites. The effects of changes in sodium chloride content on the selectivity of the zeolites for PbR_3^+ was of particular interest because of the nature of effluents currently obtained.

6.4.2 Alkyllead Analyses

6.4.2.1 Analysis of Me_3Pb^+ solutions by atomic adsorption spectrophotometry

Originally it was thought that it may be possible to analyse for suitable concentrations of Me_3Pb^+ by atomic adsorption using inorganic lead standards, followed by the application of a correction for the difference in weights of the cations:

$$(Me_3Pb^+)/ppm = (Me_3Pb^+) \text{ as ppm } Pb^{2+} \times \text{Correction factor} \quad 6.18$$

where

$$\text{Correction factor} = (\text{Weight of } Me_3Pb^+/\text{Weight of } Pb^{2+})$$

It can be seen from table 5.44 that the Me_3Pb^+ standard solutions produced adsorption readings for Pb^{2+} such that, following correction for the difference in cationic weights, the derived apparent concentrations were approximately 24-28% lower than their supposed concentrations, the discrepancy increasing as the concentration decreased. It was thought (Hodges 1984) that the manner in which Me_3Pb^+ cations enter and behave in the flame is such that not all the lead species are detected, and a lower reading for the concentration of Me_3Pb^+ is recorded than is actually present. The alternative suggestion, obviously, was that the Me_3Pb^+ standards were prepared incorrectly. To study this possibility three solutions, each containing a supposed 10ppm Me_3Pb^+, were prepared from the same stock solution as the previous standards. Before final dilution the stock solution was treated as follows: (1) No pretreatment of stock solution; (2) 5ml 1:1 HNO_3 added; and (3) 5 ml 1:1 HNO_3 added and warmed for 15 minutes.

Analyses of these solutions, carried out as previous, showed that treatment with acid and subsequently heat serves to break down the Me_3Pb^+ cation producing Pb^{2+} ion (Table 5.45). The supposed 10 ppm Me_3Pb^+ standard was shown to contain 9.705 ppm Me_3Pb^+ following acid and limited heat treatment; indeed extended pretreatment may have decreased the discrepancy still further. Thus, these results would seem to confirm the ideas of Hodges (1984).

The choice for analysis of Me_3Pb^+ by atomic absorption then is either to use Me_3Pb^+ standards directly, or to suitably pretreat the solutions as described above and then use inorganic lead standards. It is obvious that acid dissolution of the crystal phase leads to the conversion of Me_3Pb^+ ions to Pb^{2+} ions and thus analysis involves an inorganic lead calibration (see section 4.6.5.4). However, acid/heat pretreatment and subsequent dilution of the solution phases of large numbers of samples would prove unnecessarily time consuming when it is so much easier to carry out a calibration using a suitable range of Me_3Pb^+ standards.

Background interference was a problem when sufficiently high concentrations of sodium were found in solution (i.e. $E_{Pb} \rightarrow 0$). This is illustrated in table 5.46 where it can be seen that in a background of 0.1 mol dm^{-3} sodium chloride, the absorption signal was increased by up to 20%, and once again the effect was greatest at lower concentrations (Me_3Pb^+ determination was by inorganic lead calibration followed by correction for difference in cationic weights as in equation 6.18). On examining the absorption signal for a series of solutions containing 5 ppm Me_3Pb^+ in backgrounds of varying sodium content (Table 5.47), it was apparent that at

concentrations of 10^{-2} mol dm^{-3} and above the lead signal was increased. Thus a series of standards were prepared containing varying concentrations of sodium (i.e. 0, 10^{-3}, 5×10^{-3} and 10^{-2} mol dm^{-3}). Having analysed the solution phase for sodium the set of standards containing the most appropriate concentrations of sodium was used to provide an accurate determination of the Me_3Pb^+ content of that particular solution.

6.4.2.2 Polarographic analysis of the alkyllead species

The determination of Me_3Pb^+ at concentrations of less than 1 ppm was carried out by the differential pulse anodic stripping voltametric (D.P.A.S.V.) procedure laid down by Associated Octel (see section 4.7.3). However, a series of experiments were carried out to determine the optimum conditions necessary for the analysis in this particular context, and are summarised below.

6.4.2.2.1 Dimethyllead analysis

When analytical runs were carried out on both standard Me_3Pb^+ solutions and equilibrium solutions using a deposition potential set at -0.70V, no measurable levels of Me_2Pb^{2+} were found. Subsequently, it was decided to analyse for Me_3Pb^+ directly, with the deposition potential initially set at -1.0V, and to regularly check for Me_2Pb^{2+}, if only to ensure the absence of this ion from the exchange systems studied.

6.4.2.2.2 Trimethyllead analysis

Typically the (D.P.A.S.V.) analytical cycle (section 4.7.3) consists of four stages:

(1) Purge - the solution is purged with nitrogen and simultaneously stirred.

(2) Deposition - at a deposition potential of -1.0V Me_3Pb^+ ions are deposited in a mercury film at the glassy carbon anode while the solution is magnetically stirred.

(3) Equilibrium - the solution is allowed to settle before the stripping stage.

(4) Scan - stripping of Pb^{2+} back into solution (Hodges and Noden 1979).

Only in the initial purge stage is nitrogen fed directly into the solution. In the latter three stages nitrogen is fed into the top of the cell to act as a blanket, preventing the absorption of O_2 into the solution.

In the original procedure (section 4.7.3) an initial purge time of 4 minutes was used to de-aerate the solution. However by repeatedly purging for 4 minutes then carrying out single blank determinations, it was found that up to 12 minutes initial purge was required to obtain a steady baseline. It was revealed (Hodges 1984) that the procedure in section 4.7.3 has now been modified so that 3 scans on the blank solution are now carried out prior to sample analysis. This revised procedure presumably provides the necessary purge time to obtain a steady baseline.

Providing that a very small lead peak at -0.52V is obtained for the blank determination, and that it remains the same and comparatively negligible during the analysis, its subsequent subtraction from Me_3Pb^+ peaks can be disregarded.

After an initial nitrogen purge of approximately 12 minutes, a standard calibration, according to the procedure in section 4.7.3, would entail a standard addition followed by resetting the purge time to 1 minute. Subsequently, three analytical cycles would run successively on this addition, in which there would be a 1 minute nitrogen purge before the first cycle and automatic 30 second purges before the second and third cycles. It can be seen from table 5.48 and figure 5.30 that for each addition the height of the peak for a particular standard addition increased in successive scans, and that there was a disproportionate increase in peak height for successive standard additions of 20 ppb Me_3Pb^+ producing a non-linear calibration (Figure 5.32: curve 1). Although readings for a particular peak may be acceptable within experimental error, when one requires a more accurate determination one must attempt to improve a particular analytical technique where possible.

It was discovered that by increasing the purge time to 2 minutes, following a standard addition, and manually starting successive cycles on a particular addition (so that before each scan the solution will have been de-aerated for 2 minutes), it was possible to obtain nearly reproducible successive peak heights (Table 5.49 and Figure 5.31). However, the non-linear calibration remained (Figure 5.32: curve 2).

Replicate successive peak heights indicate that in the original procedure (section 4.73) oxygen must have been leaking into the cell system during those times when nitrogen is used merely as a blanket, and that purge times of 30 seconds between scans were insufficient to remove all the oxygen present in the system.

Thus, an increase in a particular peak height may be due to an increase in background signal. This idea would not account for a non-linear calibration however, and a feasible explanation for this observation has been discussed recently (Hodges 1984). It was suggested that as one carries out a number of repeat scans, producing a film of mercury of increasing thickness containing ever increasing quantities of Me_3Pb^+, the Hg : Me_3Pb^+ ratio in the film is altered in such a way that proportionally more Pb^{2+} is stripped into solution producing a non-linear calibration.

The current procedure, in practice at Associated Octel (Hodges 1984), of initially carrying out 3 runs on a blank solution may serve a dual purpose, not only of eliminating oxygen from the cell to provide a steady baseline, but also to provide a film of mercury more suitable for a standard calibration or sample determination.

When constructing a calibration consisting of 20 ppb standard additions the most suitable sensitivity setting for the instrument was found to be a current of 5μA full scale deflection, as shown in figure 5.30. It was observed that as a number of analyses were carried out over the day the sensitivity of the instrument appeared to decrease from one analysis to the next (columns 1A-1C in Table 5.50 and figure 5.33). The possibility that this was due to the concentrated standard (100 ppm Me_3Pb^+) "going off" (i.e. the conversion of Me_3Pb^+ to some other ionic lead species), was discounted when the following day a virtually identical calibration (2A) to the first (1A) was prepared (Table 5.50).

Invariably, as discussed above, the sensitivity of the instrument was observed to decrease over the day. On several occasions,

however, a large increase in sensitivity would occur for one particular analysis (column 3B in Table 5.50) which would necessitate a reduction of the sensitivity setting. It can be seen from columns 3A-3D in table 5.50 that the sensitivity would then return to that normally obtained. This phenomenon had not been observed elsewhere (Hodges 1984), but it was suggested that this may have been caused by a blockage of the hole in the vibrator/stirrer which may in turn affect the deposition of Me_3Pb^+ in the mercury film on the glassy carbon electrode. There was no evidence to support this idea, and further examination of this phenomenon may be necessary.

Although the sensitivity of the instrument appears to decrease over the day, sample analyses were not affected since the sample : standard peak height ratio remained the same. This was illustrated by the fact that samples of an equilibrium solution gave readings of 15.4 and 16 ppb (equivalent to 77 and 80 ppm in the original solutions respectively) in successive analyses. When one considers that one is adding such small quantities of sample and standard (10µl to 50 ml) by use of a micropipette, this is within experimental uncertainty.

Bearing these observations in mind, the D.P.A.S.V. procedure laid down by Associated Octel (Hodges 1984), for the analysis of Me_3Pb^+ (section 4.7.3) was altered appropriately for the particular requirements of this study, and was as follows:

Depending on the suspected level of Me_3Pb^+ in the sample one could calculate the required volume of sample to produce an adequate peak height for subsequent analytical determination (for example, for a solution containing a total of approximately 1ppm Me_3Pb^+ one

might add 1 ml to the cell, and this would produce a peak height equivalent to 20 ppb). The total volume of the cell was kept constant at 50 ml (microlitre standard additions are negligible) and since one should not alter the volumes of acetate buffer, mercuric chloride or CDTA solutions, the volume of electrolyte added initially was adjusted accordingly.

The electrolyte solution, acetate buffer, mercuric chloride solution and CDTA solution were measured into the cell. The deposition potential was set to -1.0V and the cell purged for approximately 12 minutes, after which the analysis cycle was allowed to run. This produced a blank determination with a peak at -0.52V. A suitable aliquot of sample was added to the cell, the purge time set to 2 minutes, and a single analysis cycle allowed to run. Without altering the instrument settings a further cycle was initiated which usually produced a virtually replicate peak height for the sample, but, if not, one more cycle proved to be sufficient. A suitable aliquot of Me_3Pb^+ standard was then added and single analyses run as previous.

From peak heights obtained for the sample and standard addition, the concentration of Me_3Pb^+ in the original sample could be obtained.

Regular checks for Me_2Pb^{2+} in samples were run by carrying out a deposition at -0.70V, prior to Me_3Pb^+ analysis (see section 4.7.3), and noting any increase in peak height at -0.52V above that of the blank.

6.4.2.3 Stability of trimethyllead ions

When the D.P.A.S.V. analysis was applied to waters of a low sodium chloride content it was apparent that trimethyllead was rather unstable (Hodges and Noden 1979). When replicate scans for dialkyllead were carried out on sample containing added trimethyllead, successive cycles using a reduction potential of -0.8v produced peaks of increasing heights. Investigation showed that this increase in peak height was related to the time which had elapsed after the addition of the mercuric chloride. It appeared that a metathetical reaction was taking place between trimethyllead and mercuric mercury:

$$Me_3Pb^+ + Hg^{2+} \rightarrow MeHg^+ + Me_2Pb^{2+} \qquad 6.19$$

As this effect had not been observed with sea water samples it was thought that a high chloride ion concentration may inhibit this metathetical reaction with the mercuric ion. Indeed it was shown that the "stability" of the trimethyllead was much improved by addition of sodium chloride.

It has been stated (Associated Octel 1981) that sodium chloride at a concentration of 3.5% (approximately 0.6N) is sufficient to obtain a significant shift in the equilibrium (equation 1.23) between the cation, R_3Pb^+, and the anionic complex, $(R_3PbCl_2)^-$ in favour of the latter. It can be argued that this conversion, which may be preferred compared to the metathesis reaction, could be the cause of the much slower reduction of Me_3Pb^+ to Me_2Pb^{2+} observed by Hodges and Noden (1981), rather than the so called "stabilising effect" of a high chloride concentration. Should such a situation exist in D.P.A.S.V. analysis one could not obtain

deposition of Me_3Pb^+ at the anode since the anionic complex would be formed in the high chloride (approximately 0.5N) background. However, D.P.A.S.V. has been shown to be a successful technique for analysis of alkyllead species (Hodges and Noden 1979) and is used on a daily basis.

The association of Me_3Pb^+ to a dichloro-anionic complex is of prime importance in the ion exchange system to be studied, since the effluent stream currently obtained contains low levels of Me_3Pb^+ in the presence of high concentrations of sodium chloride. The possibility of association of the trimethyl lead salt to form this complex could be studied by comparing the Me_3Pb^+/Na^+ ion exchange characteristics for solutions having a similar $Me_3Pb^+:Na^+$ ratio, but using anions of sodium of differing complexing ability, viz. sodium chloride, sodium nitrate and sodium perchlorate. On the assumption that such an association occurs in a high saline environment, $\bar{E}_{Me_3Pb}$ would be much lower in a chloride background compared to a similar exchange in a nitrate or perchlorate background, because as E_{Me_3Pb} decreases (and the concentration of chloride concurrently increases) less Me_3Pb^+ would be available for cationic exchange with the zeolite. Table 5.51 shows that there was no significant difference between similar exchanges for the same zeolite in the three systems studied, and significant complex formation could be discounted at this concentration.

It was noted that the total solution normalities after exchange were greater than the apparent initial solution concentration (T_N = 0.01g equiv. dm^{-3}) and that recoveries increased as $E_{Me_3Pb} \rightarrow 1$ (Appendix 3 : Tables 1 and 2). This increase in final solution concentrations agreed with similar decreases in cation recoveries from the crystal phase. Such observations indicated

hydronium exchange, and signified non-stoichiometric exchange of Me_3Pb^+ for Na^+ (i.e. rather than Na^+ ions being replaced in a 1 : 1 exchange with Me_3Pb^+ ions, H_3O^+ ions exchange for the majority of these Na^+ ions).

Three possibilities arose as to the cause of this non-stoichiometric exchange of Me_3Pb^+ for Na^+:

(1) the zeolites are non-selective for Me_3Pb^+ ion and it is difficiult for this ion to penetrate these zeolites

(2) association to form the dichloro-anionic complex in a high chloride background, and subsequently the reverse reaction continues, as the cation is removed from solution, until an equilibrium exists between the three species:

$$\begin{array}{ccc} E_{Me_3Pb^+} & \rightleftharpoons & E_{(Me_3PbCl_2)^-} \\ \Updownarrow & & \\ \bar{E}_{Me_3Pb^+} & & \end{array} \qquad 6.20$$

(3) some decomposition of the trimethyl lead salt in the crystal occurs

$$(CH_3)_3Pb^+ \rightleftharpoons Pb^{2+} + 3CH_3 \rightarrow \text{products} \qquad 6.21$$

and the inorganic lead remains in the crystal, so that the equilibrium is shifted, and the dissociation continues until an equilibrium between the two phases is reached:

$$E_{Me_3Pb^+} \rightleftharpoons \bar{E}_{Me_3Pb^+} + \bar{E}_{Pb} + \text{organic products} \qquad 6.22$$

All these possibilities may involve slow processes, and therefore it was thought that a one week exchange may be insufficient to attain full equilibrium. Exchanges with the chloride and nitrate anionic systems, carried out for up to 2 weeks (Table 5.52),

showed that there was no significant difference between similar exchanges for the same zeolite, so a one week exchange must be adequate. It is also noteworthy that recoveries for the 2 week exchanges were approximately the same as those over a 1 week period which signifies that no further hydronium exchange had occurred.

Scheme 2, above, was thought to be highly unlikely considering that similar recoveries were observed for exchanges involving the various anions of sodium over a week (Table 5.51), but a comparison of the nitrate and chloride systems studied here ruled out any longer-term association effects.

Infra-red analysis of Me_3Pb^+ exchanged forms of zeolites X and Y (section 4.2.3) failed to reveal the presence of an organolead species. However, this test was limited because organolead salts are thermally unstable (Shapiro and Frey 1968), which meant that the Me_3Pb^+ exchanged forms were dried at temperatures no greater than 30°C. Considering the zeolites' natural affinity for water it is not surprising that this procedure proved inconclusive. The broad band characteristic of hydrogen bonded OH^- at about 3400 cm^{-1} (Breck 1973(o)) would obscure the aliphatic carbon-hydrogen stretching frequency at about 2900 cm^{-1} which would result from the presence of an organic species. In addition, the presence of a lead-carbon asymmetric stretch at 493 cm^{-1} (Shapiro and Frey 1968) was not obvious and, if present, was probably obscured by the T-O bending mode at 420-500 cm^{-1} (Breck 1973(o)).

To determine which lead species had exchanged into the zeolite, a sample of zeolite Z1(II) which had been exchanged with 0.01N

Me_3PbCl solution was washed briefly with water, and re-exchanged with 0.01N NaCl solution. The solution and zeolite were separated, and the solution analysed for inorganic lead by D.P.A.S.V. using the silver/silver chloride electrode system (section 4.7.2), and for Me_3Pb^+ using the glassy carbon electrode system (section 6.4.2.2.2). 14.2 ppm of Me_3Pb^+ were determined in the solution whereas only 260 ppb Pb^{2+} were present. This proportion of Pb^{2+} is the quantity of $PbCl_2$ impurity one may expect to find in the original Me_3PbCl solid material as synthesized by Associated Octel. This result establishes the fact that the Me_3Pb^+ ion is exchanged into the zeolite.

Using atomic absorption spectrophotometry with Me_3Pb^+ standards (section 6.4.2.1), the concentration of Me_3Pb^+ in this same solution was determined as 14.5 ppm, which is in very good agreement with the analysis above, especially considering the dilution errors involved in D.P.A.S.V. analysis (one is adding microlitre quantities by means of a micropipiette). This confirms that D.P.A.S.V. analysis for the determination of Me_3Pb^+ is a more than satisfactory technique in this context.

6.4.3 Me_3Pb^+ Ion Exchange in Zeolites X and Y

The Me_3Pb^+/Na^+ isotherms for exchanges in zeolites X and Y are highly rectangular, and show a strong preference for sodium (Figures 5.34 and 5.35). The experimental selectivities for Me_3Pb^+ ions over Na^+ ions, quantified using the separation factor, α(Table 5.53 and Figure 5.36), emphasise this preference for sodium. Although there are quite a large scatter of data points (possibly due to losses following multiple exchanges) it can be seen from figure 5.36 that generally as the loading of sodium

decreases the selectivity for Me_3Pb^+ increases in NaX, and conversely decreases in NaY, but the zeolites are still highly selective for Na^+ compared to Me_3Pb^+. The selectivity for sodium is such that following a single exchange of 0.3g of zeolite with 50ml 0.01N Me_3Pb^+ solution only about 10% of sodium ions had been replaced in both zeolites. When the zeolite : solution ratio was increased to 0.1g in 250 ml 0.01N Me_3Pb^+ solution approximately 35% of sodium ions were replaced, but to attain greater loadings multiple exchanges were necessary.

Table 6.1 Estimated dimensions ($\AA$) of alkyllead ions

Ion	Shape	Length	Height	Breadth	Volume ($\AA^3$)
$(CH_3)_3Pb^+$	Trigonal planar	5.22	4.52	2.19	25.84
$(CH_3)_2Pb^{2+}$	Linear	6.03	2.19	2.53	16.71

Infra-red spectra of trimethyllead compounds suggested that the cation probably has a planar configuration (Okawara and Sato 1961), thus the dimensions of the trigonal planar structure (Table 6.1) could be estimated from measurements in the literature (Wong and Schomaker 1958; Pauling 1967) and the application of simple geometry. Theng and his co-workers (1968) commented that in exchanges involving large ingoing ions the extent of exchange may be limited by the available intracrystalline space of the faujasites. The volume of the Me_3Pb^+ ion (Table 6.1) is such that 100% exchange in the available space of the large cavities (Barrer and Sutherland 1956; Yates 1966) is possible, but its size

precludes entry into the cuboctahedra. Whereas Theng and his co-workers (1968) showed that the maximum extent of exchange obtained was generally less than would be expected from a consideration of the space requirements alone, results here indicate that replacement of sodium ions in the cuboctahedra has occurred. Two ideas arose to explain such an observation:

(1) A decomposition reaction, similar to that proposed in scheme (3) - section 6.4.2.3, exists and inorganic lead is able to pass through the 2.5Å windows and exchange for sodium ions in the cuboctahedra.

(2) The alkyllead halides are unstable and tend to decompose slowly at room temperature, and simple thermal disproportionation of Me_3Pb^+ ion to form the Me_2Pb^{2+} ion is possible (Shapiro and Frey 1968):

$$2Me_3PbCl \rightleftharpoons Me_2PbCl_2 + Me_4Pb \qquad 6.23$$

The dimethyllead ion has been shown to be linear (Cotton and Wilkinson 1972) and the estimated dimensions of the ion (Table 6.1) are such that it is possible for this divalent ion to exchange for sodium within the cuboctahedra. Thus, decomposition of the trimethyllead salt could occur in the crystal, and the dimethyllead ion then exchange into the cuboctahedra of the faujasites, so that the equilibrium is shifted and the dissocation continues until an equilibrium is attained:

$$E_{Me_3Pb^+} \rightleftharpoons \bar{E}_{Me_3Pb^{2+}} + \bar{E}_{Me_2Pb^{2+}} \qquad 6.24$$

In the reversibility test carried out previously (section 6.4.2.3) no check for Me_2Pb^{2+} ions was carried out, and since further

oxidation beyond Me_2Pb^{2+} is difficult (Associated Octel 1981) this scheme may be more feasible than that above (equation 6.22).

The difference in maximum exchange levels attained can be accounted for in terms of the proportion of sodium ions in the smaller cages of the faujasites (18% and 33% for zeolites X and Y respectively), together with the increased difficulty for a large cation (be it Pb^{2+} or Me_2Pb^{2+}) to pass through the interconnecting windows between the supercages and the sodalite cages in zeolite Y compared to X, due to lattice contraction when SiO_2 isomorphously replaces AlO_2^- in the framework (Sherry 1966).

The final solution normalities were greater than the initial solution concentration (T_N = 0.01g equiv. dm^{-3}) and relatively constant (Tables 5 and 6: Appendix 3) contrary to observations made previously (section 6.4.2.3). There were shortages in crystal phase cation recoveries in all exchanges, and recoveries decreased as $\bar{E}_{Me_3Pb}$ increases (Figure 5.37). These observations indicate non-stoichiometric exchange of Me_3Pb^+ for Na^+, but the replacement of Na^+ by hydronium ions (H_3O^+). One would expect the effect to be greater in the more aluminous zeolite and figure 5.37 shows this to be the case. The level of hydronium exchange also depends on the ratio of weight of zeolite to volume of solution (section 6.5.1), and when the weight : volume ratio was decreased from 0.3g in 50ml to 0.1g in 250ml the recoveries decreases from 80% to 50% and 70% for zeolites X and Y respectively. Loss of finely suspended zeolite particles during multiple exchanges is inevitable and this was reflected by the fact that crystal phase recoveries decreased as the number of exchanges increased, to 15% and 35% for zeolites X and Y respectively.

Since the relationship between $\bar{\varepsilon}$ and ε (the macro permittivities of the zeolite and the solution phases respectively) is $\bar{\varepsilon} < \varepsilon$ (Barrer, Rees and Shamuzzoha 1966) and $r_{Me_3Pb} > r_{Na}$ simple dielectric theory predicts (equation 6.7) that the standard free energy change for the Me_3Pb^+/Na^+ exchange reaction should be negative for all zeolites. In addition it has been shown (Fletcher and Townsend 1981(a)) that simple dielectric theory also implies ΔG^θ should be more negative for the zeolite of lower framework charge (equation 6.8). On the basis of framework charge densities presented in table 5.31 therefore, according to simple dielectric theory, zeolite Y should have a greater affinity for the Me_3Pb^+ ion than zeolite X.

The contribution of the last integral in equation 6.13 may increase the selectivity trend shown in the α values (Table 5.53 and Figure 5.36), and since the value of the first integral is the same and constant for exchanges in both zeolites, then the ΔG^θ values must follow a trend in qualitative agreement with the values. Although there is a scatter of data, it can be seen from figure 5.36 that the observed selectivity trends do not agree with the affinity trends produced using dielectric theory (i.e. zeolite Y > X).

The activity coefficient ratio (Γ) is constant throughout the isotherm, since one is dealing with a uni-univalent exchange, but its value is indeterminable because there are no data available for the mean molal stoichiometric activity coefficients of Me_3PbCl. The α values are $<<1$ (Table 5.52) and the same is true for the ratio $(m_{Na}/\bar{E}_{Na})$ given in equations 6.12 and 6.13. From

the shape of the isotherms (Figures 5.34 and 5.35) one would surmise that by taking equation 6.13 as a whole the measured ΔG^{θ} values for both systems must be strongly positive.

Theng and his co-workers (1968) showed there to be a good linear relationship between polarisability and the molecular weight of their respective alkylammonium ions (viz. the polarisabilities of the alkylammonium ions were greater than the NH_4^+ ion, and that polarisability increases with increasing molecular weight). Thus one might expect the polarisability of the Me_3Pb^+ ion to be similarly greater than that of the respective Pb^{2+} ion. Once more, the assumption that the macropermittivity, $\bar{\varepsilon}$, for a given zeolite, hardly charges when different ions are exchanged has been shown to be dubious if the exchanging ion is highly polarisable (Fletcher and Townsend 1981(a)).

6.4.3.1 Removal of low trimethyllead levels from high salt backgrounds

In the real effluent stream system one would be dealing with low levels of Me_3Pb^+ in the presence of high concentrations of sodium chloride, so an investigation of the isotherms studied previously (section 6.4.3) as $E_{Me_3Pb} \longrightarrow 0$ was necessary. Subsequently, the removal of similar Me_3Pb^+ levels from a background of 0.1N NaCl was carried out to note the effect, if any, of changes in the sodium chloride content on the selectivity of these zeolites for Me_3Pb^+. This is of particular interest because of the nature of effluents currently obtained.

Examinations were carried out using zeolite X (NaZ1(II)), since this appeared to be the more selective of the two zeolites studied previously (section 6.4.3).

The concentration of Me_3Pb^+ in several exchange and equilibrium solutions was initially measured by D.P.A.S.V. (section 6.4.2.2.2), but the selectivity for Na^+ over Me_3Pb^+ exhibited by zeolite X is such that very little Me_3Pb^+ was removed from solution, and so any difference between the solution phases before and after exchange was difficult to determine by measuring peak heights "by eye". Since it was established that very little Me_3Pb^+ was removed, analysis of the solutions by atomic absorption spectrophotometry (section 6.4.2.1) was thought to provide equally adequate information to D.P.A.S.V. and is a much more rapid technique.

Dissolution of the zeolite phase in 1:1 HNO_3 converts any organolead into the inorganic species. Thus, the concentration of Me_3Pb^+ in the crystal phase required D.P.A.S.V. analysis for Pb^{2+} (section 4.7.2) and subsequent correction for difference in the cationic weights (section 6.4.2.1).

It is obvious from tables 5.54 and 5.55 that there was poor agreement between the expected concentration of Me_3Pb^+ in the crystal phase, and that which was measured. The problem lies in the fact that very little Me_3Pb^+ is removed from solution (column 4 : tables 5.54 and 5.55), so there is little difference between the solutions before and after exchange. Atomic absorption spectrophotometry is not sufficiently sensitive to detect such small differences, and attempts to use D.P.A.S.V. proved equally inadequate (see previous comments). A difference

in absorption readings between the exchange and equilibrium solutions of only one or two absorption units (which may be due to "baseline drift" of the spectrophotometer) can have a significant effect on the apparent amount of Me_3Pb^+ removed, and this difference is further exaggerated by dilution factors.

Rather than attempt to measure the difference between exchange and equilibrium solutions, it seems more realistic to determine the actual amount removed derived from the measured concentration of Me_3Pb^+ in the crystal phase. Tables 5.56 and 5.57 show the very low levels of Me_3Pb^+ that are removed from solution (such levels involve the use of less than 0.02% of the exchange capacity of this zeolite i.e. 4.67 mol kg^{-1}), but it is only when one compares the relative proportion of Me_3Pb^+ removed that an interesting trend becomes apparent. As the concentration of Me_3Pb^+ in the solution phase decreases from 100 to 20 ppm the proportion of Me_3Pb^+ removed decreases, but thereafter the proportion of this ion removed increases, the effect being greater in the lower salt background (Tables 5.56 and 5.57, and Figure 5.38). If a sufficient concentration of ion is available to occupy all availables sites on the surface of the crystal and approximately the same weight of zeolite is used in each exchange system then the quantity of ion removed for surface adsorption alone (i.e. no entry of ion into the crystal) should be approximately the same. In such a case the proportion of ion removed would naturally increase as the concentration of ion originally in solution decreases, and this was observed as the concentration of the Me_3Pb^+ ion decreases from about 20 ppm down to 1 ppm. On increasing the concentration of Me_3Pb^+ ion above 20 ppm the

proportion removed increased and presumably this reflects entry of the Me_3Pb^+ ion into the crystal itself.

It is apparent that for the majority of comparable exchanges there is very little difference between the proportion of Me_3Pb^+ ion removed, although it was slightly greater in the higher salt background. However, for the lowest Me_3Pb^+ levels there was a change in this trend (significantly so in the case of approximately 1 ppm Me_3Pb^+ ion). It is difficult to explain this anomalous behaviour, apart from the possibility of insufficient washing of the zeolite phase prior to analysis, and this anomaly needs to be confirmed by further examination.

6.4.4 Me_3Pb^+ Ion Exchange in Natural and Acid Treated Clinoptilolite

It has been shown for clinoptilolite (section 6.3.3.1) that it is difficult to decompose this highly siliceous zeolite. The determination of crystal phase composition by acid dissolution gave inconsistent cation recoveries and results that were in poor agreement with those derived from the initial crystal composition and analyses of the solution phases before and after exchange. It was decided therefore, that the only way to obtain meaningful results was to use the difference technique. Thus, determination of the crystal phase composition for exchanges involving Me_3Pb^+ in clinoptilolite used this same procedure (section 6.3.3.1).

From the estimated size of the Me_3Pb^+ ion (Table 6.1) it was thought that this ion could enter the clinoptilolite crystal. It has been shown that alkylammonium ions of similar and greater dimensions to the Me_3Pb^+ cation attain up to 100% exchange in

clinoptilolite (Barrer, Papadopoulos and Rees 1967), their entry into both the wider and narrower channels being facilitated by some distortion of windows and of ions (Barrer 1959).

From Table 5.58 it appears that there is some uptake of this ion by clinoptilolite, but the relatively small amount is evidence of the poor selectivity for Me_3Pb^+ exhibited by this zeolite. It has been shown previously (section 6.4.3.1) that it is almost impossible to determine the composition of the crystal phase accurately, by determination of the difference between exchange and equilibrium solutions, when there is very little removal of the entering ion. Although atomic absorption spectrophotometric analysis of exchange and equilibrium solutions were carried out simultaneously so that conditions were identical, it can be seen from table 5.59 that the uptake of this ion was based on small differences in absorption readings (which may be due to "baseline drift" of the spectrophotometer) and that these small differences can be grossly exaggerated by dilution factors. It is therefore very difficult to state with any certainty the degree of exchange attained, but it is apparent that there is little improvement, if any, in the selectivity of the clinoptilolite by producing more siliceous (partly dealmuminated) forms (Table 5.58). The data were not presented as an isotherm because the data are so scattered that there are no real trends to be seen.

As previously noted (section 6.3.3.1), in exchanges involving NAT.CLI, the presence of Ca^{2+} and Mg^{2+} ions in solution was once again identified and measured, but the concentrations of these ions were not significant in derivation of the equivalent fraction of Me_3Pb^+ in the solution and crystal phases.

As one might expect, crystal phase cation recoveries of the natural form were appreciably lower (approximately 80%) than the exchange capacity (based on aluminium content) of the zeolite (Appendix 3 : Table 11), but it is noticeable that recoveries were much lower than similar exchanges involving the Pb^{2+} ion (Appendix 2 : Table 16). When one also takes into account that the final solution concentrations (Appendix 3 : Table 10) were up to 13% greater than the initial total normalities (Appendix 3 : Table 9) it can be assumed that these observations are due to Na^{+} and K^{+} ions being replaced partly by hydronium ions (K^{+} ion content hardly changes compared to the Na^{+} ion content because of the relative selectivity of clinoptilolite for these ions).

Ca^{2+}, Mg^{2+} and K^{+} ions were not detected in equilibrium solutions of those exchanges involving 2N CLI and 4N CLI. In the case of Ca^{2+} ions this was to be expected since the CaO content of the acid-treated forms was not measurable by X.R.F. (Table 5.3). The quantity of K_2O present in 2N CLI has been inferred to represent the clay component of the zeolitic material (section 6.3.3.1) and as such was not available for exchange. Presumably this also applies to the MgO component which may be present, together with potassium, in a clay such as montmorillonite (see section 6.1.3.2).

In exchanges involving solutions 1 to 4 with 2N CLI, and solutions 1 to 3 with 4N CLI, the concentration of sodium in the equilibrium solutions was less than in the exchange solutions (Appendix 3 : Tables 9 and 10). On comparing the total number of equivalents in the crystal phase (Appendix 3 : Table 11) with the original Na_2O content of the zeolites (1.023 and 0.984 meq g^{-1} for 2NCLI and 4N

CLI respectively) it can be seen that there is an increase in the total number of measurable ions. These observations are indicative of the overall movement of Na^+ ions from the solution to the zeolite phase in exchange for hydronium ions. Final solution concentrations were lower than the initial total normalities (Appendix 3 : Tables 9 and 10), and reflect the presence of these non-measurable hydronium ions in the solution phase.

As the concentration of Me_3Pb^+ in the solution increases (solutions 5 to 7 with 2N CLI and solutions 4 to 7 with 4N CLI) the overall reaction was ternary, involving the replacement of Na^+ and H_3O^+ ions by Me_3Pb^+ ions, so once more non-measurable H_3O^+ ions would account for the decrease in the total normalities of these solutions (Appendix 3 : Tables 9 and 10).

The crystal phase cation recoveries for exchanges involving 2N CLI and 4N CLI were some 20% lower than similar exchanges involving NAT CLI (Appendix 3 : Table 11) which can be construed as being due to non-measurable H_3O^+ ions in the zeolite phase.

6.4.5 Concluding Remarks on Ion Exchange of Me_3Pb^+ in Zeolites

A study of the selectivity of a variety of zeolites of varying silica:alumina ratios for Me_3Pb^+ ions in the presence of Na^+ ions was carried out. Improvements in current analytical methods were a prerequisite, but subsequently proved inadequate when attempting to detect small differences between exchange and equilibrium solutions. Stability of the Me_3Pb^+ ion in solution was assured, and this ion was confirmed to be the lead species entering the zeolites, but exchange limits suggested a possible dissocation

within the zeolite. None of the zeolites studied were selective for the Me_3Pb^+ ion, and in the case of clinoptilolite very little, if any, uptake of this ion was observed. The deficiences of simple dielectric theory, when the exchanging ion is highly polarisable, were once again illustrated.

6.5 HYDRONIUM ION EXCHANGE IN ZEOLITES

6.5.1 Hydronium Ion Exchange of Zeolites in Water

The high-silica natural clinoptilolite samples showed a much reduced pH response, compared to the synthetic zeolites, when the rates and levels of hydronium exchange were investigated (Figures 5.39 and 5.40). The difference in pH changes between the unexchanged and "fully" exchanged forms of the two clinoptilolite samples studied is presumably a result of the different quantities of basic impurities (e.g. calcite), but the increase in pH observed for the acid treated samples must be a result of hydronium ion uptake (see concluding remarks section 6.5.2.2). The synthetic zeolites showed initial fast rises in pH, and within one minute the pH of the solution normally reached equilibrium. The initial rates of change in pH were seen to be inversely proportional to the silica : alumina ratio in the zeolite. In all cases (bar the "hydrophobic" clinoptilolite samples) the equilibrium pH was alkaline (Appendix 4 : Table 1) and becomes progressively higher the more aluminous the material.

The inverse correlation between the final solution pH and the framework silica : alumina ratio suggests that the response must be at least in part, an exchange process in which some of the

sodium ions initially in the zeolite are replaced by hydronium ions:

$$\overline{Na^+} + (H^+OH^-) \rightleftharpoons \overline{H^+} + Na^+ + OH^- \qquad 6.25$$

The observed rise in pH will obviously be in proportion to the number of exchangeable sodium ions in the zeolite, which in turn is of course inversely proportional to the framework silica : alumina ratio.

As would be expected when calcium zeolites are placed in water the pH changes are much smaller (calcium hydroxide being a weaker base than sodium hydroxide). The kinetics of exchange were also noteably slower in A than X, reflecting the large hydration shell of calcium compared to sodium, and the smaller channel size in A compared to X.

The initial rapid increase in hydroxyl ion concentration is accompanied by a rapid rise in the concentration of sodium ions, but whereas the sodium concentration continues to rise slowly the concentration of hydroxyl ions was found to level out and eventually fall again (Drummond, De Jonge and Rees 1983; Franklin 1984; Hart and Townsend 1984). The concentrations of Na^+ and OH^- ions differed considerably which suggests that the exchange mechanism involves more than a simple stoichiometric H_3O^+/Na^+ exchange.

The concentration of hydronium ions initially in solution is insufficient to account for the levels of sodium removed from these zeolites. Drummond, De Jonge and Rees (1983) proposed a tentative mechanism in which the process was autocatalytic with the release of hydronium ions back into solution, following

zeolite breakdown which resulted from the initial hydronium exchange. The released H_3O^+ ions continue the reaction. Their mechanism involved the release of aluminium and silicon into solution, though in what form (oxide/hydroxide) was not known. Cook and co-workers (1982) proposed an incongruent dissolution mechanism for NaA hydrolysis, that is initiated by proton exchange and is then followed by silicic acid release. Semmens (1981) observed that silicon and aluminium release from clinoptilolite was pronounced at the pH extrema (below pH3 and above 11), but that aluminium was preferentially leached.

Table 5.59 (column 2) shows there to be a release of aluminium ions into those solutions containing zeolites X and A, but not Y, and as one would expect the effect was greatest with the most aluminous zeolite.

The degree of hydronium exchange was found not only to be a function of the weight of zeolite to volume of solution ratio (viz. the level of sodium removed increases as the weight : volume ratio decreases), but was also found to be a function of dissolved carbon dioxide (viz. the level of sodium removed increases as the amount of dissolved carbon dioxide increases (Franklin 1984)). Thus a mechanism to explain the large levels of sodium removal observed in terms of a reaction involving atmospheric carbon dioxide is required.

The initial rapid increase in sodium and hydroxide concentration is the result of the simple exchange reaction proposed in equation 6.25. The hydronium ion concentration may be supplemented by carbon dioxide dissolved in solution:

$$CO_2(g) \rightleftharpoons CO_2\ (aq) \rightleftharpoons HCO_3^- + H^+ \qquad 6.26$$

As the pH of the solution increases due to the exchange reaction, the predominant reaction of carbon dioxide with solution becomes (Cotton and Wilkinson 1972):

$$CO_2(g) + OH^- \rightleftharpoons HCO_3^- \qquad 6.27$$

This bicarbonate ion is itself in equilibrium with the carbonate ion:

$$HCO_3^- \rightleftharpoons H^+ + CO_3^{2-} \qquad 6.28$$

Equations 6.27 and 6.28 result in a production of hydronium ions in the solution, which allows further hydronium exchange to occur. This explains why the hydroxide concentration falls while the sodium concentration continues to rise. It also explains why the levels of sodium removed are greater as the amount of dissolved carbon dioxide increases. This also explains why the pH of a solution in an open beaker drops back to about 7 within a few hours (Hart and Townsend 1984), while that contained in a sealed bottle (limited supply of carbon dioxide) remains high (Franklin 1984). Hart and Townsend (1984) confirmed a high concentration of bicarbonate/carbonate in solution after hydronium exchange in the presence of carbon dioxide, and that in a carbon dioxide free atmosphere the level of hydronium exchange is much reduced.

The analytical data (Table 5.5) show that cation deficient forms of the synthetic zeolites were used for this work (except in the case of CaA) which was due to hydronium exchange during preparation of the zeolites. However, the data also show that the sodium : aluminium ratio of NaA is 0.98:1 compared to that of

0.88:1 for NaZ1(I), and that on more careful preparation, a sample of zeolite X with a sodium : aluminium ratio of 0.99:1 (NaZ1(II)) was prepared. This suggests that the method of preparation of the zeolite also determines the degree of hydronium exchange (Drummond, De Jonge and Rees 1983; Franklin, O'Connor and Townsend 1984). Therefore the cation : aluminium ratio seems to depend upon the composition of the starting material before preparation, the method of preparation and the silica : alumina ratio of the zeolites.

6.5.2 Hydronium Ion Exchange of Zeolites in Salt Solutions

6.5.2.1 Hydronium ion exchange in inorganic lead exchange systems

It has been shown previously (section 6.3) that in general for exchanges involving Pb^{2+} ions there were shortages in crystal phase cation recoveries, especially in the region $E_B \longrightarrow E_{B(max)}$, and that the final solution concentrations were greater than the initial total normalities. As the concentration of lead in the crystal phase increased the crystal phase recoveries increased and the final solution concentrations decreased (Figures 5.20, 5.21 and 5.24). (The anomalous behaviour of NaZ2 cannot be explained in terms of experimental error. Although NaZ2 had a chemical composition which was entirely consistent with its being a low-silica Y material (Table 5.1), and the X-ray pattern confirmed the structure (Table 5.15), nevertheless this sample frequently exhibited anomalous behaviour. For other examples, see also the kinetic uptake behaviour shown in figure 5.7, and the kinetic pH responses in figure 5.42. This zeolite did show on chemical analysis a low Na : Al ratio, even in the original material (Table 5.1), and this may explain this anomolous behaviour). Examination

of hydronium ion exchange as a function of pH was therefore carried out by adding zeolites to exchange solutions and monitoring the pH changes.

In accord with the results obtained in distilled water (section 6.5.1) the high silica clinoptilolite samples show a much reduced kinetic pH response (Figure 5.41) compared to the synthetic zeolites. Indeed in 0.1N $Pb(NO_3)_2$ solution the pH change was insignificant over the first 5 minutes of contact (Appendix 4 : Table 3).

Figure 5.42 shows that in 0.1N $NaNO_3$ there was an initial positive pH jump, due to hydronium ion exchange with the zeolites, followed by a levelling off of the pH change as a result of the partial formation of the hydronium exchanged form of the zeolite. The behaviour is qualitatively similar to that observed in distilled water (section 6.5.1). The size of the initial jump decreased as the silica : alumina ratio increased, which is accounted for in terms of the sodium : aluminium ratios of the analysed zeolites generally increasing in the same direction.

When calcium zeolites were added to 0.1N $Ca(NO_3)_2$ solutions (Figure 5.43), as would be expected with the weaker base, the pH changes are much smaller when calcium replaces sodium, and the kinetics of exchange are slower in A than X (see section 6.5.1).

While one assumes that inevitable losses of some finely suspended zeolite particles during separation and analysis of the crystal phase must account in part for the shortages in total exchange cation recoveries, these losses never amounted to more than approximately 2%, as proved by total aluminium analyses.

Therefore, hydronium exchange must account primarily for the significantly low recoveries in the region $\bar{E}_B \rightarrow \bar{E}_{B(max)}$. However, there does not appear to be a significant increase in percentage recovery as the silica : alumina ratio increases; indeed, it is often for exchanges with zeolite 5 that some of the lowest recoveries occurred (Figure 5.21).

When zeolites were immersed in 0.1N $Pb(NO_3)_2$ solution there is very little pH change, and the final pH values were all strongly acid (Figures 5.43 and 5.44). As the concentration of lead in the solution phase decreases (i.e. as one moves across the isotherm), the pH change increases but the presence of only a relatively small amount of Pb^{2+} ion (0.005N Pb^{2+} : 0.095N Na^+) is still sufficient to buffer the pH change (Figure 5.45). In all cases a similar final pH trend with silica : alumina ratio is seen (Figure 5.43 indicates that after 5 minutes the pH of the 0.1N $Pb(NO_3)_2$ solution containing CaA is more acidic than that containing CaX, but the final pH follows the overall trend - Appendix 4 : Table 3).

The degree of dealumination in the faujasites seems to be related to (but not proportional to) the silica : alumina ratio (Table 5.60). In comparison to studies in distilled water (section 6.5.1), this trend does not appear to extend to the most aluminous zeolite. However, as the concentration of lead in the exchange solution decreases ($E_{Pb} \rightarrow 0$), while aluminium was detected in those exchange solutions containing NaA, none was detected in similar exchanges involving the faujasites.

The "hydrolysis" of zeolites has been partially rationalised by consideration of the association constants for acid hydrolysis of ions in aqueous solution (Fletcher and Townsend 1985):

$$M^{2+} + n\,OH^- + n\,H^+ \rightleftharpoons M(OH)_n^{(2-n)+} + nH^+ \quad 6.29$$

Consideration of the first association constants (n=1) shows that calcium has a relatively low acidic reaction with water. In contrast, copper and iron have association constants around 10^6, and both these ions are known to encourage hydronium exchange in zeolites or even dealuminate them (Fletcher and Townsend 1980(a)). Lead has an association constant two orders of magnitude greater than this, so not only does this mean that significant irreversibility of exchange is inevitable (see section 6.3.1.1) but that in turn this hydrolysis reaction releases further protons for hydronium exchange.

The change in cation recoveries for Pb^{2+} ion exchange in the synthetic zeolites can be explained in the following terms. In the region $E_B \rightarrow E_{B(max)}$, hydronium ions exchange with sodium ions from the zeolite so that the pH increases (one must also take into account the reactions of dissolved carbon dioxide in section 6.5.1). As the concentration of lead in the solution increases hydronium exchange must continue as before, but the increasingly acidic reaction of the lead containing solution buffers the system. A minimal pH change is therefore seen, and at the same time the acidic solution must allow some crystal breakdown. Despite the consequent decrease in exchange capacity, nevertheless, the total metal content in the solid continues to increase, since the concentration of Pb^{2+} ions leads to more precipitation in the crystal.

The pH data on lead exchanges serve to emphasize the fact that stoichiometric exchange under the pH conditions using aluminous zeolites is not possible, due to hydrolysis, de-alumination and precipitation of the metal ion within the zeolite matrix. Stamovlasis and Seff (1985) observed just such a problem for Pb^{2+} ion exchange in NaA, when $PbOH^{+}$ was identified in the crystal and at the same time hydrolysis and loss of aluminium from the framework was indicated. As the framework silica : alumina ratio is increased, stoichiometric exchange becomes progressively more feasible (Barrer and Townsend 1976(b); Fletcher and Townsend 1980(a)).

6.5.2.2 Hydronium ion exchange in organolead exchange systems

Studies in 0.01N $NaNO_3$ solution (Figures 5.47 and 5.48) show once again that the pH change for a given zeolite is greater in the more dilute solution because more hydronium ions are available for exchange.

The poor selectivity exhibited by the zeolites for Me_3Pb^{+} ions resulted in the non-stoichiometric exchange of Me_3Pb^{+} ions for the respective counterions. Final solution concentrations were greater than the initial total normalities, and shortages in crystal phase cation recoveries in all exchanges leads one to surmise that hydronium exchange occurred throughout the isotherm (see section 6.4.3). A much smaller pH change was recorded in solutions of Me_3Pb^{+} ions compared to that of a similar concentration of a sodium solution (Figures 5.47 and 5.48). The organolead ion appeared to buffer the pH change to about the same degree as a similar concentration of inorganic lead (Figures 5.46 and 5.47).

Exchanges using the acid-treated clinoptilolite samples obviously involved the release of protons, and this accounts for the decrease in pH observed in figure 5.48. When these same zeolites were immersed in distilled water (Figure 5.39) an initial decrease in the pH of the solution was recorded, but the complete reaction involved a pH increase. It is very unlikely that these zeolites contain any soluble basic impurities; therefore it must be concluded that the overall reaction was one of hydronium uptake.

6.5.3 Concluding Remarks on Hydronium Ion Exchange

In summary, a study of the pH responses in aqueous solutions reveals the following: (1) on suspending a zeolite in aqueous solution, hydronium exchange occurs, resulting normally in a rise in the pH of the bathing electrolyte solution. For the same exchange cation in a set of isomorphous zeolites, this pH rise is inversely proportional to the framework silica : alumina ratio; (2) hydronium ion concentration is encouraged by dissolved carbon dioxide in solution; (3) if the exchange cation is an alkali metal or alkaline earth metal cation, this pH rise is self-stabilising, in that the final near-neutral or alkaline pH slows de-alumination of the less stable low-silica zeolites; (4) if the metal salt yields an acid pH value in solution, then even with the low-silica zeolites, the extent of hydronium exchange into the zeolite cannot raise the pH sufficiently to halt the de-alumination process; (5) washing an exchanged zeolite after its preparation should be kept to an absolute minimum if substantial hydronium exchange is to be avoided; (6) most exchange reactions which appear to be binary are in fact at least ternary in nature due to intervention of the hydronium ion, so values of binary "standard free energies of

exchange", especially in aluminous zeolites, must be viewed with caution.

6.6 CONCLUDING COMMENTS

It is clear from this study that zeolites do not appear over-encouraging for the removal of trimethyllead ions from effluent streams. Despite the advantages of such an ion exchanger, it's use is obviously limited when the selectivity for the ion of interest is poor, and especially when this ion is in low concentration in the presence of high concentrations of other salts, as in this case.

Understandably another approach is required, and one such idea may be to develop and utilise a resin which prefers the Me_3Pb^+ cation very strongly compared to all others. Such resins are said to be "specific" for the preferred cation. The basic principle is that the Me_3Pb^+ ion would associate with the fixed ionic groups or with components of the resin matrix. A cation which forms strong complexes with, or is precipitated by, a certain reagent should thus be preferred by a resin into which this reagent has been incorporated.

An unattractive feature that is common to all specific resins is that the strong affinity for the preferred cation is such that the mobility of the cation in the resin is greatly reduced. The gain in selectivity must be paid for by a loss of ion exchange rate. Also, resins with extreme specificity are difficult to regenerate and may even hold chelated cations so strongly that ion exchange no longer occurs. Hence, a reasonable compromise between selectivity, ease of regeneration and rate of ion exchange needs

to be reached. In addition of course, operating any such system is subject to the restrictions and problems that prevail in the effluent stream and these need to be considered when deciding upon any removal system.

REFERENCES

ABE, M. and SUDOH, K., (1980), J. Inorg. Nucl. Chem., 42, 1051

ABE, M. and SUDOH, K., (1981), J. Inorg. Nucl. Chem., 43, 2537

ALBERTI, A., (1975), Tschermaks. Min. Petr. Mitt., 22, 25

ALLEN, H., CHO, S.H. and NEUBECKER, T.A., (1983), Water Res., 17, 1871

ALLETTI, A., (1972), Amer. Mineral., 57, 1448

AMES, L.L., (1959), Unclass. Report., HY-62607, U.S. Atomic Energy Comm.

AMES, L.L., (1960), Amer. Mineral., 45, 689

ANDERSON, J.C., (1964), "Dielectrics", Chapman and Hall, New York

ANGELL, C.L. and SCHAFFER, P.C., (1965), J. Phys. Chem., 69, 3463

ARAYA, A., (1979), Ph.D. Thesis, Salford University, Manchester

ARAYA, A. and DYER, A., (1981), J. Inorg. Nucl. Chem., 43, 589

ARGAUER, R.J. and LANDOLT, G.R., (1972), U.S. Pat. 3,702,886

ASSOCIATED OCTEL CO. LTD, (1970), "Liquid Effluent Treatment"

ASSOCIATED OCTEL CO. LTD, (1981), personal communication

AUDEH, C.A., (1978), Ger. Offen. 2,756,222

BARRER, R.M., (1959), Br. Chem Engng., 4, 267

BARRER, R.M., (1964), "Non-stoichiometric Inclusion Compounds", (Ed. MANDELCORN, L.), Academic Press, New York

BARRER, R.M., (1978(a)), "Zeolites and Clay Minerals", Academic Press, London, 16

BARRER, R.M., (1978(b)), Ibid, 71

BARRER, R.M., (1982), "Hydrothermal Chemistry of Zeolites", Academic Press, London

BARRER, R.M., BUSER, W. and GRUTTER, W.F., (1956), Helv. Chim. Acta., 39, 518

BARRER, R.M. and COUGHLAN, B., (1968), Molecular Sieves, Society of Chemical Industry, London, 141

BARRER, R.M. and DAVIES, J.A., (1969), J. Phys. Chem. Solids, 30, 1921

BARRER, R.M., DAVIES, J.A. and REES, L.V.C., (1969(a)), J. Inorg. Nucl. Chem., 31, 219

BARRER, R.M., DAVIES, J.A. and REES, L.V.C., (1969(b)), J. Inorg. Nucl. Chem., 31, 2599

BARRER, R.M. and FALCONER, J.D., (1956), Proc. Roy. Soc., A236, 227

BARRER, R.M. and HINDS, J., (1953), J. Chem. Soc., 1879

BARRER, R.M. and KLINOWSKI, J., (1972), J. Chem. Soc. Faraday Trans. 1, 68, 1956

BARRER, R.M. and KLINOWSKI, J., (1974(a)), J. Chem. Soc. Faraday Trans. 1, 70, 2080

BARRER, R.M. and KLINOWSKI, J., (1974(b)), J. Chem. Soc. Faraday Trans. 1, 70, 2362

BARRER, R.M. and KLINOWSKI, J., (1977), Phil. Trans. Roy. Soc., 285, 637

BARRER, R.M., KLINOWSKI, J. and SHERRY, H.S. (1973), J. Chem. Soc., Faraday Trans. II, 69, 1669

BARRER, R.M. and MAKKI, M.B., (1964), Can. J. Chem., 42, 1481

BARRER, R.M. and MEIER, W.M., (1958), Trans. Faraday Soc., 54, 1074

BARRER, R.M. and MEIER, W.M., (1959), Trans. Faraday Soc.. 55, 130

BARRER, R.M. and MUNDAY, B.M., (1971), J. Chem. Soc. A, 2914

BARRER, R.M., PAPADOPOULOS, R. and REES, L.V.C., (1967), J. Inorg. Nucl. Chem., 29, 2047

BARRER, R.M. and PETERSON, D.L., (1964), Proc. Roy. Soc. Ser. A, 280, 466

BARRER, R.M., REES, L.V.C. and SHAMSUZZOHA, M., (1966), J. Inorg. Nucl. Chem., 30, 3333

BARRER, R.M., REES, L.V.C. and WARD, D.J., (1963), Proc. Roy. Soc. (London), A273, 180

BARRER, R.M. and TOWNSEND, R.P., (1976(a)), J. Chem. Soc. Faraday Trans. 1, 72, 661

BARRER, R.M. and TOWNSEND, R.P., (1976(b)), J. Chem. Soc. Faraday Trans. 1, 72, 2650

BARRER, R.M. and WALKER, A.J., (1964), Trans. Faraday Soc., 60, 171

BARRI, S.A.I. and REES, L.V.C., (1980), J. Chrom., 201, 21

BENDIXEN, C.L. and KNECHT, (1976), "Proceedings of the International Symposium on the Management of Wastes from the L.W.R. Fuel Cycle", 343

BOLTON, A.P., (1971), J. Catal., 22, 9

BOTTCHER, C.J.F., (1952), "Theory of Electrostatic Polarisation", Elsevier, Amsterdam

BRECK, D.W., (1973(a)), "Zeolite Molecular Sieves", Wiley-Interscience, 5

BRECK, D.W., (1973(b)), Ibid., 45

BRECK, D.W., (1973(c)), Ibid., 133-180

BRECK, D.W., (1973(d)), Ibid., 93

BRECK, D.W., (1973(e)), Ibid., 176-177

BRECK, D.W., (1973(f)), Ibid.,, 95

BRECK, D.W., (1973(g)), Ibid., 128

BRECK, D.W., (1973(h)), Ibid., 535

BRECK, D.W., (1973(i)), Ibid., 63

BRECK, D.W., (1973(j)), Ibid., 436-437

BRECK, D.W., (1973(k)), Ibid., 273

BRECK, D.W., (1973(l)), Ibid., 386

BRECK, D.W., (1973(m)), Ibid., 353

BRECK, D.W., (1973(n)), Ibid., 279

BRECK, D.W., (1973(o)), Ibid., 424

BRECK, D.W., (1980), "The Properties and Applications of Zeolites", City Univ. Proc., (Ed. TOWNSEND, R.P.), Chem. Soc. Spec. Publ., 33, 391

BRECK, D.W., EVERSOLE, W.G., MILTON, R.M., REED, T.B., and THOMAS, T.L., (1956), J. Am. Chem. Soc., 78, 5963

BRECK, D.W. and FLANIGEN, E.M., (1968), Molecular Sieves, Society of Chemical Industry, London, 47

BROUSSARD, L. and SHOEMAKER, D.P., (1960). J. Am. Chem. Soc., 82, 1041

BROWN, R.A., (1976), "Proceedings of the International Symposium on the Management of Wastes from the L.W.R, Fuel Cycle", 364

BURSILL, L.A., LODGE, E.A. and THOMAS, J.M., (1981), J. Phys. Chem., 85, 2409

CALINGAERT, G., DYKSTRA, F.J. and SHAPIRO, H., (1948), J. Am. Chem. Soc., 70, 3902

CHELISHCHEV, N.F., BERENSHTEIN, B.G. and MARTYNOVA, N.S., (1975) Izv. Akad. Nauk. S.S.S.R., Neorg. Mater., 11, 704

CHELISHCHEV, N.F., MARTYNOVA, N.S., FAKINA, L.K. and BERENSHTEIN, B.F., (1974), Dokl. Akad. Nauk. S.S.S.R., 217, 5, 1140

CHEN, N.Y. and WEISZ, P.B., (1967), Chem. Eng. Progr. Symp. Ser., 63, 86

CHU, C.C. and KAEDING, W.W., (1983), U.S. Pat. 4,394,300

CHU, P. and DWYER, F.G., (1983), Zeolites, 3, 72

COOK, T.E., CILLEY, W.A., SAVITSKY, A.C. and WIERS, B.H., (1982), Environ. Sci. Technol., 16, 344

COOL, W.M. and WILLARD, J.M., (1982), Nutri. Rep. Int., 26, 759

COTTON, F.A. and WILKINSON, G., (1972), "Advanced Inorganic Chemistry", Wiley-Interscience, 335

CREMERS, A., (1977), A.C.S. Symp. Ser. (Mol. Sieves-2, Int. Conf. 4th), 40, 181

CRONSTEDT, A.F., (1756), Akad. Handl. Stockholm, 17, 120

DAMOUR, A., (1840), Ann. Mines, 17, 191

DAVIDOVA, N.P., VALCHEVA, M.L. and SHOPOV, D.M., (1981), Zeolites, 1, 2, 72

DONNER, C. and TAMBERG, T., (1972), Z. Naturforsch A, 27, 1323

DRUMMOND, D., DE JONGE, A. and REES, L.V.C., (1983), J. Phys. Chem., 87, 1967

DYER, A. and BARRI, S.A.I., (1977), J. Inorg. Nucl. Chem., 39, 1061

DYER, A., ENAMY, E. and TOWNSEND, R.P., (1981), Sep. Sci. Techn. 16, (2), 173

DYER, A., GETTINS, R.B. and BROWN, J.G., (1970), J. Inorg. Nucl. Chem., 32, 2389

EDMONDSON, T., (1975), U.K. Pat. 1,410,435

EDMONDSON, T., (1977), U.K. Pat. 1,468,989

EICHORN, H., (1858), Poggendorf Ann. Phys. Chem., 105, 126

EISENMAN, G., (1962), Biophys. J., 2, 259

FILIZOVA, L., (1974), Izv. Geol. Inst. Bulg. Akad. Nauk., Ser. Rudni, Nerudni, Polezni. Izkopaemi, 23, 311

FLANIGEN, E.M., (1980), "Proc. Fifth Inter. Conf. on Zeolites, Naples", (Ed. REES, L.V.C.), Heyden, 760

FLANIGEN, E.M. and BENNETT, J.M., (1978), Nature, 271, 512

FLETCHER, P. and TOWNSEND, R.P., (1980(a)), "Proc. Fifth Int. Conf. on Zeolites, Naples", (Ed. REES, L.V.C.), Heyden, 311

FLETCHER, P. and TOWNSEND, R.P., (1980(b)), J. Chromatogr., 201, 93

FLETCHER, P. and TOWNSEND, R.P., (1981(a)), J. Chem. Soc. Faraday Trans. 1, 77, 497

FLETCHER, P. and TOWNSEND, R.P., (1981(b)), J. Chem. Soc. Faraday Trans. II, 77, 965

FLETCHER, P. and TOWNSEND, R.P., (1983), Zeolites, 3, 129

FLETCHER, P. and TOWNSEND, R.P., (1985), J. Chem. Soc. Faraday Trans. 1, 81, 7, 1731

FLETCHER, P., TOWNSEND, R.P. and LOIZIDOU, M., (1984), "Proc. Sixth Inter. Conf. on Zeolites, Reno", (Ed. OLSON, D. and BISIO, A.), Butterworths, 110

FOSTER, B.A., PENCE, D.T. and STAPLES, B.A., (1974), "Proc. A.E.C. Air Clean Conf. 13th", 293

FRANKLIN, K.R., (1984), Ph.D. Thesis, City University, London

FRANKLIN, K.R., O'CONNOR, J.F. and TOWNSEND, R.P., (1984), Adsorp. Sci. and Techn., 1, 269

GAINES, G.L. and THOMAS, H.C., (1953), J. Chem. Phys., 21, 714

GAL, I.J., JANKOVIC, O., MALCIC, S., RADOVANOV, P. and TODOROVIC, M., (1971), Trans. Faraday Soc., 67, 999

GAL, I.J., and RADOVANOV, P., (1975), Trans. Faraday Soc., 71, 167

GLUECKAUF, E., (1949), Nature, 163, 414

GRADL, R., SCIMMEL, G. and KRAUSE, W., (1983), Heymer. Ger. Offen. DE 3,202, 658

GRAMLICH, V. and MEIER, W.M., (1971), Zeit. Kristallogr., 133, 134

GRAVES, A.B. and McARTHEY, B.J., Associated Octel Company Internal Report, RA 5936

GUGGENHEIM, E.A., (1935), Phil. Mag., 19, 588

HART, R. and TOWNSEND, R.P., (1984), personal communication

HELFFERICH, F., (1962), "Ion Exchange", MacGraw-Hill, 166

HERTZENBERG, E.P. and SHERRY, H.S., (1980), A.C.S. Symp Ser., No. 135, 187

HODGES, D.J., (1984), personal communication

HODGES, D.J. and NODEN, F.G., (1979), "Proc. Int. Conf. Manage. and Control of Heavy Metals in the Environ., London", 408

JEZL, J.L. and MILLS, I.W., (1956), U.S. Pat. 2,745,793

JOERGENSEN, S.E., LIBOR, O., GRABER, K.L. and BARKACO, K., (1976), Water Res., 10, 3, 213

JOHNSON, P.W. and SIEBURTH, J. McN., (1974), Aquaculture, 4, 1, 61

KIELLAND, J., (1935), J. Chem. Soc. Ind., 54, 232

KOKOTAILO, G.T. and MEIER, W.M., (1980), "The Properties and Applications of Zeolites", City Univ. Proc., (Ed. TOWNSEND, R.P.), Chem. Soc. Spec. Publ., 33, 133

KOYAMA, K. and TAKEUCHI. Y., (1977), Zeit. Kristallogr., 145, 216

KUHL, G.H. and SHERRY H.S., (1980), "Proc. Fifth Inter. Conf. on Zeolites, Naples", (Ed. REES, L.V.C.), Heyden, 813

KURZENDORFER, C.P., SCHWUGER, M.J. and SMOLKA, H.G., (1979) Tenside Det., 16, 3

LEVENSPIEL, O., (1966), "Chemical Reaction Engineering", J. Wiley and Sons Inc.

LEWIS, B. and VON ELBE, G., (1961), "Combustion, Flames and Explosions of Gases", 2nd Edition, Academic Press, New York

LIBERTI, L. and BOARI, G., (1981), Water Res., 15, 337

LIBERTI, L., BOARI, G. and PASSINO, R., (1979), Water Res., 13, 65

LILL, D.E., Associated Octel Company Internal Report, GC 1/19/55

LIPTAY, G., (1971), "The Atlas of Thermoanalytical Curves", Heyden and Son Ltd., London

LOWENSTEIN, W., (1954), Amer. Min., 39, 92

LOIZIDOU M., (1983), Ph.D. Thesis, City University, London

LORES, C. and MOORE, R.B., (1973), U.S. Pat. 3,770,423

LUTZ, W., FAHLKE, B., LOHSE, U., BULOW, M. and RICHTER-MENDAU, J., (1983), Crystal Res. and Technol., 4, 513

MAECK, W.J., PENCE, D.T. and KELLER, J.H., (1968), U.S. Atom. Energy Comm., IN-1224

MAES, A. and CREMERS, A., (1973), Adv. Chem. Series, 121, 230

MAES, A. and CREMERS, A., (1975), J. Chem. Soc. Faraday Trans. 1, 71, 265

MANSON, R.A. and SHEPPARD, R.A., (1974), Mineral Science and Engineering, 6, 1

MARSHALL, C.E., (1964), "Physical Chemistry and Mineralogy of Soils", Vol. 1, Soil Materials, John Willey, New York, 283

MARTIN, W.P., (1982), Ph.D. Thesis, University of Minnesota, Minneapolis, Minnesota

McBAIN, J.W., (1932), "The Sorption of Gases and Vapours by Solids", Rutledge and Sons, London

McCUSKER, L.B. and SEFF, K., (1978), J. Am. Chem. Soc., 100, 16, 5052

McDANIEL, C.V. and MAHER, P.K., (1976), A.C.S. Monogr., No. 171, 285

MEIER, W.M., (1968), "Molecular Sieves", Soc. Chem. Ind., London

MELCHIOR, M.T., VAUGHAN, D.E.W., JARMEN, R.H. and JACOBSON, A.J., (1982), Nature, 298, 455

MERCER, B.W. and AMES, L.L., (1970), J. Water Poll. Cont. Fed., 42, R95

MERCER, B.W., and SCHMIDT, W.C., (1965), A.E.C. Accession No. 14466, Report No. RL-SA-58

MERKLE, A.B. and SLAUGHTER, M., (1965), Conf. Geol. Soc. Am.

MERKLE, A.B. and SLAUGHTER, M., (1968), Amer. Min., 53, 1120

MIDGELEY, T. Jr. and BOYD, T.A., (1922), Ind. Eng. Chem., 14, 894

MILTON, R.M., (1959(a)), U.S. Pat. 2,882,243

MILTON, R.M., (1959(b)), U.S. Pat. 2,882,244

MINACHEV, K.M. and ISAKOV, Y.I., (1973), "Molecular Sieves", (Ed. MEIER W.M. and UYTTERHOEVEN, J.B.), Advances in Chemistry Series, No. 121, Amer. Chem. Soc., 451

MINATO, H., (1980), "Proc. Fifth Inter. Conf. on Zeolites, Naples", (Ed. REES, L.V.C.), Heyden, 179

MOBIL Co., (1971), Netherland Pat. 7,014,807

MOREY, G.W. and INGERSON, E., (1937), Econ. Geol., 32, 607

MORTIER, W.J., (1982), "Compilation of Extra Framework Sites in Zeolites", Butterworths

MUMPTON, F.A., (1978), "Natural Zeolites: Properties, Occurence and Uses", (Ed. MUMPTON, F.A. and SAND, L.B.), Pergamon Press, New York, 3

MUMPTON, F.A., (1977), Short Course Notes, Mineral Soc. Am., 4, 177

MUMPTON, F.A. and FISHMAN, P.H., (1977), J. Anim. Sci., 45, 1188

NEEF, F.E., (1945), U.S. Pat. 2,368,261

NOZAK, M. and HATOTANI, H., (1967), Water Research, 1, 167

OBENG, L.A., CARRONDO, M.J.T., PERRY, R. and LESTER, J.N., (1981), J. Am. Oil Chem. Soc., 58, 81

O'CONNOR, J.F. and TOWNSEND, R.P., (1985), Zeolites, 5, 158

OKAWARA, R. and SATO, A., (1961), J. Inorg. Nucl. Chem., 16, 204

PARAKRAMA, R., (1983), Ph.D. Thesis, City University, London

PAULING, L., (1960), "Nature of the Chemical Bond", Cornell University Press, Ithaca, New York

PENCHEV, V., DAVIDOVA, N., KANAZIREV, V., MINCHEV, H. and NEINSKA, Y., (1973), "Molecular Sieves", (Ed. MEIER, W.M. and UYTTERHOEVEN, J.B.), Advances in Chemistry Series, No. 121, Amer. Chem. Soc., 461

PHILLIPS, C.S.G. and WILLIAMS, R.J.P., (1965), "Inorganic Chemistry", Vol 1, Clarendon Press, Oxford, 176

POND, W.G., YEN, J.T. and HILL, D.A., (1981), Proc. Soc. Exp. Biol. Med., 166, 369

REED, T.B. and BRECK, D.W., (1956), J. Am. Chem. Soc., 78, 5972

REES, L.V.C., (1980), "The Properties and Applications of Zeolites", City Univ. Proc., (Ed. TOWNSEND, R.P.), Chem. Soc. Spec. Publ., 33

ROBINSON, R.A. and STOKES, R.H., (1970), "Electrolyte Solutions", 2nd Edition, Butterworths, London, 229

RONAY, C., (1984), MSc. Thesis, University of Hawaii

RONAY, C. and SEFF, K., (1984), J. Phys. Chem., 89, 10, 1965

ROSSEINSKY, D.R., (1965), Chem. Rev., 65, 467

ROSSIN, A.C., PERRY, R. and LESTER, J.N., (1982), Water Res., 16, 1223

SAND, L.B., (1967), Molecular Sieves, Pap. Conf., 71

SATO, MIKIO and FUKAGAURA, (1976), Japan Kokai, 76,068,967

SCHOONHEYDT, R.A. and VELGHE, F., (1976), J. Chem. Soc. Faraday Trans. 1, 72, 172

SCHWUGER, M.J. and SMOLKA, H.G., (1977), Molecular Sieves 2, Fourth Int. Conf., A.C.S. Symp. Ser., 40

SCHWUGER, M.J., SMOLKA, H.G. and KURZENDORFER, C.P., (1976), Tenside Deterg., 13, 6, 305

SELBA, F., (1959), Nature, 184, 1062

SEMMENS, M.J., (1980), "Proc. Fifth Inter. Conf. on Zeolites, Naples", (Ed. REES, L.V.C.), Heyden, 795

SEMMENS, M.J., (1981), Final Report, Proj. B-150-MIN, Minnesota Water Resources Center, University of Minnesota, Minneapolis, MN, 102

SEMMENS, M.J. and MARTIN, W., (1979), A.I.Ch.E. Symp. Ser., 76, 197, 367

SEMMENS, M.J. and SEYFARTH, M., (1978), "Natural Zeolites: Properties, Occurence and Uses", (Ed. MUMPTON, F.A. and SAND, L.B.), Pergamon Press, New York, 517

SHAPIRO, H. and FREY, F.W., (1968), "The Organic Compounds of Lead", Interscience

SHEPPARD, R.A. and GUDE, A.J., (1968), U.S. Geol. Surv. Prof. Pap., 597

SHEPPARD, R.A. and GUDE, A.J., (1969), U.S. Geol. Surv. Prof. Pap., 634

SHERRY, H.S., (1966), J. Phys. Chem., 70, 1158

SHERRY, H.S., (1968), J. Phys. Chem., 72, 4086

SHERRY, H.S., (1969), The Ion Exchange Properties of Zeolites, in "Ion Exchange", Vol. 2, (Ed. MARINSKY, J.A.), Marcel Dekker, New York, 89

SHERRY, H.S., (1975), Phys. Chem. Sci. Res. Rep., 1, 523

SHERRY, H.S. and WALTON, H.F., (1967), J. Phys. Chem., 71, 1457

SHREVE, R.N., (1930), "Greens and Bibliography to 1930", U.S. Bur. Mines, Bull., 328

SMITH, J.V., (1971), "Molecular Sieve Zeolites - 1", Adv. Chem. Ser., 101, 109

SMITH, A.M. and MARTELL, A.E., (1976), "Inorganic Complexes", Vol. 4, Plenum Press, New York

STAMBERG, J.B., BISHOP, D.F. and KUMKE, G., (1972), A.I.Ch.E. Symp. Ser., 68, 124, 25

STAMOVLASIS, D. and SEFF, K., (1985), personal communication

STOVELAND, S., LESTER, J.N. and PERRY, R. (1980), Environ. Int., 3, 49

TAKAISHI, T., YATSURGI, Y., YUSA, A. and KURAMTOMI, T., (1975), J. Chem. Soc. Faraday Trans. 1, 71, 97

THENG, B.K.G., VANSANT, E. and UYTTERHOEVEN, J.B., (1968), Trans. Faraday Soc., 64, 3370

TORII, K., (1978), "Natural Zeolites: Occurence, Properties and Uses", (Ed. MUMPTON, F.A. and SAND, L.B.), Pergamon Press, New York, 441

TOWNSEND, R.P., (1977), D.I.C. Thesis, Imperial College, London

TURKEVICH, J. and ONO, Y., (1969), Advan. Catalysis, 20, 135

VANSANT, E.F., and UYTTERHOEVEN, J.B., (1971), Trans. Faraday Soc., 67, 2961

VENUTO, P.B., (1971), "Molecular Sieve Zeolites", (Ed. GOULD, R.F.), Adv. Chem. Ser., No. 102, Amer. Chem. Soc., 261

VENUTO, P.B., and LANDIS, P.S., (1968), Advan. Catalysis, 18, 259

VOGEL, A., (1978(a)), "Textbook of Quantitative Inorganic Analysis", 436

VOGEL, A., (1978(b)), Ibid., 823

VOGEL, A., (1978(c)), Ibid., 325

VOGEL, A., (1978(d)), Ibid., 329

VOGEL, A., (1978(e)), Ibid., 729

VON BALLMOOS, R., (1984), "Collection of Simulated XRD Powder Patterns for Zeolites", Butterworth Scientific Ltd., Guildford, Surrey

WARD, J.W., (1968), J. Catal., 10, 34

WEISZ, P.B., and FRILETTE, V.J., (1960), J. Phys. Chem. 64, 382

WEISZ, P.B., FRILETTE, V.J., MAATMAN, V.J. and MOWER, E.B., (1962), J. Catalysis, 1, 307

WIEGEL, O. and STEINHOFF, E., (1925). Z. Kristallogr., 61, 125

WIERS, B.H., GROSSE, R.J. and CILLEY, W.A. (1982), Environ. Sci. Technol., 16, 617

WISE, W.S., NOKLEBURG, W.S. and KOKINOS, M., (1969), Amer. Mineral., 54, 887

WOLF, VON F., CEACAREANU, D. and PILCHOWSKI, K., (1973), Z. phys. Chemie, Leipzig, 252, 50

APPENDIX 1

Data for the removal of Pb^{2+} ions from a 10^{-3} mol dm^{-3} $Pb(NO_3)_2$ solution by the faujasites

APPENDIX 1

Table 1(a) Z1(0.1% w/v)

Equilibrium concentration = 6.881×10^{-7} mol dm^{-3}

t/s	$t^{\frac{1}{2}}$/s	F.A.E./%	$\log_{10} c_{Pb}$	c_{Pb}/mol dm^{-3}
5	2.236	72.059	-3.554	2.792×10^{-4}
10	3.162	81.605	-3.735	1.841×10^{-4}
15	3.872	85.369	-3.833	1.468×10^{-4}
20	4.472	87.528	-3.903	1.250×10^{-4}
25	5	88.943	-3.954	1.111×10^{-4}
30	5.477	89.922	-3.994	1.013×10^{-4}
35	5.916	90.643	-4.027	9.39×10^{-5}
40	6.324	91.252	-4.055	8.81×10^{-5}
45	6.708	91.726	-4.079	8.33×10^{-5}
50	7.071	92.138	-4.101	7.92×10^{-5}
55	7.416	92.512	-4.122	7.55×10^{-5}
60	7.745	93.209	-4.165	6.83×10^{-5}
70	8.366	93.472	-4.181	6.59×10^{-5}
80	8.944	93.898	-4.21	6.16×10^{-5}
90	9.486	94.297	-4.24	5.75×10^{-5}
100	10	94.62	-4.265	5.43×10^{-5}
110	10.488	95.053	-4.301	5.00×10^{-5}
120	10.954	95.334	-4.325	4.73×10^{-5}
180	13.416	96.526	-4.452	3.53×10^{-5}
240	15.491	97.287	-4.556	2.77×10^{-5}
300	17.32	97.76	-4.638	2.30×10^{-5}
450	21.213	98.49	-4.803	1.57×10^{-5}
600	24.494	98.898	-4.933	1.16×10^{-5}
750	27.386	99.132	-5.029	9.3×10^{-6}
900	30	99.295	-5.112	7.7×10^{-6}
990	31.464	99.371	-5.158	6.9×10^{-6}

where F.A.E. is fractional attainment of equilibrium

This data is illustrated in figures 5.6(a) and 5.7(a)

APPENDIX 1

Table 1(b) Z1(0.2% w/v)

Equilibrium concentration = 1×10^{-7} mol dm^{-3}

t/s	t /s	F.A.E./%	$\log_{10} c_{Pb}$	c_{Pb}/mol dm^{-3}
5	2.236	95.234	-4.322	4.76×10^{-5}
10	3.162	97.781	-4.653	2.22×10^{-5}
15	3.872	98.424	-4.801	1.58×10^{-5}
20	4.472	98.721	-4.891	1.28×10^{-5}
25	5	98.923	-4.964	1.08×10^{-5}
30	5.477	99.052	-5.019	9.5×10^{-6}
35	5.916	99.118	-5.051	8.8×10^{-6}
40	6.324	99.226	-5.107	7.8×10^{-6}
45	6.708	99.287	-5.141	7.2×10^{-6}
50	7.071	99.333	-5.17	6.7×10^{-6}
55	7.416	99.387	-5.206	6.2×10^{-6}
60	7.745	99.433	-5.24	5.7×10^{-6}
70	8.366	99.505	-5.298	5.0×10^{-6}
80	8.944	99.562	-5.35	4.4×10^{-6}
90	9.486	99.61	-5.4	3.9×10^{-6}
100	10	99.647	-5.441	3.6×10^{-6}
110	10.488	99.681	-5.483	3.2×10^{-6}
120	10.954	99.709	-5.522	3.0×10^{-6}
180	13.416	99.807	-5.695	2.0×10^{-6}
240	15.491	99.858	-5.82	1.5×10^{-6}
300	17.32	99.887	-5.913	1.2×10^{-6}
450	21.213	99.928	-6.092	8×10^{-7}
600	24.494	99.947	-6.206	6×10^{-7}

This data is illustrated in figures 5.6(a) and 5.7(b)

APPENDIX 1

Table 1(c) Z1(0.4% w/v)

Equilibrium concentration = 1 x 10^{-7} mol dm^{-3}

t/s	$t^{\frac{1}{2}}$/s	F.A.E./%	$\log_{10}c_{Pb}$	c_{Pb}/mol dm^{-3}
5	2.236	99.701	-5.511	$3.1x10^{-6}$
10	3.162	99.842	-5.778	$1.6x10^{-6}$
15	3.872	99.871	-5.86	$1.3x10^{-6}$
20	4.472	99.886	-5.911	$1.2x10^{-6}$
25	5	99.897	-5.948	$1.1x10^{-6}$
30	5.477	99.905	-5.98	$1.0x10^{-6}$
35	5.916	99.912	-6.009	$9x10^{-7}$
40	6.324	99.917	-6.036	$9x10^{-7}$
45	6.708	99.922	-6.058	$8x10^{-7}$
50	7.071	99.926	-6.079	$8x10^{-7}$
55	7.416	99.93	-6.098	$8x10^{-7}$
60	7.745	99.933	-6.117	$8x10^{-7}$
70	8.366	99.939	-6.154	$7x10^{-7}$
80	8.944	99.945	-6.188	$7x10^{-7}$

This data is illustrated in figures 5.6(a) and 5.7(c)

APPENDIX 1

Table 2(a) Z2(0.1% w/v)

Equilibrium concentration = 9.6×10^{-6} mol dm^{-3}

t/s	$t^{\frac{1}{2}}$/s	F.A.E./%	$\log_{10} c_{Pb}$	c_{Pb}/mol dm^{-3}
5	2.236	40.548	-3.223	5.984×10^{-4}
10	3.162	50.713	-3.304	4.865×10^{-4}
15	3.872	55.24	-3.344	4.528×10^{-4}
20	4.472	58.488	-3.377	4.197×10^{-4}
25	5	60.587	-3.398	3.999×10^{-4}
30	5.477	62.581	-3.42	3.801×10^{-4}
35	5.916	63.799	-3.435	3.672×10^{-4}
40	6.324	65.472	-3.454	3.515×10^{-4}
45	6.708	66.756	-3.471	3.381×10^{-4}
50	7.071	67.688	-3.483	3.288×10^{-4}
55	7.416	68.744	-3.497	3.184×10^{-4}
60	7.745	69.838	-3.511	3.083×10^{-4}
70	8.366	71.376	-3.533	2.931×10^{-4}
80	8.944	72.773	-3.554	2.792×10^{-4}
90	9.486	73.793	-3.571	2.685×10^{-4}
100	10	74.896	-3.588	2.582×10^{-4}
110	10.488	76.069	-3.609	2.460×10^{-4}
120	10.954	77.135	-3.628	2.355×10^{-4}
180	13.416	80.915	-3.703	1.981×10^{-4}
240	15.491	83.861	-3.772	1.690×10^{-4}
300	17.32	85.965	-3.828	1.485×10^{-4}
450	21.213	89.588	-3.948	1.127×10^{-4}
600	24.494	91.866	-4.045	9.01×10^{-5}
750	27.386	93.292	-4.119	7.60×10^{-5}
900	30	94.267	-4.178	6.63×10^{-5}
990	31.464	94.743	-4.21	6.16×10^{-5}

This data is illustrated in figures 5.6(b) and 5.7(a)

APPENDIX 1

Table 2(b) Z2(0.2% w/v)

Equilibrium concentration = 1.455×10^{-6} mol dm^{-3}

t/s	$t^{\frac{1}{2}}$/s	F.A.E./%	$\log_{10} c_{Pb}$	c_{Pb}/mol dm^{-3}
5	2.236	91.302	-4.054	8.83×10^{-5}
10	3.162	93.97	-4.21	6.16×10^{-5}
15	3.872	95.056	-4.294	5.08×10^{-5}
20	4.472	95.651	-4.348	4.48×10^{-5}
25	5	96.103	-4.394	4.03×10^{-5}
30	5.477	96.39	-4.427	3.74×10^{-5}
35	5.916	96.665	-4.46	3.46×10^{-5}
40	6.324	96.852	-4.483	3.28×10^{-5}
45	6.708	97.058	-4.511	3.08×10^{-5}
50	7.071	97.19	-4.53	2.95×10^{-5}
55	7.416	97.349	-4.554	2.79×10^{-5}
60	7.745	97.462	-4.573	2.67×10^{-5}
70	8.366	97.687	-4.61	2.45×10^{-5}
80	8.944	97.882	-4.647	2.25×10^{-5}
90	9.486	98.024	-4.674	2.11×10^{-5}
100	10	98.142	-4.699	1.99×10^{-5}
110	10.488	98.285	-4.732	1.85×10^{-5}
120	10.954	98.401	-4.759	1.74×10^{-5}
180	13.416	98.8	-4.872	1.34×10^{-5}
240	15.491	99.003	-4.943	1.14×10^{-5}
300	17.32	99.2	-5.026	9.4×10^{-6}
450	21.213	99.433	-5.148	7.1×10^{-6}
600	24.494	99.56	-5.233	5.8×10^{-6}
750	27.386	99.643	-5.301	5.0×10^{-6}
900	30	99.699	-5.351	4.4×10^{-6}
990	31.464	99.73	-5.383	4.1×10^{-6}

This data is illustrated in figures 5.6(b) and 5.7(b)

APPENDIX 1

Table 2(c) Z2(0.4% w/v)

Equilibrium concentration = 1 x 10^{-7} mol dm^{-3}

t/s	$t^{\frac{1}{2}}$/s	F.A.E./%	$\log_{10} c_{Pb}$	c_{Pb}/mol dm^{-3}
5	2.236	99.065	-5.026	9.4×10^{-6}
10	3.162	99.172	-5.078	8.3×10^{-6}
15	3.872	99.305	-5.153	7.0×10^{-6}
20	4.472	99.419	-5.23	5.8×10^{-6}
25	5	99.462	-5.263	5.4×10^{-6}
30	5.477	99.513	-5.305	4.9×10^{-6}
35	5.916	99.544	-5.333	4.6×10^{-6}
40	6.324	99.569	-5.356	4.4×10^{-6}
45	6.708	99.595	-5.383	4.1×10^{-6}
50	7.071	99.614	-5.404	3.9×10^{-6}
55	7.416	99.631	-5.423	3.7×10^{-6}
60	7.745	99.645	-5.438	3.6×10^{-6}
70	8.366	99.671	-5.471	3.3×10^{-6}
80	8.944	99.695	-5.503	3.1×10^{-6}
90	9.486	99.708	-5.521	3.0×10^{-6}
100	10	99.721	-5.541	2.8×10^{-6}
110	10.488	99.74	-5.57	2.6×10^{-6}
120	10.954	99.748	-5.584	2.6×10^{-6}
180	13.416	99.795	-5.668	2.1×10^{-6}
240	15.491	99.82	-5.722	1.8×10^{-6}
300	17.32	99.84	-5.771	1.6×10^{-6}
450	21.213	99.87	-5.856	1.3×10^{-6}
600	24.494	99.889	-5.92	1.2×10^{-6}
750	27.386	99.9	-5.963	1.1×10^{-6}
900	30	99.91	-6.003	1.0×10^{-6}
990	31.464	99.914	-6.022	9.0×10^{-7}

This data is illustrated in figures 5.6(b) and 5.7(c)

APPENDIX 1

Table 2(d) Z2(0.6% w/v)

Equilibrium concentration = 1×10^{-7} mol dm^{-3}

t/s	$t^{\frac{1}{2}}$/s	F.A.E./%	$\log_{10} c_{Pb}$	c_{Pb}/mol dm^{-3}
5	2.236	99.653	-5.448	3.5×10^{-6}
10	3.162	99.752	-5.59	2.5×10^{-6}
15	3.872	99.799	-5.678	2.1×10^{-6}
20	4.472	99.827	-5.74	1.8×10^{-6}
25	5	99.845	-5.786	1.6×10^{-6}
30	5.477	99.86	-5.826	1.4×10^{-6}
35	5.916	99.871	-5.858	1.3×10^{-6}
40	6.324	99.879	-5.884	1.3×10^{-6}
45	6.708	99.886	-5.911	1.2×10^{-6}
50	7.071	99.893	-5.935	1.1×10^{-6}
55	7.416	99.898	-5.954	1.1×10^{-6}
60	7.745	99.903	-5.971	1.0×10^{-6}
70	8.366	99.91	-6.001	9×10^{-7}
80	8.944	99.916	-6.03	9×10^{-7}
90	9.486	99.921	-6.053	8×10^{-7}
100	10	99.925	-6.071	8×10^{-7}
110	10.488	99.928	-6.092	8×10^{-7}
120	10.954	99.931	-6.108	7×10^{-7}
180	13.416	99.944	-6.185	6×10^{-7}
240	15.491	99.952	-6.238	5×10^{-7}
300	17.32	99.957	-6.28	5×10^{-7}
450	21.213	99.965	-6.35	4×10^{-7}

This data is illustrated in figures 5.6(b) and 5.7(d)

APPENDIX 1

Table 3(a) Z3(0.1% w/v)

Equilibrium concentration = 6.818×10^{-5} mol dm^{-3}

t/s	$t^{\frac{1}{2}}$/s	F.A.E./%	$\log_{10} c_{Pb}$	c_{Pb}/mol dm^{-3}
5	2.236	70.277	-3.463	3.443×10^{-4}
10	3.162	77.554	-3.558	2.766×10^{-4}
15	3.872	80.729	-3.607	2.471×10^{-4}
20	4.472	82.332	-3.633	2.328×10^{-4}
25	5	83.456	-3.653	2.223×10^{-4}
30	5.477	84.107	-3.666	2.157×10^{-4}
35	5.916	84.635	-3.675	2.113×10^{-4}
40	6.324	85.049	-3.684	2.070×10^{-4}
45	6.708	85.455	-3.691	2.037×10^{-4}
50	7.071	85.854	-3.699	1.999×10^{-4}
55	7.416	86.246	-3.708	1.958×10^{-4}
60	7.745	86.535	-3.713	1.936×10^{-4}
70	8.366	87.148	-3.727	1.874×10^{-4}
80	8.944	87.653	-3.738	1.828×10^{-4}
90	9.486	88.1	-3.747	1.791×10^{-4}
100	10	88.538	-3.758	1.745×10^{-4}
110	10.488	89.007	-3.768	1.706×10^{-4}
120	10.954	89.217	-3.773	1.686×10^{-4}
180	13.416	91.036	-3.82	1.513×10^{-4}
240	15.491	92.468	-3.86	1.380×10^{-4}
300	17.32	93.395	-3.888	1.294×10^{-4}
450	21.213	95.108	-3.945	1.135×10^{-4}
600	24.494	96.335	-3.991	1.021×10^{-4}
750	27.386	97.162	-4.025	9.44×10^{-5}
900	30	97.796	-4.053	8.85×10^{-5}
990	31.464	98.182	-4.071	8.49×10^{-5}

This data is illustrated in figures 5.6(c) and 5.7(a)

APPENDIX 1

Table 3(b) Z3(0.2% w/v)

Equilibrium concentration = 9.103×10^{-6} mol dm^{-3}

t/s	$t^{\frac{1}{2}}$/s	F.A.E./%	$\log_{10} c_{Pb}$	c_{Pb}/mol dm^{-3}
5	2.236	90.179	-3.973	1.064×10^{-4}
10	3.162	95.461	-4.268	5.39×10^{-5}
15	3.872	97.037	-4.416	3.83×10^{-5}
20	4.472	97.69	-4.496	3.19×10^{-5}
25	5	98.054	-4.548	2.83×10^{-5}
30	5.477	98.276	-4.583	2.61×10^{-5}
35	5.916	98.412	-4.606	2.47×10^{-5}
40	6.324	98.531	-4.627	2.36×10^{-5}
45	6.708	98.622	-4.643	2.27×10^{-5}
50	7.071	98.7	-4.658	2.19×10^{-5}
55	7.416	98.756	-4.669	2.14×10^{-5}
60	7.745	98.81	-4.68	2.08×10^{-5}
70	8.366	98.909	-4.702	1.98×10^{-5}
80	8.944	98.977	-4.717	1.91×10^{-5}
90	9.486	99.03	-4.729	1.86×10^{-5}
100	10	99.082	-4.741	1.81×10^{-5}
110	10.488	99.136	-4.754	1.76×10^{-5}
120	10.954	99.18	-4.765	1.71×10^{-5}
180	13.416	99.369	-4.814	1.53×10^{-5}
240	15.491	99.506	-4.854	1.39×10^{-5}
300	17.32	99.591	-4.882	1.31×10^{-5}
450	21.213	99.735	-4.931	1.17×10^{-5}
600	24.494	99.854	-4.978	1.05×10^{-5}
750	27.386	99.932	-5.01	9.7×10^{-6}
900	30	99.987	-5.036	9.2×10^{-6}
990	31.464	100.019	-5.051	8.8×10^{-6}

This data is illustrated in figures 5.6(c) and 5.7(b)

APPENDIX 1

Table 3(c) Z3(0.4% w/v)

Equilibrium concentration = 2.338×10^{-6} mol dm^{-3}

t/s	$t^{\frac{1}{2}}$/s	F.A.E./%	$\log_{10} c_{Pb}$	c_{Pb}/mol dm^{-3}
5	2.236	98.257	-4.706	1.96×10^{-5}
10	3.162	99.357	-5.059	8.7×10^{-6}
15	3.872	99.587	-5.191	6.4×10^{-6}
20	4.472	99.691	-5.266	5.4×10^{-6}
25	5	99.746	-5.313	4.8×10^{-6}
30	5.477	99.788	-5.353	4.4×10^{-6}
35	5.916	99.816	-5.38	4.1×10^{-6}
40	6.324	99.839	-5.405	3.9×10^{-6}
45	6.708	99.857	-5.426	3.7×10^{-6}
50	7.071	99.872	-5.443	3.6×10^{-6}
55	7.416	99.886	-5.46	3.4×10^{-6}
60	7.745	99.896	-5.472	3.3×10^{-6}
70	8.366	99.915	-5.498	3.1×10^{-6}
80	8.944	99.929	-5.518	3.0×10^{-6}
90	9.486	99.943	-5.538	2.8×10^{-6}
100	10	99.953	-5.553	2.7×10^{-6}
110	10.488	99.963	-5.568	2.7×10^{-6}
180	13.416	100.003	-5.639	2.2×10^{-6}
240	15.491	100.023	-5.678	2.1×10^{-6}
300	17.32	100.037	-5.706	1.9×10^{-6}
450	21.213	100.061	-5.764	1.7×10^{-6}
600	24.494	100.076	-5.805	1.6×10^{-6}
750	27.386	100.085	-5.828	1.5×10^{-6}
900	30	100.096	-5.862	1.4×10^{-6}
990	31.464	100.101	-5.88	1.3×10^{-6}

This data is illustrated in figures 5.6(c) and 5.7(c)

APPENDIX 1

Table 3(d) Z3(0.6% w/v)

Equilibrium concentration = 1.12×10^{-6} mol dm^{-3}

t/s	t /s	F.A.E./%	$\log_{10} c_{Pb}$	c_{Pb}/mol dm^{-3}
5	2.236	99.127	-5.008	9.8×10^{-6}
10	3.162	99.638	-5.325	4.7×10^{-6}
15	3.872	99.765	-5.461	3.4×10^{-6}
20	4.472	99.824	-5.541	2.8×10^{-6}
25	5	99.863	-5.606	2.4×10^{-6}
30	5.477	99.886	-5.648	2.2×10^{-6}
35	5.916	99.905	-5.685	2.1×10^{-6}
40	6.324	99.92	-5.718	1.9×10^{-6}
45	6.708	99.932	-5.746	1.7×10^{-6}
50	7.071	99.94	-5.766	1.7×10^{-6}
55	7.416	99.948	-5.786	1.6×10^{-6}
60	7.745	99.954	-5.803	1.5×10^{-6}
70	8.366	99.965	-5.835	1.4×10^{-6}
80	8.944	99.974	-5.861	1.3×10^{-6}
90	9.486	99.98	-5.88	1.3×10^{-6}
100	10	99.986	-5.901	1.2×10^{-6}
110	10.488	99.99	-5.917	1.2×10^{-6}
120	10.954	99.994	-5.931	1.1×10^{-6}
180	13.416	100.012	-6	9×10^{-7}
240	15.491	100.021	-6.043	9×10^{-7}
300	17.32	100.027	-6.075	8×10^{-7}
450	21.213	100.034	-6.113	7×10^{-7}
600	24.494	100.042	-6.155	6×10^{-7}
750	27.386	100.045	-6.178	6×10^{-7}
900	30	100.049	-6.203	6×10^{-7}
990	31.464	100.05	-6.213	6×10^{-7}

This data is illustrated in figures 5.6(c) and 5.7(d)

APPENDIX 1

Table 3(e) Z3(0.8% w/v)

Equilibrium concentration = 7.423×10^{-7} mol dm^{-3}

t/s	$t^{\frac{1}{2}}$/s	F.A.E./%	$\log_{10} c_{Pb}$	c_{Pb}/mol dm^{-3}
5	2.236	99.702	-5.43	3.7×10^{-6}
10	3.162	99.822	-5.6	2.5×10^{-6}
15	3.872	99.863	-5.676	2.1×10^{-6}
20	4.472	99.885	-5.725	1.8×10^{-6}
25	5	99.897	-5.755	1.7×10^{-6}
30	5.477	99.906	-5.776	1.6×10^{-6}
35	5.916	99.914	-5.798	1.5×10^{-6}
40	6.324	99.921	-5.816	1.5×10^{-6}
45	6.708	99.928	-5.838	1.4×10^{-6}
50	7.071	99.931	-5.846	1.4×10^{-6}
55	7.416	99.934	-5.856	1.3×10^{-6}
60	7.745	99.939	-5.871	1.3×10^{-6}
70	8.366	99.946	-5.893	1.2×10^{-6}
80	8.944	99.952	-5.913	1.2×10^{-6}
90	9.486	99.958	-5.936	1.1×10^{-6}
100	10	99.961	-5.95	1.1×10^{-6}
110	10.488	99.966	-5.968	1.1×10^{-6}
120	10.954	99.969	-5.981	1.0×10^{-6}
180	13.416	99.986	-6.055	8×10^{-7}
240	15.491	99.995	-6.106	7×10^{-7}
300	17.32	100.002	-6.146	7×10^{-7}
450	21.213	100.013	-6.213	6×10^{-7}
600	24.494	100.018	-6.256	5×10^{-7}
750	27.386	100.022	-6.291	5×10^{-7}
900	30	100.025	-6.316	5×10^{-7}
990	31.464	100.027	-6.328	4×10^{-7}

This data is illustrated in figures 5.6(c) and 5.7(e)

APPENDIX 1

Table 3(f) Z3(1% w/v)

Equilibrium concentration = 1 x 10^{-7} mol dm^{-3}

t/s	$t^{\frac{1}{2}}$/s	F.A.E./%	$\log_{10}c_{Pb}$	c_{Pb}/mol dm^{-3}
5	2.236	99.695	-5.504	$3.1x10^{-6}$
10	3.162	99.8	-5.678	$2.1x10^{-6}$
15	3.872	99.842	-5.776	$1.6x10^{-6}$
20	4.472	99.86	-5.825	$1.4x10^{-6}$
25	5	99.876	-5.875	$1.3x10^{-6}$
30	5.477	99.886	-5.908	$1.2x10^{-6}$
35	5.916	99.894	-5.938	$1.1x10^{-6}$
40	6.324	99.9	-5.96	$1.1x10^{-6}$
45	6.708	99.905	-5.98	$1.0x10^{-7}$
50	7.071	99.91	-6.001	$1.0x10^{-7}$
55	7.416	99.913	-6.016	$9x10^{-7}$
60	7.745	99.917	-6.036	$9x10^{-7}$
70	8.366	99.923	-6.063	$8x10^{-7}$
80	8.944	99.928	-6.088	$8x10^{-7}$
90	9.486	99.932	-6.111	$7x10^{-7}$
100	10	99.935	-6.129	$7x10^{-7}$
110	10.488	99.938	-6.148	$7x10^{-7}$
120	10.954	99.941	-6.166	$6x10^{-7}$
180	13.416	99.953	-6.248	$5x10^{-7}$
240	15.491	99.959	-6.295	$5x10^{-7}$
300	17.32	99.965	-6.348	$4x10^{-7}$
450	21.213	99.97	-6.408	$3x10^{-7}$
600	24.494	99.974	-6.446	$3x10^{-7}$
750	27.386	99.975	-6.469	$3x10^{-7}$
900	30	99.977	-6.492	$3x10^{-7}$
990	31.464	99.978	-6.503	$3x10^{-7}$

This data is illustrated in figures 5.6(c) and 5.7(f)

APPENDIX 1

Table 4(a) Z4(0.1% w/v)

Equilibrium concentration = 1.721×10^{-4} mol dm^{-3}

t/s	$t^{\frac{1}{2}}$/s	F.A.E./%	$\log_{10} c_{Pb}$	c_{Pb}/mol dm^{-3}
5	2.236	60.667	-3.304	4.965×10^{-4}
10	3.162	68.665	-3.366	4.305×10^{-4}
15	3.872	73.251	-3.405	3.935×10^{-4}
20	4.472	76.116	-3.433	3.689×10^{-4}
25	5	77.732	-3.448	3.564×10^{-4}
30	5.477	78.615	-3.458	3.483×10^{-4}
35	5.916	79.385	-3.466	3.419×10^{-4}
40	6.324	79.67	-3.468	3.404×10^{-4}
45	6.708	80.141	-3.473	3.365×10^{-4}
50	7.071	80.698	-3.479	3.318×10^{-4}
55	7.416	80.974	-3.483	3.288×10^{-4}
60	7.745	81.339	-3.486	3.265×10^{-4}
70	8.366	81.791	-3.491	3.228×10^{-4}
80	8.944	82.414	-3.498	3.176×10^{-4}
90	9.486	82.591	-3.5	3.162×10^{-4}
100	10	82.854	-3.504	3.133×10^{-4}
110	10.488	83.288	-3.508	3.104×10^{-4}
120	10.954	83.717	-3.513	3.069×10^{-4}
180	13.416	85.71	-3.538	2.897×10^{-4}
240	15.491	87.057	-3.554	2.792×10^{-4}
300	17.32	88.277	-3.571	2.685×10^{-4}
450	21.213	90.932	-3.608	2.466×10^{-4}
600	24.494	92.472	-3.63	2.344×10^{-4}
750	27.386	93.621	-3.648	2.249×10^{-4}
900	30	94.544	-3.663	2.172×10^{-4}
990	31.464	95.2	-3.674	2.118×10^{-4}

This data is illustrated in figures 5.6(d) and 5.7(a)

APPENDIX 1

Table 4(b) Z4(0.2% w/v)

Equilibrium concentration = 3.275×10^{-5} mol dm^{-3}

t/s	$t^{\frac{1}{2}}$/s	F.A.E./%	$\log_{10} c_{Pb}$	c_{Pb}/mol dm^{-3}
5	2.236	79.864	-3.643	2.275×10^{-4}
10	3.162	88.714	-3.848	1.419×10^{-4}
15	3.872	91.892	-3.954	1.111×10^{-4}
20	4.472	93.375	-4.015	9.66×10^{-5}
25	5	94.235	-4.053	8.85×10^{-5}
30	5.477	94.806	-4.082	8.27×10^{-5}
35	5.916	95.154	-4.099	7.96×10^{-5}
40	6.324	95.452	-4.116	7.65×10^{-5}
45	6.708	95.65	-4.127	7.46×10^{-5}
50	7.071	95.809	-4.135	7.32×10^{-5}
55	7.416	95.981	-4.145	7.16×10^{-5}
60	7.745	96.167	-4.156	6.98×10^{-5}
70	8.366	96.282	-4.163	6.87×10^{-5}
80	8.944	96.492	-4.177	6.65×10^{-5}
90	9.486	96.602	-4.184	6.54×10^{-5}
100	10	96.71	-4.191	6.44×10^{-5}
110	10.488	96.802	-4.197	6.35×10^{-5}
120	10.954	96.907	-4.203	6.26×10^{-5}
180	13.416	97.395	-4.237	5.79×10^{-5}
240	15.491	97.73	-4.263	5.45×10^{-5}
300	17.32	97.96	-4.28	5.24×10^{-5}
450	21.213	98.46	-4.323	4.75×10^{-5}
600	24.494	98.735	-4.347	4.49×10^{-5}
750	27.386	98.975	-4.371	4.25×10^{-5}
900	30	99.125	-4.385	4.12×10^{-5}
990	31.464	99.212	-4.394	4.03×10^{-5}

This data is illustrated in figures 5.6(d) and 5.7(b)

APPENDIX 1

Table 4(c) Z4(0.4% w/v)

Equilibrium concentration = 8.904×10^{-6} mol dm^{-3}

t/s	$t^{\frac{1}{2}}$/s	F.A.E./%	$\log_{10} c_{Pb}$	c_{Pb}/mol dm^{-3}
5	2.236	95.479	-4.27	5.37×10^{-5}
10	3.162	97.858	-4.522	3.01×10^{-5}
15	3.872	98.472	-4.619	2.40×10^{-5}
20	4.472	98.746	-4.672	2.12×10^{-5}
25	5	98.935	-4.711	1.94×10^{-5}
30	5.477	99.049	-4.737	1.83×10^{-5}
35	5.916	99.128	-4.757	1.74×10^{-5}
40	6.324	99.192	-4.772	1.69×10^{-5}
45	6.708	99.258	-4.79	1.62×10^{-5}
50	7.071	99.306	-4.803	1.57×10^{-5}
55	7.416	99.349	-4.814	1.53×10^{-5}
60	7.745	99.388	-4.825	1.49×10^{-5}
70	8.366	99.453	-4.845	1.42×10^{-5}
80	8.944	99.502	-4.86	1.38×10^{-5}
90	9.486	99.549	-4.874	1.33×10^{-5}
100	10	99.589	-4.888	1.29×10^{-5}
110	10.488	99.625	-4.9	1.25×10^{-5}
120	10.954	99.657	-4.911	1.22×10^{-5}
180	13.416	99.792	-4.96	1.09×10^{-5}
240	15.491	99.882	-4.997	1.01×10^{-5}
300	17.32	99.952	-5.029	9.3×10^{-6}
450	21.213	100.072	-5.088	8.1×10^{-6}
600	24.494	100.143	-5.126	7.4×10^{-6}
750	27.386	100.184	-5.151	7.1×10^{-6}
900	30	100.233	-5.181	6.5×10^{-6}
990	31.464	100.254	-5.196	6.3×10^{-6}

This data is illustrated in figures 5.6(d) and 5.7(c)

APPENDIX 1

Table 4(d) Z4(0.6% w/v)

Equilibrium concentration = 4.614×10^{-6} mol dm^{-3}

t/s	$t^{\frac{1}{2}}$/s	F.A.E./%	$\log_{10} c_{Pb}$	c_{Pb}/mol dm^{-3}
5	2.236	97.366	-4.511	3.08×10^{-5}
10	3.162	98.558	-4.722	1.89×10^{-5}
15	3.872	98.911	-4.812	1.54×10^{-5}
20	4.472	99.102	-4.868	1.35×10^{-5}
25	5	99.227	-4.911	1.22×10^{-5}
30	5.477	99.323	-4.946	1.13×10^{-5}
35	5.916	99.384	-4.97	1.07×10^{-5}
40	6.324	99.449	-4.997	1.01×10^{-5}
45	6.708	99.499	-5.018	9.5×10^{-6}
50	7.071	99.536	-5.036	9.2×10^{-6}
55	7.416	99.572	-5.053	8.8×10^{-6}
60	7.745	99.602	-5.067	8.5×10^{-6}
70	8.366	99.658	-5.097	7.9×10^{-6}
80	8.944	99.706	-5.123	7.5×10^{-6}
90	9.486	99.735	-5.141	7.2×10^{-6}
100	10	99.766	-5.159	6.9×10^{-6}
110	10.488	99.795	-5.178	6.6×10^{-6}
120	10.954	99.817	-5.192	6.4×10^{-6}
180	13.416	99.917	-5.266	5.4×10^{-6}
240	15.491	99.978	-5.316	4.8×10^{-6}
300	17.32	100.018	-5.355	4.4×10^{-6}
450	21.213	100.08	-5.42	3.8×10^{-6}
600	24.494	100.116	-5.463	3.4×10^{-6}
750	27.386	100.143	-5.497	3.1×10^{-6}
900	30	100.157	-5.516	3.0×10^{-6}
990	31.464	100.169	-5.534	2.9×10^{-6}

This data is illustrated in figures 5.6(d) and 5.7(d)

APPENDIX 1

Table 4(e) Z4(0.8% w/v)

Equilibrium concentration = 3.342×10^{-6} mol dm^{-3}

t/s	$t^{\frac{1}{2}}$/s	F.A.E./%	$\log_{10} c_{Pb}$	c_{Pb}/mol dm^{-3}
5	2.236	99.161	-4.933	1.16×10^{-5}
10	3.162	99.601	-5.136	7.3×10^{-6}
15	3.872	99.727	-5.218	6.1×10^{-6}
20	4.472	99.788	-5.265	5.4×10^{-6}
25	5	99.826	-5.295	5.1×10^{-6}
30	5.477	99.852	-5.318	4.8×10^{-6}
35	5.916	99.877	-5.342	4.5×10^{-6}
40	6.324	99.894	-5.358	4.3×10^{-6}
45	6.708	99.907	-5.371	4.2×10^{-6}
50	7.071	99.92	-5.384	4.1×10^{-6}
55	7.416	99.934	-5.4	3.9×10^{-6}
60	7.745	99.943	-5.408	3.9×10^{-6}
70	8.366	99.961	-5.43	3.7×10^{-6}
80	8.944	99.967	-5.436	3.6×10^{-6}
90	9.486	99.985	-5.458	3.4×10^{-6}
100	10	99.996	-5.472	3.3×10^{-6}
110	10.488	100.009	-5.488	3.2×10^{-6}
120	10.954	100.017	-5.5	3.1×10^{-6}
180	13.416	100.059	-5.561	2.7×10^{-6}
240	15.491	100.083	-5.601	2.5×10^{-6}
300	17.32	100.102	-5.634	2.3×10^{-6}
450	21.213	100.133	-5.696	2.0×10^{-6}
600	24.494	100.153	-5.742	1.8×10^{-6}
750	27.386	100.167	-5.776	1.6×10^{-6}
900	30	100.179	-5.809	1.5×10^{-6}
990	31.464	100.184	-5.823	1.5×10^{-6}

This data is illustrated in figures 5.6(d) and 5.7(e)

APPENDIX 1

Table 4(f) Z4(1% w/v)

Equilibrium concentration = 3.011×10^{-6} mol dm^{-3}

t/s	$t^{\frac{1}{2}}$/s	F.A.E./%	$\log_{10} c_{Pb}$	c_{Pb}/mol dm^{-3}
5	2.236	99.467	-5.081	8.2×10^{-6}
10	3.162	99.821	-5.321	4.7×10^{-6}
15	3.872	99.909	-5.408	3.9×10^{-6}
20	4.472	99.954	-5.46	3.4×10^{-6}
25	5	99.981	-5.496	3.1×10^{-6}
30	5.477	100.002	-5.526	2.9×10^{-6}
35	5.916	100.019	-5.551	2.8×10^{-6}
40	6.324	100.032	-5.571	2.6×10^{-6}
45	6.708	100.044	-5.59	2.5×10^{-6}
50	7.071	100.052	-5.605	2.4×10^{-6}
55	7.416	100.06	-5.62	2.3×10^{-6}
60	7.745	100.067	-5.633	2.3×10^{-6}
70	8.366	100.081	-5.658	2.1×10^{-6}
80	8.944	100.09	-5.676	2.1×10^{-6}
90	9.486	100.098	-5.693	2.0×10^{-6}
100	10	100.105	-5.708	1.9×10^{-6}
110	10.488	100.112	-5.723	1.8×10^{-6}
120	10.954	100.117	-5.736	1.8×10^{-6}
180	13.416	100.142	-5.798	1.5×10^{-6}
240	15.491	100.157	-5.84	1.4×10^{-6}
300	17.32	100.169	-5.879	1.3×10^{-6}
450	21.213	100.186	-5.941	1.1×10^{-6}
600	24.494	100.196	-5.979	1.0×10^{-6}
750	27.386	100.201	-6	1.0×10^{-6}
900	30	100.21	-6.038	9×10^{-7}
990	31.464	100.213	-6.053	8×10^{-7}

This data is illustrated in figures 5.6(d) and 5.7(f)

APPENDIX 1

Table 5(a) Z5(0.1% w/v)

Equilibrium concentration = 3.174×10^{-4} mol dm^{-3}

t/s	$t^{\frac{1}{2}}$/s	F.A.E./%	$\log_{10} c_{Pb}$	c_{Pb}/mol dm^{-3}
5	2.236	33.562	-3.113	7.709×10^{-4}
10	3.162	50.152	-3.183	6.561×10^{-4}
15	3.872	59.234	-3.225	5.956×10^{-4}
20	4.472	64.683	-3.254	5.571×10^{-4}
25	5	68.365	-3.273	5.333×10^{-4}
30	5.477	71.365	-3.291	5.116×10^{-4}
35	5.916	72.906	-3.299	5.023×10^{-4}
40	6.324	74.746	-3.31	4.897×10^{-4}
45	6.708	75.893	-3.317	4.819×10^{-4}
50	7.071	76.862	-3.323	4.753×10^{-4}
55	7.416	78.133	-3.332	4.655×10^{-4}
60	7.745	78.76	-3.335	4.623×10^{-4}
70	8.366	80.454	-3.347	4.497×10^{-4}
80	8.944	81.51	-3.354	4.425×10^{-4}
90	9.486	82.402	-3.36	4.365×10^{-4}
100	10	83.281	-3.366	4.305×10^{-4}
110	10.488	84.005	-3.371	4.255×10^{-4}
120	10.954	84.72	-3.375	4.216×10^{-4}
180	13.416	88.042	-3.399	3.990×10^{-4}
240	15.491	90.156	-3.416	3.837×10^{-4}
300	17.32	91.943	-3.429	3.723×10^{-4}
450	21.213	94.518	-3.451	3.539×10^{-4}
600	24.494	96.514	-3.468	3.404×10^{-4}
750	27.386	97.876	-3.479	3.318×10^{-4}
900	30	99.092	-3.491	3.228×10^{-4}
990	31.464	99.635	-3.496	3.191×10^{-4}

This data is illustrated in figures 5.6(e) and 5.7(a)

APPENDIX 1

Table 5(b) Z5(0.2% w/v)

Equilibrium concentration = 8.596×10^{-5} mol dm^{-3}

t/s	$t^{\frac{1}{2}}$/s	F.A.E./%	$\log_{10} c_{Pb}$	c_{Pb}/mol dm^{-3}
5	2.236	62.949	-3.372	4.246×10^{-4}
10	3.162	78.427	-3.548	2.831×10^{-4}
15	3.872	84.456	-3.642	2.280×10^{-4}
20	4.472	87.575	-3.701	1.991×10^{-4}
25	5	89.496	-3.741	1.815×10^{-4}
30	5.477	90.696	-3.767	1.710×10^{-4}
35	5.916	91.205	-3.779	1.663×10^{-4}
40	6.324	92.025	-3.799	1.588×10^{-4}
45	6.708	92.807	-3.82	1.513×10^{-4}
50	7.071	93.259	-3.832	1.472×10^{-4}
55	7.416	93.627	-3.842	1.438×10^{-4}
60	7.745	93.986	-3.852	1.406×10^{-4}
70	8.366	94.509	-3.866	1.361×10^{-4}
80	8.944	94.781	-3.874	1.336×10^{-4}
90	9.486	94.982	-3.88	1.318×10^{-4}
100	10	95.503	-3.897	1.267×10^{-4}
110	10.488	95.788	-3.905	1.244×10^{-4}
120	10.954	96.006	-3.913	1.221×10^{-4}
180	13.416	97.043	-3.947	1.129×10^{-4}
240	15.491	97.6	-3.968	1.076×10^{-4}
300	17.32	97.921	-3.979	1.049×10^{-4}
450	21.213	99.004	-4.022	9.51×10^{-5}
600	24.494	99.608	-4.048	8.95×10^{-5}
750	27.386	99.941	-4.063	8.64×10^{-5}
900	30	100.241	-4.078	8.35×10^{-5}
990	31.464	100.367	-4.084	8.24×10^{-5}

This data is illustrated in figures 5.6(e) and 5.7(b)

APPENDIX 1

Table 5(c) Z5(0.4% w/v)

Equilibrium concentration = 2.119×10^{-5} mol dm^{-3}

t/s	$t^{\frac{1}{2}}$/s	F.A.E./%	$\log_{10} c_{Pb}$	c_{Pb}/mol dm^{-3}
5	2.236	84.163	-3.754	1.761×10^{-4}
10	3.162	92.652	-4.031	9.31×10^{-5}
15	3.872	94.898	-4.148	7.11×10^{-5}
20	4.472	95.908	-4.213	6.12×10^{-5}
25	5	96.446	-4.253	5.58×10^{-5}
30	5.477	96.84	-4.283	5.21×10^{-5}
35	5.916	97.091	-4.304	4.96×10^{-5}
40	6.324	97.286	-4.322	4.76×10^{-5}
45	6.708	97.462	-4.338	4.59×10^{-5}
50	7.071	97.559	-4.347	4.49×10^{-5}
55	7.416	97.715	-4.361	4.35×10^{-5}
60	7.745	97.836	-4.373	4.23×10^{-5}
70	8.366	97.993	-4.39	4.07×10^{-5}
80	8.944	98.116	-4.403	3.95×10^{-5}
90	9.486	98.226	-4.415	3.84×10^{-5}
100	10	98.307	-4.423	3.77×10^{-5}
110	10.488	98.377	-4.431	3.71×10^{-5}
120	10.954	98.446	-4.439	3.63×10^{-5}
180	13.416	98.766	-4.479	3.31×10^{-5}
240	15.491	98.963	-4.504	3.13×10^{-5}
300	17.32	99.107	-4.525	2.98×10^{-5}
450	21.213	99.351	-4.56	2.75×10^{-5}
600	24.494	99.538	-4.59	2.57×10^{-5}
750	27.386	99.662	-4.611	2.44×10^{-5}
900	30	99.764	-4.629	2.34×10^{-5}
990	31.464	99.813	-4.639	2.29×10^{-5}

This data is illustrated in figures 5.6(e) and 5.7(c)

APPENDIX 1

Table 5(d) Z5(0.6% w/v)

Equilibrium concentration = 1.397×10^{-5} mol dm^{-3}

t/s	$t^{\frac{1}{2}}$/s	F.A.E./%	$\log_{10} c_{Pb}$	c_{Pb}/mol dm^{-3}
5	2.236	94.103	-4.143	7.19×10^{-5}
10	3.162	97.189	-4.38	4.16×10^{-5}
15	3.872	98.004	-4.473	3.36×10^{-5}
20	4.472	98.389	-4.526	2.97×10^{-5}
25	5	98.604	-4.558	2.76×10^{-5}
30	5.477	98.791	-4.588	2.58×10^{-5}
35	5.916	98.91	-4.608	2.46×10^{-5}
40	6.324	99.011	-4.625	2.37×10^{-5}
45	6.708	99.066	-4.635	2.31×10^{-5}
50	7.071	99.146	-4.651	2.23×10^{-5}
55	7.416	99.208	-4.663	2.17×10^{-5}
60	7.745	99.253	-4.672	2.12×10^{-5}
70	8.366	99.322	-4.685	2.06×10^{-5}
80	8.944	99.388	-4.699	1.99×10^{-5}
90	9.486	99.439	-4.71	1.94×10^{-5}
100	10	99.484	-4.721	1.90×10^{-5}
110	10.488	99.532	-4.732	1.85×10^{-5}
120	10.954	99.567	-4.74	1.81×10^{-5}
180	13.416	99.725	-4.779	1.66×10^{-5}
240	15.491	99.824	-4.804	1.57×10^{-5}
300	17.32	99.895	-4.824	1.49×10^{-5}
450	21.213	100.026	-4.863	1.37×10^{-5}
600	24.494	100.089	-4.883	1.31×10^{-5}
750	27.386	100.145	-4.903	1.25×10^{-5}
900	30	100.194	-4.919	1.21×10^{-5}
990	31.464	100.219	-4.928	1.18×10^{-5}

This data is illustrated in figures 5.6(e) and 5.7(d)

APPENDIX 1

Table 5(e) Z5(0.8% w/v)

Equilibrium concentration = 8.543×10^{-6} mol dm^{-3}

t/s	$t^{\frac{1}{2}}$/s	F.A.E./%	$\log_{10} c_{Pb}$	c_{Pb}/mol dm^{-3}
5	2.236	95.469	-4.272	5.34×10^{-5}
10	3.162	97.38	-4.463	3.44×10^{-5}
15	3.872	97.952	-4.541	2.87×10^{-5}
20	4.472	98.257	-4.588	2.58×10^{-5}
25	5	98.436	-4.619	2.40×10^{-5}
30	5.477	98.54	-4.639	2.29×10^{-5}
35	5.916	98.619	-4.654	2.21×10^{-5}
40	6.324	98.71	-4.672	2.12×10^{-5}
45	6.708	98.768	-4.684	2.07×10^{-5}
50	7.071	98.811	-4.692	2.03×10^{-5}
55	7.416	98.858	-4.703	1.98×10^{-5}
60	7.745	98.899	-4.711	1.94×10^{-5}
70	8.366	98.948	-4.722	1.89×10^{-5}
80	8.944	98.992	-4.733	1.84×10^{-5}
90	9.486	99.038	-4.743	1.81×10^{-5}
100	10	99.068	-4.75	1.77×10^{-5}
110	10.488	99.096	-4.758	1.74×10^{-5}
120	10.954	99.14	-4.768	1.71×10^{-5}
180	13.416	99.263	-4.801	1.58×10^{-5}
240	15.491	99.342	-4.823	1.50×10^{-5}
300	17.32	99.403	-4.84	1.44×10^{-5}
450	21.213	99.519	-4.877	1.32×10^{-5}
600	24.494	99.583	-4.897	1.26×10^{-5}
750	27.386	99.637	-4.916	1.21×10^{-5}
900	30	99.684	-4.934	1.16×10^{-5}
990	31.464	99.711	-4.943	1.14×10^{-5}

This data is illustrated in figures 5.6(e) and 5.7(e)

APPENDIX 1

Table 5(f) Z5(1% w/v)

Equilibrium concentration = 6.444×10^{-6} mol dm^{-3}

t/s	t /s	F.A.E./%	$\log_{10} c_{Pb}$	c_{Pb}/mol dm^{-3}
5	2.236	97.238	-4.471	3.38×10^{-5}
10	3.162	98.289	-4.63	2.34×10^{-5}
15	3.872	98.644	-4.702	1.98×10^{-5}
20	4.472	98.812	-4.74	1.81×10^{-5}
25	5	98.939	-4.77	1.69×10^{-5}
30	5.477	99.027	-4.793	1.61×10^{-5}
35	5.916	99.078	-4.808	1.55×10^{-5}
40	6.324	99.132	-4.823	1.50×10^{-5}
45	6.708	99.17	-4.834	1.46×10^{-5}
50	7.071	99.193	-4.84	1.44×10^{-5}
55	7.416	99.223	-4.849	1.41×10^{-5}
60	7.745	99.252	-4.858	1.38×10^{-5}
70	8.366	99.29	-4.871	1.34×10^{-5}
80	8.944	99.318	-4.879	1.32×10^{-5}
90	9.486	99.342	-4.888	1.29×10^{-5}
100	10	99.363	-4.894	1.27×10^{-5}
110	10.488	99.384	-4.902	1.25×10^{-5}
120	10.954	99.404	-4.908	1.23×10^{-5}
180	13.416	99.49	-4.939	1.15×10^{-5}
240	15.491	99.547	-4.961	1.09×10^{-5}
300	17.32	99.582	-4.975	1.05×10^{-5}
450	21.213	99.651	-5.004	9.9×10^{-6}
600	24.494	99.7	-5.027	9.3×10^{-6}
750	27.386	99.736	-5.043	9.1×10^{-6}
900	30	99.761	-5.055	8.8×10^{-6}
990	31.464	99.782	-5.066	8.5×10^{-6}

This data is illustrated in figures 5.6(e) and 5.7(f)

APPENDIX 2

Inorganic lead ion exchange data

APPENDIX 2

Table 1 Pb/NaZ1 exchange at T_N = 0.05g equiv. dm^{-3}

Sol.Phase Conc./ ($x10^{-2}$ mol dm^{-3})		(a)	Cryst. Phase Conc./(mol kg^{-1})		(b)		(c)	
		T_N/			Total/	Percentage	Isotherm data	
Pb^{2+}	Na^+	($x10^{-2}$g equiv. dm^{-3})	Pb^{2+}	Na^+	(equiv. kg^{-1})	recovery	E_{Pb}	$\bar{E}_{Pb}$
-	4.540	4.540	-	4.216	4.216	88.09	-	-
$8.953x10^{-6}$	4.820	4.820	0.102	4.075	4.279	89.40	$3.715x10^{-6}$	0.048
$1.794x10^{-5}$	4.820	4.820	0.210	3.832	4.252	88.84	$7.444x10^{-6}$	0.099
$1.919x10^{-5}$	4.820	4.820	0.105	4.127	4.337	90.61	$7.963x10^{-6}$	0.048
$2.169x10^{-5}$	4.881	4.881	0.052	4.260	4.364	91.18	$8.887x10^{-6}$	0.024
$2.775x10^{-5}$	4.746	4.746	0.447	3.601	4.495	93.91	$1.169x10^{-5}$	0.199
$5.332x10^{-5}$	4.746	4.746	0.886	2.780	4.552	95.11	$2.246x10^{-5}$	0.389
$6.837x10^{-5}$	4.746	4.746	1.271	2.018	4.560	95.27	$2.881x10^{-5}$	0.558
$2.542x10^{-4}$	4.728	4.729	1.762	1.131	4.655	97.26	$1.075x10^{-4}$	0.757
$6.228x10^{-3}$	4.667	4.680	2.233	0.359	4.825	100.81	$2.662x10^{-3}$	0.926
0.089	4.304	4.482	2.398	0.084	4.880	101.96	0.040	1.002
0.237	3.951	4.425	2.527	0.051	5.105	106.66	0.107	1.056
0.406	3.518	4.330	2.548	0.039	5.135	107.29	0.188	1.065
0.628	3.578	4.834	2.706	0.032	5.444	113.74	0.260	1.131
0.822	2.624	4.268	2.791	0.031	5.613	117.27	0.385	1.166

(a) refer to figure 5.20(a); (b) refer to figure 5.21(a); (c) data plotted in figure 5.8

APPENDIX 2

Table 2 Pb/NaZ2 exchange at T_N = 0.05g equiv. dm^{-3}

Sol.Phase Conc./ ($x10^{-2}$ mol dm^{-3})		(a)	Cryst. Phase Conc./(mol kg^{-1})		(b)		(c)	
		T_N/			Total/	Percentage	Isotherm data	
Pb^{2+}	Na^+	($x10^{-2}$g equiv. dm^{-3})	Pb^{2+}	Na^+	(equiv. kg^{-1})	recovery	E_{Pb}	$\bar{E}_{Pb}$
-	4.645	4.645	-	3.527	3.527	83.58	-	-
$7.004x10^{-5}$	4.984	4.984	0.231	3.796	4.258	100.91	$2.811x10^{-5}$	0.109
$1.372x10^{-4}$	4.954	4.954	0.427	3.247	4.101	97.19	$5.539x10^{-5}$	0.208
$1.420x10^{-4}$	5.042	5.042	0.108	3.891	4.107	97.33	$5.632x10^{-5}$	0.053
$1.789x10^{-4}$	5.042	5.042	0.059	3.919	4.037	95.67	$7.096x10^{-5}$	0.029
$2.106x10^{-4}$	5.042	5.042	0.108	3.883	4.099	97.14	$8.353x10^{-5}$	0.053
$6.274x10^{-4}$	5.042	5.043	0.868	2.470	4.206	99.68	$2.488x10^{-4}$	0.413
$2.869x10^{-3}$	4.587	4.593	1.302	1.647	4.251	100.74	$1.249x10^{-3}$	0.613
$5.890x10^{-3}$	4.587	4.599	1.613	0.703	3.929	93.11	$2.562x10^{-3}$	0.821
0.048	4.412	4.508	1.966	0.286	4.218	99.96	0.021	0.932
0.288	3.961	4.537	2.144	0.156	4.444	105.32	0.127	1.016
0.434	3.532	4.400	2.248	0.128	4.624	109.58	0.197	1.066
0.617	3.074	4.308	2.335	0.100	4.770	113.04	0.286	1.107
0.843	2.596	4.282	2.344	0.089	4.777	113.21	0.394	1.111
1.074	2.108	4.256	2.405	0.075	4.885	115.77	0.505	1.140

(a) refer to figure 5.20(a); (b) refer to figure 5.21(a); (c) data plotted in figure 5.9

APPENDIX 2

Table 3 Pb/NaZ3 exchange at T_N = 0.05g equiv. dm^{-3}

Sol.Phase Conc./ ($x10^{-2}$ mol dm^{-3})		(a)	Cryst. Phase Conc./(mol kg^{-1})		(b)		(c)	
		T_N/			Total/	Percentage	Isotherm data	
Pb^{2+}	Na^+	($x10^{-2}$g equiv. dm^{-3})	Pb^{2+}	Na^+	(equiv. kg^{-1})	recovery	E_{Pb}	$\bar{E}_{Pb}$
-	4.738	4.738	-	3.680	3.680	97.85	-	-
$3.341x10^{-5}$	5.071	5.071	0.052	3.656	3.760	99.99	$1.318x10^{-5}$	0.028
$5.356x10^{-5}$	5.071	5.071	0.105	3.604	3.814	101.42	$2.112x10^{-5}$	0.055
$6.158x10^{-5}$	5.071	5.071	0.109	3.587	3.805	101.18	$2.429x10^{-5}$	0.057
$6.938x10^{-5}$	5.042	5.042	0.207	3.550	3.964	105.40	$2.752x10^{-5}$	0.104
$4.416x10^{-4}$	4.620	4.621	0.423	2.387	3.233	85.97	$1.911x10^{-4}$	0.262
$1.134x10^{-3}$	4.620	4.622	0.738	2.004	3.480	92.53	$4.907x10^{-4}$	0.424
$4.350x10^{-3}$	4.620	4.629	1.102	1.307	3.511	93.36	$1.880x10^{-3}$	0.628
0.059	4.444	4.562	1.529	0.572	3.630	96.52	0.026	0.842
0.260	4.140	4.660	1.685	0.348	3.718	98.86	0.112	0.906
0.429	3.756	4.614	1.791	0.303	3.885	103.30	0.186	0.922
0.632	3.409	4.673	1.685	0.288	3.658	97.27	0.270	0.921
0.910	2.772	4.592	1.794	0.235	3.823	101.65	0.396	0.939
1.110	2.365	4.585	1.710	0.206	3.626	96.42	0.484	0.943
1.313	1.945	4.571	1.793	0.193	3.779	100.48	0.574	0.949
1.899	1.089	4.887	2.044	0.154	4.242	112.80	0.777	1.087

APPENDIX 2

Table 3 (cont.) Pb/NaZ3 exchange at T_N = 0.05g equiv. dm^{-3}

Sol.Phase Conc./ ($x10^{-2}$ mol dm^{-3})		(a) T_N/	Cryst. Phase Conc./(mol kg^{-1})		(b) Total/ (equiv. kg^{-1})	Percentage recovery	(c) Isotherm data	
Pb^{2+}	Na^+	($x10^{-2}$g equiv. dm^{-3})	Pb^{2+}	Na^+			E_{Pb}	$\bar{E}_{Pb}$
2.202	0.557	4.961	2.036	0.108	4.180	111.15	0.888	1.083
2.313	0.328	4.954	2.120	0.091	4.331	115.16	0.934	1.127
2.363	0.244	4.970	2.013	0.072	4.098	108.97	0.951	1.071
2.399	0.218	5.016	1.917	0.087	3.921	104.26	0.957	1.019

(a) refer to figure 5.20(a)

(b) refer to figure 5.21(a)

(c) data plotted in figure 5.10

APPENDIX 2

Table 4 Pb/NaZ4 exchange at T_N = 0.05g equiv. dm^{-3}

Sol.Phase Conc./ ($x10^{-2}$ mol dm^{-3})		(a) T_N/	Cryst. Phase Conc./(mol kg^{-1})		Total/ (equiv. kg^{-1})	(b) Percentage recovery	(c) Isotherm data	
Pb^{2+}	Na^+	($x10^{-2}$g equiv. dm^{-3})	Pb^{2+}	Na^+			E_{Pb}	$\bar{E}_{Pb}$
-	4.884	4.884	-	3.430	3.430	98.89	-	-
$3.707x10^{-5}$	5.071	5.071	0.053	3.312	3.418	98.54	$1.462x10^{-5}$	0.031
$5.612x10^{-5}$	5.071	5.071	0.105	3.173	3.383	97.53	$2.213x10^{-5}$	0.062
$6.636x10^{-5}$	5.071	5.071	0.110	3.210	3.430	98.89	$2.617x10^{-5}$	0.064
$1.751x10^{-4}$	5.042	5.042	0.211	2.996	3.418	98.54	$6.945x10^{-5}$	0.124
$5.309x10^{-4}$	5.042	5.043	0.439	2.571	3.449	99.43	$2.106x10^{-4}$	0.255
$4.269x10^{-3}$	5.042	5.051	0.897	1.759	3.553	102.43	$1.691x10^{-3}$	0.505
0.031	4.646	4.708	1.277	0.894	3.448	99.41	0.013	0.741
0.194	4.354	4.742	1.403	0.620	3.426	98.77	0.082	0.819
0.416	3.962	4.794	1.426	0.502	3.354	96.70	0.174	0.850
0.592	3.637	4.821	1.489	0.498	3.476	100.21	0.246	0.857
0.872	3.074	4.818	1.534	0.435	3.503	100.99	0.362	0.876
1.112	2.550	4.774	1.572	0.423	3.567	102.84	0.466	0.881
1.326	2.150	4.802	1.546	0.384	3.476	100.21	0.552	0.890
1.571	1.621	4.763	1.819	0.367	3.605	103.93	0.660	0.898
2.015	0.923	4.953	1.593	0.244	3.430	98.89	0.814	0.929

APPENDIX 2

Table 4 (cont.) Pb/NaZ4 exchange at T_N = 0.05g equiv. dm^{-3}

Sol.Phase Conc./ ($x10^{-2}$ mol dm^{-3})		(a) T_N/	Cryst. Phase Conc./(mol kg^{-1})		Total/ (equiv. kg^{-1})	(b) Percentage recovery	(c) Isotherm data	
Pb^{2+}	Na^+	($x10^{-2}$g equiv. dm^{-3})	Pb^{2+}	Na^+			E_{Pb}	$\bar{E}_{Pb}$
2.227	0.529	4.983	1.774	0.177	3.725	107.39	0.894	1.023
2.338	0.325	5.001	1.748	0.120	3.616	104.25	0.935	1.007
2.389	0.218	4.996	1.687	0.125	3.499	100.97	0.956	0.964
2.409	0.212	5.030	1.824	0.097	3.745	102.43	0.958	1.052

(a) refer to figure 5.20(a)

(b) refer to figure 5.21(a)

(c) data plotted in figure 5.11

APPENDIX 2

Table 5 Pb/NaZ5 exchange at T_N = 0.05g equiv. dm^{-3}

Sol.Phase Conc./ ($x10^{-2}$ mol dm^{-3})		(a)	Cryst. Phase Conc./(mol kg^{-1})		(b)		(c)	
		T_N/			Total/	Percentage	Isotherm data	
Pb^{2+}	Na^+	($x10^{-2}$g equiv. dm^{-3})	Pb^{2+}	Na^+	(equiv. kg^{-1})	recovery	E_{Pb}	$\bar{E}_{Pb}$
-	5.162	5.162	-	2.809	2.809	87.75	-	-
$7.619x10^{-5}$	5.071	5.071	0.059	2.755	2.873	89.73	$3.005x10^{-5}$	0.041
$1.569x10^{-4}$	5.071	5.071	0.106	2.700	2.912	90.94	$6.188x10^{-5}$	0.073
$1.716x10^{-4}$	5.071	5.071	0.108	2.667	2.883	90.04	$6.767x10^{-5}$	0.075
$5.126x10^{-4}$	5.042	5.043	0.222	2.479	2.923	91.29	$2.033x10^{-4}$	0.152
$1.710x10^{-3}$	5.071	5.074	0.489	1.893	2.871	89.66	$6.740x10^{-4}$	0.341
0.019	5.071	5.109	0.795	1.274	2.864	89.45	$7.438x10^{-3}$	0.555
0.084	4.747	4.915	1.075	0.917	3.067	95.79	0.034	0.701
0.338	4.195	4.871	1.161	0.743	3.065	95.72	0.139	0.758
0.579	3.784	4.942	1.158	0.688	3.004	93.82	0.234	0.771
0.792	3.392	4.976	1.169	0.698	3.036	94.82	0.318	0.770
1.025	2.922	4.972	1.244	0.657	3.145	98.22	0.412	0.791
1.289	2.394	4.972	1.208	0.630	3.046	95.13	0.519	0.793
1.528	1.884	4.940	1.230	0.599	3.059	95.54	0.619	0.804
1.766	1.403	4.935	1.250	0.559	3.059	95.54	0.716	0.817
2.121	0.699	4.941	1.429	0.508	3.366	105.12	0.859	0.849

APPENDIX 2

Table 5 (cont.) Pb/NaZ5 exchange at T_N = 0.05g equiv. dm^{-3}

Sol.Phase Conc./ ($x10^{-2}$ mol dm^{-3})		(a) T_N/	Cryst. Phase Conc./(mol kg^{-1})		(b) Total/ (equiv. kg^{-1})	Percentage recovery	(c) Isotherm data	
Pb^{2+}	Na^+	($x10^{-2}$g equiv. dm^{-3})	Pb^{2+}	Na^+			E_{Pb}	$\bar{E}_{Pb}$
2.232	0.459	4.923	1.431	0.337	3.199	99.91	0.907	0.895
2.323	0.338	4.984	1.492	0.317	3.299	103.03	0.932	0.905
2.358	0.255	4.971	1.464	0.220	3.148	98.32	0.949	0.930
2.419	0.172	5.010	1.608	0.171	3.387	105.78	0.966	1.004
2.444	0.153	5.041	1.599	0.149	3.347	104.53	0.970	0.956

(a) refer to figure 5.20(a)

(b) refer to figure 5.21(a)

(c) data plotted in figure 5.12

APPENDIX 2

Table 6 Pb/NaZl exchange at T_N = 0.1g equiv. dm^{-3}

Sol.Phase Conc./ ($x10^{-2}$ mol dm^{-3})		(a)	Cryst. Phase Conc./(mol kg^{-1})		(b) Total/ (equiv. kg^{-1})	Percentage recovery	(c) Isotherm data	
Pb^{2+}	Na^+	T_N/ ($x10^{-2}$g equiv. dm^{-3})	Pb^{2+}	Na^+			E_{Pb}	$\bar{E}_{Pb}$
-	10.055	10.055	-	4.146	4.146	92.27	-	-
$1.943x10^{-5}$	9.684	9.684	0.108	4.191	4.407	92.08	$4.013x10^{-6}$	0.049
$1.083x10^{-5}$	9.562	9.562	0.216	4.034	4.466	93.31	$2.265x10^{-6}$	0.097
$3.417x10^{-5}$	9.562	9.562	0.208	3.853	4.269	89.19	$7.147x10^{-6}$	0.098
$3.471x10^{-5}$	9.562	9.562	0.416	3.499	4.331	90.49	$7.260x10^{-6}$	0.192
$7.801x10^{-5}$	9.396	9.396	0.909	2.801	4.619	96.51	$1.660x10^{-5}$	0.394
$8.180x10^{-4}$	9.958	9.960	1.631	1.179	4.441	92.79	$1.643x10^{-4}$	0.735
0.081	9.958	10.012	2.258	0.141	4.657	97.30	0.016	0.970
0.419	8.738	9.576	2.505	0.050	5.060	105.72	0.088	1.047
0.832	7.592	9.256	2.827	0.038	5.692	118.92	0.180	1.181
1.274	6.560	9.108	2.859	0.038	5.756	120.26	0.280	0.195
1.812	5.474	9.098	2.743	0.028	5.514	115.20	0.398	1.146
2.206	4.422	8.834	2.753	0.025	5.531	115.56	0.499	1.150
2.672	3.472	8.816	2.926	0.023	5.875	122.75	0.606	1.223
3.182	2.485	8.849	2.857	0.020	5.734	119.80	0.719	1.193

(a) refer to figure 5.20(b); (b) refer to figures 5.21(b) and 5.24; (c) data plotted in figure 5.13

APPENDIX 2

Table 7 Pb/NaZ2 exchange at T_N = 0.1g equiv. dm^{-3}

Sol.Phase Conc./ ($x10^{-2}$ mol dm^{-3})		(a)	Cryst. Phase Conc./(mol kg^{-1})		Total/ (equiv. kg^{-1})	Percentage recovery	(b) Isotherm data	(c)
Pb^{2+}	Na^+	T_N/ ($x10^{-2}$g equiv. dm^{-3})	Pb^{2+}	Na^+			E_{Pb}	$\bar{E}_{Pb}$
-	9.530	9.530	-	3.726	3.726	88.29	-	-
$4.509x10^{-5}$	9.684	9.684	0.207	3.452	3.866	91.62	$9.312x10^{-6}$	0.107
$5.408x10^{-5}$	9.562	9.562	0.210	3.498	3.918	92.85	$1.131x10^{-5}$	0.107
$1.184x10^{-4}$	9.684	9.684	0.103	3.703	3.909	92.64	$2.445x10^{-5}$	0.053
$1.204x10^{-4}$	9.684	9.684	0.433	3.172	4.038	95.70	$2.487x10^{-5}$	0.215
$5.068x10^{-4}$	9.530	9.531	1.838	2.368	6.044	143.24	$1.064x10^{-4}$	0.608
0.200	9.530	9.570	2.115	0.927	5.157	122.22	$4.180x10^{-3}$	1.003
0.333	9.130	9.796	2.415	1.228	6.058	143.57	0.068	1.145
0.709	8.126	9.544	2.312	0.893	5.517	130.75	0.149	1.096
1.154	7.174	9.482	2.311	0.712	5.334	126.41	0.243	1.095
1.638	6.143	9.419	2.320	0.724	5.364	127.12	0.347	1.100
2.086	5.126	9.298	2.524	0.523	5.571	132.03	0.449	1.196
2.515	4.191	9.221	2.960	0.286	6.206	147.08	0.546	1.403
3.010	3.235	9.225	2.573	0.316	5.462	129.44	0.651	1.220
3.520	2.126	9.166	2.519	0.418	5.456	129.30	0.768	1.194

(a) refer to figure 5.20(b); (b) refer to figure 5.21(b); (c) data plotted in figure 5.14

APPENDIX 2

Table 8 Pb/NaZ3 exchange at T_N = 0.1g equiv. dm^{-3}

Sol.Phase Conc./ ($x10^{-2}$ mol dm^{-3})		(a) T_N/	Cryst. Phase Conc./(mol kg^{-1})		Total/ (equiv. kg^{-1})	Percentage recovery	(b) Isotherm data	(c)
Pb^{2+}	Na^+	($x10^{-2}$g equiv. dm^{-3})	Pb^{2+}	Na^+			E_{Pb}	$\bar{E}_{Pb}$
-	10.141	10.141	-	3.754	3.754	99.84	-	-
$1.024x10^{-4}$	9.684	9.684	0.101	3.470	3.672	97.64	$2.115x10^{-5}$	0.055
$1.874x10^{-4}$	9.562	9.562	0.201	3.175	3.577	95.11	$3.920x10^{-5}$	0.112
$2.208x10^{-4}$	9.562	9.562	0.213	3.118	3.544	94.24	$4.618x10^{-5}$	0.120
$6.216x10^{-4}$	9.562	9.563	0.421	2.732	3.574	95.03	$1.300x10^{-4}$	0.236
$4.374x10^{-3}$	9.865	9.874	0.865	2.079	3.809	101.28	$8.860x10^{-4}$	0.454
0.087	9.707	9.881	1.551	0.848	3.950	105.03	0.018	0.785
0.440	8.935	9.815	1.771	0.793	4.335	115.27	0.090	0.817
0.920	7.974	9.814	1.842	0.358	4.042	107.48	0.188	0.911
1.340	7.198	9.878	1.893	0.311	4.097	108.94	0.271	1.007
1.869	5.929	9.667	1.904	0.254	4.062	108.01	0.387	1.013
2.358	4.943	9.659	2.043	0.234	4.320	114.87	0.488	1.086
2.879	3.980	9.738	2.163	0.216	4.542	120.77	0.591	1.150
3.348	2.957	9.653	2.148	0.165	4.461	118.62	0.694	1.142
3.788	2.010	9.586	2.127	0.127	4.381	116.49	0.790	1.131

(a) refer to figure 5.20(b); (b) refer to figure 5.21(b); (c) data plotted in figure 5.15

APPENDIX 2

Table 9 Pb/NaZ4 exchange at T_N = 0.1g equiv. dm^{-3}

Sol.Phase Conc./ ($x10^{-2}$ mol dm^{-3})		(a)	Cryst. Phase Conc./(mol kg^{-1})		(b)		(c)	
		T_N/			Total/	Percentage	Isotherm data	
Pb^{2+}	Na^+	($x10^{-2}$g equiv. dm^{-3})	Pb^{2+}	Na^+	(equiv. kg^{-1})	recovery	E_{Pb}	$\bar{E}_{Pb}$
-	10.060	10.060	-	3.197	3.197	92.16	-	-
$2.435x10^{-4}$	9.978	9.979	0.112	3.075	3.299	95.11	$4.880x10^{-5}$	0.068
$5.043x10^{-4}$	9.857	9.858	0.216	2.907	3.339	96.26	$1.023x10^{-4}$	0.129
$5.473x10^{-4}$	9.857	9.858	0.212	2.676	3.100	89.37	$1.110x10^{-4}$	0.137
$2.646x10^{-3}$	9.737	9.742	0.439	2.353	3.231	93.15	$5.432x10^{-4}$	0.272
0.015	10.060	10.090	0.837	1.651	3.325	95.86	$2.973x10^{-3}$	0.504
0.249	9.501	9.999	1.384	0.827	3.595	103.64	0.050	0.770
0.677	8.576	9.993	1.474	0.614	3.562	102.69	0.136	0.828
1.141	7.693	9.975	1.355	0.443	3.153	90.90	0.229	0.860
1.621	6.786	10.028	1.534	0.507	3.575	103.07	0.323	0.858
2.101	5.739	9.941	1.555	0.493	3.603	103.87	0.422	0.863
2.576	4.709	9.861	1.589	0.429	3.607	103.99	0.523	0.881
3.076	3.819	9.971	1.603	0.377	3.583	103.30	0.617	0.895
3.560	2.813	9.933	1.660	0.339	3.659	105.49	0.717	0.907
3.995	1.927	9.917	1.686	0.304	3.676	105.98	0.806	0.917
4.575	0.867	10.017	1.791	0.188	3.770	108.69	0.914	1.033

APPENDIX 2

Table 9 (cont.) Pb/NaZ4 exchange at T_N = 0.1g equiv. dm^{-3}

Sol.Phase Conc./ ($x10^{-2}$ mol dm^{-3})		(a) T_N/	Cryst. Phase Conc./(mol kg^{-1})		Total/ (equiv. kg^{-1})	Percentage recovery	(b) Isotherm data	(c)
Pb^{2+}	Na^+	($x10^{-2}$g equiv. dm^{-3})	Pb^{2+}	Na^+			E_{Pb}	$\bar{E}_{Pb}$
4.676	0.639	9.991	1.883	0.177	3.943	113.68	0.936	1.086
4.777	0.473	10.027	1.901	0.130	3.932	113.36	0.953	1.096
4.833	0.345	10.011	1.927	0.135	3.989	115.00	0.966	1.111
4.909	0.206	10.024	1.913	0.290	4.116	118.66	0.980	1.103
4.936	0.149	10.021	2.052	0.112	4.216	121.55	0.985	1.183

(a) refer to figure 5.20(b)

(b) refer to figure 5.21(b)

(c) data plotted in figure 5.16

APPENDIX 2

Table 10 Pb/NaZ5 exchange at T_N = 0.1g equiv. dm^{-3}

Sol.Phase Conc./ ($x10^{-2}$ mol dm^{-3})		(a)	Cryst. Phase Conc./(mol kg^{-1})		(b)		(c)	
		T_N/			Total/	Percentage	Isotherm data	
Pb^{2+}	Na^+	($x10^{-2}$g equiv. dm^{-3})	Pb^{2+}	Na^+	(equiv. kg^{-1})	recovery	E_{Pb}	$\bar{E}_{Pb}$
-	10.041	10.041	-	2.768	2.768	86.45	-	-
$9.899x10^{-4}$	10.223	10.224	0.114	2.558	2.786	87.01	$1.936x10^{-4}$	0.082
$2.291x10^{-3}$	9.978	9.983	0.229	2.365	2.823	88.16	$4.590x10^{-4}$	0.162
$2.757x10^{-3}$	9.857	9.863	0.229	2.253	2.711	84.67	$5.591x10^{-4}$	0.169
$8.473x10^{-3}$	9.857	9.874	0.455	1.954	2.864	89.45	$1.716x10^{-3}$	0.318
0.053	9.820	9.926	0.781	1.444	3.006	93.88	0.011	0.520
0.383	9.578	10.344	1.056	0.891	3.003	93.79	0.074	0.703
0.858	8.702	10.418	1.137	0.752	3.026	94.50	0.165	0.751
1.315	7.352	9.982	1.151	0.718	3.020	94.32	0.263	0.762
1.808	6.374	9.990	1.182	0.707	3.071	95.91	0.362	0.770
2.278	5.398	9.954	1.203	0.670	3.076	96.07	0.458	0.782
2.772	4.320	9.864	1.218	0.635	3.071	95.91	0.562	0.793
3.283	3.450	10.016	1.237	0.600	3.074	96.00	0.656	0.805
3.752	2.258	9.762	1.274	0.574	3.122	97.50	0.769	0.816
4.257	1.325	9.839	1.602	0.477	3.681	114.96	0.865	1.001
4.560	0.736	9.856	1.408	0.364	3.180	99.31	0.925	0.886

APPENDIX 2

Table 10 (cont.) Pb/NaZ5 exchange at T_N = 0.1g equiv. dm^{-3}

Sol.Phase Conc./ ($x10^{-2}$ mol dm^{-3})		(a)	Cryst. Phase Conc./(mol kg^{-1})		Total/ (equiv. kg^{-1})	Percentage recovery	(b) Isotherm data	(c)
Pb^{2+}	Na^+	T_N/ ($x10^{-2}$g equiv. dm^{-3})	Pb^{2+}	Na^+			E_{Pb}	$\bar{E}_{Pb}$
4.717	0.476	9.910	1.465	0.288	3.218	100.50	0.952	0.911
4.803	0.368	9.974	1.490	0.251	3.231	100.91	0.963	0.922
4.899	0.253	10.051	1.627	0.199	3.453	107.84	0.975	1.016
4.929	0.188	10.046	1.694	0.136	3.524	110.06	0.981	1.058
4.939	0.172	10.050	1.671	0.126	3.468	108.31	0.983	1.044

(a) refer to figure 5.20(b)

(b) refer to figure 5.21(b)

(c) data plotted in figure 5.17

APPENDIX 2

Table 11 Pb/CaX exchange at T_N = 0.1g equiv. dm^{-3}

Sol.Phase Conc./ ($x10^{-2}$ mol dm^{-3})		(a)	Cryst. Phase Conc./(mol kg^{-1})		(b)		(c)	
		T_N/			Total/	Percentage	Isotherm data	
Pb^{2+}	Ca^{2+}	($x10^{-2}$g equiv. dm^{-3})	Pb^{2+}	Na^{+}	(equiv. kg^{-1})	recovery	E_{Pb}	$\bar{E}_{Pb}$
-	5.100	10.200	-	2.072	4.144	90.01	-	-
$1.375x10^{-4}$	5.090	10.180	0.107	0.781	1.776	38.58	$2.701x10^{-5}$	0.120
$1.689x10^{-4}$	5.100	10.200	0.203	0.901	2.208	47.96	$3.312x10^{-5}$	0.184
$3.079x10^{-4}$	5.090	10.181	0.214	1.563	3.554	77.20	$6.049x10^{-5}$	0.121
$6.655x10^{-4}$	5.090	10.181	0.436	1.406	3.684	80.02	$1.307x10^{-4}$	0.237
$6.158x10^{-3}$	5.045	10.102	0.862	1.146	4.016	87.23	$1.219x10^{-3}$	0.429
0.079	4.980	10.118	1.460	0.586	4.092	88.88	0.016	0.714
0.102	4.930	10.064	1.595	0.562	4.314	93.70	0.020	0.739
0.400	4.540	9.880	1.835	0.448	4.566	99.18	0.081	0.804
0.780	4.100	9.760	2.116	0.433	5.098	110.73	0.160	0.830
1.170	3.655	9.650	2.107	0.382	4.978	108.13	0.243	0.847
1.815	3.090	9.810	2.244	0.404	5.296	115.03	0.370	0.847
2.180	2.620	9.600	2.237	0.401	5.276	114.60	0.454	0.848
2.630	2.140	9.540	2.283	0.400	5.366	116.55	0.551	0.851
3.200	1.600	9.600	2.283	0.404	5.374	116.73	0.667	0.850
3.560	1.115	9.350	2.257	0.408	5.330	115.77	0.762	0.847

APPENDIX 2

Table 11 (cont.) Pb/CaX exchange at T_N = 0.1g equiv. dm^{-3}

Sol.Phase Conc./ ($x10^{-2}$ mol dm^{-3})		(a)	Cryst. Phase Conc./(mol kg^{-1})		Total/ (equiv. kg^{-1})	Percentage recovery	(b) Isotherm data	(c)
Pb^{2+}	Ca^{2+}	T_N/ ($x10^{-2}$g equiv. dm^{-3})	Pb^{2+}	Na^{+}			E_{Pb}	$\bar{E}_{Pb}$
4.650	0.278	9.856	2.292	0.399	5.382	116.90	0.944	0.852
4.815	0.140	9.910	2.235	0.386	5.242	113.86	0.972	0.853
4.860	0.120	9.960	2.281	0.395	5.352	116.25	0.976	0.852
4.805	$1.638x10^{-3}$	9.613	2.201	0.291	4.984	108.26	1.000	0.883
4.805	$1.678x10^{-3}$	9.613	2.190	0.284	4.948	107.47	1.000	0.885
4.691	$1.773x10^{-3}$	9.386	1.945	0.087	4.064	88.27	1.000	0.957
4.691	$1.773x10^{-3}$	9.386	1.897	0.081	3.956	85.93	1.000	0.959
4.987	$2.000x10^{-3}$	9.978	2.365	0.268	5.266	114.38	1.000	1.027
4.987	$2.000x10^{-3}$	9.978	2.395	0.300	5.390	117.07	1.000	1.040

(a) refer to figure 5.24

(b) data plotted in figure 5.22

APPENDIX 2

Table 12 Pb/NaA exchange at T_N = 0.1g equiv. dm^{-3}

Sol.Phase Conc./ ($x10^{-2}$ mol dm^{-3})		(a)	Cryst. Phase Conc./(mol kg^{-1})		(b)		(c)	
		T_N/			Total/	Percentage	Isotherm data	
Pb^{2+}	Na^+	($x10^{-2}$g equiv. dm^{-3})	Pb^{2+}	Na^+	(equiv. kg^{-1})	recovery	E_{Pb}	$\bar{E}_{Pb}$
-	9.740	9.740	-	4.805	4.805	88.51	-	-
$1.425x10^{-5}$	10.010	10.010	0.212	4.216	4.640	85.46	$2.847x10^{-6}$	0.091
$4.144x10^{-5}$	9.740	9.740	0.211	4.245	4.667	85.96	$8.509x10^{-6}$	0.090
$5.019x10^{-5}$	10.010	10.010	1.369	2.588	5.326	98.10	$1.003x10^{-5}$	0.514
$6.371x10^{-5}$	10.010	10.010	0.101	4.356	4.558	83.95	$1.273x10^{-5}$	0.044
$8.977x10^{-5}$	9.740	9.740	0.376	3.765	4.517	83.20	$1.843x10^{-5}$	0.167
$3.769x10^{-5}$	9.740	9.741	1.704	1.908	5.316	97.91	$7.739x10^{-5}$	0.641
0.058	9.470	9.586	2.417	0.417	5.251	96.71	0.012	0.921
0.434	8.805	9.673	2.652	0.203	5.507	101.43	0.090	0.963
0.848	7.914	9.610	2.673	0.136	5.482	100.97	0.177	0.975
1.345	6.946	9.636	2.763	0.100	5.626	103.62	0.279	1.018
1.892	6.032	9.816	2.744	0.078	5.566	102.52	0.386	1.011
2.346	5.303	9.995	2.773	0.061	5.607	103.27	0.489	1.022
2.806	4.117	9.729	2.724	0.056	5.504	101.37	0.577	1.003
3.337	3.266	9.940	2.805	0.049	5.659	104.23	0.671	1.003
4.168	1.647	9.983	2.880	0.046	5.806	106.94	0.835	1.061

APPENDIX 2

Table 12 (cont.) Pb/NaA exchange at T_N = 0.1g equiv. dm^{-3}

Sol.Phase Conc./ ($x10^{-2}$ mol dm^{-3})		(a)	Cryst. Phase Conc./(mol kg^{-1})		(b)		(c)	
		T_N/			Total/	Percentage	Isotherm data	
Pb^{2+}	Na^+	($x10^{-2}$g equiv. dm^{-3})	Pb^{2+}	Na^+	(equiv. kg^{-1})	recovery	E_{Pb}	$\bar{E}_{Pb}$
4.775	0.423	9.933	2.752	0.099	5.603	103.20	0.957	1.014
4.830	0.283	9.943	2.842	0.075	5.759	106.07	0.971	1.047
4.825	0.269	9.919	3.040	0.086	6.166	113.57	0.972	1.120

(a) refer to figure 5.20(b)

(b) refer to figures 5.21(b) and 5.24

(c) data plotted in figure 5.25

APPENDIX 2

Table 13 Pb/CaA exchange at T_N = 0.1g equiv. dm^{-3}

Sol.Phase Conc./ ($x10^{-2}$ mol dm^{-3})		T_N/	Cryst. Phase Conc./(mol kg^{-1})		Total/ (equiv. kg^{-1})	Percentage recovery	(a) Isotherm data	(b)
Pb^{2+}	Ca^{2+}	($x10^{-2}$g equiv. dm^{-3})	Pb^{2+}	Na^{+}			E_{Pb}	$\bar{E}_{Pb}$
-	4.400	8.800	-	2.153	4.306	80.65	-	-
$2.748x10^{-4}$	4.455	8.911	0.883	1.069	3.904	73.12	$6.168x10^{-5}$	0.452
$2.824x10^{-4}$	4.424	8.849	0.219	2.046	4.530	84.84	$6.383x10^{-5}$	0.097
$3.086x10^{-4}$	4.419	8.839	0.210	0.975	2.370	44.39	$6.983x10^{-5}$	0.177
$3.131x10^{-4}$	4.414	8.829	0.108	0.994	2.204	41.28	$7.093x10^{-5}$	0.098
$3.240x10^{-4}$	4.424	8.849	0.425	1.719	4.288	80.31	$7.323x10^{-5}$	0.198
$6.810x10^{-4}$	4.495	8.991	1.775	0.366	4.282	80.20	$1.515x10^{-4}$	0.829
0.053	4.460	9.026	2.346	0.209	5.110	95.71	0.012	0.918
0.428	4.184	9.224	2.709	0.907	5.612	105.11	0.093	1.014
0.971	3.694	9.330	2.807	0.050	5.714	107.02	0.208	1.052
1.325	3.373	9.396	2.873	0.040	5.826	109.12	0.282	1.076
1.842	2.913	9.510	2.797	0.012	5.618	105.22	0.387	1.048
2.372	2.437	9.618	2.823	$4.28x10^{-3}$	5.655	105.91	0.493	1.058
2.843	2.027	9.740	2.852	$4.83x10^{-3}$	5.714	107.01	0.584	1.068
3.298	1.622	9.840	2.854	*	5.708	106.91	0.670	1.069
4.109	0.862	9.942	2.997	*	5.994	112.26	0.827	1.123

APPENDIX 2

Table 13 (cont.) Pb/CaA exchange at T_N = 0.1g equiv. dm^{-3}

Sol.Phase Conc./ ($x10^{-2}$ mol dm^{-3})		T_N/	Cryst. Phase Conc./(mol kg^{-1})		Total/ (equiv. kg^{-1})	Percentage recovery	(a) Isotherm data	(b)
Pb^{2+}	Ca^{2+}	($x10^{-2}$g equiv. dm^{-3})	Pb^{2+}	Na^{+}			E_{Pb}	$\bar{E}_{Pb}$
4.575	0.403	9.956	3.211	*	6.422	120.28	0.919	1.203
4.770	0.209	9.958	3.169	*	6.388	118.71	0.958	1.187
4.815	0.163	9.956	3.273	*	6.546	122.60	0.967	1.226

* Concentration of Ca^{2+} too low to be analysed accurately

(a) refer to figure 5.24

(b) data plotted in figure 5.26

APPENDIX 2

Table 14 Pb^{2+}/Na^{+} solutions for exchange with clinoptilolite

Solution number	Concentration/($x10^{-2}$ mol dm^{-3})		T_N/ ($x10^{-2}$g equiv. dm^{-3})
	Pb^{2+}	Na^{+}	
1	-	10.012	10.012
2	0.248	9.493	9.989
3	0.500	8.929	9.929
4	0.995	8.211	10.201
5	1.501	7.206	10.208
6	1.990	6.160	10.140
7	2.497	5.123	10.117
8	3.002	4.088	10.092
9	3.491	3.160	10.142
10	3.991	2.149	10.131
11	4.488	1.099	10.075
12	4.995	-	9.990

APPENDIX 2

Table 15 Solution phase analysis for Pb^{2+} exchange with NAT.CLI at T_N = 0.1g equiv. dm^{-3}

(a) Solution Number	Weight of zeolite/(g)	Volume of solution/(ml)	(b) Solution Phase Concentration/($x10^{-2}$ mol dm^{-3}) Na^+	K^+	Pb^{2+}	T_N/ ($x10^{-2}$g equiv. dm^{-3}
1	0.3031	50	9.837	0.120	0	9.957
2	0.6085	25	9.607	0.205	$1.513x10^{-3}$	9.815
2	0.6046	50	9.607	0.214	0.011	9.843
2	0.2995	25	9.607	0.214	0.018	9.857
2	0.3025	50	9.607	0.193	0.058	9.916
3	0.2974	50	9.152	0.230	0.229	9.840
4	0.2963	50	8.214	0.261	0.689	9.853
5	0.2997	50	7.375	0.272	1.189	10.026
6	0.3050	50	6.480	0.293	1.634	10.041
7	0.2992	50	5.511	0.298	2.140	10.090
8	0.2955	50	4.437	0.307	2.616	9.977
9	0.2955	50	3.536	0.303	3.106	10.051
10	0.2997	50	2.576	0.322	3.564	10.026
11	0.2956	50	1.635	0.334	4.035	10.041
12	0.2981	50	0.620	0.334	4.534	10.021

APPENDIX 2

Table 15 (cont.) Solution phase analysis for Pb^{2+} exchange with NAT.CLI at T_N = 0.1g equiv. dm^{-3}

(a) Solution Number	Weight of zeolite/(g)	Volume of solution/(ml)	(b) Solution Phase Concentration/($x10^{-2}$ mol dm^{-3}) Na^+	K^+	Pb^{2+}	T_N/ ($x10^{-2}$g equiv. dm^{-3}
12	0.3014	100	0.323	0.202	4.756	10.037
12	0.1386	100	0.135	0.098	4.876	9.985
12	0.1471	200	0.081	0.061	4.935	10.012
12	0.1308	250	0.058	0.046	4.935	9.976
12	0.1535	500	0.032	0.027	4.760	9.578
12	0.1160	500	0.025	0.021	4.760	9.566

(a) refers to Table 14

(b) data is input into computer programme as moles per volume of exchange solution

APPENDIX 2

Table 16 Derived[a] results for Pb^{2+} exchange with NAT.CLI at T_N = 0.1g equiv. dm^{-3}

(b) Solution Number	Crystal Phase Concentration/mol kg^{-1})			Total/ (equiv. kg^{-1})	Percentage recovery	(c) Isotherm data	
	Na^+	K^+	Pb^{2+}			E_{Pb}	$\bar{E}_{Pb}$
1	1.245	0.657	0	1.902	91.42	0	0
2	0.914	0.771	0.101	1.887	90.71	3.083×10^{-4}	0.107
2	0.867	0.679	0.196	1.937	93.12	2.273×10^{-3}	0.202
2	0.865	0.677	0.192	1.926	92.59	3.553×10^{-3}	0.200
2	0.753	0.537	0.315	1.919	92.26	0.012	0.328
3	0.588	0.469	0.455	1.967	94.56	0.047	0.463
4	0.958	0.415	0.516	2.406	115.64	0.140	0.429
5	0.678	0.402	0.521	2.120	101.92	0.237	0.491
6	0.437	0.375	0.584	1.979	95.11	0.326	0.590
7	0.313	0.357	0.598	1.866	89.71	0.424	0.641
8	0.369	0.337	0.653	2.012	96.71	0.524	0.649
9	0.325	0.342	0.653	1.974	94.87	0.618	0.662
10	0.251	0.318	0.714	1.997	96.00	0.711	0.715
11	0.055	0.291	0.765	1.875	90.10	0.804	0.816
12	0	0.295	0.775	1.845	88.70	0.905	0.840

APPENDIX 2

Table 16 (cont.) Derived[a] results for Pb^{2+} exchange with NAT.CLI at T_N = 0.1g equiv. dm^{-3}

(b) Solution Number	Crystal Phase Concentration/mol kg^{-1})			Total/ (equiv. kg^{-1})	Percentage recovery	(c) Isotherm data	
	Na^+	K^+	Pb^{2+}			E_{Pb}	$\bar{E}_{Pb}$
12	0	0.184	0.793	1.770	85.01	0.948	0.896
12	0	0.147	0.851	1.849	88.89	0.977	0.921
12	0	0.022	0.816	1.653	79.48	0.986	0.987
12	0	0	1.147	2.294	110.25	0.990	1.103
12	0	0	1.303	2.606	125.26	0.994	1.253
12	0	0	1.724	3.448	165.75	0.995	1.658

(a) derived from data in Table 15

(b) refers to Table 14

(c) data plotted in figure 5.27

APPENDIX 2

Table 17 Solution phase analysis for Pb^{2+} exchange with F.EX.CLI at T_N = 0.1g equiv. dm^{-3}

(a) Solution Number	Weight of zeolite/(g)	Volume of solution/(ml)	(b) Solution Phase Concentration ($x10^{-2}$ mol dm^{-3})		T_N/ ($x10^{-2}$g equiv. dm^{-3})
			Na^+	Pb^{2+}	
1	0.3010	50	9.837	0	9.837
2	0.5951	25	9.780	2.028×10^{-3}	9.782
2	0.5991	50	9.780	3.831×10^{-3}	9.783
2	0.2990	25	9.723	4.816×10^{-3}	9.728
2	0.2990	50	9.723	0.024	9.747
3	0.2959	50	9.436	0.163	9.762
4	0.2968	50	8.651	0.595	9.751
5	0.2998	50	7.838	1.115	10.068
6	0.2996	50	6.836	1.575	9.986
7	0.2970	50	5.894	2.080	10.054
8	0.2959	50	4.878	2.527	9.934
9	0.2966	50	4.008	3.002	10.012

APPENDIX 2

Table 17 (cont.) Solution phase analysis for Pb^{2+} exchange with F.EX.CLI at T_N = 0.1g equiv. dm^{-3}

(a) Solution Number	Weight of zeolite/(g)	Volume of solution/(ml)	(b) Solution Phase Concentration ($x10^{-2}$ mol dm^{-3})		T_N/ ($x10^{-2}$g equiv. dm^{-3})
			Na^+	Pb^{2+}	
10	0.2962	50	3.049	3.476	10.002
11	0.2986	50	2.218	3.947	9.918
12	0.3022	50	1.182	4.270	9.722
12	0.2994	100	0.603	4.637	9.877
12	0.1426	100	0.305	4.756	9.817
12	0.1515	200	0.153	4.816	9.785
12	0.1493	250	0.111	4.876	9.863
12	0.1398	500	0.054	4.770	9.594
12	0.1110	500	0.045	4.760	9.565

(a) refers to Table 14

(b) data is input into computer programme as moles per volume of exchange solution

APPENDIX 2

Table 18 Derived[a] results for Pb^{2+} exchange with F.EX.CLI at T_N = 0.1g equiv. dm^{-3}

(b) Solution Number	Crystal Phase Concentration/mol kg^{-1}) Na^+	Pb^{2+}	Total/ (equiv. kg^{-1})	Percentage recovery	(c) Isotherm data E_{Pb}	$\bar{E}_{Pb}$
1	2.128	0	2.128	99.02	0	0
2	1.721	0.103	1.928	102.74	4.146×10^{-4}	0.107
2	1.603	0.204	2.011	95.61	7.830×10^{-4}	0.203
2	1.648	0.203	2.055	93.57	9.896×10^{-4}	0.198
2	1.457	0.375	2.208	89.70	4.831×10^{-3}	0.340
3	0.987	0.569	2.124	98.84	0.033	0.535
4	1.101	0.751	2.602	121.08	0.113	0.577
5	0.788	0.644	2.075	96.56	0.222	0.620
6	0.714	0.693	2.099	97.67	0.315	0.660
7	0.546	0.704	1.953	90.88	0.414	0.721
8	0.507	0.801	2.109	98.14	0.509	0.760
9	0.412	0.826	2.065	96.09	0.600	0.800
10	0.323	0.871	2.065	96.09	0.695	0.844
11	0.296	0.904	2.105	97.95	0.796	0.859
12	0	1.201	2.402	111.77	0.878	1.118

APPENDIX 2

Table 18 (cont.) Derived[a] results for Pb^{2+} exchange with F.EX.CLI at T_N = 0.1g equiv. dm^{-3}

(b) Solution Number	Crystal Phase Concentration/mol kg^{-1}) Na^+	Pb^{2+}	Total/ (equiv. kg^{-1})	Percentage recovery	(c) Isotherm data E_{Pb}	$\bar{E}_{Pb}$
12	0	1.196	2.391	111.26	0.939	1.113
12	0	1.676	3.352	155.98	0.969	1.560
12	0	2.363	4.726	219.92	0.984	2.200
12	0	2.009	4.019	187.02	0.989	1.870
12	0	1.073	2.146	99.86	0.994	1.000
12	0	1.802	3.604	167.71	0.995	1.677

(a) derived from data in Table 17

(b) refers to Table 14

(c) data plotted in figure 5.28

APPENDIX 3

Organolead ion exchange data

APPENDIX 3

Table 1(i) Analytical data [a] for Me_3Pb^+/NaZl(II) exchange at T_N = 0.01g equiv. dm^{-3} using anions of sodium of differing complexing ability (1 week exchange)

Solution number	Counter anion	Sol. Phase Conc./ ($x10^{-2}$ mol dm^{-3}) Me_3Pb^+	Sol. Phase Conc./ ($x10^{-2}$ mol dm^{-3}) Na^+	T_N/ ($x10^{-2}$g equiv. dm^{-3})	Crystal Phase Conc./ (mol kg^{-1}) Me_3Pb^+	Crystal Phase Conc./ (mol kg^{-1}) Na^+	Total/ (equiv. kg^{-1})	Percentage recovery
I	Cl^-	0.107	1.041	1.148	0.013	4.407	4.420	94.68
II	Cl^-	0.269	0.942	1.211	0.061	4.051	4.112	88.08
III	Cl^-	0.453	0.776	1.229	0.120	3.842	3.962	84.86
IV	Cl^-	0.599	0.678	1.277	0.187	3.788	3.975	85.14
I	NO_3^-	0.109	1.035	1.144	0.012	4.121	4.133	88.53
II	NO_3^-	0.272	0.919	1.191	0.064	3.866	3.930	84.18
III	NO_3^-	0.456	0.787	1.243	0.130	3.875	4.005	85.79
IV	NO_3^-	0.599	0.688	1.287	0.198	3.745	3.943	84.46
I	ClO_4^-	0.110	1.035	1.145	0.011	4.525	4.536	97.16
II	ClO_4^-	0.269	0.908	1.177	0.064	4.141	4.205	90.07
III	ClO_4^-	0.456	0.798	1.254	0.119	3.865	3.984	85.34
IV	ClO_4^-	0.578	0.708	1.286	0.185	3.740	3.925	84.07

(a) isotherm data for the respective exchanges are presented in Table 1(ii)

APPENDIX 3

Table 1(ii) Isotherm data for Me_3Pb^+/NaZl(II) exchange at T_N = 0.01g equiv. dm^{-3} using anions of sodium of differing complexing ability (1 week exchange)

Solution number	Counter anion	Isotherm data	
		E_{Me_3Pb}	$\bar{E}_{Me_3Pb}$
I	Cl^-	0.093	2.941×10^{-3}
II	Cl^-	0.222	0.015
III	Cl^-	0.369	0.030
IV	Cl^-	0.469	0.047
I	NO_3^-	0.095	2.904×10^{-3}
II	NO_3^-	0.228	0.016
III	NO_3^-	0.367	0.033
IV	NO_3^-	0.465	0.050
I	ClO_4^-	0.096	2.425×10^{-3}
II	ClO_4^-	0.229	0.015
III	ClO_4^-	0.364	0.030
IV	ClO_4^-	0.450	0.047

APPENDIX 3

Table 2(i) Analytical data [(a)] for Me_3Pb^+/NaZ5(II) exchange at T_N = 0.01g equiv. dm^{-3} using anions of sodium of differing complexing ability (1 week exchange)

Solution number	Counter anion	Sol. Phase Conc./ (x10^{-2} mol dm^{-3}) Me_3Pb^+	Sol. Phase Conc./ (x10^{-2} mol dm^{-3}) Na^+	T_N/ (x10^{-2}g equiv. dm^{-3})	Crystal Phase Conc./ (mol kg^{-1}) Me_3Pb^+	Crystal Phase Conc./ (mol kg^{-1}) Na^+	Total/ (equiv. kg^{-1})	Percentage recovery
I	Cl^-	0.108	0.985	1.093	0.016	2.667	2.683	84.15
II	Cl^-	0.326	0.803	1.129	0.059	2.627	2.686	84.25
III	Cl^-	0.502	0.662	1.164	0.104	2.545	2.649	83.09
IV	Cl^-	0.674	0.519	1.193	0.181	2.438	2.619	82.15
I	NO_3^-	0.110	0.979	1.089	0.016	2.644	2.660	83.44
II	NO_3^-	0.332	0.793	1.125	0.057	2.657	2.714	85.13
III	NO_3^-	0.498	0.668	1.166	0.098	2.481	2.579	80.90
IV	NO_3^-	0.676	0.507	1.183	0.181	2.365	2.546	79.86
I	ClO_4^-	0.106	0.985	1.091	0.015	2.677	2.692	84.44
II	ClO_4^-	0.321	0.797	1.118	0.059	2.621	2.680	84.07
III	ClO_4^-	0.501	0.657	1.158	0.106	2.536	2.642	82.87
IV	ClO_4^-	0.665	0.536	1.201	0.186	2.434	2.620	82.18

(a) isotherm data for the respective exchanges are presented in Table 2(ii)

APPENDIX 3

Table 2(ii) Isotherm data for Me_3Pb^+/NaZ5(II) exchange at T_N = 0.01g equiv. dm^{-3} using anions of sodium of differing complexing ability (1 week exchange)

Solution number	Counter anion	Isotherm data	
		E_{Me_3Pb}	$\bar{E}_{Me_3Pb}$
I	Cl^-	0.099	5.964×10^{-3}
II	Cl^-	0.289	0.022
III	Cl^-	0.431	0.039
IV	Cl^-	0.565	0.069
I	NO_3^-	0.101	6.015×10^{-3}
II	NO_3^-	0.295	0.021
III	NO_3^-	0.427	0.038
IV	NO_3^-	0.571	0.071
I	ClO_4^-	0.097	5.572×10^{-3}
II	ClO_4^-	0.287	0.022
III	ClO_4^-	0.433	0.040
IV	ClO_4^-	0.554	0.071

APPENDIX 3

Table 3(i) Analytical data [(a)] for Me_3Pb^+/NaZl(II) exchange at T_N = 0.01g equiv. dm^{-3} using anions of sodium of differing complexing ability (1 and 2 week exchanges)

Exchange time (days)	Solution number	Counter anion	Sol. Phase Conc./ ($x10^{-2}$ mol dm^{-3}) Me_3Pb^+	Sol. Phase Conc./ ($x10^{-2}$ mol dm^{-3}) Na^+	T_N/ ($x10^{-2}$g equiv. dm^{-3})	Crystal Phase Conc./ (mol kg^{-1}) Me_3Pb^+	Crystal Phase Conc./ (mol kg^{-1}) Na^+	Total (equiv. kg^{-1})	Percentage recovery
7	V	Cl^-	0.432	0.768	1.200	0.175	3.776	3.951	84.63
7	VI	Cl^-	0.585	0.616	1.201	0.272	3.583	3.855	82.57
7	V	NO_3^-	0.444	0.772	1.216	0.154	3.702	3.856	83.59
7	VI	NO_3^-	0.613	0.625	1.238	0.252	3.502	3.754	80.41
14	V	Cl^-	0.454	0.754	1.208	0.169	3.761	3.930	84.18
14	VI	Cl^-	0.604	0.623	1.227	0.276	3.559	3.835	82.15
14	V	NO_3^-	0.441	0.759	1.200	0.179	3.771	3.950	84.61
14	VI	NO_3^-	0.628	0.617	1.245	0.291	3.588	3.879	83.09

(a) isotherm data for the respective exchanges are presented in Table 3(ii)

APPENDIX 3

Table 3(ii) Isotherm data for Me_3Pb^+/NaZl(II) exchange at T_N = 0.01g equiv. dm^{-3} using anions of sodium of differing complexing ability (1 and 2 week exchanges)

Exchange time (days)	Solution number	Counter anion	Isotherm data	
			E_{Me_3Pb}	$\bar{E}_{Me_3Pb}$
7	V	Cl^-	0.360	0.044
7	VI	Cl^-	0.487	0.071
7	V	NO_3^-	0.365	0.040
7	VI	NO_3^-	0.495	0.067
14	V	Cl^-	0.376	0.043
14	VI	Cl^-	0.492	0.072
14	V	NO_3^-	0.368	0.045
14	VI	NO_3^-	0.504	0.075

APPENDIX 3

Table 4(i) Analytical data [(a)] for Me_3Pb^+/NaZ5(II) exchange at T_N = 0.01g equiv. dm^{-3} using anions of sodium of differing complexing ability (1 and 2 week exchanges)

Exchange time (days)	Solution number	Counter anion	Sol. Phase Conc./ ($x10^{-2}$ mol dm^{-3}) Me_3Pb^+	Sol. Phase Conc./ ($x10^{-2}$ mol dm^{-3}) Na^+	T_N/ ($x10^{-2}$g equiv. dm^{-3})	Crystal Phase Conc./ (mol kg^{-1}) Me_3Pb^+	Crystal Phase Conc./ (mol kg^{-1}) Na^+	Total/ (equiv. kg^{-1})	Percentage recovery
7	V	Cl^-	0.520	0.606	1.126	0.144	2.698	2.842	89.15
7	VI	Cl^-	0.708	0.411	1.119	0.258	2.530	2.788	87.45
7	V	NO_3^-	0.581	0.603	1.184	0.124	2.476	2.600	81.56
7	VI	NO_3^-	0.819	0.398	1.217	0.244	2.402	2.646	83.00
14	V	Cl^-	0.535	0.594	1.129	0.136	2.589	2.725	85.47
14	VI	Cl^-	0.776	0.434	1.210	0.246	2.403	2.649	83.08
14	V	NO_3^-	0.519	0.636	1.155	0.134	2.533	2.667	83.66
14	VI	NO_3^-	0.769	0.437	1.206	0.226	2.344	2.570	80.62

(a) isotherm data for the respective exchanges are presented in Table 4(ii)

APPENDIX 3

Table 4(ii) Isotherm data for Me_3Pb^+/NaZ5(II) exchange at T_N = 0.01g equiv. dm^{-3} using anions of sodium of differing complexing ability (1 and 2 week exchanges)

Exchange time (days)	Solution number	Counter anion	Isotherm data	
			E_{Me_3Pb}	$\bar{E}_{Me_3Pb}$
7	V	Cl^-	0.462	0.051
7	VI	Cl^-	0.632	0.093
7	V	NO_3^-	0.490	0.048
7	VI	NO_3^-	0.673	0.092
14	V	Cl^-	0.474	0.050
14	VI	Cl^-	0.641	0.093
14	V	NO_3^-	0.449	0.050
14	VI	NO_3^-	0.638	0.088

APPENDIX 3

Table 5 Me_3Pb^+/NaZl(II) exchange at T_N = 0.01g equiv. dm^{-3}

Sol. Phase Conc./ ($x10^{-2}$ mol dm^{-3})		T_N/	Cryst. Phase Conc./ (mol kg^{-1})		Total/	Percentage[a]	Isotherm data[b]	
Me_3Pb^+	Na^+	($x10^{-2}$ mol dm^{-3})	Me_3Pb^+	Na^+	(equiv. kg^{-1})	recovery	E_{Me_3Pb}	$\bar{E}_{Me_3Pb}$
0.107	1.041	1.148	0.013	4.407	4.420	94.68	0.093	$2.941x10^{-3}$
0.188	0.969	1.157	0.038	3.907	3.945	84.50	0.163	$9.632x10^{-3}$
0.269	0.942	1.211	0.061	4.051	4.112	88.08	0.222	0.015
0.366	0.838	1.202	0.088	3.727	3.815	81.72	0.305	0.023
0.366	0.727	1.093	0.179	3.679	3.858	82.64	0.335	0.046
0.453	0.776	1.229	0.120	3.842	3.962	84.86	0.369	0.030
0.457	0.645	1.102	0.245	3.590	3.835	82.14	0.415	0.064
0.523	0.690	1.213	0.165	3.679	3.844	82.34	0.431	0.043
0.599	0.678	1.277	0.187	3.788	3.975	85.14	0.469	0.047
0.679	0.627	1.306	0.213	3.568	3.781	80.99	0.520	0.056
0.720	0.574	1.294	0.260	3.438	3.698	79.21	0.556	0.070
0.735	0.537	1.272	0.283	3.414	3.697	79.19	0.578	0.077
0.718	0.407	1.125	0.379	3.413	3.792	81.22	0.638	0.100
0.865	0.372	1.237	0.443	3.164	3.607	77.26	0.699	0.123

APPENDIX 3

Table 5 (cont.) Me_3Pb^+/NaZl(II) exchange at T_N = 0.01g equiv. dm^{-3}

Sol. Phase Conc./ ($x10^{-2}$ mol dm^{-3})		T_N/	Cryst. Phase Conc./ (mol kg^{-1})		Total/	Percentage[a]	Isotherm data[b]	
Me_3Pb^+	Na^+	($x10^{-2}$ mol dm^{-3})	Me_3Pb^+	Na^+	(equiv. kg^{-1})	recovery	E_{Me_3Pb}	$\bar{E}_{Me_3Pb}$
0.822	0.271	1.093	0.568	2.777	3.345	71.65	0.752	0.169
0.929	0.253	1.182	0.698	2.444	3.142	67.30	0.786	0.222
0.962	0.209	1.171	0.746	2.094	2.840	60.83	0.822	0.263
1.021	0.168	1.189	0.854	1.700	2.554	54.71	0.859	0.334
1.047	0.146	1.193	0.823	1.584	2.407	51.56	0.878	0.342
1.093	0.090	1.183	0.717	1.149	1.866	39.97	0.924	0.384
1.115	0.034	1.149	0.709	0.781	1.490	31.92	0.970	0.476
1.116	0.014	1.130	0.692	0.677	1.369	29.32	0.988	0.506
1.024	0.011	1.035	0.690	0.095	0.785	16.81	0.989	0.879
0.977	0.010	$9.87x10^{-3}$	0.723	0.047	0.770	16.49	0.990	0.939
0.977	$9x10^{-3}$	$9.86x10^{-3}$	0.688	0.038	0.726	15.55	0.991	0.948

(a) refer to figure 5.37

(b) data plotted in figure 5.34

APPENDIX 3

Table 6 Me_3Pb^+/NaZ5(II) exchange at T_N = 0.01g equiv. dm^{-3}

Sol. Phase Conc./ ($x10^{-2}$ mol dm^{-3})		T_N/	Cryst. Phase Conc./ (mol kg^{-1})		Total/	Percentage[a]	Isotherm data[b]	
Me_3Pb^+	Na^+	($x10^{-2}$ mol dm^{-3})	Me_3Pb^+	Na^+	(equiv. kg^{-1})	recovery	E_{Me_3Pb}	$\bar{E}_{Me_3Pb}$
0.108	0.985	1.093	0.016	2.667	2.683	84.15	0.099	$5.964x10^{-3}$
0.215	0.886	1.101	0.038	2.678	2.716	85.19	0.195	0.014
0.326	0.803	1.129	0.059	2.627	2.686	84.25	0.289	0.022
0.397	0.729	1.126	0.082	2.583	2.665	83.59	0.353	0.031
0.370	0.676	1.046	0.123	2.628	2.751	86.29	0.354	0.045
0.502	0.662	1.164	0.104	2.545	2.649	83.09	0.431	0.039
0.598	0.578	1.176	0.147	2.494	2.641	82.84	0.508	0.056
0.529	0.506	1.035	0.205	2.473	2.678	84.00	0.511	0.077
0.674	0.519	1.193	0.181	2.438	2.619	82.15	0.565	0.069
0.758	0.463	1.221	0.207	2.349	2.556	80.17	0.621	0.081
0.828	0.418	1.246	0.247	2.268	2.515	78.89	0.665	0.098
0.888	0.349	1.237	0.293	2.310	2.603	81.64	0.718	0.113
0.899	0.252	1.151	0.368	2.453	2.821	88.48	0.781	0.131
1.029	0.252	1.231	0.407	2.067	2.474	77.60	0.836	0.165
0.995	0.155	1.150	0.510	2.173	2.683	84.15	0.865	0.190
1.038	0.134	1.172	0.601	1.967	2.568	80.55	0.886	0.234
1.038	0.105	1.143	0.677	1.791	2.468	77.41	0.908	0.274

APPENDIX 3

Table 6 (cont.) Me_3Pb^+/NaZ5(II) exchange at T_N = 0.01g equiv. dm^{-3}

Sol. Phase Conc./ ($x10^{-2}$ mol dm^{-3})		T_N/	Cryst. Phase Conc./ (mol kg^{-1})		Total/	Percentage[a]	Isotherm data[b]	
Me_3Pb^+	Na^+	($x10^{-2}$ mol dm^{-3})	Me_3Pb^+	Na^+	(equiv. kg^{-1})	recovery	E_{Me_3Pb}	$\bar{E}_{Me_3Pb}$
1.151	0.082	1.233	0.726	1.557	2.283	71.61	0.934	0.318
1.195	0.071	1.266	0.808	1.434	2.242	70.32	0.944	0.360
1.071	0.048	1.119	0.827	1.278	2.105	66.02	0.957	0.393
1.112	0.025	1.137	0.827	0.913	1.740	54.58	0.978	0.475
1,159	0.014	1.173	0.878	0.804	1.682	52.76	0.988	0.522
0.977	0.012	$9.89x10^{-3}$	0.961	0.435	1.396	43.79	0.988	0.688
0.977	0.011	$9.88x10^{-3}$	1.021	0.404	1.425	44.70	0.989	0.717
0.986	$6x10^{-3}$	$9.92x10^{-3}$	0.734	0.438	1.172	36.76	0.994	0.626

(a) refer to figure 5.37

(b) data plotted in figure 5.35

APPENDIX 3

Table 7[a] Low level Me_3Pb^+ ion exchange in NaZl(II) at T_N = 0.01g equiv. dm^{-3}

Exchange sol. conc./(mol dm^{-3})		Equilibrium sol. conc./(mol dm^{-3})		Crystal phase conc./(mol kg^{-1})		Percentage
$Me_3Pb^+/(x10^{-4})$	$Na^+(x10^{-2})$	$Me_3Pb^+/(x10^{-4})$	$Na^+/(x10^{-2})$	$Me_3Pb^+/(x10^{-4})$	Na^+	recovery
0.035	1.024	0.035	1.113	0.781	4.268	91.39
0.070	1.024	0.070	1.113	0.330	4.331	92.74
0.194	1.024	0.181	1.113	0.293	4.294	91.95
0.393	1.024	0.372	1.113	0.324	4.353	93.21
0.786	1.024	0.743	1.113	0.467	4.379	93.77
1.953	1.024	1.732	1.113	1.557	4.354	93.23
3.983	1.024	3.265	1.113	5.612	4.314	92.38

(a) Data derived from these results are presented in tables 5.53 and 5.55, and figure 5.38

APPENDIX 3

Table 8[a] Low level Me_3Pb^+ ion exchange in NaZ1(II) at T_N = 0.1g equiv. dm^{-3}

Exchange sol. conc./(mol dm^{-3})		Equilibrium sol. conc./(mol dm^{-3})		Crystal phase conc./(mol kg^{-1})		Percentage
$Me_3Pb^+/(x10^{-4})$	$Na^+(x10^{-2})$	$Me_3Pb^+/(x10^{-4})$	$Na^+/(x10^{-2})$	$Me_3Pb^+/(x10^{-4})$	Na^+	recovery
0.033	9.508	0.033	9.776	0.285	4.392	94.05
0.078	9.508	0.078	9.776	0.279	4.320	92.51
0.199	9.508	0.199	9.776	0.387	4.318	92.46
0.395	9.508	0.395	9.776	0.462	4.349	93.13
0.752	9.508	0.739	9.776	0.569	4.327	92.66
1.958	9.508	1.748	9.776	2.388	4.318	92.46
3.931	9.508	3.648	9.776	6.529	4.299	92.06

(a) Data derived from these results are presented in tables 5.54 and 5.56, and figure 5.38

APPENDIX 3

Table 9 Me_3Pb^+/Na^+ solutions for exchange with clinoptilolite

Solution number	Concentration/($x10^{-2}$ mol dm^{-3})		T_N/ ($x10^{-2}$ mol. dm^{-3})
	Me_3Pb^+	Na^+	
1	0.107	0.877	0.984
2	0.217	0.807	1.024
3	0.434	0.579	1.013
4	0.536	0.481	1.017
5	0.742	0.288	1.030
6	0.867	0.200	1.067
7	1.072	-	1.072

APPENDIX 3

Table 10 Solution phase analysis for Me_3Pb^+ exchange with NAT.CLI, 2N CLI and 4N CLI at T_N = 0.01g equiv. dm^{-3}

Zeolite	Solution[a] number	Weight of zeolite/(g)	Volume of solution/(ml)	(b)Solution Phase Concentration/($x10^{-2}$ mol dm^{-3}) Na^+	K^+	Me_3Pb^+	T_N/ ($x10^{-2}$ mol dm^{-3})
NAT CLI	1	0.3013	50	0.991	0.031	0.103	1.125
NAT CLI	2	0.2812	50	0.894	0.029	0.207	1.130
NAT CLI	3	0.2645	50	0.727	0.027	0.413	1.167
NAT CLI	4	0.2415	50	0.619	0.025	0.505	1.149
NAT CLI	5	0.2206	50	0.433	0.018	0.711	1.162
NAT CLI	6	0.2043	50	0.347	0.016	0.826	1.189
NAT CLI	7	0.1824	50	0.154	0.009	1.031	1.195
2N CLI	1	0.3012	50	0.844	-	0.107	0.951
2N CLI	2	0.2816	50	0.743	-	0.212	0.955
2N CLI	3	0.2602	50	0.567	-	0.434	1.001
2N CLI	4	0.2442	50	0.472	-	0.526	0.998
2N CLI	5	0.2197	50	0.305	-	0.690	0.995
2N CLI	6	0.2043	50	0.218	-	0.826	1.044
2N CLI	7	0.1830	50	0.051	-	1.011	1.062

APPENDIX 3

Table 10 (cont.) Solution phase analysis for Me_3Pb^+ exchange with NAT.CLI, 2N CLI and 4N CLI at T_N = 0.01g equiv. dm^{-3}

Zeolite	Solution[a] number	Weight of zeolite/(g)	Volume of solution/(ml)	(b)Solution Phase Concentration/($x10^{-2}$ mol dm^{-3}) Na^+	K^+	Me_3Pb^+	T_N/ ($x10^{-2}$ mol dm^{-3})
4N CLI	1	0.3009	50	0.844	-	0.105	0.949
4N CLI	2	0.2832	50	0.743	-	0.212	0.955
4N CLI	3	0.2605	50	0.567	-	0.413	0.980
4N CLI	4	0.2432	50	0.484	-	0.526	1.010
4N CLI	5	0.2232	50	0.305	-	0.711	1.016
4N CLI	6	0.2039	50	0.218	-	0.826	1.044
4N CLI	7	0.1809	50	0.054	-	1.031	1.085

(a) refers to table 9

(b) data is input into computer system as moles per volume of exchange solution

APPENDIX 3

Table 11 Derived[a] results for Me_3Pb^+ exchange with NAT.CLI, 2N CLI^- and 4N CLI at T_N = 0.01g equiv. dm^{-3}

Zeolite	Solution[b] number	Crystal Phase Concentration/(mol kg^{-1}) Na+	K^+	Me_3Pb^+	Total/ (equiv. kg^{-1})	Percentage recovery	Isotherm data[c] E_{Me_3Pb}	$\bar{E}_{Me_3Pb}$
NAT CLI	1	0.877	0.846	0.007	1.730	84.85	0.092	3.97×10^{-3}
NAT CLI	2	0.909	0.846	0.018	1.773	86.91	0.183	0.010
NAT CLI	3	0.785	0.847	0.039	1.671	81.95	0.354	0.023
NAT CLI	4	0.778	0.846	0.064	1.688	82.79	0.440	0.038
NAT CLI	5	0.735	0.857	0.070	1.662	81.51	0.612	0.042
NAT CLI	6	0.706	0.858	0.100	1.664	81.66	0.695	0.060
NAT CLI	7	0.642	0.872	0.114	1.628	79.79	0.864	0.070
2N CLI	1	1.077	-	0	1.077	60.09	0.113	0
2N CLI	2	1.136	-	0.009	1.145	63.89	0.222	8.07×10^{-3}
2N CLI	3	1.046	-	0	1.046	58.36	0.434	0
2N CLI	4	1.040	-	0.021	1.061	59.20	0.527	0.020
2N CLI	5	0.984	-	0.117	1.101	61.43	0.693	0.106
2N CLI	6	0.980	-	0.100	1.080	60.26	0.791	0.093
2N CLI	7	0.883	-	0.168	1.051	58.64	0.952	0.160

APPENDIX 3

Table 11 (cont.) Derived[a] results for Me_3Pb^+ exchange with NAT.CLI, 2N CLI and 4N CLI at T_N = 0.01g equiv. dm^{-3}

Zeolite	Solution[b] number	Crystal Phase Concentration/(mol kg^{-1}) Na+	K^+	Me_3Pb^+	Total/ (equiv. kg^{-1})	Percentage recovery	Isotherm data[c] E_{Me_3Pb}	$\bar{E}_{Me_3Pb}$
4N CLI	1	1.039	-	0.003	1.042	62.74	0.111	3.25×10^{-3}
4N CLI	2	1.096	-	0.009	1.105	66.53	0.222	8.31×10^{-3}
4N CLI	3	1.008	-	0.040	1.048	63.10	0.422	0.038
4N CLI	4	0.978	-	0.021	0.999	60.15	0.521	0.021
4N CLI	5	0.946	-	0.069	1.015	61.12	0.700	0.068
4N CLI	6	0.941	-	0.101	1.042	62.74	0.791	0.097
4N CLI	7	0.836	-	0.114	0.950	57.20	0.951	0.121

(a) derived from data in table 10

(b) refers to table 9

(c) data summarised in table 5.57

APPENDIX 4

Kinetic pH response data

APPENDIX 4

Table 1 Kinetic pH responses[a] of zeolites of different framework density after immersion in distilled water

	pH									
Time / Zeolite	0	5s	10s	15s	30s	45s	60s	180s	300s	7 days
NaA	5.04	9.91	10.33	10.45	10.60	10.66	10.72	10.86	10.95	10.30
NaZ1	5.04	10.06	10.24	10.33	10.45	10.51	10.54	10.66	10.66	10.26
NaZ2	5.04	9.05	9.50	9.59	9.82	9.94	10.02	10.18	10.21	9.90
NaZ3	5.04	8.87	9.29	9.35	9.41	9.44	9.44	9.44	9.41	9.35
NaZ4	5.04	7.36	8.10	8.31	8.55	8.73	8.78	8.93	8.90	7.80
NaZ5	5.04	5.87	6.17	6.26	6.38	6.50	6.59	7.03	7.09	7.55
CaA	5.04	5.55	5.81	5.96	6.29	6.62	7.00	9.08	9.14	8.62
CaX	5.04	5.69	5.93	6.02	6.20	6.29	6.35	6.65	6.76	7.48
NAT.CLI	5.04	5.22	5.28	5.34	5.46	5.52	5.58	5.96	6.20	9.50
F.EX.CLI	5.04	5.13	5.13	5.13	5.16	5.19	5.22	5.46	5.66	7.22
2N CLI	5.04	5.01	5.01	4.98	4.92	4.92	4.92	4.98	5.04	5.55
4N CLI	5.04	5.01	5.01	5.01	5.01	5.01	5.01	5.13	5.25	5.88
NAT.CLI(II)	5.04	5.07	5.10	5.13	5.19	5.22	5.25	5.55	5.72	7.68
F.EX.CLI(II)	5.04	5.13	5.13	5.13	5.15	5.16	5.19	5.37	5.55	7.03

(a) data for the various clinoptilolite forms, and the synthetic zeolites are plotted in figures 5.39 and 5.40 respectively

APPENDIX 4

Table 2 Kinetic pH responses[a] of zeolites of different framework density after immersion in 0.1N $NaNO_3$

	pH									
Time / Zeolite	0	5s	10s	15s	30s	45s	60s	180s	300s	7 days
NaA	5.74	9.47	9.64	9.67	9.73	9.75	9.76	9.82	9.84	9.94
NaZ1	5.74	8.25	9.42	9.56	9.64	9.70	9.72	9.76	9.76	9.58
NaZ2	5.74	7.16	8.14	8.67	9.07	9.14	9.17	9.25	9.26	8.62
NaZ3	5.74	7.34	8.31	8.73	8.98	9.01	9.02	9.02	9.02	7.25
NaZ4	5.74	6.76	7.29	7.59	8.22	8.49	8.59	8.64	8.65	7.00
NaZ5	5.74	5.92	6.09	6.20	6.34	6.45	6.51	6.71	6.74	6.53
NAT.CLI	5.56	5.59	5.62	5.65	5.71	5.74	5.77	6.09	6.27	8.84
F.EX.CLI	5.56	5.62	5.64	5.65	5.68	5.70	5.71	5.78	5.83	6.70
NAT.CLI(II)	5.56	5.58	5.60	5.62	5.65	5.68	5.71	5.95	6.12	7.30
F.EX.CLI(II)	5.56	5.57	5.58	5.59	5.60	5.61	5.62	5.65	5.69	6.26

(a) data for the various clinoptilolite forms, and the synthetic zeolites are plotted in figures 5.41 and 5.42 respectively

APPENDIX 4

Table 3 Kinetic pH responses[a] of zeolites of different framework density after immersion in 0.1N $Pb(NO_3)_2$

	pH									
Time / Zeolite	0	5s	10s	15s	30s	45s	60s	180s	300s	7 days
NaA	4.00	4.40	4.38	4.35	4.33	4.32	4.31	4.30	4.30	4.73
NaZ1	4.00	4.25	4.26	4.25	4.24	4.22	4.21	4.15	4.12	4.70
NaZ2	4.00	4.10	4.13	4.14	4.14	4.13	4.12	4.11	4.09	4.55
NaZ3	4.00	4.10	4.13	4.14	4.15	4.14	4.13	4.12	4.12	4.65
NaZ4	4.00	4.00	4.00	4.00	4.00	4.00	4.00	4.00	4.00	4.85
NaZ5	4.00	3.98	3.97	3.96	3.94	3.96	3.97	3.99	4.00	5.10
CaA	4.00	3.91	3.87	3.85	3.82	3.82	3.82	3.85	3.88	5.47
CaX	4.00	4.05	4.11	4.14	4.17	4.18	4.20	4.24	4.25	4.87
NAT.CLI	4.00	-	-	-	-	-	4.00	4.02	4.03	4.94
F.EX.CLI	4.00	-	-	-	-	-	4.02	4.03	4.03	5.67
NAT.CLI(II)	4.00	-	-	-	-	-	4.00	4.01	4.02	4.77
F.EX.CLI(II)	4.00	-	-	-	-	-	4.00	4.00	4.01	5.60

(a) data for the calcium and sodium forms of the synthetic zeolites are plotted in figures 5.43 and 5.44 respectively

APPENDIX 4

Table 4 Kinetic pH responses[a] of zeolites of different framework density after immersion in 0.1N $CaNO_3$, 0.05N Pb^{2+} : 0.05N Na^+, or 0.005N Pb^{2+} : 0.095N Na^+

	pH									
Time / Zeolite	0	5s	10s	15s	30s	45s	60s	180s	300s	7 days
0.1N $CaNO_3$[a]										
CaA	5.12	5.26	5.44	5.58	5.82	5.99	6.09	6.73	7.14	7.70
CaX	5.12	5.32	5.44	5.52	5.60	5.62	5.64	5.67	5.72	6.52
0.05N Pb^{2+} : 0.05N Na^+[b]										
NaA	4.39	4.92	5.13	5.16	5.16	5.13	5.10	4.86	4.80	5.02
NaZ1	4.39	4.72	4.81	4.79	4.75	4.72	4.69	4.57	4.45	4.38
NaZ5	4.39	4.35	4.33	4.33	4.36	4.36	4.36	4.39	4.39	5.06
0.005N Pb^{2+} : 0.095N Na^+[b]										
NaA	4.91	5.55	6.18	6.55	7.10	7.36	7.64	8.18	8.24	9.15
NaZ1	4.91	5.87	5.88	5.89	5.92	5.95	5.98	6.04	6.10	6.99
NaZ5	4.91	5.15	5.22	5.22	5.23	5.24	5.25	5.29	5.32	5.83

(a) data plotted in figure 5.43

(b) data plotted in figure 5.45

APPENDIX 4

Table 5 Kinetic pH responses[a] of zeolites of different framework density after immersion in 0.01N $Pb(NO_3)_2$

	pH									
Time / Zeolite	0	5s	10s	15s	30s	45s	60s	180s	300s	7 days
NaA	5.03	5.73	6.13	6.55	7.61	8.21	8.50	8.95	8.95	8.81
NaZ1	5.03	5.48	5.51	5.51	5.51	5.52	5.57	6.13	6.13	7.00
NaZ2	5.03	5.11	5.08	5.06	5.03	5.03	5.06	5.51	5.69	6.25
NaZ3	5.03	5.48	6.07	6.19	6.22	6.24	6.26	6.31	6.37	6.15
NaZ4	5.03	5.15	5.36	5.43	5.46	5.48	5.49	5.75	5.84	6.12
NaZ5	5.03	5.18	5.23	5.27	5.33	5.36	5.36	5.54	5.63	5.91
CaA	5.03	5.02	4.99	4.93	4.89	4.92	4.96	6.04	6.28	7.15
CaX	5.03	4.80	4.71	4.69	4.69	4.71	4.74	5.02	5.12	5.37
NAT.CLI	5.03	5.05	5.05	5.06	5.08	5.09	5.12	5.12	5.12	5.55
F.EX.CLI	5.03	5.03	5.03	5.03	5.03	5.03	5.03	5.06	5.06	5.42
NAT.CLI(II)	5.03	5.03	5.03	5.03	5.03	5.03	5.03	5.05	5.06	5.15
F.EX.CLI(II)	5.03	5.03	5.03	5.03	5.03	5.03	5.03	5.03	5.03	5.27

(a) data for the calcium and sodium forms of the synthetic zeolites are plotted in figures 5.46

APPENDIX 4

Table 6 Kinetic pH responses[a] of zeolites of different framework density after immersion in 0.01N NaCl or 0.01N $(CH_3)_3PbCl$

	pH									
Time / Zeolite	0	5s	10s	15s	30s	45s	60s	180s	300s	7 days
0.01N NaCl										
NaZ1	5.21	8.57	10.06	10.21	10.35	10.41	10.44	10.51	10.52	10.03
NaZ5	5.21	5.81	6.13	6.27	6.45	6.52	6.56	6.76	6.83	6.93
NAT CLI	5.21	5.25	5.28	5.31	5.38	5.43	5.47	5.83	6.04	8.95
F.EX.CLI	5.21	5.22	5.24	5.25	5.27	5.30	5.31	5.59	5.77	7.10
2N CLI	5.21	5.06	4.91	4.82	4.61	4.53	4.44	4.14	4.10	3.58
4N CLI	5.21	4.97	4.88	4.82	4.73	4.64	4.58	4.26	4.14	3.58
0.01N $(CH_3)_3PbCl$										
NaZ1	6.31	7.69	7.83	7.86	7.90	7.93	7.95	8.01	8.02	8.26
NaZ5	6.31	6.68	6.86	6.86	6.86	6.86	6.86	6.87	6.88	7.00
NAT CLI	6.31	6.34	6.37	6.39	6.43	6.46	6.49	6.76	6.93	7.79
F.EX.CLI	6.31	6.33	6.34	6.36	6.39	6.42	6.43	6.65	6.79	6.95
2N CLI	6.31	6.31	6.30	6.28	6.25	6.24	6.22	6.12	6.06	4.24
4N CLI	6.31	6.28	6.27	6.25	6.22	6.19	6.18	6.12	6.09	4.66

(a) data for the synthetic and natural zeolites are plotted in figures 5.47 and 5.48 respectively